NASA CR-54881
LAC ER-8434

GPO PRICE $ _____

CFSTI PRICE(S) $ _____

Hard copy (HC) 7.00

Microfiche (MF) 1.75

ff 653 July 65

EFFECT OF NUCLEAR RADIATION ON MATERIALS AT CRYOGENIC TEMPERATURES

by

LOCKHEED NUCLEAR PRODUCTS

C. A. Schwanbeck, Project Manager

prepared for

NATIONAL AERONAUTICS AND SPACE ADMINISTRATION

Contract NAS3-7987
(Contract NASw-114)

N66 24695

(ACCESSION NUMBER) (THRU)

303 (PAGES) 1 (CODE)

CR-54881 (NASA CR OR TMX OR AD NUMBER) 17 (CATEGORY)

FACILITY FORM 602

LOCKHEED NUCLEAR PRODUCTS

This report was prepared as an account of Government sponsored work. Neither the United States, nor the National Aeronautics and Space Administration (NASA), nor any person acting on behalf of NASA:

A.) Makes any warranty or representation, expressed or implied, with respect to the accuracy, completeness, or usefulness of the information contained in this report, or that the use of any information, apparatus, method, or process disclosed in this report may not infringe privately owned rights; or

B.) Assumes any liabilities with respect to the use of, or for damages resulting from the use of any information, apparatus, method or process disclosed in this report.

As used above, "person acting on behalf of NASA" includes any employee or contractor of NASA, or employee of such contractor, to the extent that such employee or contractor of NASA, or employee of such contractor prepares, disseminates, or provides access to, any information pursuant to his employment or contract with NASA, or his employment with such contractor.

Requests for copies of this report should be referred to

National Aeronautics and Space Administration
Office of Scientific and Technical Information
Attention: AFSS-A
Washington, D.C. 20546

NASA CR-54881
LAC ER-8434

FINAL REPORT

EFFECT OF NUCLEAR RADIATION ON MATERIALS AT CRYOGENIC TEMPERATURES

by

LOCKHEED NUCLEAR PRODUCTS

C. A. Schwanbeck, Project Manager

prepared for

NATIONAL AERONAUTICS AND SPACE ADMINISTRATION

January 1965

Contract NAS 3-7987
(Contract NASw-114)

Technical Management
NASA Lewis Research Center
Cleveland, Ohio
Nuclear Systems Division
Charles L. Younger

LOCKHEED NUCLEAR PRODUCTS
LOCKHEED-GEORGIA COMPANY

A DIVISION OF LOCKHEED AIRCRAFT CORPORATION

If this document is supplied under the requirements of a United States Government contract, the following legend shall apply unless the letter U appears in the coding box:

This data is furnished under a United States Government contract and only those portions hereof which are marked (for example, by circling, underscoring or otherwise) and indicated as being subject to this legend shall not be released outside the Government (except to foreign governments, subject to these same limitations), nor be disclosed, used, or duplicated, for procurement or manufacturing purposes, except as otherwise authorized by contract, without the permission of Lockheed-Georgia Company, A Division of Lockheed Aircraft Corporation, Marietta, Georgia. This legend shall be marked on any reproduction hereon in whole or in part.

The "otherwise marking" and "indicated portions" as used above shall mean this statement and includes all details or manufacture contained herein respectively.

Code: U Contract: NAS 3-7987

FOREWORD

This report is submitted to the National Aeronautics and Space Administration, Lewis Research Center, by the Lockheed-Georgia Company in accordance with the requirements of NASA Contract NAS 3-7987.

TABLE OF CONTENTS

SECTION		PAGE
	FOREWORD	iii
	TABLE OF CONTENTS	v
	LIST OF TABLES	vii
	LIST OF FIGURES	ix
	LIST OF SYMBOLS	xi
1	SUMMARY	1
2	INTRODUCTION	3
3	TEST MATERIALS AND SPECIMENS	7
3.1	Material Selection	7
3.2	Specimen Design and Fabrication	18
4	TEST PROCEDURES	21
4.1	Test Equipment	21
4.2	Test Methods	34
5	TEST RESULTS	61
5.1	Test Values	61
5.2	Validity of Test Values	68
6	ANALYSIS OF TEST RESULTS	83
6.1	Aluminum Alloys	83
6.2	Titanium Alloys	96
6.3	Nickel Alloys	99
6.4	Ferrous Alloys	102
7	QUALITATIVE INTERPRETATION OF CERTAIN TEST RESULTS	115
7.1	Background	115
7.2	Interpretation	119
8	EVALUATION OF TEST RESULTS AS DESIGN CRITERIA	121
9	CONCLUSIONS AND RECOMMENDATIONS	123
9.1	Conclusions	123
9.2	Recommendations Regarding Use of Test Results as Design Criteria	129
9.3	Recommendations For Fundamentally Oriented Tests	131
10	REFERENCES	133
Appendix A	Material Pedigree Data	A-1
Appendix B	Test Results	B-1
Appendix C	Photomicrographs of Specimens	C-1
Appendix D	Stress-Strain Diagrams	D-1
Appendix E	Distribution	E-1

LIST OF TABLES

TABLE		PAGE
1	Materials Tested In The Screening Program	4
2	Specimen Temperature Distribution At 30°R (Nominal)	43
3	Foils Used For Spectral Measurements Of Fast Neutron Flux In HB-2	45
4	Summary of Test Results, Aluminum Alloys	63
5	Summary of Test Results, Titanium And Nickel Alloys	65
6	Summary of Test Results, Ferrous Alloys	67
Appendix A		
TABLES A 1 THROUGH A 3	Material Pedigree Data	A-2 A-7
Appendix B		
TABLES B 1 THROUGH B 33	Test Results	B-2 B-67
B 34	Approximate Modulus Values For 33 Alloys	B-68

LIST OF FIGURES

FIGURE		PAGE
1	Notched and Unnotched Miniature Tensile Specimens	19
2	System Layout	22
3	Tensile Test Loop, Drawing	24
4	Tensile Test Loop, Photograph	25
5	Schematic Diagram of Refrigeration System	27
6	Refrigeration System	28
7	Hot Cave - Overall View	30
8	Transfer Tables	33
9	Cask, Bridge and Airlock	35
10	Extensometer	36
11	Calibration Curves For Copper-Constantan Thermocouples	40
12	Typical Wire Test Data	41
13	Upper and Lower Limit Spectral Curves of Fast Flux In HB-2	46
14	Fast Neutron Flux in Test Location Vs. Control Rod Position	48
15	$\phi > E/\phi > 0.5$ Mev As A Function of Neutron Energy	50
16	Load-Elongation And Load-Time Curves From Tensile Test Showing Well Defined Modulus Slope and Well Defined Zero (A) After Specimen Fracture	53
17	Curves Showing Effects Of Ice Formation On Actuator Rod Yielding Invalid Test Results	54
18	Load-Elongation Curve Without Load-Time Extension	55
19	Load-Time Curves From Tensile Notch Tests Showing Ductile (A) And Non-Ductile (B) Behavior Under Triaxial Loading	56

LIST OF FIGURES (Cont'd)

FIGURE		PAGE
20	Load-Elongation And Load-Time Curves From Three Test Conditions For 17-7PH Stainless Steel	57
21	Changes In Certain Functions For Aluminum Alloys Due To Cryogenic and Irradiation Environment	62
22	Changes In Certain Functions For Titanium And Nickel Alloys Due to Cryogenic And Irradiation Environment	64
23	Changes In Certain Functions For Ferrous Alloys Due To Cryogenic And Irradiation Environment	66
24	Test Value Ratios For Aluminum Alloys	69
25	Test Value Ratios For Titanium And Nickel Alloys	70
26	Test Value Ratios For Ferrous Alloys	71
27	X-Ray Diffraction Patterns From Aluminum 1099	88
28	Elastic And Early Plastic Portion Of Typical Stress-Strain Curves - Type 304 Stainless Steel	106
29	Stress-Strain Curves For AISI Type 440C Stainless Steel	113
30	Tensile Yield Strength To Weight Ratios For 33 Alloys At Various Test Conditions In Order Of Decreasing Value In-Pile At 30°R	122

Appendix C

FIGURES C 1		C-4
THROUGH C 33	Photomicrographs of Test Specimen	C-69

Appendix D

FIGURES D 1		D-2
THROUGH D 5	Typical Stress-Strain Diagrams	D-6

LIST OF SYMBOLS

°R	Degrees Rankine
nvt (n/cm^2)	Time Integrated Flux in Neutrons Per Square Centimeter
E	Neutron Energy (Mev)
Mev	Million Electron Volts
ϕ ($n/cm^2 sec.$)	Fast Neutron Flux
F_{tu}	Ultimate Tensile Strength
F_{ty}	Tensile Yield Strength (0.2% Offset)
F_{tun}	Notched Ultimate Tensile Strength
ksi	Thousands of Pounds (kips) per Square Inch
k_t	Theoretical Stress Concentration Factor
ELI	Extra Low Interstitial Content
Std. I	Standard Interstitial Content
BHN	Brinell Hardness Number
P.M.	Permanent Mold Casting
R_c	Rockwell "C" Scale Hardness
LVDT	Linear Variable Differential Transformer
RT	Room Temperature (Out-Of-Pile)
OP	Out-Of-Pile
IP	In-Pile
Bias	Difference Between Two Arithmetic Means
Bias Range	Interval In Which Values of Bias Would Fall In 90% Of Similar Tests
d	Density in lb/in^3
bcc	Body Centered Cubic
fcc	Face Centered Cubic
hcp	Hexagonal, Close Packed

1 SUMMARY

This is a summary report on a test program to determine the effects of a combined nuclear-cryogenic environment on the tensile properties of thirty-three (33) structural alloys.

The tensile testing was performed under three conditions; at room temperature without irradiation, at 30°R without irradiation, at 30°R in a high flux zone of a nuclear reactor after 1×10^{17} nvt ($E > 0.5$ Mev) at the same temperature. The irradiation times varied from 11 to 17 hours.

Special remote handling and test equipment was designed and fabricated and installed at the HB-2 location of the NASA Plum Brook Reactor Facility to allow remote manipulation and testing under 20 feet of shielding water. Specimen temperature control was provided by a 1150 watt refrigeration system using gaseous helium as the cryogenic fluid.

The materials tested included thirteen (13) aluminum alloys; six (6) different titanium alloys or alloy conditions; four (4) nickel alloys and ten (10) different iron alloys or alloy conditions. The properties that were measured were the yield strength, the ultimate strength, the elongation, the reduction of area and, in some materials, the notched ultimate strength.

Aluminum 1099 (-H14) showed a previously unreported reduction in tensile yield strength at 30°R unirradiated which was fully recovered with irradiation. The heat treatable high-copper aluminum alloys and the aluminum-magnesium silicon alloy 6061 show a consistent reduction of ultimate strength due to irradiation at 30°R. The high-magnesium-low-zinc aluminum alloys gave no indication of serious deterioration of mechanical properties due to irradiation.

The titanium alloys tested exhibited similar cryogenic and irradiation effects. They showed generally increased strength due to the cryogenic environment and, with the exception of the 5% Al-2 1/2% Sn, with extra low interstitial content, also showed generally increased strengths due to irradiation at 30°R.

The nickel alloys, René 41 and Inconel X show significant decreases in notch strength due to irradiation, while K-Monel shows an increase in yield strength and Inconel shows an increase in notch strength due to irradiation at 30°R.

The cryogenic and nuclear cryogenic effects in the austenitic stainless steels appear to be a function of the austenitic stability.

ASTM A 353 appears to be the only non-austenitic steel tested to show improved characteristics due to both cryogenic and nuclear cryogenic environments.

2 INTRODUCTION

The combination of a fast neutron and cryogenic environment encountered in the structural members of a liquid hydrogen nuclear rocket imposes service conditions dissimilar to those encountered in other engineering applications. Both fast neutron bombardment and extremely low temperatures affect the mechanical properties of engineering materials; therefore the magnitude of the combined effect must be determined to provide basic design information before materials for a reliable nuclear rocket system can be selected. Since the neutron irradiation effects are self-healing through spontaneous annealing even at low temperatures, tests to provide the desired information concerning the combined effect must be conducted with the specimens held at the temperature of interest during the entire irradiation and testing period.

A screening program, authorized by Contract NASw-114 between the National Aeronautics and Space Administration and the Lockheed-Georgia Company, was undertaken to assess the effect of fast neutron irradiation on selected engineering alloys at temperatures near the boiling point of liquid hydrogen (-423°F). The thirty-three (33) materials selected for the screening program, including thirteen (13) aluminum alloys, six (6) different conditions of titanium alloys, four (4) nickel alloys and ten (10) different ferrous alloy conditions, are shown in Table 1.

The principal objective of the screening program was to determine which of the several alloys were least susceptible to deterioration of mechanical properties in a combined nuclear-cryogenic environment. An additional, although secondary, objective was to investigate the possibility of formulating theoretical models of the nature of low-temperature irradiation effects to allow prediction of their magnitude in other materials.

Test results from the screening program are reported herein and consist of tensile tests on parallel samples of unnotched specimens (3 to 5 specimens per sample) for each alloy at room temperature unirradiated; at 30°R (-430°F) unirradiated; and at 30°R irradiated to 1×10^{17} nvt (energies greater than 0.5 Mev). Notched specimen data were also obtained for each alloy tested at room temperature unirradiated; at 30°R unirradiated; and several alloys at 30°R irradiated to 1×10^{17} nvt ($E > 0.5$ Mev).

All testing was performed at the NASA Plum Brook Reactor Facility using testing equipment specially designed and built by the Lockheed-Georgia Company for the program. Temperature control was maintained with an 1150 watt helium refrigerator designed for the project by the A.D. Little Company.

TABLE 1

MATERIALS TESTED IN THE SCREENING PROGRAM

ALUMINUM ALLOYS		TITANIUM AND NICKEL ALLOYS		FERROUS ALLOYS	
Alloy	Temper	Alloy	Temper	Alloy	Temper
1099	H-14	Titanium Alloys		Stainless Steel AISI Type 304	Annealed
2014	T-651	55A	Annealed	Stainless Steel AISI Type 310	Annealed
2024	T-351	5% Al, 2 1/2% Sn, Std.	Annealed	Stainless Steel AISI Type 347	Annealed
2219	T-87	5% Al, 2 1/2% Sn, Eli	Annealed	Stainless Steel Type A-286	AMS 5735
5083	H-321	6% Al - 4% V	Annealed	Stainless Steel Type A-286	AMS 5737
5086	H-32	6% Al - 4% V	Solution Treated and Aged	Austenitic Manganese Steel, Union Carbide T-450	Annealed
5456	H-321	8% Al, 1% Mo, 1% V	Duplex Annealed	Stainless Steel Type AM 350	Water Quenched, Sub-Zero Cooled and Tempered
6061	T-6				
7079	T-6	Nickel Alloys		Stainless Steel 17-7 PH	RH-950
7178	T-651	René 41	Solution Treated	Nickel Alloy Steel, ASTM A-353, Grade B	Normalized
X-250	T-4	K Monel	Annealed and Aged	Stainless Steel AISI Type 440C	Quenched and Drawn to R_c 60
B-750	T-5	Inconel	Cold Drawn		
A-356	T-61	Inconel X	Solution Treated and Aged		

A summary of pedigree data supplied by the manufacturer is included in Appendix A. Complete pedigree data has been previously published in LNP ER-5542, February 1962 and Addendum to ER-5542, September 1963.

All test specimens for each material were made from one special lot of the material with a common melting and fabrication history. The raw material was subjected to a rigorous inspection program including ultra-sonic, X-ray and eddy current techniques to insure uniform quality. A complete pedigree containing full chemical analysis, mechanical properties and metallurgical characteristics was supplied by the vendor with each lot of material. A summary of this pedigree data is given in Appendix A. The complete material history has been published in Pedigree of Metals and Alloys, Lockheed ER-5542 of February 1962 and its Addendum of September 1963.

3 TEST MATERIALS AND SPECIMENS

The materials selected for testing and the design and techniques for fabrication of the test specimens were dependent on many factors and are discussed in the following paragraphs.

3.1 MATERIAL SELECTION

The extent of the screening program was necessarily limited by the need to produce experimental data for use as design criteria for the first generation of nuclear powered extra-terrestial vehicles. Major components located in a high flux radiation environment on such a vehicle include cryogenic fluid pumps, liquid hydrogen storage vessels, shells, nozzles, ducts, bellows and bearings. The diverse nature of such hardware required in a functioning nuclear rocket involves a fairly wide range of material types.

The materials selected for inclusion in the screening program, summarized in Table 1, reflect the opinions of numerous governmental installations and industrial laboratories with design responsibilities in the aerospace field from whom suggestions had been invited. These materials fall into four general material classes: aluminum alloys, titanium alloys, nickel alloys and ferrous alloys.

The literature describing the effects of cryogenic temperatures on materials is extensive and has been ably compiled in the Cryogenic Material Data Handbook,(1) initially by the Bureau of Standards and more recently by the Martin Company under Air Force contract. Likewise, the literature on the effects of nuclear irradiation at normal temperatures is widely disseminated and has been competently indexed by the Radiation Effects Information Center(2) at Battelle Memorial Institute. However, reported test data on the combined effects of nuclear irradiation and low temperatures is fragmentary.

3.1.1 Aluminum Alloys

The aluminum alloys are logically divided according to those which are fabricated in the wrought condition and those which are fabricated in the cast condition.

---

(1) References are listed in Section 10.

3.1.1.1 Wrought Aluminum Alloys

Since the wrought aluminum alloys, being of a face centered cubic lattice, usually exhibit desirable cryogenic behaviour,[3] ten were selected for the screening program. The light weight of the aluminum alloys makes them attractive for aerospace application and the wide range of properties available offers broad design flexibility. The individual alloys tested in the screening program are listed in increasing numerical order of their standard designations, together with the most probable usage in nuclear rocketry.

Aluminum Alloy 1099 - H14

This alloy is an ultra-high purity aluminum. Due to the low strength of 1099 (F_{tu}* $\approx$ 13 ksi at room temperature), applications in a nuclear rocket seem unlikely, but it offers interest in relating observed phenomena to solid state mechanisms in the formulation of irradiation effects models.

Aluminum Alloy 2014 - T 651

This is a high strength ($F_{tu} \approx 70$ ksi at room temperature) aluminum alloy with a history of successful application in welded cryogenic pressure vessels. It was included in the program primarily for consideration as a material for the storage vessels for liquid hydrogen rocket fuel.

Aluminum Alloy 2024 - T 351

This high strength ($F_{tu} \approx 70$ ksi at room temperature) aluminum alloy has been one of the most widely used aluminum alloys in the aircraft industry for many years. It has been extensively studied at room and cryogenic temperatures and has satisfactory cryogenic behaviour for general structural use.

Aluminum Alloy 2219 - T 87

This alloy, another in the same general strength range as 2014 and 2024, is a fairly recently developed 6 percent copper material

* F_{tu} designates Ultimate Tensile Strength

Aluminum Alloy 2219 - T 87 (Continued)

with small additions of titanium, vanadium and zirconium to improve strength at elevated temperatures. This material had not been widely tested at cryogenic temperatures at the time of its selection. However, from both metallographic and chemical considerations, it appeared potentially useful for cryogenic applications. Probable rocket applications are ducts and bellows assemblies.

Aluminum Alloy 5083 - H 321

This moderate strength ($F_{tu} \approx 50$ ksi at room temperature) alloy has shown unusual tear strength at cryogenic temperatures.[4] It also develops unusually high joint efficiencies in weldments in the as-welded condition.[4] Possible rocket applications include liquid hydrogen fuel tanks and internal pump parts.

Aluminum Alloy 5086 - H 32

This moderate strength ($F_{tu} \approx 45$ ksi at room temperature) alloy has been extensively used in missile applications and might be used in rockets for general structural applications.

Aluminum Alloy 5456 - H 321

An intermediate alloy ($F_{tu} \approx 55$ ksi at room temperature), 5456-H 321 would have similar applications in rocketry as 5083 - H 321.

Aluminum Alloy 6061 - T 6

This moderate strength alloy ($F_{tu} \approx 45$ ksi at room temperature) which develops its hardness through aging rather than work hardening was included to study possible differences in nuclear-cryogenic effects on the two mechanisms. This material also was included specifically for evaluation for liquid hydrogen storage tank applications.

Aluminum Alloy 7079 - T 6

This high strength ($F_{tu} \approx 90$ ksi at room temperature) alloy was included as a potential alloy for general structural rocket applications due to the high strength-weight ratio of the material.

Aluminum Alloy 7178 - T 651

This high strength ($F_{tu} \approx 90$ ksi at room temperature) alloy was included for reasons similar to those for including 7079-T 6. Although a reported notch sensitivity at cryogenic temperatures [5] makes the use of this alloy for liquid hydrogen environments unlikely, the high strength-weight ratio makes applications for other structural members a possibility.

3.1.1.2 Aluminum Casting Alloys

Three aluminum casting alloys were included in the testing program for evaluation as possible materials for use in applications such as cryogenic pump housings in a nuclear radiation environment.

Aluminum Alloy X 250 - T 4

Aluminum Alloy X 250 is an experimental material developed by the Aluminum Company of America. This material contains a nominal 1.5 percent zinc and 8 percent magnesium. It is a heat treatable alloy and, in the T4 condition, develops a F_{tu} of $\approx$ 60 ksi with a hardness of $\approx$90 Brinell (500 Kg load). The Aluminum X 250 alloy test slugs were sand cast.

Aluminum Alloy A 356 - T 6

Aluminum Alloy A 356 is a 7 percent silicon (nominal) alloy with a trace addition of magnesium which responds to thermal hardening treatment. In the T 6 condition, this material has a F_{tu} of $\approx$42 ksi and a Brinell hardness (500 Kg load) of about 80. The test slugs of A 356 were 0.5 inch diameter permanent mold castings.

Aluminum Alloy B 750 - T 5

This alloy, another heat treatable casting alloy, has a nominal alloying element content of 2 percent copper, 0.75 percent magnesium and 1.25 percent nickel. In the T 5 condition, it has a F_{tu} of $\approx$30 ksi with a hardness of $\approx$65 BHN (500 Kg load). The B 750 test slugs were cast in a 0.5 inch diameter permanent mold.

3.1.2 Titanium Alloys

The titanium alloys of primary alpha structure usually exhibit good cryogenic properties due to the hexagonal close-packed lattice of this phase. The alpha-beta alloys can be expected to show a reduction of ductility parameters due to the body centered cubic structure of the beta phase; however, all of titanium alloys except the beta-stable types have useful cryogenic properties. The titanium alloys have several characteristics which make them of interest to nuclear rocket designers: a strength-weight ratio comparable with that of the aluminum alloys, an increase in the modulus of rigidity of $\approx$50 percent, and a higher allowable working temperature for rocket parts which, although initially at cryogenic temperatures, see elevated temperatures during rocket firing. Four basic titanium alloys were included in the screening program with two being tested in different conditions.

Titanium Alloy 55A, Annealed

This alloy is essentially commercially pure elemental titanium. In the annealed condition, it is a moderate strength material ($F_{tu}\approx$70 ksi at room temperature) with good forming properties. Alloy 55A was included in this program to serve a dual purpose: to allow evaluation of this material for nuclear rocket applications and to provide a relatively pure metal for comparison with test results of alloyed titanium alloys for evaluation of the effects of "foreign" atoms on the nuclear-cryogenic behavior of titanium alloys.

Titanium Alloy, 5% Al, 2 1/2% Sn, Annealed

Titanium 5% Al, 2 1/2% Sn is a fairly high strength alpha phase alloy ($F_{tu}\approx$120 ksi at room temperature). Samples from two separate

lots were included in this program: one manufactured using the vacuum melting of consumable electrode techniques standard in the titanium industry and the other manufactured with extra precautions during melting and rolling to limit the total interstitial content to less than 0.125 percent. This was done to allow the evaluation of the effects of interstitial contents on the irradiation induced changes in material properties. Since this alloy is now commercially available in the extra low interstitial grade (designated as ELI) it is practicable for designers to specify it as such. Probable use in nuclear rockets would be for shells, pressure vessels and pump parts.

Titanium Alloy 6% Al, 4% V

This alpha-beta alloy was also tested in two conditions; annealed and in the solution treated and aged condition. The presence of the metastable beta phase in the annealed material, largely retransformed into alpha during aging in the other material, will permit an estimation of the effect of a second crystallographic phase of both cryogenic and irradiation behaviour in titanium alloys. This higher strength titanium alloy ($F_{tu} \approx 170$ ksi aged, ≈ 140 ksi annealed, at room temperature) should be suitable for shells and pressure vessels if the presence of the body centered cubic beta phase does not show a deleterious effect on cryogenic or irradiated properties.

Titanium Alloy 8% Al, 1% Mo, 1% V, Duplex Annealed

This alloy is stable alpha at room temperature, but in industrial practice, it is rolled in the elevated temperature beta phase. After rolling, it is double annealed to ensure complete transformation of the beta to the alpha phase. After annealing it develops a F_{tu} of ≈ 140 ksi at room temperature. Although not extensively tested at cryogenic temperatures, the complete transformation to the hexagonal close-packed lattice should provide good low temperature properties. This alloy would probably be considered for duct and bellows applications as well as pump and pressure vessel parts.

3.1.3 Nickel Alloys

Many high nickel alloys were developed for use at elevated temperatures; however, many also have useful cryogenic properties.[1] Some components such as nozzles and turbine parts are precooled by low temperature gaseous hydrogen prior to experiencing elevated temperatures during the rocket blast. Combination cryogenic and heat resistant alloys, such as the nickel alloys and the austenitic stainless steels, are obvious candidates for such applications. Additionally, nuclear-cryogenic properties of certain nickel alloys may prove useful for such applications as internal pump parts, tank and shell components and general structural members. Four nickel alloys were selected for testing in the screening program.

René 41, Solution Treated

This alloy was tested in the solution treated rather than in the aged condition to reduce the loss of ductility at cryogenic temperatures reported in the NBS Cryogenic Materials Data Handbook[6] for this material in the aged condition. This material in this condition has desirable mechanical properties ($F_{tu} \approx 140$ ksi at temperature from room temperature to 1400°F) over an extreme temperature range and its probable use in nuclear rocketry would be for components, such as the nozzle, which must withstand both cryogenic and elevated temperature environments.

K Monel, Cold Drawn, Annealed and Aged

This copper-nickel alloy has excellent formability and can easily be fabricated into complex shapes. It is a fairly high strength ($F_{tu} \approx 150$ ksi at room temperature) material in the aged condition and probably would be used for such components as fuel vessels and structural members in nuclear rockets.

Inconel 600, Cold Drawn

This is a moderate strength alloy ($F_{tu} \approx 135$ ksi at room temperature) with reported high notch toughness at cryogenic temperatures.[6]

Inconel 600, Cold Drawn (Continued)

Probable applications in nuclear rocketry would include components in the cryogenic zone which might be subjected to impact loading.

Inconel X 750, Solution Treated and Precipitation Hardened

This alloy is a higher strength ($F_{tu} \approx 190$ ksi at room temperature) material than the other nickel alloys included in the screening program. Likely applications would include pump parts as well as pressure vessel hardware. Inclusion of Inconel X 750 in the aged condition in the screening program allows, through comparison with the test results for cold drawn Inconel 600, an evaluation of the effect of neutron irradiation on the finely dispersed precipitates which form the strengthening agent in Inconel X 750.

3.1.4 Ferrous Alloys

The ferrous alloys tested are logically divided into two groups: those which are austenitic steels and those which are not.

3.1.4.1 Austenitic Steels

The face centered cubic crystal lattice of the gamma phase of iron, characteristic of the austenitic alloys, is not subject to the low temperature nil-ductility transformation frequently encountered in materials with a face centered cubic lattice. For this reason, the austenitic steels, particularly the chromium-nickel grades, have been widely used in cryogenic applications. In general, austenites have fairly low F_{ty}*/F_{tu} ratios which lead to ease of formability. Although austenite is not entirely stable at extremely low temperatures,[7] the austenitic alloys have generally been reported to retain a fair degree of ductility at low temperatures.[1]

AISI Type 304 Stainless Steel, Annealed

This material, an 18-8 type chrome-nickel stainless steel, is perhaps the most widely used structural stainless steel. It has been

---

* F_{ty} designates Tensile Yield Strength (0.2% offset).

AISI Type 304 Stainless Steel, Annealed (Continued)

extensively tested separately in cryogenic and normal temperature nuclear environments. AISI Type 304 ($F_{tu} \approx 90$ ksi at room temperature) would probably find applications as fuel vessel hardware, internal pump parts and as a general structural material.

AISI Type 310 Stainless Steel, Annealed

This material, a 25-20 chrome-nickel type, is similar to 304 ($F_{tu} \approx 90$ ksi at room temperature) in use except that it contains a higher nickel content to increase dimensional stability during thermal cycling and to increase austenite stability. The increased chromium content reduces the susceptability to stress corrosion cracking and generally enhances the corrosion resistance in oxidizing atmospheres.

AISI Type 347 Stainless Steel, Annealed

This is also an 18-8 chrome nickel type stainless steel ($F_{tu} \approx 90$ ksi at room temperature) distinguished from AISI Type 304 principally by the addition of columbium (niobium) as a carbide stabilizing agent to prevent the development of a susceptability to intergrannular corrosion when heated to a 900°F - 1100°F sensitizing temperature range. Its most common application is for welded structures unsuited to post-welding heat treatment to prevent sensitization by the welding heat.

A-286 Stainless Steel, Precipitation Heat Treated

This precipitation hardening super alloy is commonly used in two different heat treated conditions, annealed at 1800°F prior to aging and annealed at 1650°F prior to aging. The materials and heat treatments conform to AMS Specifications 5735D and 5737B respectively. This material in both treatments retains high strength ($F_{tu} \approx 160$ ksi at room temperature) up to 1300°F, although the lower annealing temperature generally provides better creep properties at temperatures over 1000°F. Published data from tests of A-286 at cryogenic temperatures indicate desirable ductility properties at low temperatures.(1)

A-286 Stainless Steel, Precipitation Heat Treated (Continued)

Probable applications for this material include components, such as nozzles, which must withstand an extreme variation of temperature during rocket operation.

T-450 Steel, Annealed

This material, an experimental alloy developed by the Union Carbide Corporation for cryogenic applications, uses manganese (nominal 19 percent) as an austenizing agent with minor additions of nickel, copper, chromium and nitrogen to increase low temperature austenitic stability. The substitution of manganese for nickel to produce the desired face centered cubic austenitic structure allows the development of low temperature ductility with a more economical alloy composition. Although no irradiation studies are known to have been made on this alloy, cryogenic tests run by Union Carbide [8] indicate only a 9 percent martensitic transformation of T-450 during deformation to fracture at liquid hydrogen temperature.

3.1.4.2 Non-Austenitic Steels

The face centered cubic austenitic lattice is generally preferable to a body centered cubic lattice for cryogenic applications [3] due to the absence of a low temperature nil-ductility transformation. For some components, such as bearings, the greater hardness available in the semi-austenitic or martensitic steels is necessary; therefore, three steels of this type were included in the test program. One ferritic low temperature pressure vessel steel was also included.

Type AM-350, SCT

This alloy, a proprietary stainless steel of the Allegheny Ludlum Steel Corporation, can be heat treated to $\approx$ 200 ksi F_{tu} at room temperature. The treatment consists of austenizing at 1750°F, and quenching in water, followed by holding at -100°F for a sufficient period to allow

Type AM-350, SCT (Continued)

complete martensitic transformation. The martensite is then tempered at 850°F. The resultant structure is somewhat susceptable to cryogenic embrittlement. Rocket design considerations indicate the desirability of testing some high strength materials for applications where the loading pattern is such that embrittlement is not a serious drawback and a high yield strength is a basic requirement.

Type 17-7 PH, RH - 950

17-7 PH is a proprietary high strength stainless steel, developed by Armco Steel Corporation. It also can be heat treated to a F_{tu} of 200 ksi by aging at 950°F after solution treatment. Published data indicate a nil-ductility transition at well above liquid nitrogen temperatures for this alloy,[1] but the requirement for high strength structural materials, as in the case of AM-350, indicated the desirability of including 17-7 PH in the screening program.

ASTM A 353 - 58, Grade B, Normalized

This steel is a fire box quality pressure vessel steel suitable for the construction of unfired pressure vessels built in accordance with Section VII of the ASME Boiler and Pressure Vessel Code. It is a low carbon steel ($F_{tu} \approx 100$ ksi at room temperature) with a nominal nine percent nickel to improve its cryogenic properties. The common use for this material is in welded pressure vessels.

AISI Type 440C Stainless Steel, Quenched and Drawn to Rockwell "C" 60

This martensitic stainless steel is known to develop cryogenic embrittlement[1] but was included in the test program as a high hardness material for possible bearing applications. This material can be heat treated to an approximate F_{tu} of 285 ksi.

3.2 SPECIMEN DESIGN AND FABRICATION

Standard tensile test specimens, ASTM E-8[9] could not be used in the screening program for these reasons:

- All testing was performed at the NASA Plum Brook Reactor Facility using testing equipment specially designed for operation in a horizontal beam hole (HB-2) facility of the Plum Brook Reactor with temperature control maintained with an 1150 watt helium refrigerator. For tests in the radiation environment, it was necessary to maintain a test specimen temperature of 30°R in a high flux zone of a reactor radiation spectrum. The reactor radiation spectrum, even with the maximum practicable shielding of the test zone, contained an appreciable gamma component. Since gamma radiation induces internal heating of materials at a rate proportional to mass, the entire weight of the test specimen and test equipment in the cryogenic zone was limited to keep the required refrigeration capacity within realistic limits.

- With the required gamma attenuation shield installed in the Plum Brook Reactor beam port HB-2, the internal diameter of this access hole was reduced to 6 inches. This limited the physical size of the test loop envelope containing the test equipment and refrigeration transfer lines to 6 in. in diameter.

The miniature tensile and tensile notch specimens which satisfy the above requirements are illustrated in Figure 1. The test specimens had threaded ends to allow installation in the specimen holders with the minimum increase in mass in that section.

3.2.1 Tensile Test Specimen

The nominal diameter of the mid-point in the gage length was 0.125 inch. The gage length was nominally 0.5 inch to maintain the 4:1 gage length to gage diameter established in ASTM E-8.[9] The limits of the gage length are delineated by light sand-

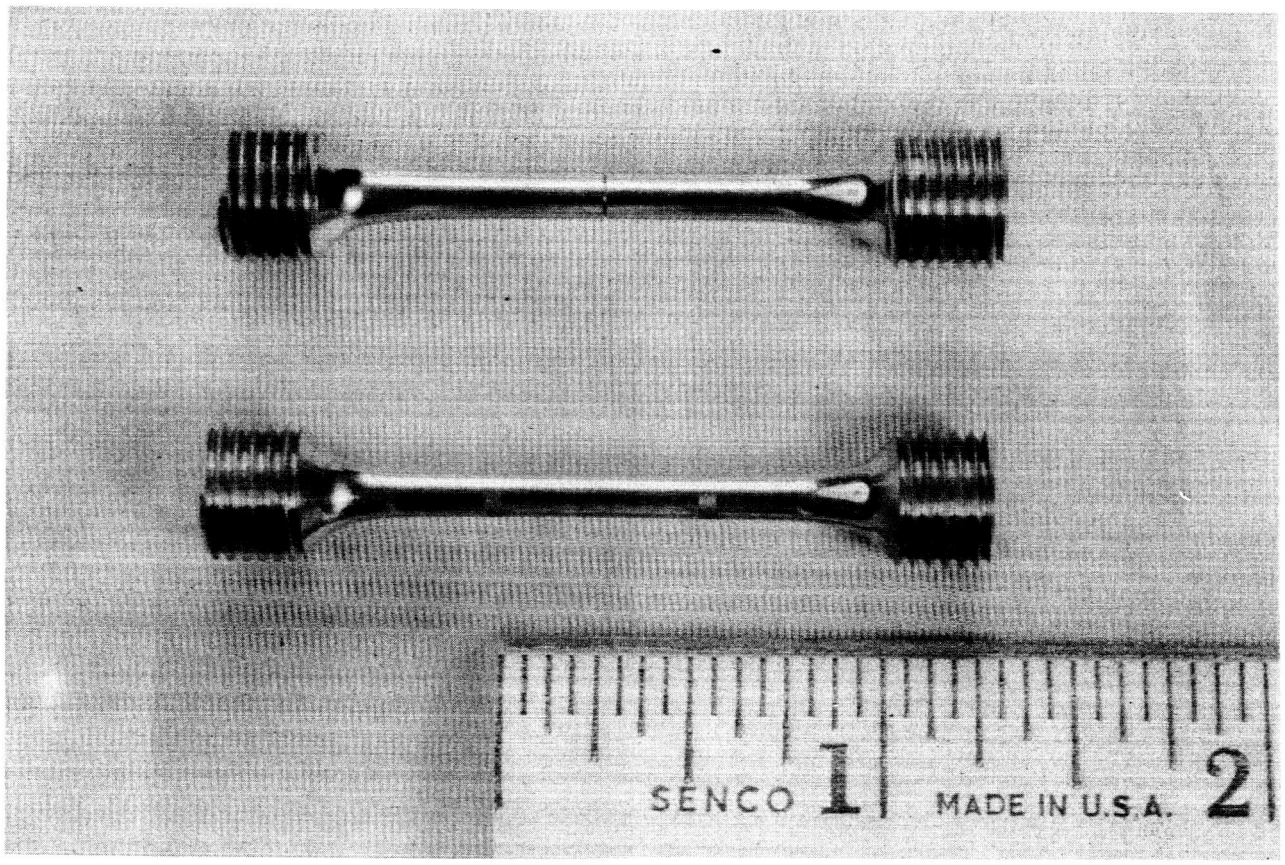

FIGURE 1 NOTCHED AND UNNOTCHED MINIATURE TENSILE SPECIMENS

blasting of gage marks over an area 0.0625 inch by 0.125 inch at each end of the gage length. This method of marking was used to avoid introducing a notch at each end of the gage length.

The raw material from which the specimens were fabricated was thoroughly inspected using both visual and non-destructive testing techniques to ensure uniform material quality of the completed specimens. After final polishing, the finished specimens in each alloy group were checked against each other using Eddy current techniques to assure the homogeniety of each sample lot of test specimens. During all machining operations unusual precautions were taken to meet the specially strict dimensional tolerances required due to the small size of the test specimens. After machining, each specimen was polished in a longitudinal direction to remove any tool marks or scratches formed during machining. After completion, all significant dimensions were recorded for each specimen using an optical comparator to measure the dimensions.

3.2.2 Tensile Notch Specimens

Notched tensile specimens were fabricated to allow the determination of any cryogenic or irradiation induced notch sensitivity in the test materials. These notched specimens were regular tensile specimens, manufactured as described above, with the addition of a mid-point notch with a nominal root diameter of 0.105 inch and a nominal notch radius of 0.0007 inch. This gives a nominal theoretical notch stress concentration (k_t) of 6.4. On the notched specimens the gage marks were, naturally, omitted. The major and root diameters and the notch radius were measured on an optical comparator for each specimen. The k_t value was determined for each specimen using the method of Peterson.[10] Precautions during machining and inspection were similar to those for the unnotched specimens.

At the time these specimens were designed there had been little effort in standardizing notched specimen design and recent efforts[11] in this area indicate that these specimens are not optimized with respect to sensitivity to embrittling effects.

4 TEST PROCEDURES

The program objective, performing tensile tests in-pile and out-of-pile at 30°R and out-of-pile at room temperature, required the development of specialized testing and handling equipment described in Section 4.1. A general layout of this equipment is shown in Figure 2.

The methods and procedures for standardizing, calibrating and operating this equipment are described in Section 4.2.

4.1 TEST EQUIPMENT

The irradiated specimens tested during this materials screening program required 11 to 17 hour exposures in the NASA Plum Brook 60 MW (th) nuclear reactor with the specimen temperature maintained at 30°R. The irradiations were conducted in a test location adjacent to the beryllium reflector on the north face of the reactor core. Access to this zone is through a 9 inch ID horizontal beam port (HB-2) located approximately 20 feet below the surface of a pool of demineralized water which provides biological shielding during reactor operations. The beam port, which penetrates a high density concrete biological shield two feet thick, the stainless steel clad pressure vessel and thermal shield, is approximately six and one-half feet in length from its external flange to the high flux test zone. However, the full ID of HB-2 was not available as a test zone since a gamma shield, required to permit specimen temperature control at 30°R with refrigeration capacity attainable at reasonable cost within the current state-of-the-art, limited the internal diameter of the beam port to 6 inches.

The operation of the test equipment can be readily followed by reference to Figure 2 . In a typical testing sequence, a test loop was inserted into the hot cave for specimen installation. After completion of loop reassembly following specimen placement, the loop was withdrawn from the hot cave to the north table in Quadrant D. Refrigerant flow was started and the table holding the loop was rotated 180°. The loop was then transferred to the south table and positioned in line with HB-2 and, after stabilization of specimen temperature at 30°R, inserted into HB-2. The loop was held at this position with the specimen maintained at 30°R until the accumulated fast neutron dose of 1×10^{17} nvt ($E > 0.5$ Mev) was attained. At this time, an axial tensile load was applied to the specimen and increased until failure occurred. After specimen failure, the loop was returned to the hot cave for specimen replacement.

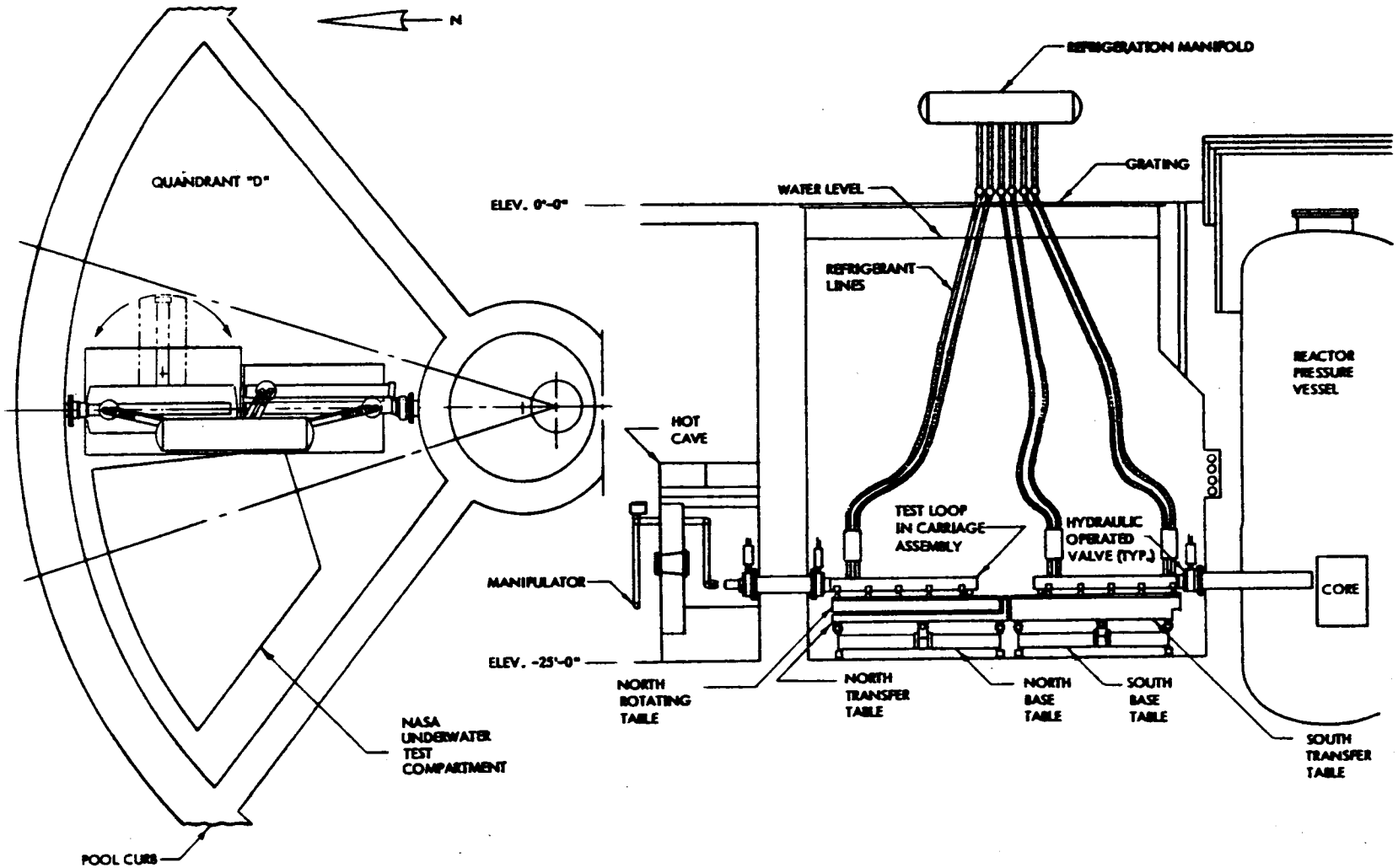

FIGURE 2 SYSTEM LAYOUT

During operation, two test loops were used for alternate insertion in HB-2 providing a maximum utilization of reactor operating time. Thus, most of the activity described above was performed during the irradiation period of a specimen in another loop.

A brief description of the system components follows.

4.1.1 Test Loops

The tensile testing conducted during this program was performed in an especially designed test loop with the following capability requirements:

- Maintain test specimen temperature at 30°R at a point near the core of an operating nuclear reactor, some nine feet forward from the external flange of the access port.
- Apply and monitor an axial load in tension up to 5000 lbs. on a test specimen.
- Monitor elongation of the specimen during testing.
- Be packaged in a 6 inch OD tubular envelope to permit insertion into the reactor beam port, HB-2.
- Permit specimen change and minor maintenance by remote methods.

The design of the test loops, fulfilling the above requirements, is shown in Figures 3 and 4 .

The tensile testing machine was actuated by a hydraulic cylinder using demineralized water as the working fluid to avoid the possible contamination of reactor primary or quadrant water with other fluids. The force was transmitted to the specimen through a push rod guided by two self-aligning graphite bearings. The load cell consisted of a ring type dynamometer equipped with a linear variable differential transformer. The output of the LVDT was a function of the deflection in the ring which, in turn, was a measure of the applied load. (Methods for strain and stress measurements are described in Sections 4.2.1 and 4.2.2.)

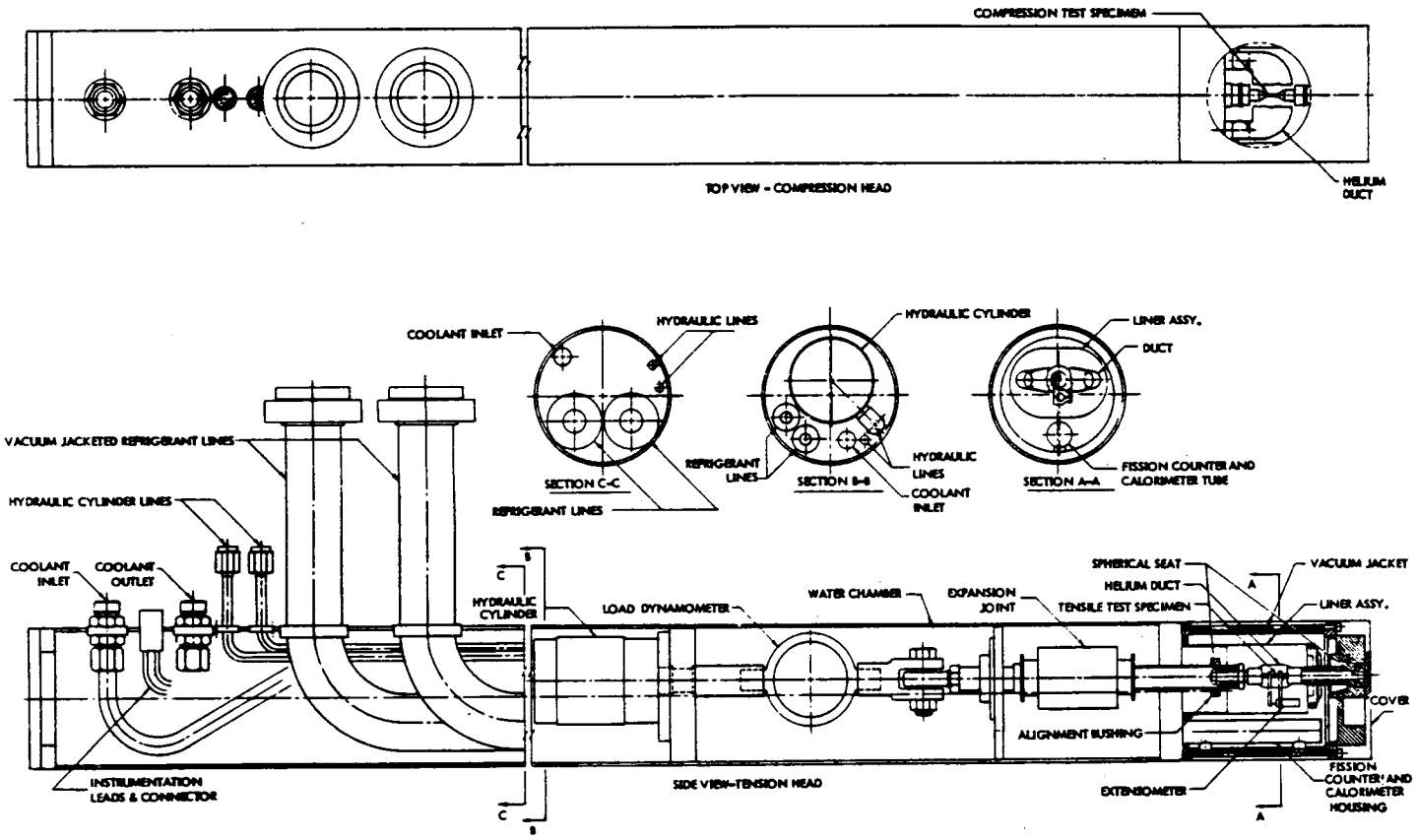

FIGURE 3 TENSILE TEST LOOP

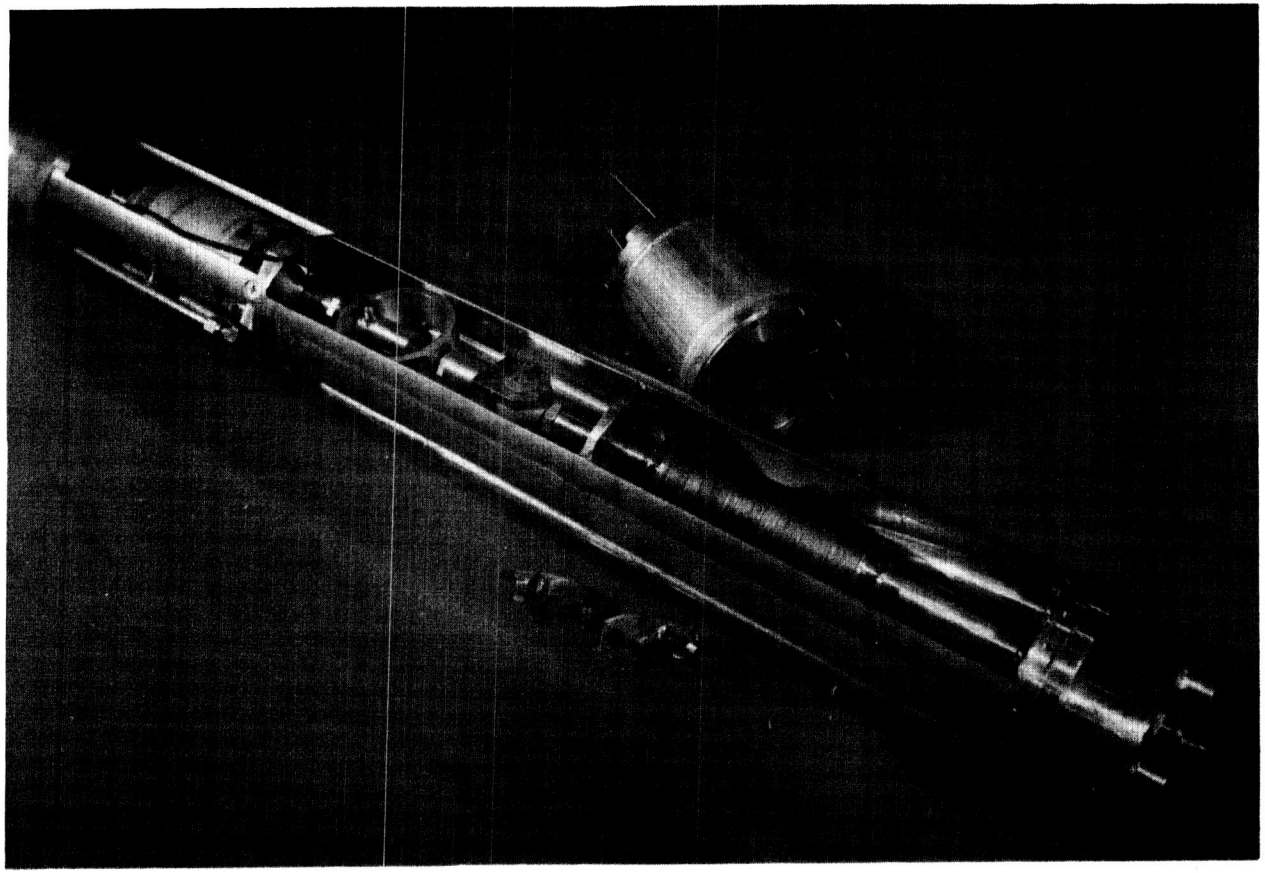

FIGURE 4 TENSILE TEST LOOP

The testing equipment contained in the test loop was calibrated by running parallel tests of specimens of a common sample population in the test loop and in standard universal testing machines verified with a proving ring immediately prior to this calibration.

The forward section, or head, of the test loop was removable to allow specimen change by remote handling methods. Figure 4 shows the forward section of the loop with the head removed.

The holders on both forward and aft ends of the test specimen were fitted with mating spherical seats to insure proper alignment during application of the test load.

Helium guides, shown in the foreground of Figure 4 , directed the refrigerant over the specimen in a flow pattern which assured adequate specimen temperature control. (The method of temperature calibration is described in Section 4.2.3.)

4.1.2 Refrigeration System

Test location temperature control was provided by a closed cycle helium refrigerator with an electrically driven positive displacement compressor, a counter-flow heat exchanger and four reciprocating expansion engines. The refrigeration system was designed and built for this application and was warranted to be capable of maintaining any temperature between 30°R and room temperature in the test location of the test loops. The refrigeration system had a rated capacity of 1150 watts with a manifold temperature of 30°R. A schematic of this system is shown in Figure 5 . A photograph of the portion of the refrigeration system located inside the reactor containment vessel is shown in Figure 6 .

As shown in Figure 5 , low pressure (≈50 psia) helium gas was drawn into the suction side of a two stage positive displacement compressor and compressed to 300 psia. The heat of compression was removed by water cooling after each compression stage. The helium gas at 300 psia and 80°F passed through an extended surface counter flow aluminum heat exchanger capable of a 600 lb/hr flow with a duty rating of 410,000 BTU/hr. With the refrigeration system operating at 30°R, the helium gas left the high pressure side of the heat exchanger at approximately 37°R and 296 psia. The cold gas entered the expansion engines where it was expanded to≈53 psia. These engines are coupled in pairs to crossheads which drive

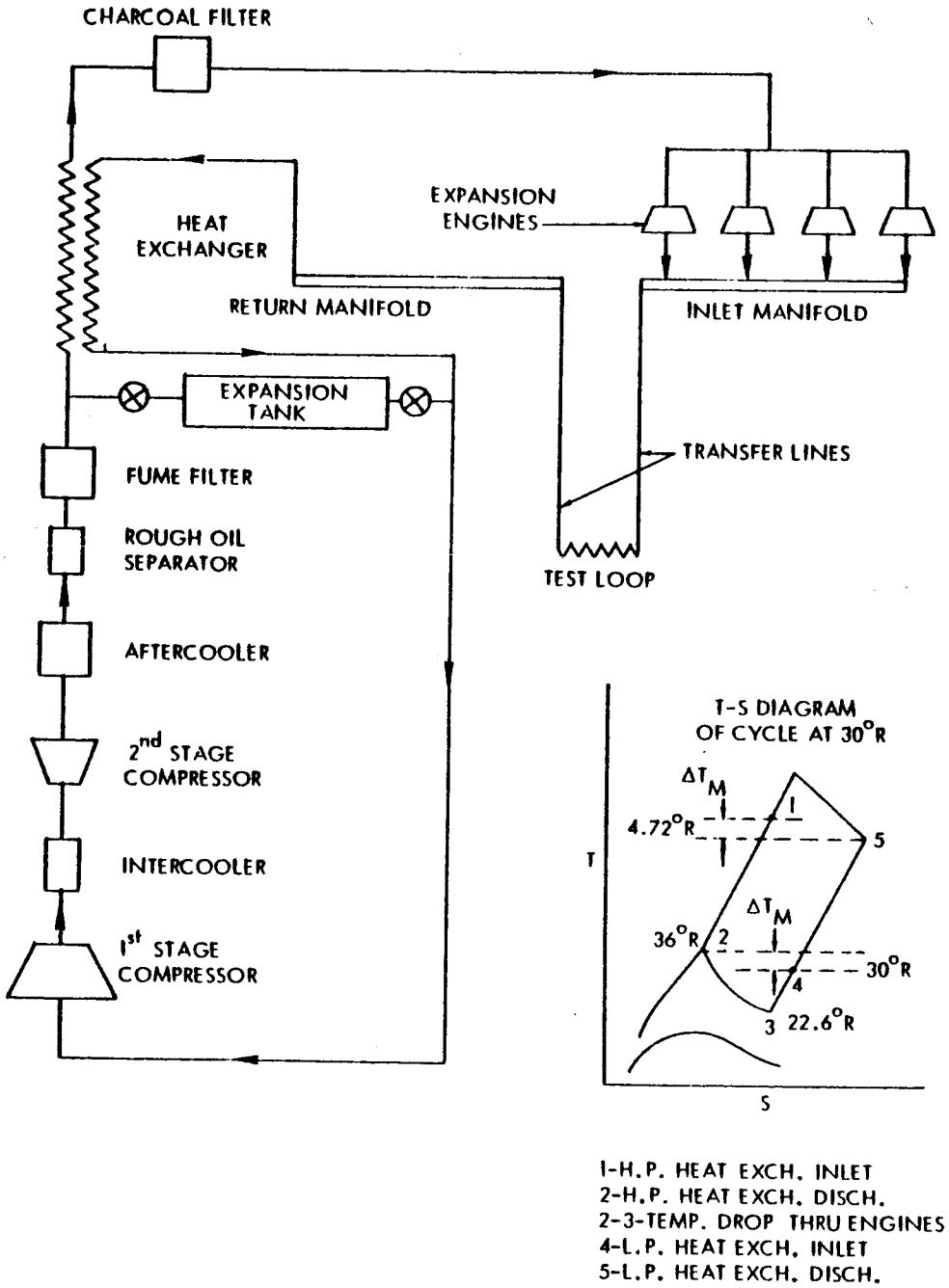

FIGURE 5 SCHEMATIC DIAGRAM OF REFRIGERATION SYSTEM

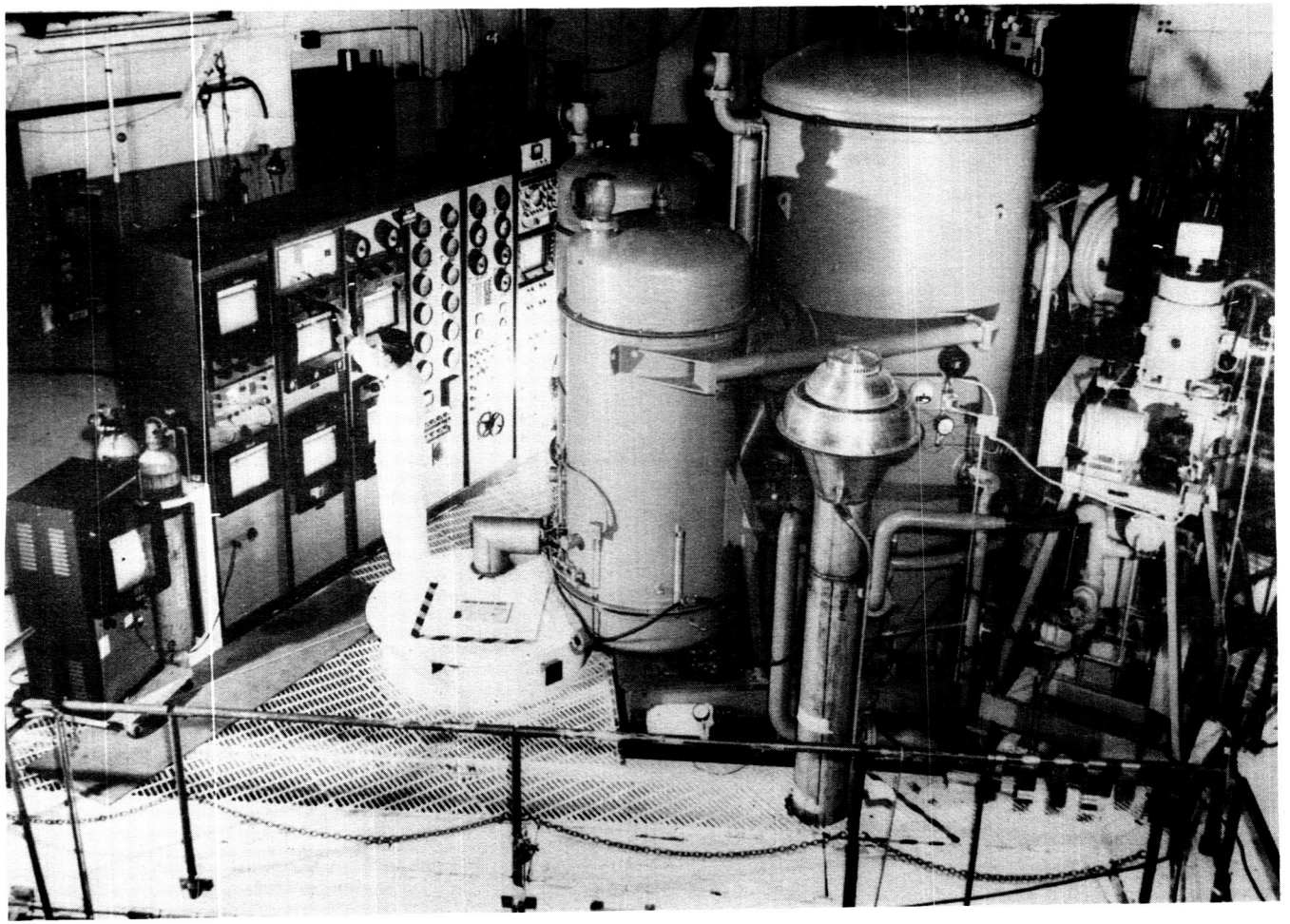

FIGURE 6 REFRIGERATION SYSTEM

oil pumps that absorb work from the system to allow adiabatic gas expansion. The design specifications for the expansion engines are given below:

Mass Flow (Total)	520 lb/hr
Inlet Temperature	37°R
Outlet Temperature	24°R
Piston Displacement	7.93 ft^3/min
Engine Speed	340 RPM

The heat exchanger and each pair of expansion engines were mounted in evacuated shells filled with powdered perlite to provide insulation.

The refrigerated gas leaving the expansion engines was transferred through vacuum insulated flexible lines to the test location in the tensile-compression test loop. After passing through the test chamber, the gas was returned through a manifold to the low pressure side of the heat exchanger and then back to the compressor suction side. A line heater of 2500 watt capacity was located in the inlet manifold and a 100 watt trim heater was located in the manifold at the inlet of each set of transfer lines to allow operation of the system at any temperature between 30°R and room temperature.

4.1.3 Sample Change Equipment

Due to the high activity level of the test loops after several in-pile exposures, remote handling techniques were required for changing specimens or routine loop maintenance. To provide operator shielding during work on the test loops, a hot cave was installed outside the wall of Quadrant D with the access port on a radial line with HB-2. An overall view of the hot cave is given in Figure 7 . The side walls, roof and base of the hot cave were constructed of high density concrete block. The front, or North, face of the hot cave consisted of a layer of lead shot 21 inches thick contained in a steel shield with a computed shielding effectiveness equivalent to 12 inches of solid lead. The front face was fitted with a viewing window consisting of five panes of lead glass with a specific gravity of 6.2, the spaces between which were filled with mineral oil to prevent surface reflection. The hot cave roof contained a removable roof block and plugs to permit insertion of tools and test equipment. This roof block was handled with a jib crane located at the northeast corner of the hot cave, as shown in Figure 7 . The hot cave was equipped with a pair of miniature Model 8, Central Research Laboratory Master Slave Manipulators and specially designed remote handling tools to facilitate test specimen change and minor loop maintenance.

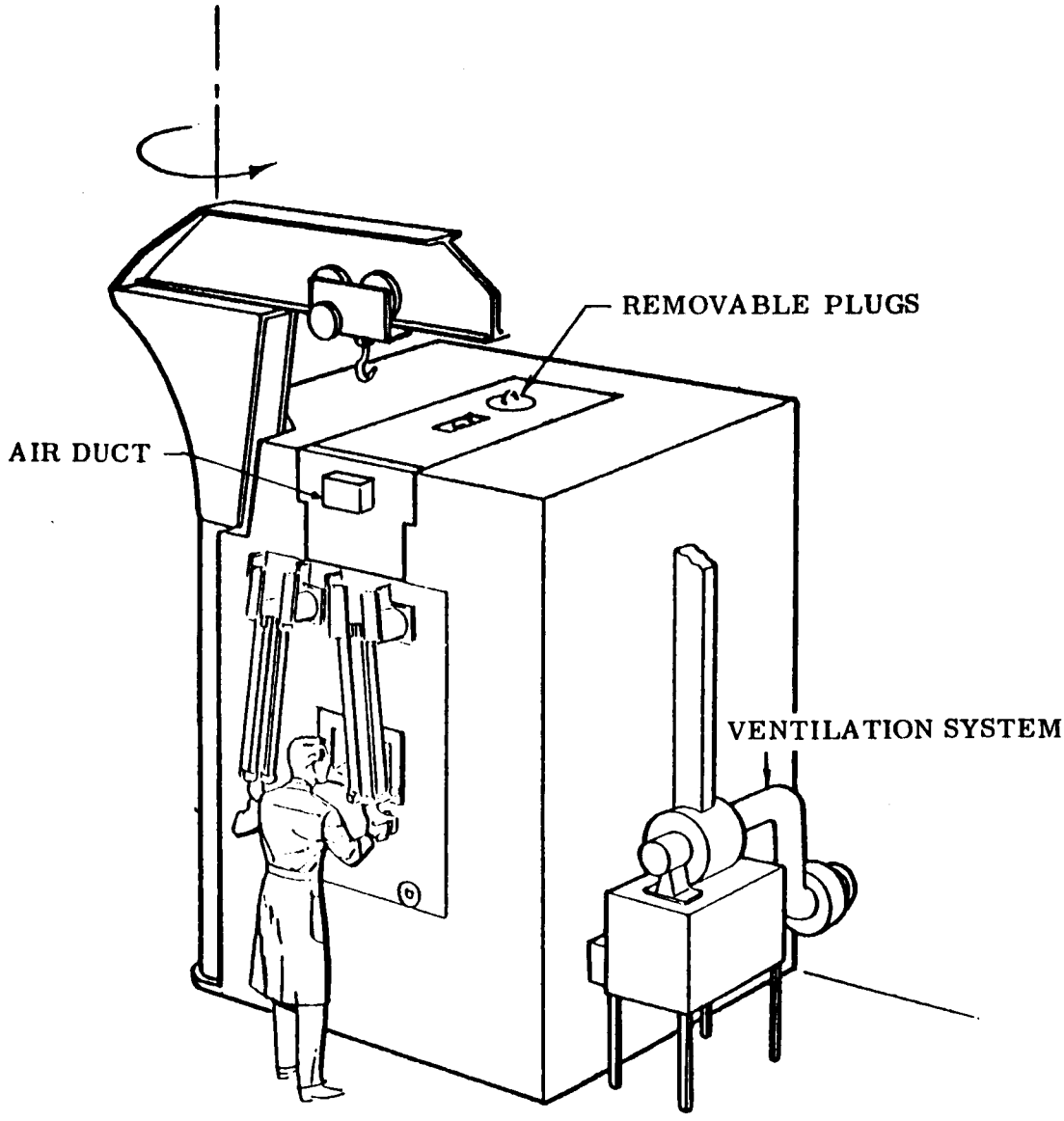

FIGURE 7 HOT CAVE - OVERALL VIEW

During the initial operation, the external surfaces of the hot cave were monitored by the Health Safety Office during each insertion of an irradiated test loop. Since the principal gamma source in an irradiated test loop was Mn^{56}, this practice was discontinued after the loops received sufficient in-pile exposure to saturate the contained manganese. The hot cave effluent gases were monitored at intervals for possible radioactive release through a particulate filter. In no instance during normal hot cave operation was a significant discharge detectable.

4.1.4 Transfer System

To permit insertion and withdrawal of the test loops at the beam port and the hot cave, a special transfer system was installed in Quadrant D of the Plum Brook Reactor Facility. The location of this system with respect to the reactor beam port HB-2 and the specimen change hot cave is shown in Figure 2 . All of the transfer equipment operated under some 20 feet of quadrant water.

The transfer system included two base tables, fastened to the floor of Quadrant D, on which were located translating tables capable of movement in the east-west direction. On each of the translating tables were three sets of tracks on which specially designed carriages traveled to transfer the test loops to the desired location. The lateral east-west translation of the transfer tables permitted the positioning of any track in proper alignment with the beam port or the hot cave port for insertion of the test loop. The north table, associated with the hot cave, had the additional capability of rotation through 180° to enable insertion of the forward end of the test loop into the hot cave. The actuating force for this translation and rotation was provided by a 10HP hydraulic pump, using demineralized water as the working fluid. Mechanical stops were situated at the limits of table travel and movable mechanical stops were located to insure accurate positioning of the tracks for beam port and hot cave insertion of the test loop.

Each of the carriages which held the test loops traveled on grooved wheels on the table tracks and were moved on the tables by a hydraulically operated rack and pinion gear actuated by a hydraulic cylinder which is driven by the 10HP pump. By suitable manipulation, the carriage could be placed on any track of the tables and positioned in front of either the beam port or the hot cave. Limit switches located on the tables were tripped by actuators on the carriages and indicated carriage locations on the tables by means of lights on the control console. Mechanical stops limited carriage travel on the tables.

After a carriage was positioned in front of the beam port or hot cave, it was advanced and coupled to the port. Both the beam port and the hot cave port were protected by 6 inch gate type valves. On the quadrant side of each valve was a chevron seal to prevent water flow past the loop during operation. The valves were interlocked with limit switches to prevent opening unless the test loop was in position in the chevron seal to block flow. After coupling the carriage to either valve, the loop was advanced into the beam port or hot cave by a high torque hydraulic motor driven by the 10HP pump. The torque was translated from the motor shaft to a lead screw through a worm-worm gear connection. This lead screw was coupled to a yoke assembly on the carriage which supported the aft end of the test loop. As the lead screw advanced the test loop, limit switches on the carriage indicated the loop position by lights on the control panel. A mechanical stop precluded the possibility of inserting the loop into HB-2 to a point which would restrict the coolant passage between the forward end of the loop and the gamma shield plug. The test loop drive system, during an insertion into the beam port, had to overcome both the primary coolant pressure of 125 psi and systematic frictions. This required a thrust force of over 4000 pounds. Limit switches and mechanical stops were installed at all places necessary to insure safe operation of the transfer system. A photograph of the system as installed is presented in Figure 8 .

4.1.5 Loop Handling Equipment

Although the hot cave has been used successfully for minor repairs in the forward section of test loops, major overhaul and maintenance work on the aft portion of the test loop could not be accomplished in this area. To provide a capability for removal of the test loops from the containment vessel to the hot laboratory area, remote loop handling equipment and shielding equipment were designed and built. A lead filled stainless steel cask was built to provide adequate shielding of irradiated test loops during transfer to the hot laboratory area or during storage outside of the quadrant. The thickness of lead at the activated end of the test loop was eight inches. The shielding integrity of the cask was demonstrated by moving an eleven curie cobalt-60 source longitudinally through the central axis of the cask while monitoring the exterior surfaces. A manually operated clam-shell lifting device inside the containment vessel permits the insertion of an irradiated test loop into the cask using quadrant water as a biological shield during loop manipulation. A similar, but remotely operated, lifting device was available to facilitate loop handling in the hot laboratory area. After placement in the lead filled cask, the irradiated loop could be removed from the containment vessel through an airlock

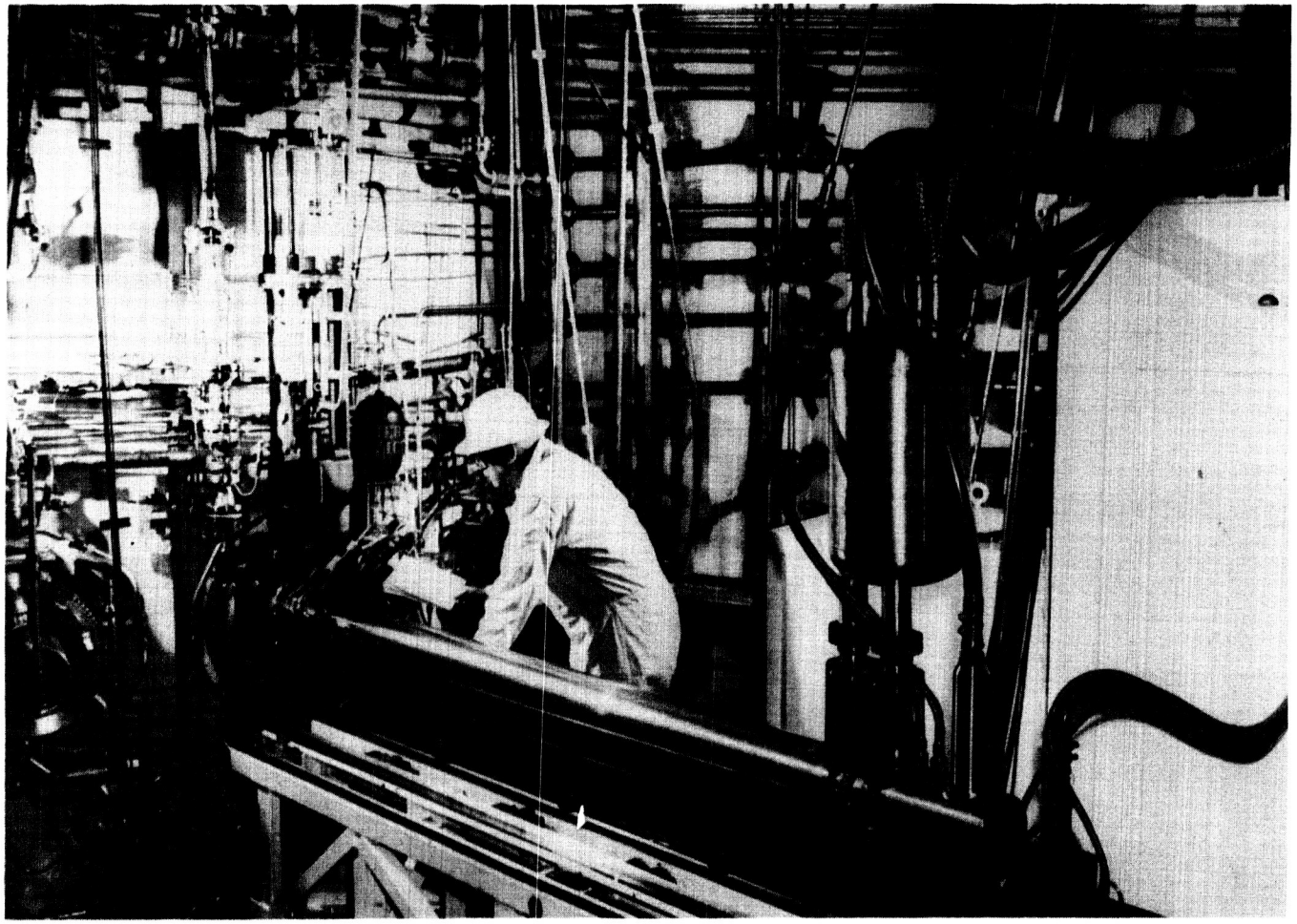

FIGURE 8 TRANSFER TABLES

penetration of the vessel wall without compromising vessel containment. A special bridge over Canal E, inside the containment vessel, and a special cart outside the vessel facilitated transfer of the cask through the airlock penetration. Figure 9 shows the cask being transferred from the bridge to the portion of the airlock inside the containment vessel.

4.2 TEST METHODS

Discussion of the methods of testing is, in the following paragraphs, divided into sections on strain and stress measurement, temperature control, flux mapping and exposure calculations, data recording and reduction.

4.2.1 Strain Measurement

Strain of unnotched tensile specimens was measured using an extensometer developed for this application. This extensometer, shown in Figure 10, measured the increase of the separation between two knife edges initially 0.50 inch apart. The measurement was accomplished through the use of a linear variable differential transformer (LVDT) specially constructed to be resistant to radiation effects.

The signal generated by the LVDT was recorded on the X axis of a Moseley X-Y Recorder used to plot a stress-strain curve for each specimen tested.

The extensometer was tested for reproducibility of signal at 30°R by repeatedly stressing an AISI 4130 steel test specimen to approximately 60 percent of its yield strength and comparing the modulus slope recorded for consistency.

The extensometers were verified and classified in accordance with ASTM Specification E-83(9) using a Tuckerman optical strain gage as a primary standard. The error in indicated strain was less than 0.0001 in/in. Thus the extensometer met the requirements for an ASTM Classification of B-1, suitable for determination of modulus values as well as yield strength. However, this classification was obtained in a standards laboratory using precision techniques and this degree of accuracy could not be expected following installation by remote means. As the extensometer was actually used, an ASTM Classification of B-2, suitable for determination of yield strength, but not of modulus, was probably a more realistic appraisal.

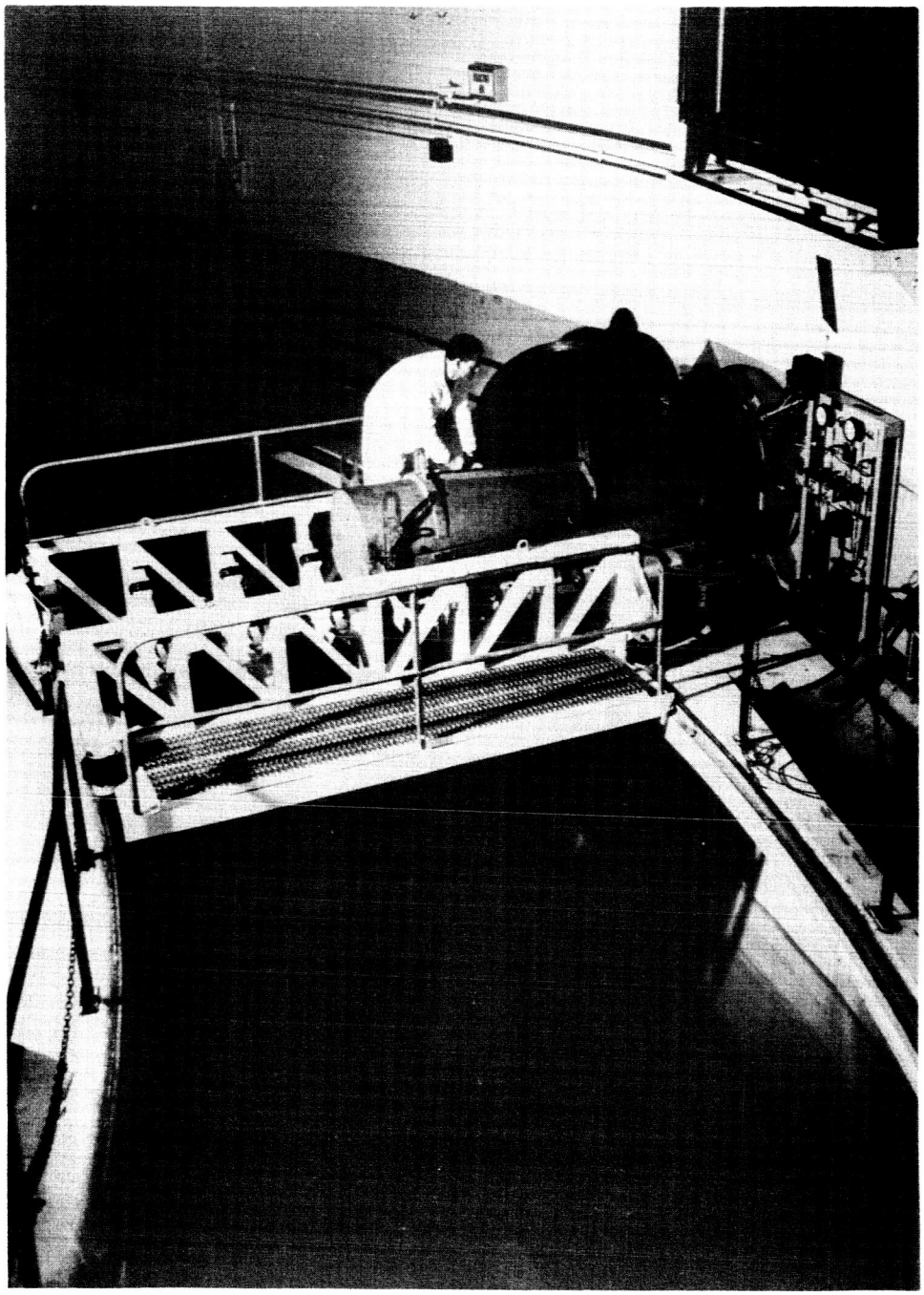

FIGURE 9 CASK, BRIDGE AND AIRLOCK

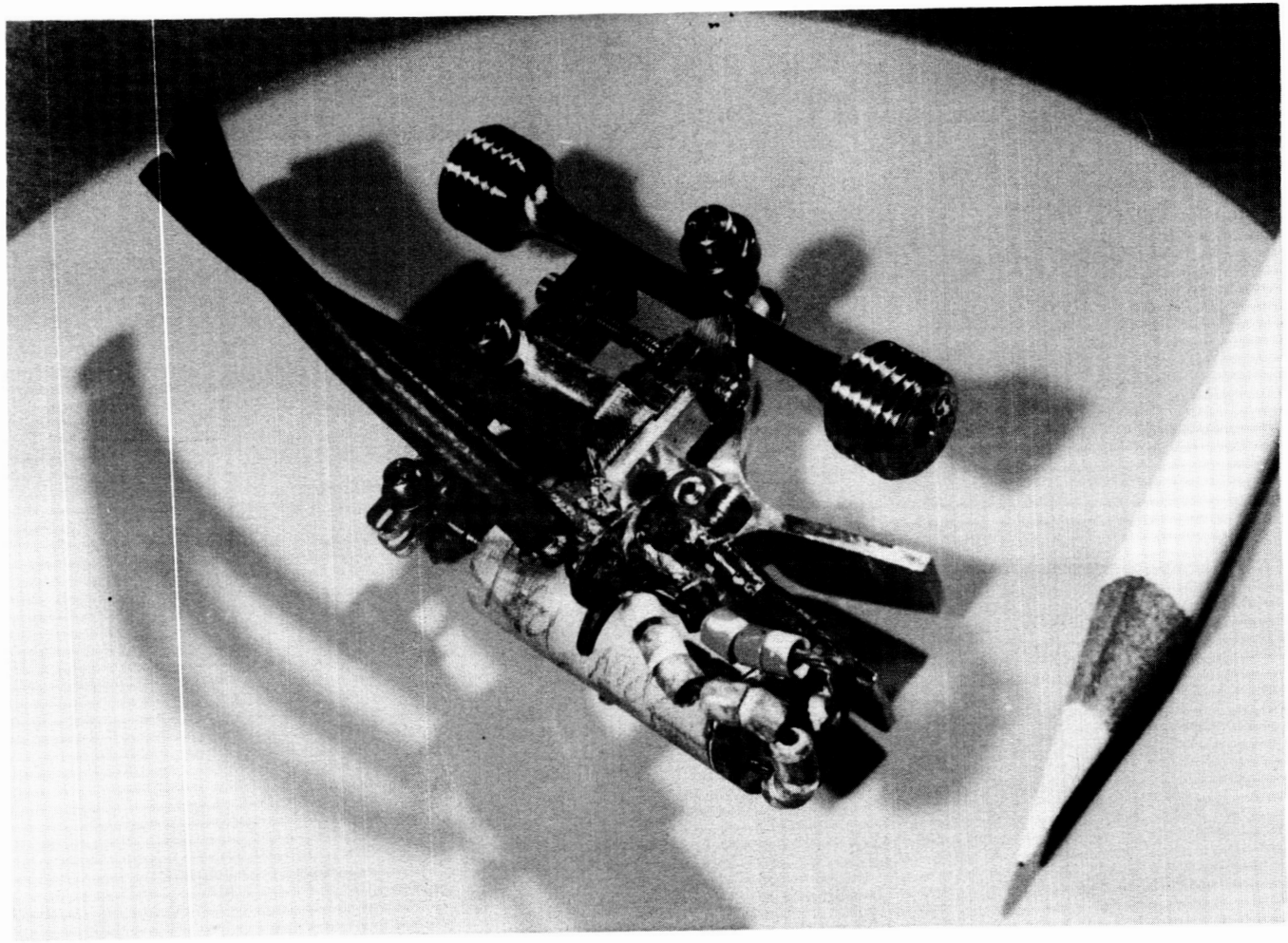

FIGURE 10 EXTENSOMETER

This extensometer had a range of reliable accuracy of approximately 0.010 inch, or some 2 percent of the specimen gage length. This was sufficient to record the elastic portion of the stress-strain curve and the initial plastic portion to well beyond the yield strength (0.2 percent offset method). However, the strain could not be measured immediately prior to failure except for rather brittle materials. During plastic behavior of the test specimen at strain levels beyond the capability of the extensometer, stress was recorded against time on the X axis to provide a record of the loading pattern and to allow accurate determination of the fracture stress. However, the recording equipment was modified to permit this stress-time plot after the screening program was begun and this plot is not available for all samples tested.

The strain rate, measured over ten second intervals during the elastic behavior of the test specimen, was approximately 0.0015 in/in/min. This method of measuring speed-of-testing conforms to ASTM E-8, paragraph 22 e.[9]

4.2.2 Stress Measurement

The stress applied to the test specimens in the test loop described in Section 4.1.1 was monitored by a proving ring type dynamometer using a linear variable differential transformer to measure the ring deflection resulting from loading. The transformer operated from a 2 kilocycle carrier oscillator and phase sensitive demodulator. The direct current output from this demodulator was fed through the X-Y Recorder where it was plotted on the Y axis as a direct measurement of stress.

Each dynamometer was calibrated prior to installation in the test loop by loading in series with a Morehouse vibrating reed proving ring calibrated by the National Bureau of Standards. The read out equipment associated with the test equipment was used to record dynamometer loading during calibration. The maximum difference in the load recorded by the dynamometer and the standard ring was less than 2 percent.

In testing notched specimens, where strain was not monitored, the load rate was controlled by measuring stress at 10 second intervals during the initial portion of the loading period. The stress rate was maintained at less than 90,000 psi/min.

This method of speed-of-testing measurement conforms to the requirement of ASTM E-8, paragraph 22 d.[9]

4.2.3 Specimen Temperature Control

Direct measurement of the specimen temperature was not feasible because of:

- Possible alteration of the mechanical properties of the specimen during attachment of the sensing device.
- Mechanical difficulties in attaching sensing devices to the individual specimens using remote handling techniques.
- Possible erroneous results from protracted irradiation exposures.
- Possible erroneous results from mechanical damage to the sensor.

Therefore it was planned to monitor the test chamber temperature with a platinum resistance thermometer mounted in the test loop helium inlet duct just aft of the forward bulkhead. However, work reported by Coltman, et. al.,[12] at ORNL indicated a gross change in the low temperature electrical resistance of platinum resulting from exposure to a fast neutron environment. This irradiation induced increase in resistivity is not completely removed by self-annealing at room temperature. Therefore, location of platinum resistance thermometers as originally planned would require recalibration after each irradiation. Even after recalibration, the sensors would have an uncertainty of measurement of about $\pm$ 10% at the test temperature.

For this reason, two platinum resistance thermometers were installed to monitor the temperature of the inlet and return helium streams in each test loop at a location remote from the fast neutron field. These pairs of sensors were located some thirty feet from the test zone, in the inlet and return legs of the refrigeration manifold shown in the upper right portion of figure 2.

Since this temperature control method does not provide direct measurement of specimen temperature, relationship between indicated sensor readings and

specimen temperature was determined with thermocouples attached to typical specimens during the following test stages:

- Calibration of direct measuring thermocouples on instrumented aluminum, titanium and stainless steel specimens.*

- Determination of temperature distribution across the gage length of each of the above specimens.

- Determination of correction to be applied to the control sensors to insure a temperature of 30°R at the gage length mid-point.

4.2.3.1 Thermocouple Calibration

Instrumented specimens of AISI Type 304 Stainless Steel, Aluminum Alloy 7178-T651 and Titanium Alloy 6% Al-4% V were prepared for this program. Longitudinal slots were milled in each specimen and copper-constantan thermocouples were welded or soldered to the base of each slot at each end of the 1/2 inch gage length and at the mid-point of the gage length, as shown in figure 11. After the thermocouples were mounted, the slots were filled with a suitable potting compound to prevent perturbations in the gas flow pattern and to increase the mechanical strength of the couple to specimen joints. Copper-constantan thermocouples were used since measurements at liquid helium temperature after a dose of 1×10^{18} nvt, made at ORNL[13] showed no significant radiation induced measurement variations in this thermoelectric pair.

The wire used for the manufacture of these thermocouples was tested for homogeneity to minimize the effect of a Peltier emf on the Thomson emf generated by the finished instrument. This was accomplished by moving a liquid air bath along a closed loop of wire and measuring the emf generated at the two high temperature gradient interfaces. Any wire showing a change greater than 3 microvolts in a 1.5 foot length was rejected for use as thermocouple material. Plots showing the emf curves of rejected and acceptable wire are shown in figure 12.

The initial stage of the temperature correlation program, calibration of each of these thermocouples, was then undertaken. The instrumented specimens were individually

---

* Nickel alloy specimen not used due to similarity of thermal conductivity with austenitic stainless steels.

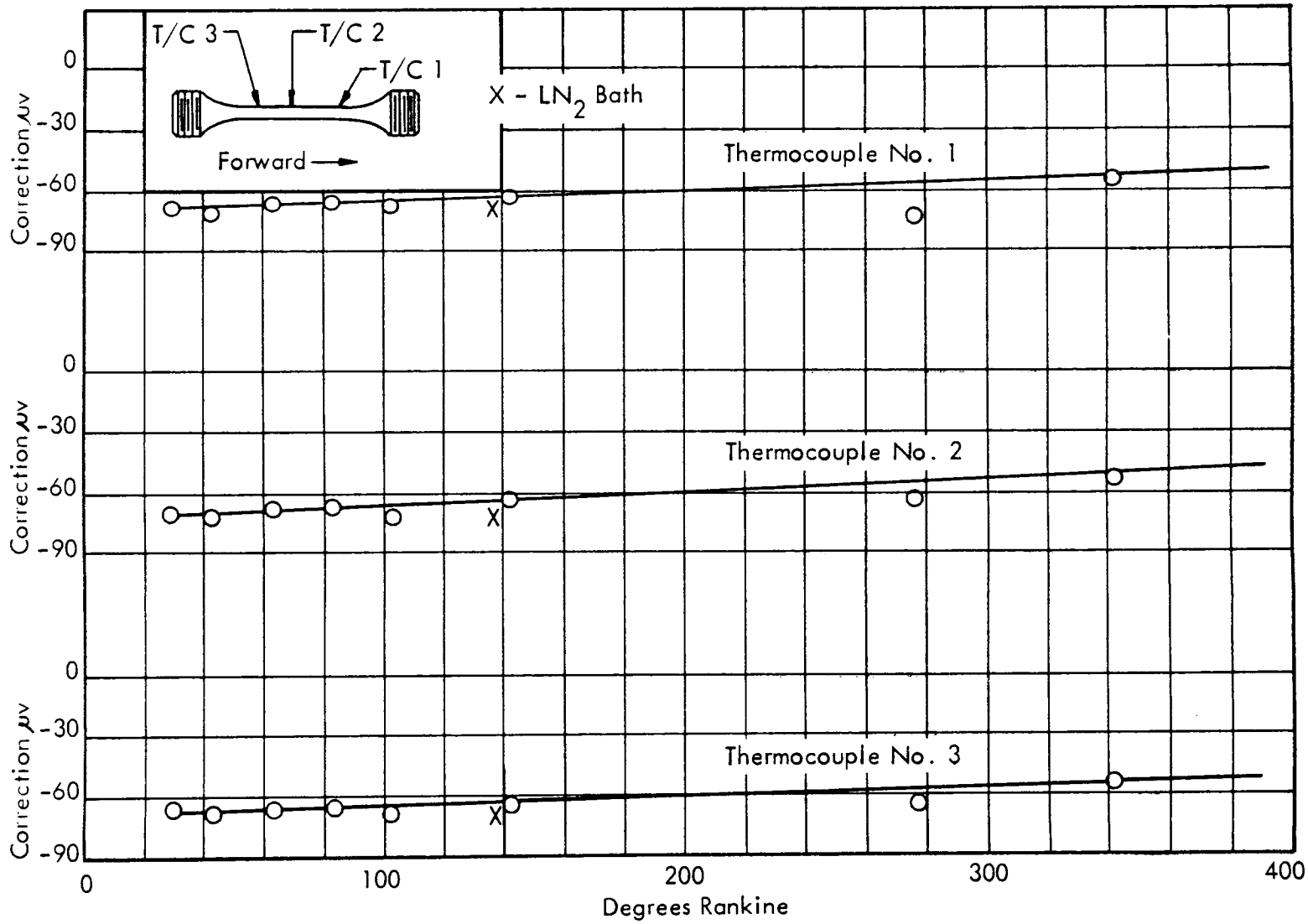

FIGURE 11 CALIBRATION CURVES FOR COPPER-CONSTANTAN THERMOCOUPLES

REJECTED WIRE

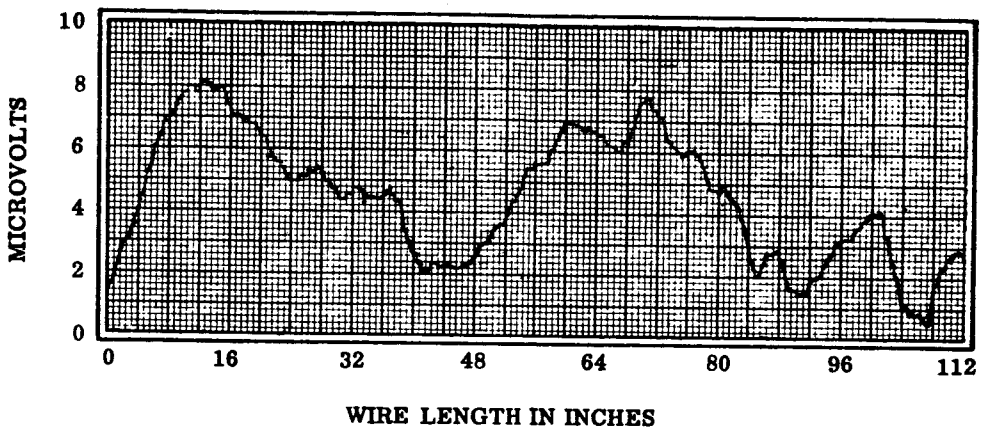

ACCEPTED WIRE

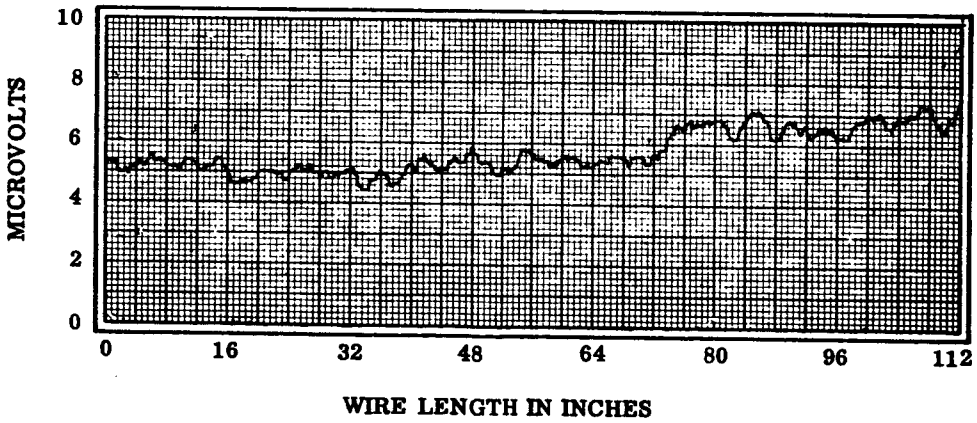

FIGURE 12 TYPICAL WIRE TEST DATA

packaged in aluminum foil with a platinum resistance bulb calibrated by the National Bureau of Standards serving as a primary standard. Each package was separately immersed in liquid nitrogen and the micro-voltage out-put from each thermocouple was recorded with the temperature measurement from the primary standard. This initial comparison at a known temperature was done to provide additional assurance against a systematic error.

After the liquid nitrogen check, each package was separately placed in the test zone inside the head of a test loop. The package was stabilized at several temperatures between liquid nitrogen and 30°R and emf readings for each couple were recorded against the temperature recorded by the primary standard. Actual temperature versus emf out-put curves were prepared for each thermocouple. At this point, the instrumented specimens were considered adequate for use as secondary, or working, standards. Typical calibration curves are shown in figure 11.

4.2.3.2 Specimen Temperature Distribution

After completion of the calibration of section 4.2.3.1, specimen temperature distribution measurements were made.

The stainless steel, aluminum alloy and titanium alloy instrumented specimens, now calibrated to serve as working standards, were individually installed in the normal test position in a test loop. The refrigeration system was stabilized at 30°R, out-of-pile, and the temperature was measured at each end and the mid-point of the specimen gage length from the emf out-put of each thermocouple with the individual calibration curves discussed in section 4.2.3.1.

Initially, a variation of several degrees R was observed among the three test points. This was corrected by internal modification of the ducts which direct the helium across the specimen to increase the mass flow at the warmer locations. The specimen temperature distribution at 30°R (nominal) is shown in table 2.

After satisfactory temperature distribution was obtained across the gage length at 30°R out-of-pile, the test loop containing the instrumented specimen was brought to the "full forward" position in HB-2 to measure the effect of gamma heating on temperature distribution. The reactor power level was nominally 50 MW during the aluminum and stainless steel temperature distribution tests

TABLE 2 SPECIMEN TEMPERATURE DISTRIBUTION AT 30°R (NOMINAL)

TEMPERATURE SENSOR	SENSOR LOCATION	INDICATED TEMPERATURE, °R Aluminum 7178	Titanium 6-4	SS 304
		OUT - OF - PILE		
TC 1	Fwd. Gage Mark	31.1	30.1	29.5
TC 2	Midpoint of Gage	29.2	30.6	29.8
TC 3	Aft Gage Mark	29.8	32.1	29.8
Pt Bulb	Helium Inlet	27.4	30.0	29.5
Pt Bulb	Helium Outlet	29.5	32.5	30.1
		IN - PILE		
TC 1	Fwd. Gage Mark	31.3	30.0	*
TC 2	Midpoint of Gage	29.3	33.0	*
TC 3	Aft Gage Mark	31.0	35.0	*
Pt Bulb	Helium Inlet	27.1	29.9	*
Pt Bulb	Helium Outlet	29.6	33.5	*

* Not available

and nominally 40 MW for the titanium tests. The temperature of the test loop was again stabilized at 30°R and brought to a steady-state, where the refrigeration capacity exactly balanced gamma heating. No appreciable increase in temperature differential between the test points was observed.

4.2.3.3 Refrigerator Control Sensor Corrections

After completion of the temperature distribution tests of 4.2.3.2, readings of the permanently installed temperature sensors of the refrigerator were taken which corresponded with a 30°R specimen temperature under in-pile steady-state conditions as measured with the secondary standard thermocouple. The use of these correction constants for each pair of permanent temperature sensors during each irradiation exposure assured the maintenance of specimen temperature under $\pm$ 1°R. The platinum resistance bulbs from the permanent temperature sensors were recalibrated by the manufacturer after the completion of the test program and gave readings within less than one degree of the initial calibrations.

4.2.4 Flux Mapping and Exposure Calculations

Fast neutron dose rates in the test location in HB-2 were determined using foil measurement techniques. Sets of foils, as shown in Table 3, were placed in the test specimen location of a test loop in an aluminum foil holder. The foils were then irradiated for thirty minutes with sufficient refrigeration provided to prevent the melting of the S^{32} foil from gamma heating. Reactor operational parameters were recorded at the time of irradiation.

After irradiation, the foils were shipped by air to the Georgia Nuclear Laboratories at Dawsonville, Georgia, for counting and evaluation by standard techniques. The upper and lower limits of spectral shape of the reactor fast flux obtained from seven (7) foil runs is given in Figure 13.

Examination of the family of spectral curves in Figure 13 shows a significant variation in flux level, particularly in the lower energy region of the spectrum. Examination of the reactor operational parameters at the time of these irradiations indicated that the flux level varied with the position of the fuel control rods in the lattice core. These control rods have an upper half consisting of cadmium

TABLE 3

FOILS USED FOR SPECTRAL MEASUREMENTS OF FAST NEUTRON FLUX IN HB-2

Type of Foil	Nominal Weight		Nuclear Reaction	Threshold Energy
	Lockheed Foils	NASA Foils		
Neptunium	20 micrograms	10 milligrams	$Np^{237}(n, f)\ Ba^{140}$	0.75 Mev
Uranium	-	10 milligrams	$U^{238}\ (n, f)\ Ba^{140}$	1.45 Mev
Thorium	50 micrograms	-	$Th^{232}(n, f)\ Ba^{140}$	1.75 Mev
Sulfur	0.5 grams	0.8 grams	$S^{32}\ (n, p)\ P^{32}$	2.90 Mev
Nickel	0.1 grams	50 milligrams	$Ni^{58}\ (n, p)\ Co^{58}$	5.0 Mev
Magnesium	0.5 grams	30 milligrams	$Mg^{24}\ (n, p)\ Na^{24}$	6.3 Mev
Aluminum*	0.5 grams	25 milligrams	$Al^{27}\ (n,\alpha)\ Na^{24}$	8.1 Mev

* The $Al^{27}(n, p)\ Mg^{27}$ reaction with a threshold energy of 5.3 Mev is not included due to the short (9.8 m) half life of the product.

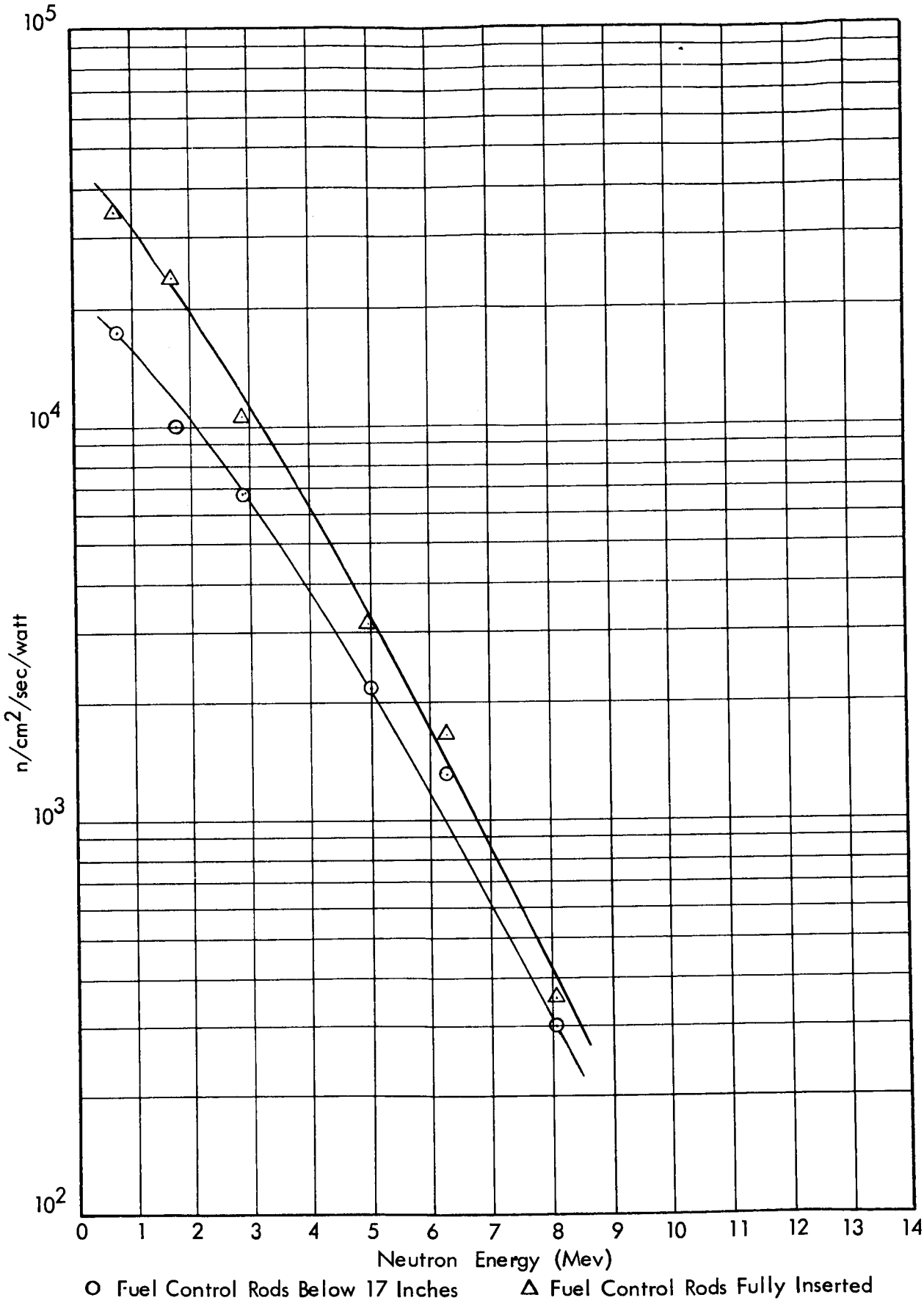

FIGURE 13 UPPER AND LOWER LIMIT SPECTRAL CURVES OF FAST FLUX IN HB-2

enclosed in AISI Type 304 stainless steel and a lower portion consisting of aluminum clad aluminum-enriched uranium alloy fuel elements of the MTR type. The rods were progressively inserted into the core, from the bottom, during reactor operations. Thus, as poison was removed from the core, fuel was added. One of the control rods, in lattice position LC-6, was located directly in front of HB-2. When the rods were in the initial operating position, the cadmium portion of the rod caused a rod shadowing effect in the test location which disappeared as further insertion brought the fueled segment of the control rod in line with HB-2. This was the cause of the observed variation in fast flux level.

To establish the fast neutron flux level at various control rod positions, additional partial sets of foils containing only the low threshold energy materials Np^{237}, Th^{232} and S^{32} were irradiated at several rod positions. Figure 14 shows the flux level at energies greater than 0.75 Mev as a function of rod position measured with the several Np^{237} foils and greater than 0.50 Mev obtained by extrapolation of the curve obtained from the evaluation of the Np^{237}, Th^{232} and S^{32} foils.

Control rod position and reactor power levels were recorded hourly in the reactor operations log. With these data and the plot of Figure 14, the incremental hourly increase in the neutron dose received by each specimen was calculated. The test specimens were irradiated until these calculations indicated an accumulated dose of 1×10^{17} nvt ($E > 0.5$ Mev) at which time the test load was applied to the specimen.

About midway in the in-pile testing phase of the screening program the reactor loading pattern was changed to provide greater fuel economy. The enriched uranium content of each of twenty-two (22) fuel elements was increased from 168 grams to 200 grams; the fueled segments of the five (5) control rods from 130 grams to 155 grams.

Spectral sets of foils were irradiated both prior to and after the change in reactor fuel loading. No significant change in flux level or spectral shape for similar power level and control rod positions was observed. During the final three foil irradiations after the change in fuel loading, the Plum Brook Nuclear Experiments Section supplied additional sets of parallel foils for evaluation by NASA personnel. The NASA foil set also is included in Table 3. Agreement between the Lockheed and NASA foil evaluation was within the expected limit of experimental uncertainty for both spectral shape and fast neutron flux levels. Cobalt and cadmium covered

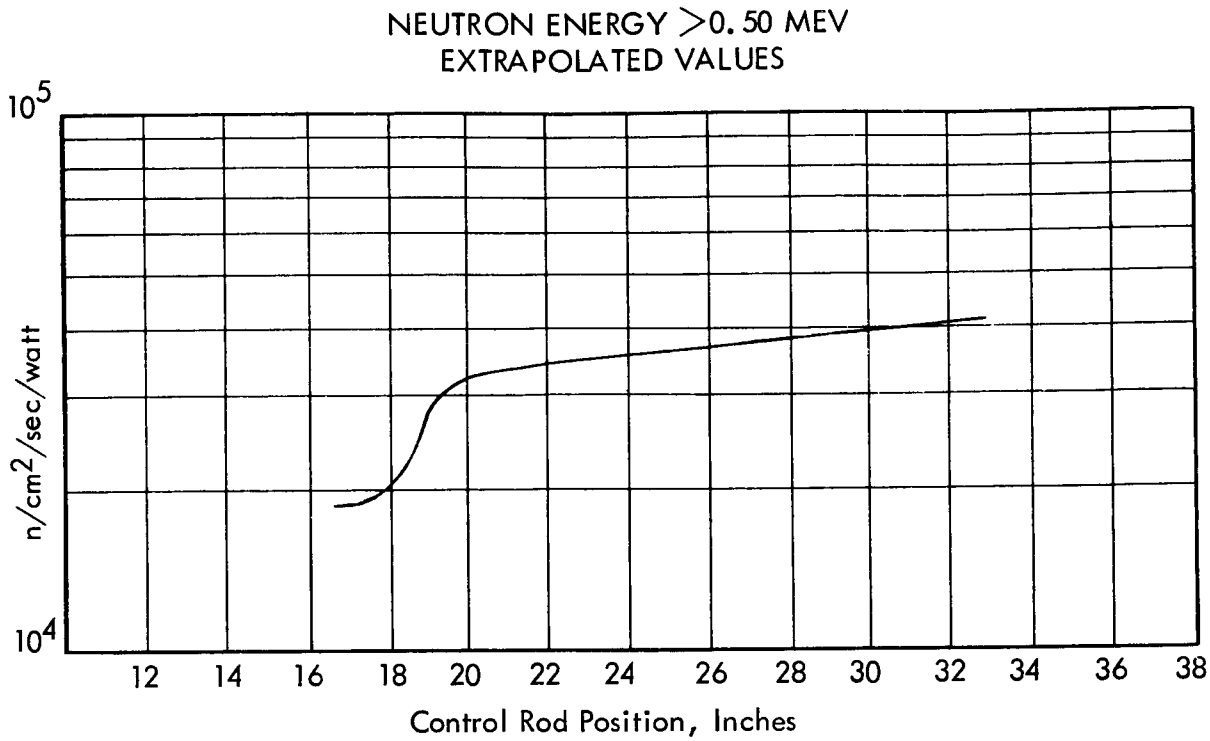

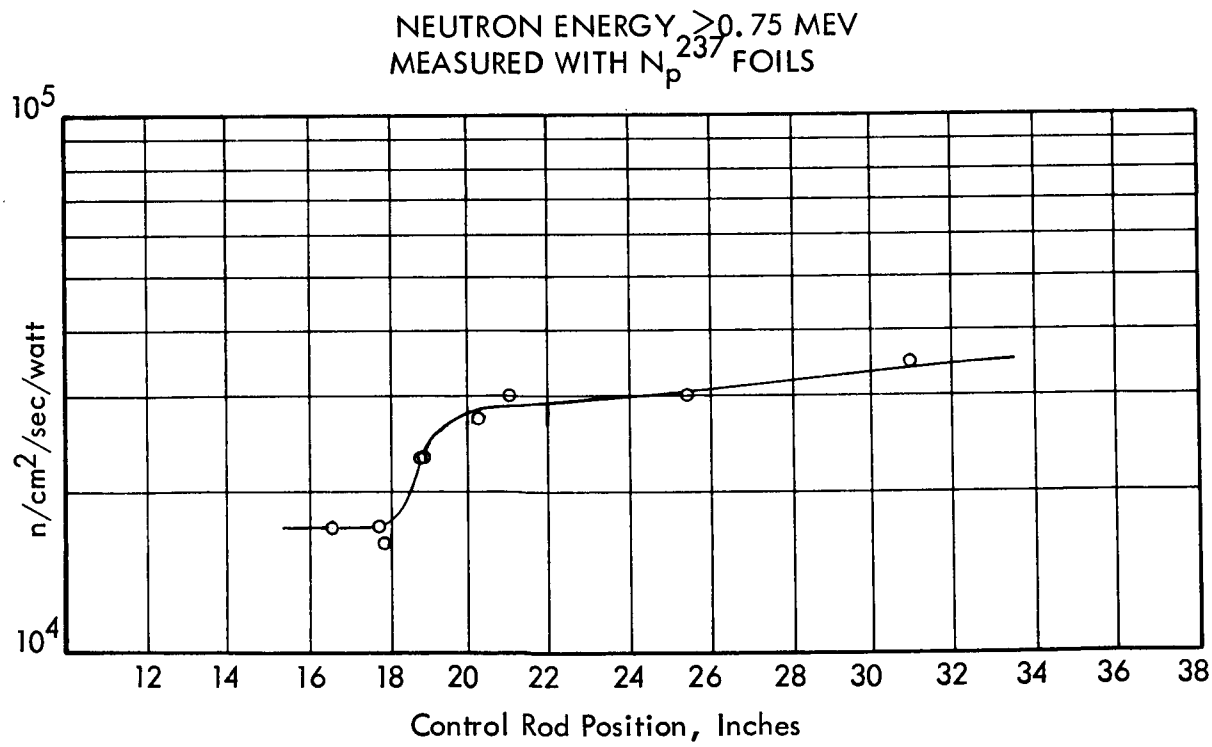

FIGURE 14 FAST NEUTRON FLUX IN TEST LOCATION VS. CONTROL ROD POSITION

cobalt were irradiated for determination of the thermal flux by NASA personnel. With the reactor power level at 60 MW and the fuel control rod location at twenty-five inches the measured thermal flux was in the order of $10^4 n/cm^2/watt/sec$ or approximately twenty-eight percent of the fast ($E > 0.5$ Mev) flux.

A curve presenting the upper and lower limits of the ratio of the flux with neutron energies greater than E to the fluxes with energies greater than 0.5 Mev in the Plum Brook Reactor spectrum observable in HB-2 is given in Figure 15 as a basis of comparison of the irradiation received by specimens in this program with test data from other sources.

4.2.5 Data Recording

The temperature of the helium gas was monitored with platinum resistance thermometers located at the helium manifold on both the test loop inlet and return transfer lines. These control sensors were monitored by the test console operator and recorded on a specimen test log at regular intervals, which documented the proper control of the specimen temperature throughout the irradiation exposure. The method used to calibrate the temperature control system is described in Section 4.2.3.

The accumulated fast neutron flux dosage was calculated hourly using the method described in Section 4.2.4. Both the incremental and accumulated flux were recorded in a data log to serve as a permanent record of the exposure received by each in-pile specimen.

4.2.5.1 Stress-Strain Recording

The strain and stress monitoring equipment are described in Sections 4.2.1 and 4.2.2. The calibration techniques used to verify these instruments are discussed in the same sections.

The monitoring instruments converted stress and strain into electrical signals proportional in strength to the magnitude of the stress or strain being measured. The

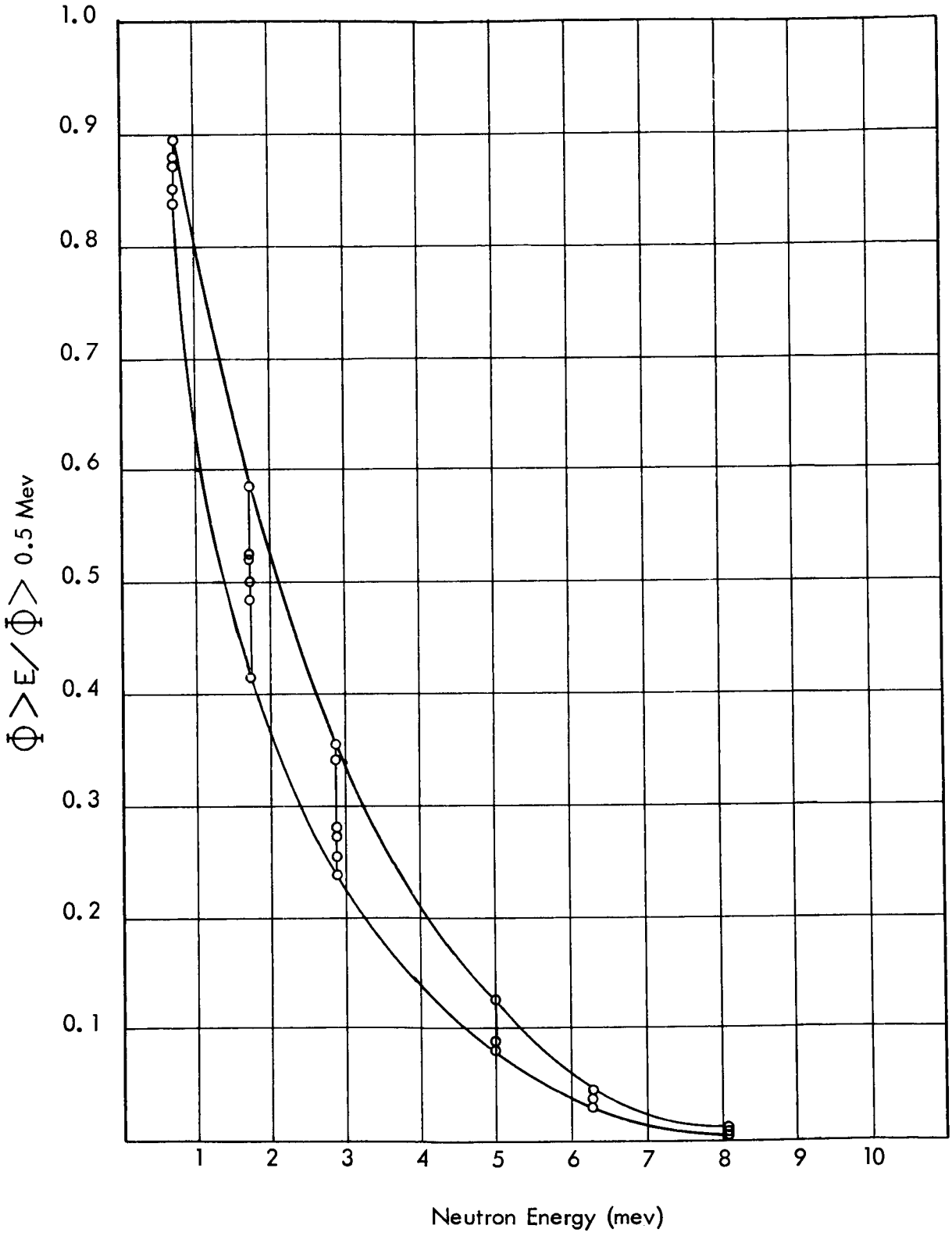

FIGURE 15 $\Phi>E/\Phi>_{0.5}$ MEV AS A FUNCTION OF NEUTRON ENERGY

electrical impulse from each of these instruments was amplified and plotted automatically by a Moseley X-Y Recorder. Stress appeared as the Y plot, strain as the X plot and the resultant stress-strain curves were recorded on graph paper as a permanent record of test data. The extensometer used in this program was capable of measuring only about 0.010 inch extension with reliable accuracy. After this limit of approximately 0.02 in/in. total strain has been reached the X axis recorder was switched to a time plot traveling at a rate of 0.02 in/sec.

The X-Y Recorder contained a calibrator which was used to provide a constant voltage of known amplitude to serve as a reference voltage. This calibration signal was continuously variable from 400 mv to 1400 mv and permitted setting the X-Y Recorder range to conform with the individual calibrations of the extensometers and dynamometers.

The stress-strain curve developed by the X-Y Recorder during testing and the initial specimen dimensions provided data for the determination of the ultimate tensile strength (F_{tu}) and the tensile yield strength (F_{ty}). The modulus of elasticity may be approximated from these curves, but an exact determination of this value was unobtainable due to the method of extensometer installation imposed by the necessity of using remote handling techniques.

4.2.5.2 Ductility Measurements

Elongation and reduction of area values were obtained by fitting the broken specimens together and measuring the fractured gage length and minimum diameter by means of a micrometer stage and hair line apparatus accurate to $\pm$ 0.0001 inch. These values are reported as the change in magnitude from original specimen dimensions expressed as a percentage of the original value.

4.2.5.3 Structural Studies, Optical Metallography

The suppliers of the test material submitted photomicrographs of the raw stock taken in both traverse and longitudinal planes. Additional photomicrographs were prepared by NASA Plum Brook Laboratory personnel from longitudinal sections of failed specimens of each alloy after testing in each of the environmental conditions of the screening program.

Due to the irradiation induced radioactivity of the in-pile test specimens, metallographic preparation and examination of these specimens was accomplished by remote handling techniques.

4.2.6 Data Reduction

As described previously, stress-strain curves were plotted up to strains of approximately two percent and thereafter the stress was plotted versus time until after failure of the specimen. The stress scale was varied to accommodate the approximate ultimate stress of the material being tested while the strain scale was held constant. In nearly all measurements of tensile specimens, it was possible to estimate the slope of the so-called elastic portion of the stress-strain curve and to thus determine a yield point corresponding to 0.2 percent plastic strain. This slope was also used to determine an approximate modulus of elasticity value.

The scale used and the yield deflection were recorded on a master calculation sheet as were the ultimate load deflection and the fracture load deflection. Early in the program, only the stress was recorded after two percent strain; consequently, the fracture load increment could not be differentiated when different from the ultimate load increment and the fracture stress was not calculable from most of the test specimens.

Figures 16 to 19 show load-elongation and load-time curves from a variety of tests. As indicated in the captions these include usable and not usable curves, tensile tests with and without a load versus time plot and tensile notch tests (ductile and non-ductile). Figure 20 shows curves from the three test conditions for 17-7PH Stainless Steel, clearly illustrating the effect of irradiation.

In nearly all tensile notch tests, the load was recorded only on the vertical scale.

The elongated gage length and reduced diameter of the failed specimens were measured and these dimensions also were recorded on the master calculation sheet for the particular material.

Arithmetic means of yield stress, ultimate stress, fracture stress, yield to ultimate ratio, elongation and reduction of area were calculated for the tensile specimens and the arithmetic mean of the ultimate stress was calculated for the tensile notch specimens.

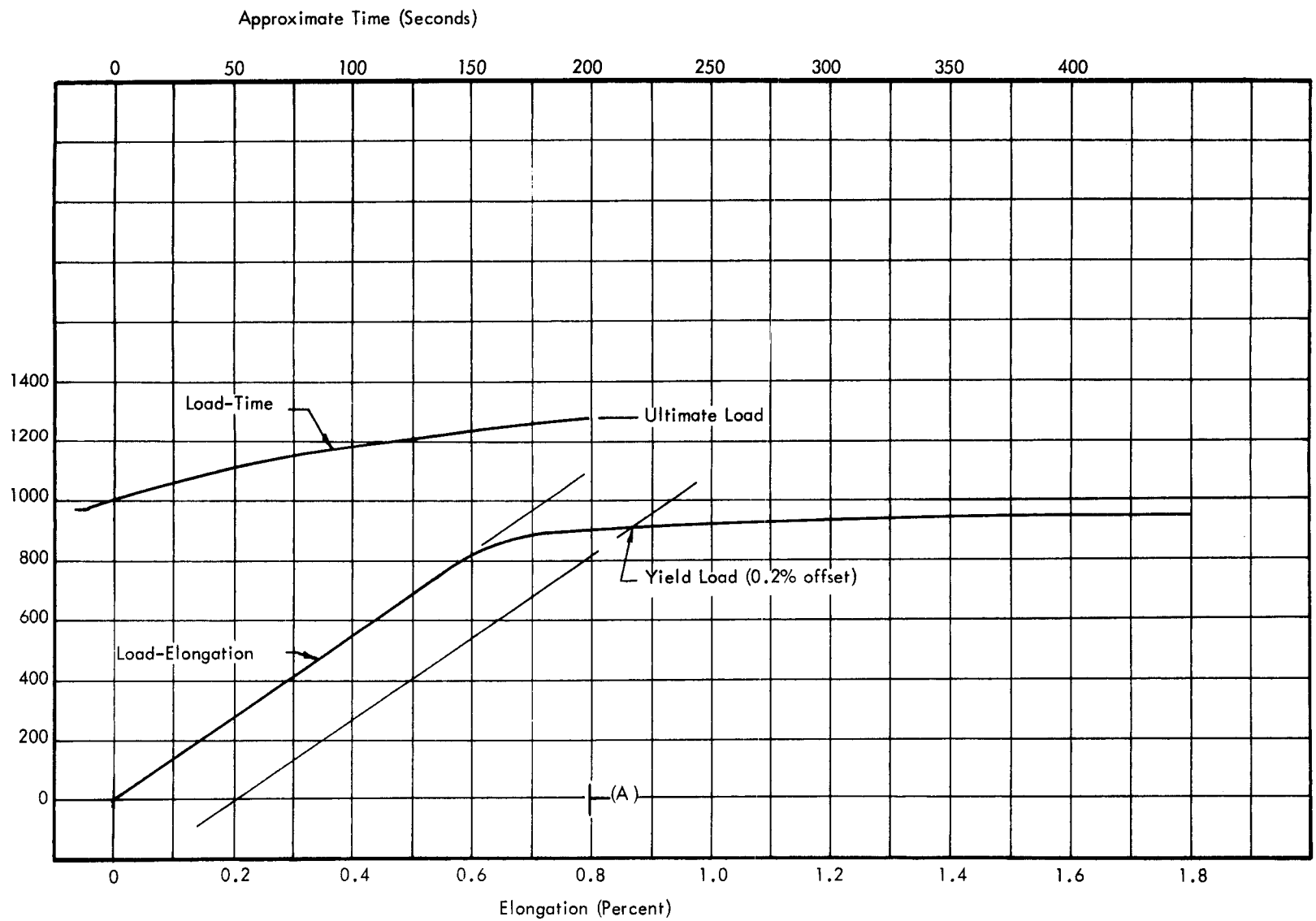

FIGURE 16 LOAD-ELONGATION AND LOAD TIME CURVES FROM TENSILE TEST SHOWING WELL DEFINED MODULUS SLOPE AND WELL DEFINED ZERO (A) AFTER SPECIMEN FRACTURE

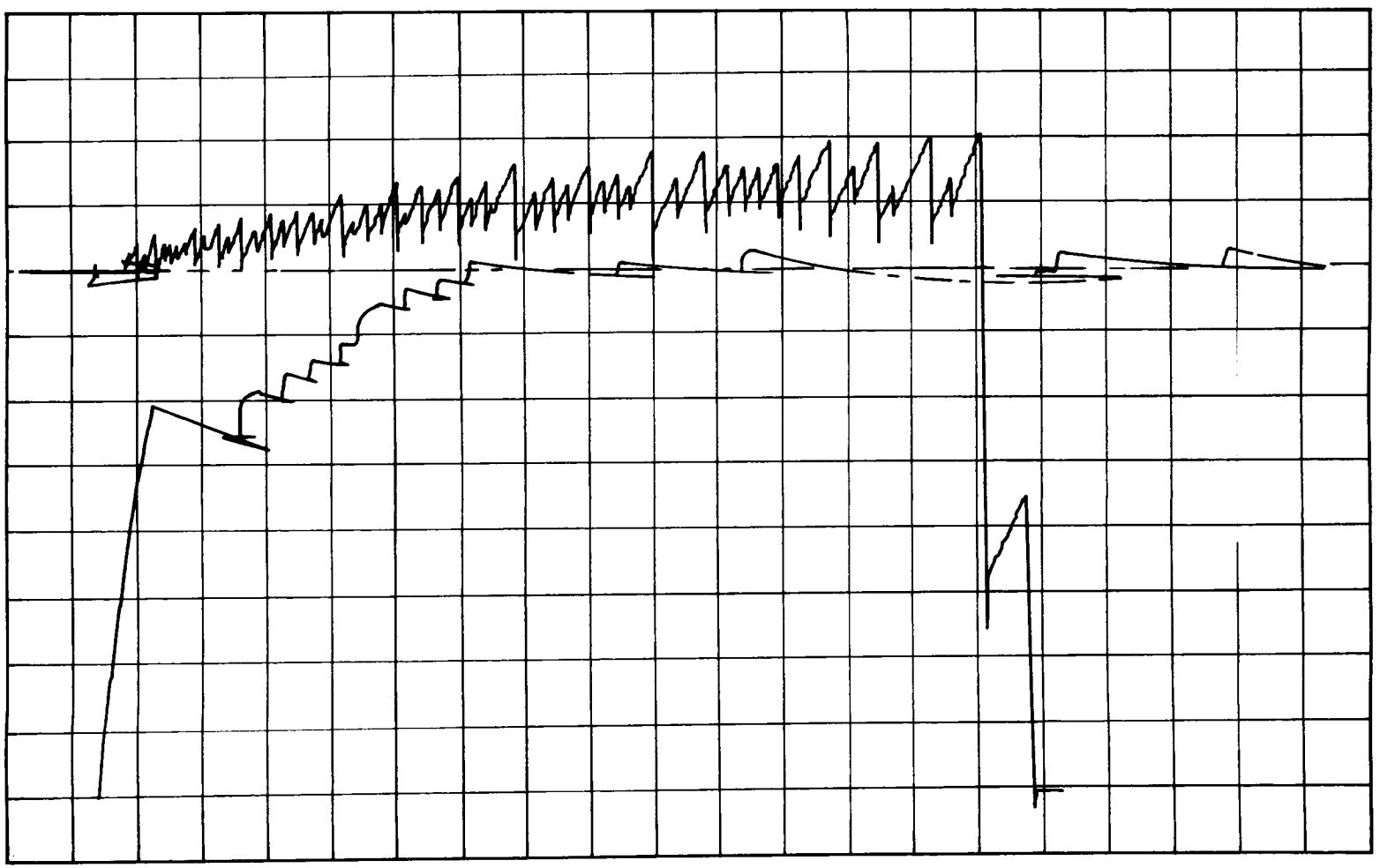

FIGURE 17 CURVES SHOWING EFFECTS OF ICE FORMATION ON ACTUATOR ROD YIELDING INVALID TEST RESULTS

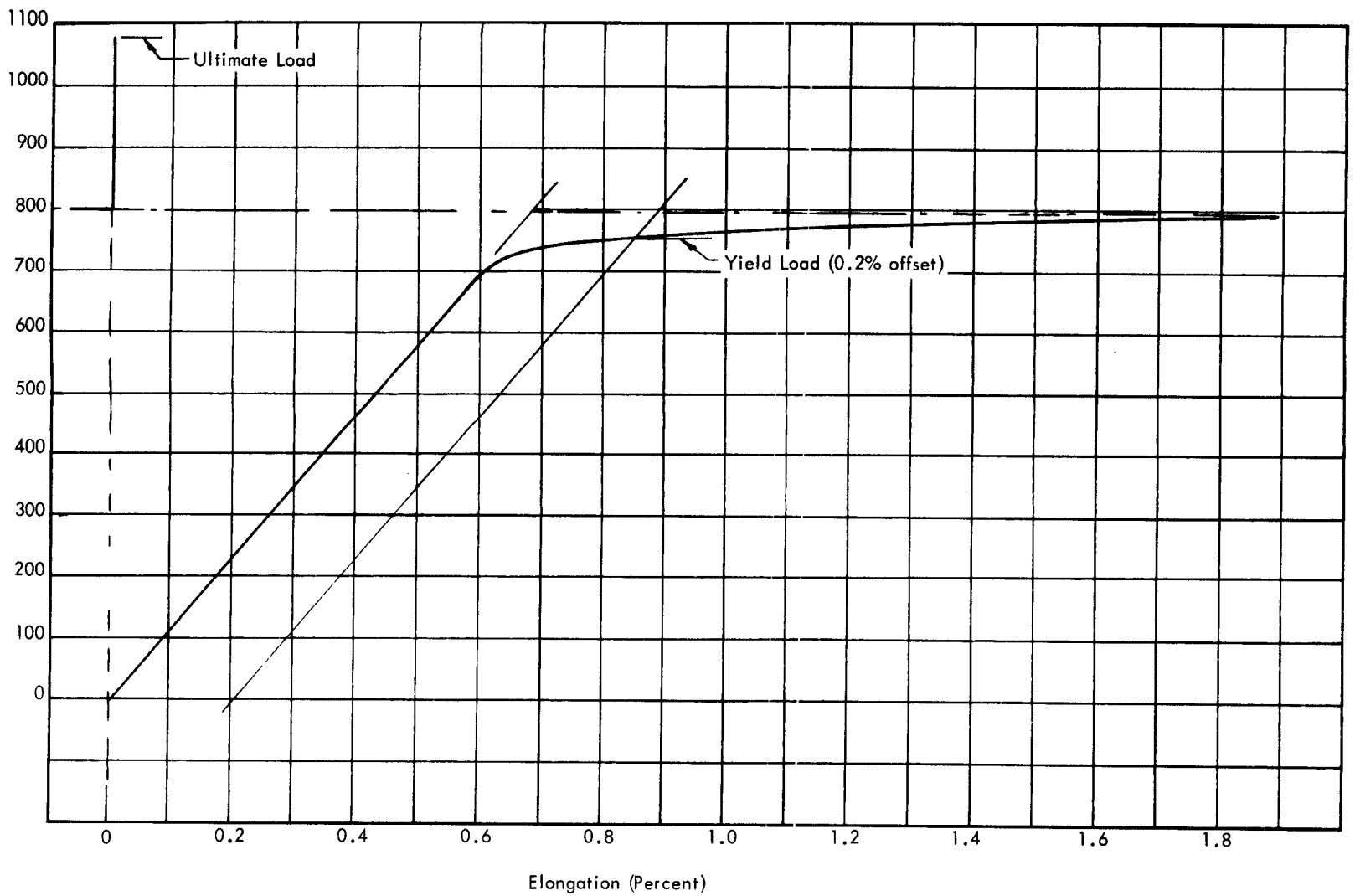

FIGURE 18 LOAD-ELONGATION CURVE WITHOUT LOAD-TIME EXTENSION

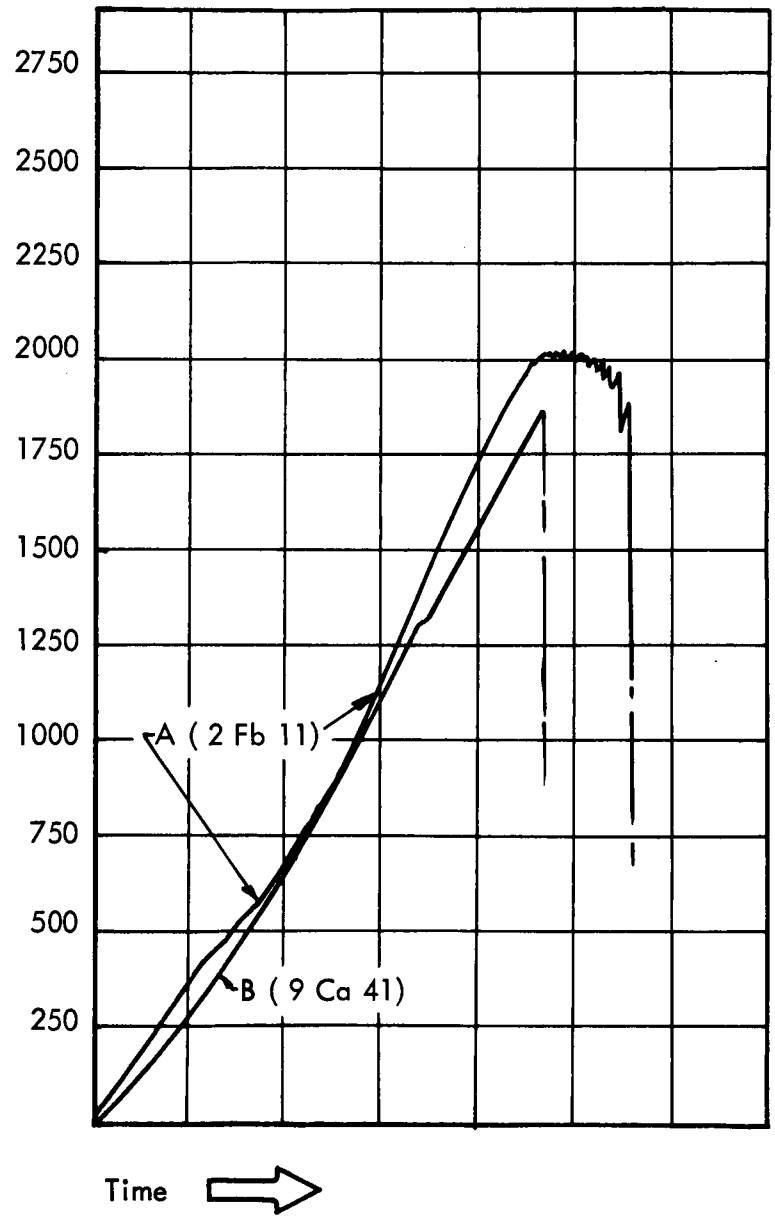

FIGURE 19 LOAD-TIME CURVES FROM TENSILE NOTCH TESTS SHOWING DUCTILE (A) AND NON-DUCTILE (B) BEHAVIOR UNDER TRIAXIAL LOADING

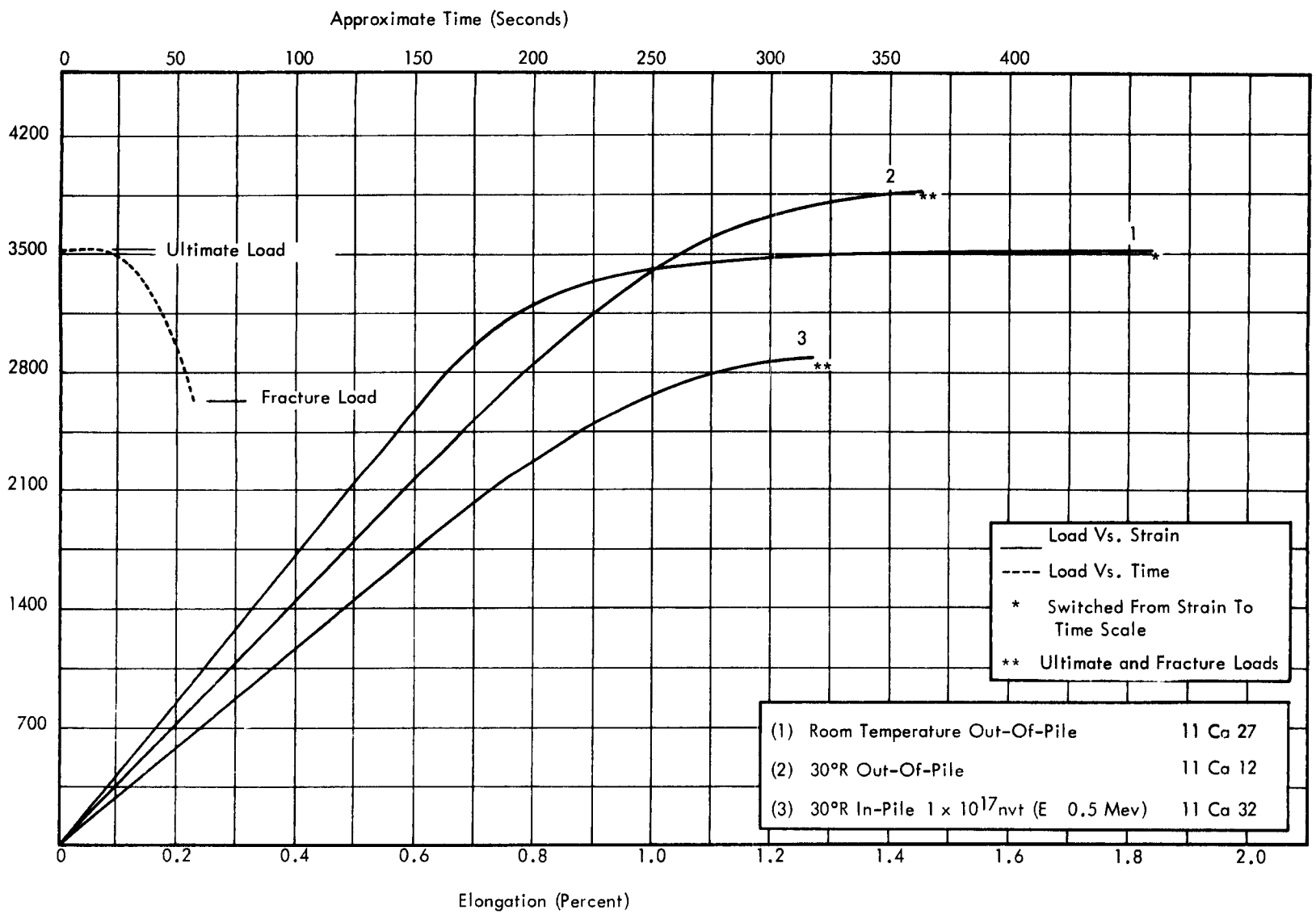

FIGURE 20 LOAD-ELONGATION AND LOAD TIME CURVES FROM THREE TEST CONDITIONS FOR 17-7PH STAINLESS STEEL

The ratio of notched ultimate stress to unnotched ultimate stress was determined randomly by choosing notched and unnotched specimens on the basis of their specimen number. Thus, five notched to unnotched ratios were available for each five specimen sample of tensile notch specimens and an arithmetic mean of the function was determined in the same manner as for the tensile yield and ultimate tensile stresses.

The objective of the screening program was to observe changes resulting from combined cryogenic and neutron irradiation environments and to compare various materials with respect to these changes. Consequently, even limited random scatter reduces the value of the data, unless it is treated statistically, because of:

- The low level of effects expected in some materials, particularly due to the low level of irradiation (10^{17} nvt) used throughout the program.

- The reduced number of in-pile specimens (three, in-pile, compared with five, out-of-pile).

Random scatter in all test values results from inhomogenities and brittleness in some materials and additional random scatter in in-pile test values can result from possible inhomogenities in irradiation effects and from errors arising from remote handling of the specimens and remote operation of the test equipment.

The standard deviation as well as the arithmetic means were determined for the tensile yield stress, ultimate tensile stress, notched ultimate tensile stress and notched to unnotched ultimate stress ratio.

The elongation and reduction of area and fracture stress data were not treated statistically because known non-random errors (such as that due to imperfect fitting together of the fractured surfaces) would tend to invalidate the statistical treatment. The yield to ultimate ratio was not treated statistically because in most cases, the statistical quantities can be inferred from the statistical quantities determined for the yield and ultimate stresses individually.

With the standard deviation of the means, the differences between the means (bias) for the room temperature values and the cryogenic temperatures were calculated with a range of values assigned based on the sample size (number of specimens) and the desired level of confidence (ninety percent). The range is the extreme values between which ninety percent of all determination of the bias would fall.[14, 15]

Similarly, the differences between the means of the results obtained out-of-pile at 30°R and the values taken in-pile at 30°R were treated statistically to determine the significance of apparent irradiation effects and to permit comparison of results from various materials.

The ninety percent confidence level is reasonably high. It permits discussing differences as real rather than as probable. It should be noted that in most cases, assuming a fifty percent confidence level would reduce the range of the biases by a factor of approximately 2.5.

For a given difference between two means (the bias), the range of the bias shows immediately if the difference is not statistically significant. If the range includes zero (one sign is positive, while the other is negative) then the difference is not significant at the chosen ninety percent confidence level. The range of the bias is also valuable in making comparisons between materials for a given test condition. For example, if the ranges of the biases for one function for two given materials overlap, then there is not significant difference between the two biases or between the two materials with respect to that particular function.

No attempt has been made to statistically eliminate outliers (those test values that appear to be extreme, probably due to an undetectable error in the observation). They are pointed out in the few cases where they might affect the significance of the results.

5 TEST RESULTS

The objective of the test program was to determine changes in tensile properties resulting from combined cryogenic and neutron irradiation environments and to compare various materials with respect to these changes. As in most testing of this sort, out-of-pile tests at room temperature and at the cryogenic temperature were performed as a control in order to determine individual cryogenic and irradiation effects. The resulting test values along with a discussion of their validity are presented in this section.

5.1 TEST VALUES

The pedigree data supplied by the vendors of the test specimen materials are summarized in Appendix A . These data served as a description of the material used in the test program as well as an indication of the validity of the room temperature test values obtained in the screening program.

The raw test data along with the important statistical parameters obtained in the screening program are compiled in Appendix B . These data include unnotched tensile and yield strengths, notched tensile strengths, elongations and reductions of area and fracture stresses and are presented with the calculated notched-to-unnotched tensile strength ratios and tensile yield to ultimate ratios. Estimated modulus of elasticity values are presented in a separate table (B-34) at the end of this appendix.

Photomicrographs taken of most of the materials as supplied by the vendors and after various test conditions are shown in Appendix C .

Some typical constructed stress-strain curves are shown in Appendix D .

The differences between means of the test values at various test conditions are probably the most important numbers calculable from the raw test data. These differences for the strength functions (F_{tu}, F_{ty} and F_{tun}) are presented in graphical form in Figures 21 , 22 and 23 with a bar to represent each positive or negative difference (bias) and an indication of the statistical range of this bias at the ninety percent confidence level (see Section 4.2.6).

The arithmetic means of all test values, at the three test conditions, including elongations, reductions of area, fracture stresses, notched-to-unnotched ratios and yield-to-ultimate ratios are presented for easy reference in Tables 4 , 5 and 6.

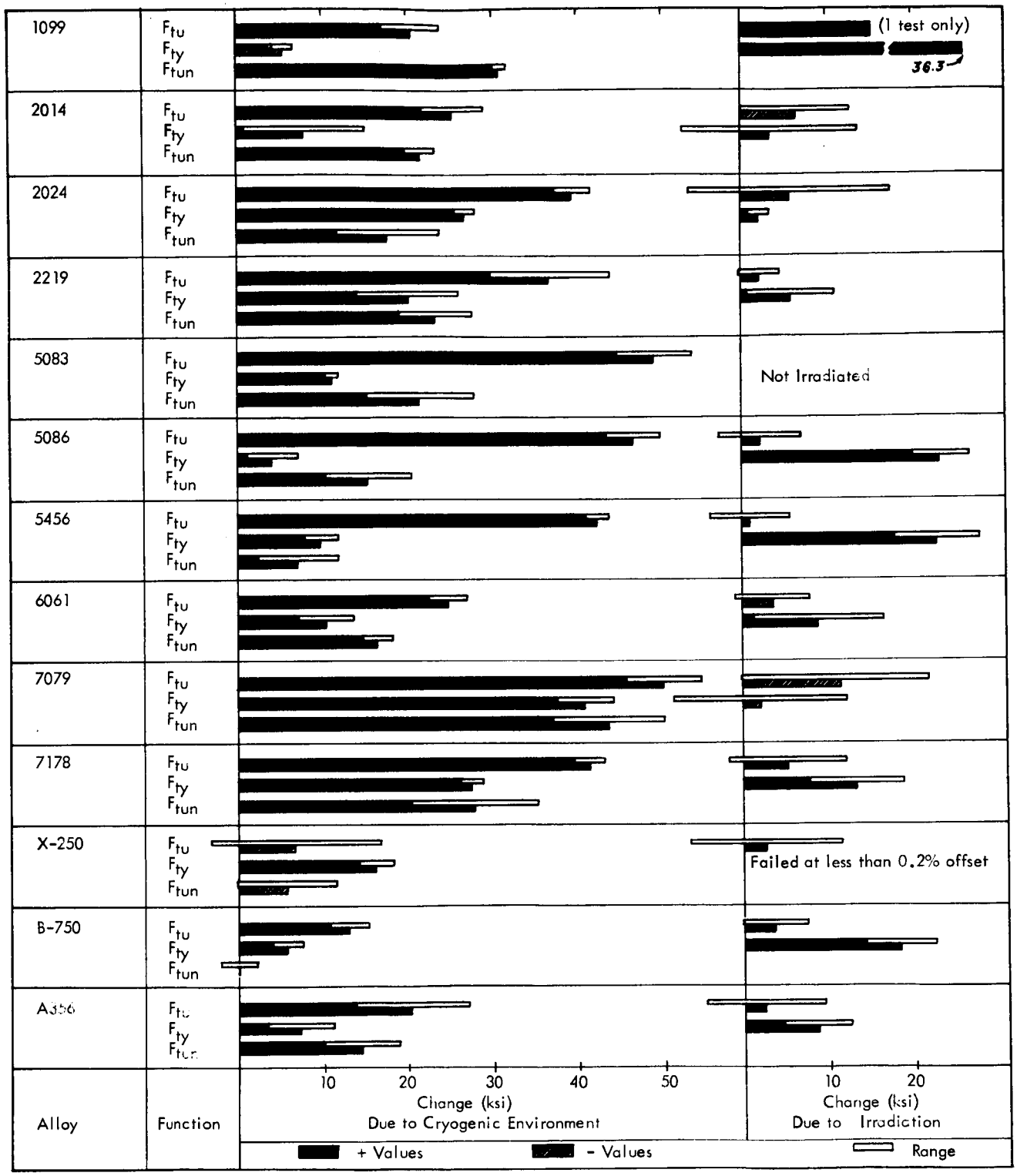

FIGURE 21 CHANGES IN CERTAIN FUNCTIONS FOR ALUMINUM ALLOYS DUE TO CRYOGENIC AND IRRADIATION ENVIRONMENTS

TABLE 4

SUMMARY OF TEST RESULTS, ALUMINUM ALLOYS

ALLOY	Test Cond.	F_{tu} (ksi)	F_{ty} (ksi)	F_{tun} (ksi)	F_{tun}/F_{tu}	F_{ty}/F_{tu}	Elongation (% in 4D)	Reduction of Area (%)	Fracture Stress (ksi)
1099	RT	13.18	12.48	16.12	1.288	0.942	22.8	79.0	-
	OP 30°R	33.78	6.97	47.16	1.412	0.216	61.4	69.2	110.0
	IP 30°R	49.20*	43.30*	-	-	0.880*	46.0*	54.0*	87.4*
2014	RT	65.64	60.34	79.50	1.210	0.920	12.2	35.0	69.3
	OP 30°R	91.10	68.28	101.16	1.110	0.750	17.7	26.3	117.0
	IP 30°R	84.60	71.77	-	-	0.847	12.7	18.3	101.6
2024	RT	67.08	50.30	72.82	1.086	0.748	21.6	28.2	-
	OP 30°R	106.60	77.20	95.64	0.894	0.724	22.3	20.3	-
	IP 30°R	100.77	79.40	-	-	0.830	16.3	18.0	123.7
2219	RT	59.04	48.02	74.68	1.290	0.812	14.2	32.2	52.4
	OP 30°R	95.86	68.18	98.10	1.030	0.710	16.4	27.2	-
	IP 30°R	93.73	74.07	-	-	0.787	15.3	18.3	111.3
5083	RT	46.36	32.16	55.08	1.190	0.692	11.4	23.8	-
	OP 30°R	95.46	43.32	76.70	0.804	0.454	21.0	24.0	130.0
	IP 30°R	-	-	-	-	-	-	-	-
5086	RT	45.34	32.00	52.88	1.170	0.704	10.6	22.0	54.2
	OP 30°R	91.96	36.18	68.40	0.750	0.394	30.0	25.0	122.7
	IP 30°R	94.23	59.47	-	-	0.630	22.3	20.0	118.0
5456	RT	49.90	34.00	59.58	1.190	0.682	12.8	10.4	-
	OP 30°R	92.20	43.86	66.78	0.720	0.478	18.2	16.8	113.0
	IP 30°R	93.15	66.70	-	-	0.720	14.0	16.5	111.5
6061	RT	43.36	40.00	56.52	1.300	0.922	18.5	48.3	-
	OP 30°R	68.14	50.42	72.96	1.070	0.738	30.0	41.4	-
	IP 30°R	64.57	59.37	-	-	0.920	30.0	34.0	95.4
7079	RT	95.12	88.96	108.20	1.140	0.936	11.4	25.2	103.5
	OP 30°R	145.20	129.80	151.80	1.050	0.894	5.8	5.8	153.4
	IP 30°R	133.70	127.70	-	-	0.953	5.3	4.3	140.0
7178	RT	87.68	80.48	100.30	1.146	0.918	12.0	22.8	-
	OP 30°R	129.00	108.00	128.20	0.994	0.834	12.4	13.0	-
	IP 30°R	134.30	121.30	-	-	0.903	6.3	4.3	138.3
X-250	RT	56.26	32.78	58.54	1.048	0.590	20.6	19.6	-
	OP 30°R	49.54	49.03	52.84	1.098	0.880	nil	nil	49.5
	IP 30°R	46.93	(g)	-	-	-	nil	nil	46.9
B-750	RT	29.54	19.46	31.10	1.048	0.658	8.8	10.8	-
	OP 30°R	42.58	25.18	31.15	0.745	0.590	7.0	4.0	-
	IP 30°R	46.20	43.53	-	-	0.940	3.3	1.0	46.8
A-356	RT	44.10	30.32	51.36	1.166	0.688	14.6	18.4	54.5
	OP 30°R	64.54	37.58	65.86	1.038	0.584	11.6	9.4	71.7
	IP 30°R	62.10	46.13	-	-	0.743	8.7	8.0	67.6

* 1 test only

\- not recorded or not available

(g) failed at less than 0.2% plastic strain

TITANIUM ALLOYS

NICKEL ALLOYS

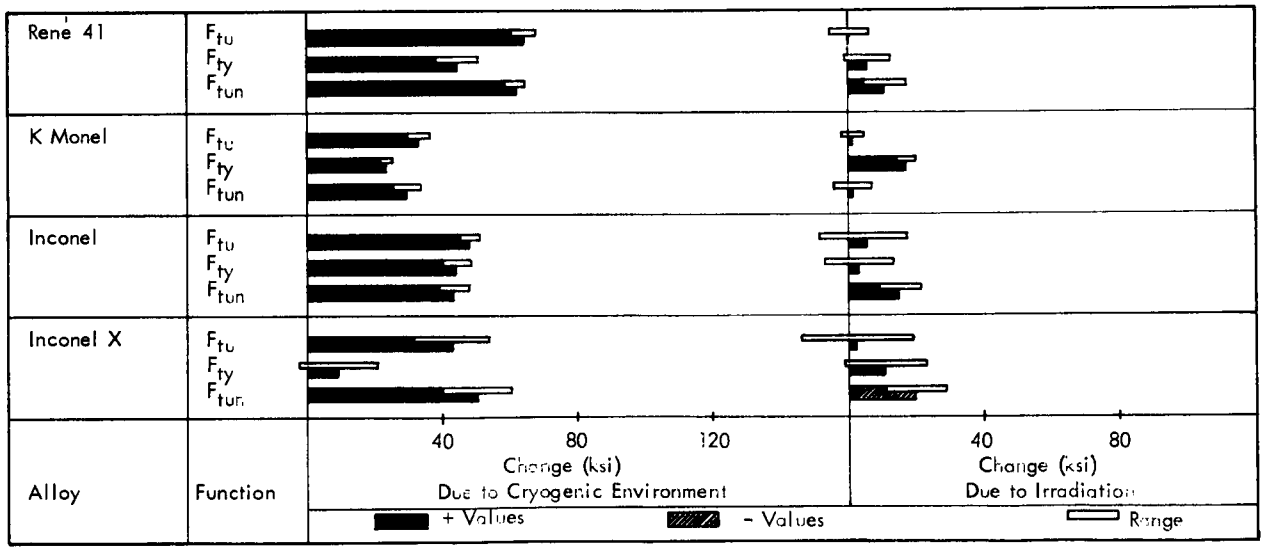

FIGURE 22 CHANGES IN CERTAIN FUNCTIONS FOR TITANIUM AND NICKEL ALLOYS DUE TO CRYOGENIC AND IRRADIATION ENVIRONMENTS

TABLE 5

SUMMARY OF TEST RESULTS, TITANIUM AND NICKEL ALLOYS

ALLOY	Test Cond.	F_{tu} (ksi)	F_{ty} (ksi)	F_{tun} (ksi)	F_{tun}/F_{tu}	F_{ty}/F_{tu}	Elongation (% in 4D)	Reduction of Area (%)	Fracture Stress (ksi)
55A	RT	67.00	53.50	84.28	1.260	0.798	30.0	62.3	-
	OP 30°R	169.40	122.00	167.20	0.990	0.722	33.3	53.0	-
	IP 30°R	192.30	131.70	187.30	0.990	0.690	34.0	53.0	-
5 Al-2.5 Sn (Std. I)	RT	125.20	114.80	166.80	1.330	0.920	23.3	50.7	-
	OP 30°R	224.80	205.25	249.60	1.110	0.915	13.8	30.0	298.0
	IP 30°R	239.00	218.00	273.00	1.150	0.913	11.5	36.0	-
5 Al-2.5 Sn (Eli)	RT	126.40	113.40	153.40	1.220	0.896	16.0	42.2	170.0
	OP 30°R	228.40	214.20	267.20	1.170	0.948	9.7	32.3	-
	IP 30°R	223.30	213.00	270.00	1.210	0.953	11.0	31.0	-
6 Al-4 V (Annealed)	RT	144.00	137.80	184.40	1.280	0.957	13.8	45.0	-
	OP 30°R	260.40	243.20	281.60	1.120	0.934	7.6	30.4	-
	IP 30°R	273.70	254.00	283.67	1.040	0.950	5.7	37.3	-
6 Al-4 V (Aged)	RT	167.60	158.60	201.80	1.210	0.946	16.5	54.0	-
	OP 30°R	282.20	275.00	288.80	1.030	0.976	6.4	25.4	-
	IP 30°R	302.30	293.30	295.00	0.980	0.970	5.0	22.5	-
8 Al-1Mo-1V	RT	138.00	131.80	175.00	1.270	0.956	22.7	52.6	-
	OP 30°R	239.00	224.20	267.20	1.120	0.938	-	-	-
	IP 30°R	261.70	242.70	282.00	1.130	0.927	5.7	29.0	-
René 41	RT	130.20	63.20	142.80	1.100	0.485	54.8	60.8	-
	OP 30°R	194.40	107.60	204.80	1.060	0.554	60.5	50.5	-
	IP 30°R	194.70	113.30	194.00	1.000	0.580	55.0	48.0	401.0
K Monel	RT	154.20	97.80	180.40	1.170	0.636	28.0	54.3	-
	OP 30°R	187.20	121.40	210.00	1.120	0.648	32.0	54.8	-
	IP 30°R	188.30	138.67	211.30	1.120	0.737	33.0	51.3	339.0
Inconel	RT	138.20	131.50	179.00	1.290	0.950	13.8	54.8	-
	OP 30°R	186.40	175.80	222.40	1.190	0.940	20.0	56.0	-
	IP 30°R	191.00	179.00	237.30	1.250	0.940	25.0	51.0	352.7
Inconel X	RT	200.60	142.20	199.75	0.990	0.710	25.3	52.3	328.0
	OP 30°R	243.20	150.80	249.80	1.030	0.620	33.0	45.6	421.8
	IP 30°R	241.0	161.30	230.30	0.960	0.667	29.0	37.3	377.7

- not recorded or not available

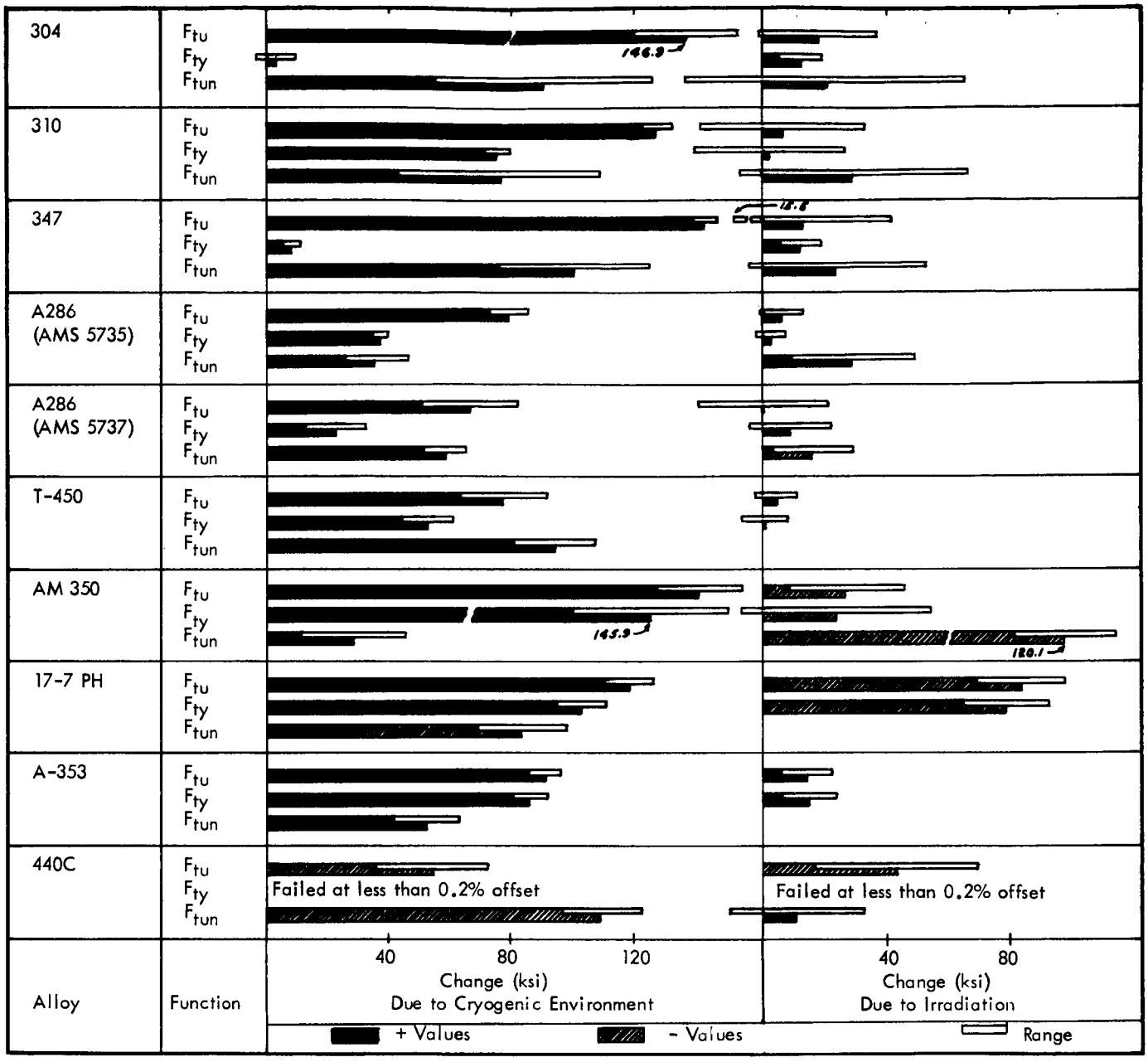

FIGURE 23 CHANGES IN CERTAIN FUNCTIONS FOR FERROUS ALLOYS DUE TO CRYOGENIC AND IRRADIATION ENVIRONMENTS

TABLE 6

SUMMARY OF TEST RESULTS, FERROUS ALLOYS

ALLOY	Test Cond.	F_{tu} (ksi)	F_{ty} (ksi)	F_{tun} (ksi)	F_{tun}/F_{tu}	F_{ty}/F_{tu}	Elongation (% in 4D)	Reduction of Area (%)	Fracture Stress (ksi)
304	RT	95.14	36.76	102.82	1.080	0.386	76.5	81.3	-
	OP 30°R	242.00	39.62	193.40	0.800	0.164	34.4	38.4	-
	IP 30°R	260.33	51.90	173.30	0.670	0.200	33.5	28.5	-
310	RT	84.90	62.64	112.40	1.330	0.736	42.8	79.0	-
	OP 30°R	212.20	137.80	188.64	0.890	0.648	42.8	56.2	462.0
	IP 30°R	218.67	135.67	218.00	1.000	0.617	48.3	21.7	278.7
347	RT	94.50	43.70	113.80	1.158	0.462	60.3	76.5	-
	OP 30°R	237.40	51.90	214.20	0.902	0.220	41.3	43.8	-
	IP 30°R	250.70	64.00	238.00	0.960	0.257	37.0	55.0	-
A286 (AMS 5735)	RT	156.00	112.20	181.00	1.160	0.720	26.3	51.0	-
	OP 30°R	235.00	149.60	216.40	0.920	0.636	34.5	46.5	-
	IP 30°R	229.00	152.00	245.67	1.070	0.663	33.5	16.0	-
A286 (AMS 5737)	RT	171.80	133.80	196.20	1.140	0.780	23.8	52.5	271.0
	OP 30°R	238.20	156.80	255.00	1.070	0.658	31.8	42.2	407.6
	IP 30°R	238.00	165.70	239.00	1.010	0.697	31.0	39.7	386.7
T-450	RT	119.60	38.68	120.20	1.020	0.324	70.2	70.8	385.5
	OP 30°R	197.20	91.46	214.40	1.090	0.464	31.2	27.2	271.4
	IP 30°R	192.70	92.27	-	-	0.480	30.3	29.7	274.3
AM 350	RT	199.00	186.40	239.60	1.210	0.936	19.3	53.7	309.5
	OP 30°R	340.60	332.30	268.40	0.790	0.995	11.0	36.0	574.0
	IP 30°R	313.30	308.30	148.30	0.470	0.983	7.3	20.7	396.3
17-7 PH	RT	234.80	226.60	266.60	1.140	0.964	13.8	45.0	279.0
	OP 30°R	335.40	330.00	182.60	0.550	0.980	nil	nil	340.0
	IP 30°R	251.30	250.70	-	-	0.997	nil	nil	251.3
A 353	RT	110.60	88.60	137.00	1.240	0.800	25.2	69.4	-
	OP 30°R	201.60	174.80	189.60	0.940	0.868	18.0	39.6	-
	IP 30°R	215.70	190.00	-	-	0.883	15.7	21.3	260.3
440 C	RT	315.80	269.80	217.40	0.690	0.854	nil	nil	315.8
	OP 30°R	261.20	(g)	107.70	0.410	(g)	nil	nil	261.2
	IP 30°R	217.70	(g)	118.70	0.550	(g)	nil	nil	217.7

- not recorded or not available

(g) failed at less than 0.2% plastic strain

Most of the discussion in this section and the following sections is based on the data as presented in Figures 21, 22 and 23 and Tables 4, 5 and 6 since they contain nearly all the information needed to discuss the validity of the test data and to analyze and interpret the results in terms of variables such as composition and structure.

Presentation of the absolute changes (biases) in the strength functions in this form, with the statistical ranges indicated, permits a ready assessment of over-all nuclear cryogenic effects as well as easy comparison of materials with respect to the cryogenic and irradiation effects individually. When the range of a bias includes zero it is not statistically significant at the chosen confidence level (90 percent) and when the ranges of two biases overlap they are not statistically different at the chosen confidence level. Trends in notched-to-unnotched strength ratios and yield-to-ultimate strength ratios are apparent at a glance.

For readers more interested in percentage changes, the ratios of test values at 30°R to test values at room temperature and the ratios of values in-pile at 30°R to values out-of-pile at 30°R are shown in Figures 24, 25 and 26.

5.2 VALIDITY OF TEST VALUES

The validity or quality of test results can generally be indicated by: 1) estimating systematic errors in the results from a careful analysis and calibration of the apparatus, 2) determining statistical parameters, such as standard deviation, which are a measure of random error (scatter) in the test results from a given population, and 3) comparing to data, perhaps of unknown quality, obtained independently in a different laboratory.

Although the program was undertaken as a controlled experiment and although this report stresses measured changes in properties due to changes in environment, it was established that the absolute test values, presented in this report as well as the changes in test values resulting from the cryogenic and irradiation environments are of a quality at least equivalent to that generally obtained in physical testing laboratories. This is of importance because the cryogenic data from some of these materials is not generally available and may be useful as such to engineers needing the absolute test values.

Alloy	Function	RT Values	OP 30°R Value/RT Value	IP 30°R Value/OP 30°R Value
1099	F_{tu}	13.18	2.56	1.46
	F_{ty}	12.48	0.56	6.21
	F_{tun}	16.12	2.93	
2014	F_{tu}	65.64	1.39	0.93
	F_{ty}	60.34	1.13	1.05
	F_{tun}	79.50	1.27	
2024	F_{tu}	67.08	1.59	0.95
	F_{ty}	50.30	1.53	1.03
	F_{tun}	72.82	1.31	
2219	F_{tu}	59.04	1.62	0.98
	F_{ty}	48.02	1.42	1.09
	F_{tun}	74.68	1.31	
5083	F_{tu}	46.36	2.06	Not Irradiated
	F_{ty}	32.16	1.35	
	F_{tun}	55.08	1.39	
5086	F_{tu}	45.34	2.03	1.02
	F_{ty}	32.00	1.13	1.64
	F_{tun}	52.88	1.29	
5456	F_{tu}	49.90	1.85	1.01
	F_{ty}	34.00	1.29	1.52
	F_{tun}	59.58	1.12	
6061	F_{tu}	43.36	1.57	0.95
	F_{ty}	40.00	1.26	1.18
	F_{tun}	56.52	1.29	
7079	F_{tu}	95.12	1.53	0.92
	F_{ty}	88.96	1.46	0.98
	F_{tun}	108.20	1.40	
7178	F_{tu}	87.68	1.47	1.04
	F_{ty}	80.48	1.34	1.12
	F_{tun}	100.30	1.28	
X-250	F_{tu}	56.26	0.88	0.95
	F_{ty}	32.78	1.50	Failed at less than 0.2% offset
	F_{tun}			
B-750	F_{tu}	29.54	1.44	1.08
	F_{ty}	19.46	1.29	1.73
	F_{tun}	31.10	1.00	
A-356	F_{tu}	44.10	1.46	0.95
	F_{ty}	30.32	1.24	1.23
	F_{tun}	51.36	1.28	

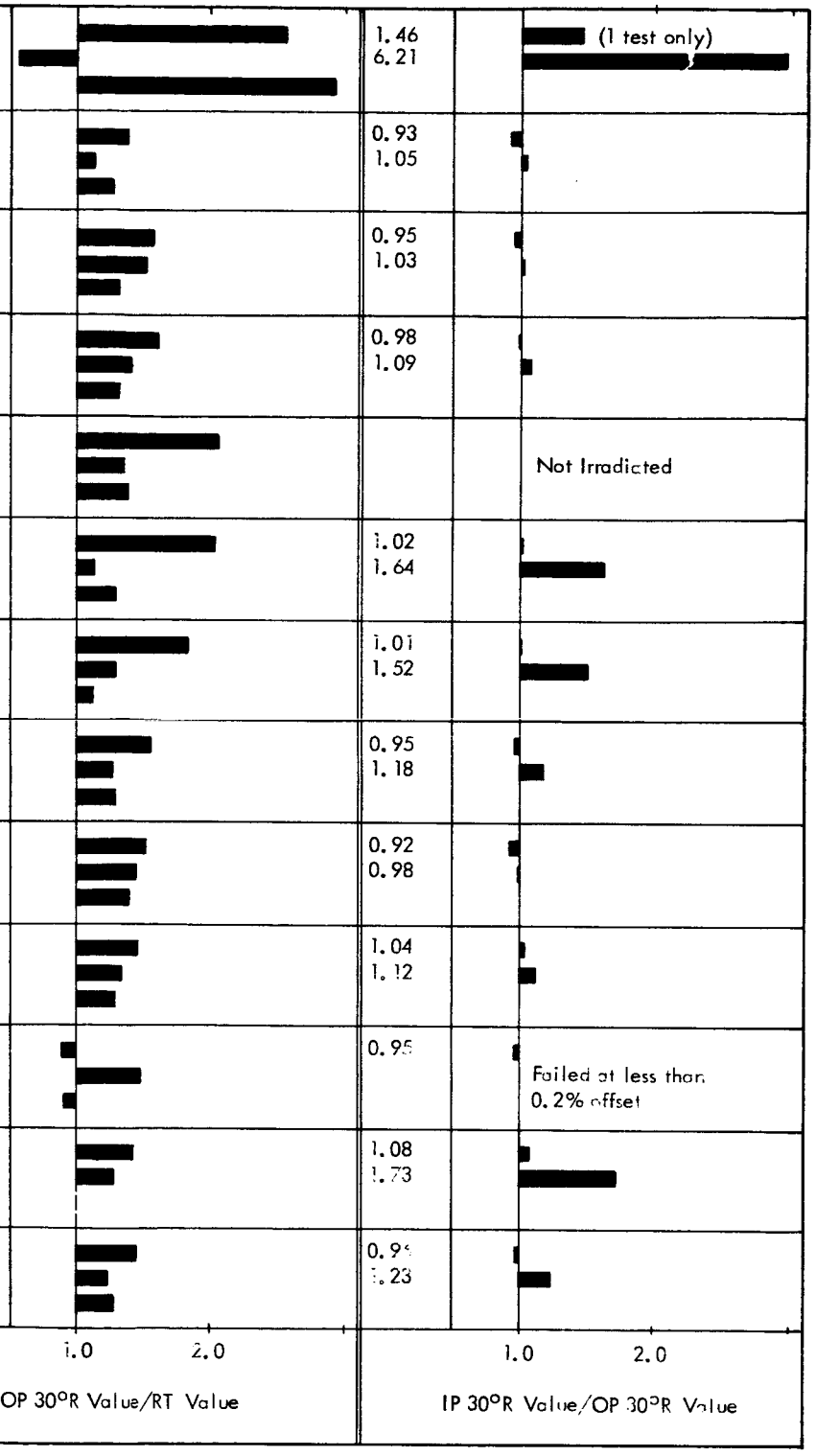

FIGURE 24 TEST VALUE RATIOS FOR ALUMINUM ALLOYS

TITANIUM ALLOYS

55A	F_{tu}	67.00	2.53	1.14	
	F_{ty}	53.50	2.28	1.08	
	F_{tun}	84.28	1.98	1.12	
5 Al-2.5 Sn (Std. I)	F_{tu}	125.20	1.80	1.06	
	F_{ty}	114.80	1.78	1.06	
	F_{tun}	166.80	1.50	1.09	
5 Al-2.5 Sn (Eli)	F_{tu}	126.40	1.81	0.98	
	F_{ty}	113.40	1.89	0.99	
	F_{tun}	153.40	1.74	1.01	
6 Al-4V (Annealed)	F_{tu}	144.00	1.81	1.05	
	F_{ty}	137.80	1.76	1.04	
	F_{tun}	184.40	1.53	1.01	
6 Al-4V (Aged)	F_{tu}	167.60	1.68	1.07	
	F_{ty}	158.60	1.73	1.07	
	F_{tun}	201.80	1.43	1.02	
8 Al-1 Mo-1V	F_{tu}	138.00	1.73	1.09	
	F_{ty}	131.80	1.70	1.08	
	F_{tun}	175.00	1.53	1.06	

NICKEL ALLOYS

Rene 41	F_{tu}	130.20	1.49	1.00	
	F_{ty}	63.20	1.70	1.05	
	F_{tun}	142.80	1.43	0.95	
K Monel	F_{tu}	154.20	1.21	1.01	
	F_{ty}	97.80	1.24	1.14	
	F_{tun}	180.40	1.16	1.01	
Inconel	F_{tu}	138.20	1.35	1.02	
	F_{ty}	131.50	1.34	1.02	
	F_{tun}	179.00	1.24	1.07	
Inconel X	F_{tu}	200.60	1.21	0.99	
	F_{ty}	142.20	1.06	1.07	
	F_{tun}	199.75	1.25	0.92	
Alloy	Function	RT Values	1.0 2.0 OP 30°R Value/ RT Value	1.0 2.0 IP 30°R Value/OP 30°R Value	

FIGURE 25 TEST VALUE RATIOS FOR TITANIUM AND NICKEL ALLOYS

Alloy	Function	RT Values	OP 30°R Value/RT Value	IP 30°R Value/OP 30°R Value
304	F_{tu}	95.14	2.54	1.07
	F_{ty}	36.76	1.07	1.31
	F_{tun}	102.82	1.88	0.90
310	F_{tu}	84.90	2.50	1.03
	F_{ty}	62.64	2.20	0.98
	F_{tun}	112.40	1.68	1.16
347	F_{tu}	94.50	2.51	1.06
	F_{ty}	43.70	1.19	1.23
	F_{tun}	113.80	1.88	1.11
A286 (AMS 5735)	F_{tu}	156.00	1.51	0.97
	F_{ty}	112.20	1.33	1.02
	F_{tun}	181.00	1.20	1.14
A286 (AMS 5737)	F_{tu}	171.80	1.39	1.00
	F_{ty}	133.80	1.17	1.06
	F_{tun}	196.20	1.30	0.94
T-450	F_{tu}	119.60	1.65	0.98
	F_{ty}	38.68	2.36	1.01
	F_{tun}	120.20	1.78	
AM 350	F_{tu}	199.00	1.71	0.92
	F_{ty}	186.40	1.78	0.93
	F_{tun}	239.60	1.12	0.55
17-7 PH	F_{tu}	234.80	1.43	0.75
	F_{ty}	226.60	1.46	0.76
	F_{tun}	266.60	0.68	
A353	F_{tu}	110.60	1.82	1.07
	F_{ty}	88.60	1.97	1.09
	F_{tun}	137.00	1.38	
440C	F_{tu}	315.80	0.83	0.83
	F_{ty}	269.80	Specimen failed at less than 0.2% offset	Specimen failed at less than 0.2% offset
	F_{tun}	217.40	0.50	1.10

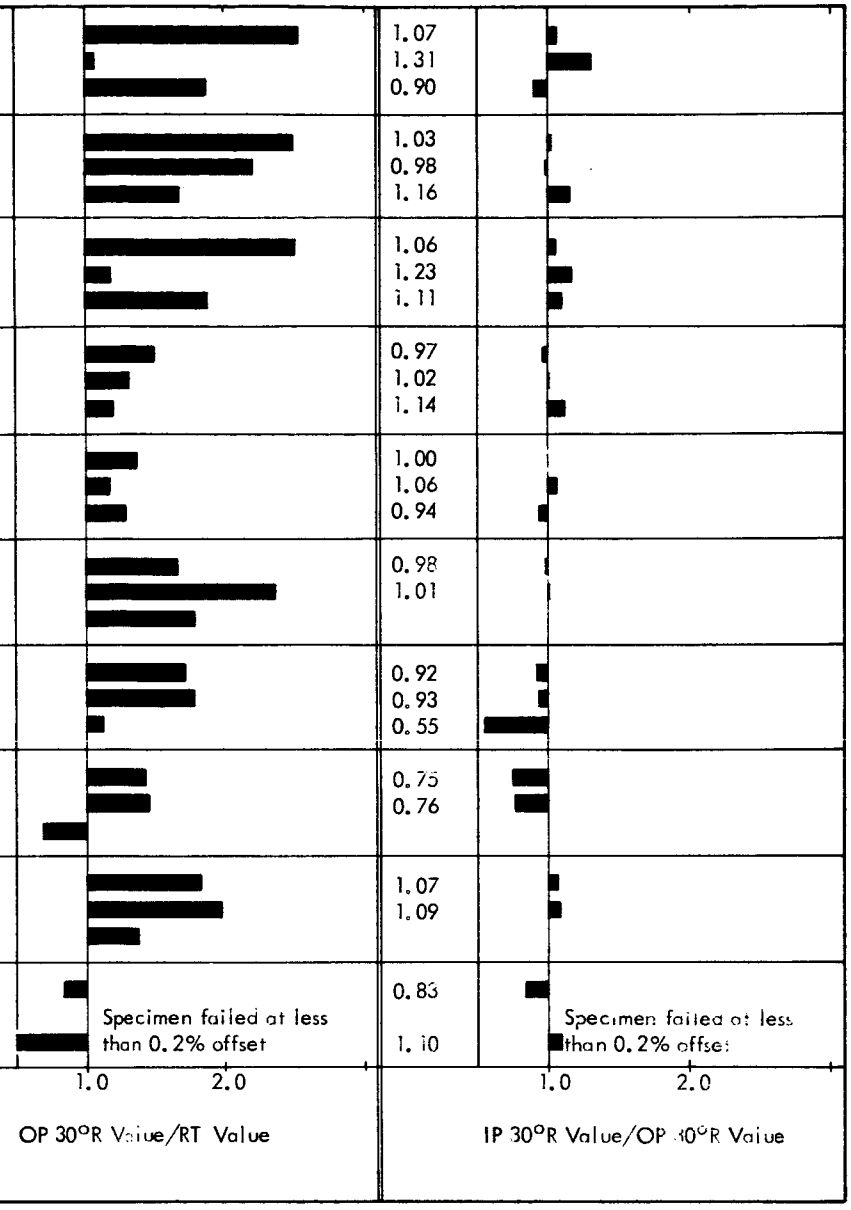

FIGURE 26 TEST VALUE RATIOS FOR FERROUS ALLOYS

5.2.1 Systematic Errors and Miscellaneous Effects

There are certain systematic errors in the control, measurement and recording system which have been discussed in Section 4.2. Some of these errors affecting the strength values may depend on the stress level of the test and on the shape of the stress-strain curve and so may vary from material to material. On the other hand, some of the errors may be compensating, particularly as they effect the biases. The maximum total of these systematic errors, even assuming them to be all cumulative, cannot be accurately assessed but may be estimated at less than a few percent in the strength functions, at least at moderate to high stress levels (50 Ksi and above).

There is a non-random error in the yield strength measurement which arises in the determination of the slope of the so-called elastic portion of the stress-strain curves and as mentioned previously (Section 4.2.5.1) the elastic modulus values must be considered strictly as estimates. However, in nearly all cases where the choice of slope is arbitrary the 0.2 percent offset slope intercepts the stress-strain curve in a region of low rate of hardening (low slope) and large variations in the offset slope do not result in large variations in the yield stress.

There are certain effects that occur in tensile testing of structural materials which, although not strictly a source of error, can account for discrepencies among data produced in different laboratories. These are strain rate effects and specimen size effects, both of which may be dependent on the material structure and grain size.

As indicated in Section 4.2.1, the strain rate used in the screening program was approximately 0.0015 in./in./minute and may have varied by 20 percent or more in certain instances. Data from other laboratories with which the screening program results will be compared was obtained at various strain rates up to 0.01 in./in./minute.

Specimen size effects have been noted in the literature and deserve some elaboration at this point. As described in Section 3.2, miniaturized tensile and tensile notch specimens were used to produce the test results described. Early in the screening program there was concern over the use of such specimens as a source of discrepancy and some comparisons were made between miniaturized and standard specimens from three materials exhibiting a variety of deformation characteristics (Stainless Steel 304, Aluminum 7178 and Titanium 55A).

Large and small round tensile and round tensile notch specimens were tested at approximately 540°R and at liquid nitrogen temperature (140°R). The tensile notch tests were conducted at liquid hydrogen temperature (36°R) as well as at the two higher temperatures. Some statistically significant differences did appear in the ductility values and in the tensile notch strengths but comparison of the screening test results to the pedigree data (produced with standard size specimens at room temperature) did not confirm these differences except in the case of the Stainless Steel 304.

Except for the yield strengths, Stainless Steel 304 shows consistent dependence on specimen size at room temperature. The ultimate strength and elongationwere higher (by approximately 15 percent) in the smaller specimens than in standard size specimens. Although there is not pedigree data to use for confirmation, the tensile notch strength appears to be approximately 15 percent lower in the small specimens than in the standard specimens.

Stainless Steel 304 is unique among the materials investigated for specimen size effects in that it is relatively ductile and has a low yield-to-ultimate strength ratio. It might be tentatively concluded that materials exhibiting these same characteristics will show similar size effects. Stainless Steel 347 is very similar to the Stainless Steel 304 and on the basis of the pedigree data and the screening program values does show the same size dependence.

Tests outside this laboratory[16] on yield and ultimate strengths of Stainless Steel 304, indicate that small specimens (0.125 inch diameter by 1/2 inch gage) have larger test values than the large specimens (0.500 inch diameter by 2 inch gage) but that the absolute magnitude of the difference in the two functions produced by irradiation is unaffected by specimen size up to 8.6×10^{20} nvt.

The possible size effects should be classed with possible material stock (whether bar or sheet) effects by design engineers, using the absolute values presented in this report with appropriate caution. It can be emphasized that the value of the screening program test values as indication of sensitivity of various materials to irradiation effects at 30°R is in no way impaired by the use of miniaturized specimens, with the exception of the tensile notch values as noted in Section 3.2.2.

5.2.2 Scatter in Test Values Due to Random Error

There are natural random errors in readings and calibrations as well as random variations in the actual properties of the materials tested, all of which are indicated

by the standard deviation of the test values from the mean of the values.

Errors in elongation and reduction-of-area measurements from tensile test specimens are generally larger than errors in strength measurements. Part of the error in elongation measurements is attributable to imperfect fitting together of failed specimen parts for the final length measurement and therefore is not totally a random error and is of more importance in the low values.

Large errors in the reduction-of-area measurements result from inability to accurately determine minimum diameters after failure and, as is seen in Tables 4 , 5 and 6 , impossible values (geometrical considerations require that the reduction in area be larger than the measured elongation) sometimes result. Further discussion in this report will generally not include mention of reduction-of-area values. Errors in the reduction-of-area measurements naturally are included in the fracture stress values.

Actual variations in material properties may be more pronounced at cryogenic temperatures. This would be expected in brittle materials or in materials having fabrication defects. It would be particularly true in the austenitic steels in which phase transformations will occur during deformation at low temperatures.

Standard deviations might be expected to be greater in the nuclear-cryogenic tests than in the cryogenic tests, partly due to errors in the integrated flux determination and partly due to differences in dose rate which can vary by about a factor of two from test to test. Also there is somewhat greater difficulty in the measurements in irradiation tests and a greater chance for specimen misalignment during the required remote operation in these tests.

The use of only three tests in the irradiation portion of the program results in a statistical increase in the standard deviation which is not apparent in the data.

A review of the standard deviations of the strength values for all the materials at all test conditions (Appendix B) reveals that for most of the tests in the screening program the standard deviations are less than 5 percent of the mean values.

The standard deviations of the elongation values are assumed to be approximately half of the difference between extreme values[14] for a particular material and test condition and nearly all of these deviations are less than twenty-five percent of the means if the tests on the aluminum alloys out-of-pile at 30°R are excepted.

Certain variations in the standard deviations as percentages of the test values are apparently dependent on the test and on the materials and test conditions and may

be grouped according to the major constituent of the alloy:

Aluminum Alloys

Low strength alloys (1099 and 5000 series) and casting alloys (X 250, B 750 and A 356) exhibit more scatter at RT than other aluminums with the exception of Al 2219 which exhibits inexplicably high scatter at RT.

In the aluminum alloys as a group there is increased scatter at 30°R particularly in F_{tun} and elongation. Also, there is no general difference in scatter with irradiation but there are no very high (> 10%) deviations as in the other two test conditions.

The high deviations in the values from the low strength materials (particularly Al 1099) can be explained in part, at least, by larger percentage errors in the measurement and recording systems at the lower load levels.

The generally high deviations in the strengths of X-250 and A-356 is due to imperfections in the cast specimen stock.

Titanium Alloys

With the exception of Ti 55A which is a low strength material, the strengths of titanium alloys exhibit less deviation than the aluminum alloys.

There is some apparent dependence in the deviations of the test values on temperature with the deviations being somewhat higher, for the titanium alloys as a group, at the out-of-pile 30°R condition than at room temperature.

Nickel Alloys

Scatter in the test values from the nickel alloys appears to be similar to that from the high strength titanium alloys with the exception of Inconel X which has standard deviations greater than five percent for all three strength functions at 30°R.

Ferrous Alloys

The variations in the strengths of the austenites, 304, 310 and 347 show a large dependence on temperature with many of the deviations at 30°R and 30°R IP being greater than 10 percent of the test values.

The A 286 (5737) values appear to exhibit more scatter than the A 286 (5735) values.

Values from 440C have consistently high deviations (5-10 percent).

Of all the alloys tested, T-450 is the only exception to the general rule that the percentage deviations are higher at the cryogenic temperature.

The random scatter in the changes due to environments as indicated by the ranges of the bias (Figures 21, 22 and 23) which represent a somewhat complex combination of the room temperature scatter and scatter at 30°R in the case of the cryogenic effects and a similar combination of the scatter at 30°R and that in-pile at 30°R in the case of irradiation tend to confirm these conclusions but indicate in addition that there is an appreciable increase in scatter in one or more of the strengths of certain materials which is associated with irradiation testing. These materials are:

Aluminum Alloys, 2024, 7079 and 7178
Titanium Alloys, 55A and Ti 5% Al-2.5% Sn (Std. I)
Stainless Steels, 310 and 347

5.2.3 Comparison of Room Temperature Test Results To The Pedigree Data

There is generally good agreement between the test values obtained at room temperature in the screening program and the pedigree data supplied by the vendors of the materials tests.

One difficulty in making this comparison is that the quality of the pedigree data is not known. The pedigree data represents results from sample lots generally smaller than the five specimen lots used in the room temperature testing in the screening

program and the vendors only supplied mean test values, without indications of scatter in the values. It is assumed for the purposes of this discussion that the quality of the pedigree data is similar to that of the screening program data.

The following alloys show very good agreement between the screening program data and the pedigree data: (The F_{tu} and F_{ty} values, including the standard deviations, from the screening program fall within plus or minus 5 percent of the pedigree values.)

Aluminum Alloys, 1099, 2014, 2219, 7079, X-250 and A 356
Titanium Alloys, 55A, Ti 5% Al-2.5% Sn (ELI) and Ti 6% Al-4% V (annealed) and Ti 6% Al-4% V (aged)
Nickel Alloy, Inconel (cold drawn)

The following alloys show small differences between the screening program data and the pedigree data, in at least one strength value, which are noted as follows:

Aluminum 2024, K Monel and A 286 (5735) all have F_{ty} values about 5 percent lower than the pedigree values.

Inconel X has F_{tu} and F_{ty} which are somewhat high with respect to the pedigree values.

The elongation values obtained at room temperature in the screening program appear to be somewhat high ($\approx$10 percent) when compared with the pedigree data from the following alloys:

Aluminum B-750
Titanium 8% Al - 1% Mo - 1% V
Stainless Steel A 286 (AMS 5735 and AMS 5737)
Austenitic Manganese Steel T-450
Stainless Steel AM 350

The room temperature elongation value from Aluminum 5086 appears to be low when compared with the pedigree data.

The following aluminum, titanium and nickel alloys tested in the screening program show room temperature values of F_{tu} and F_{ty} which are about 5 to 10 percent low

with respect to the pedigree data:

Aluminum Alloys, 5083, 5456, 6061 and 7178
Titanium 5% Al - 2.5% Sn (Std. I)
René 41 (nickel alloy)

The elongations from this group of alloys are in fair agreement with the pedigree values with the possible exception of Aluminum 5083, which gave a range of values lower than the pedigree value, and Titanium 5% Al - 2.5% Sn and René 41 which have ranges of values higher than the pedigree values.

As discussed earlier there is serious disagreement between the room temperature screening program test values and the pedigree data from the Stainless Steels 304 and 347 which may possibly be attributed to the use of miniaturized test specimens in the screening program. The Stainless Steel 310 elongations were also high with respect to the pedigree data but its F_{tu} value was low as were the F_{tu} values from SS 304 and SS 347.

Stainless Steel 17-7 PH gave strength values that were high (by more than 10 percent) with respect to the pedigree strengths while the Nickel Alloy Steel ASTM A 353 gave strength values that were low (by more than 10 percent). The elongations of both of these alloys were in fair agreement with the pedigree data. It must be noted that the pedigree specimens of A 353 were stress relieved before testing while the screening program specimens were not.

The pedigree data for Stainless Steel 440C is obviously in error but typical manufacturer values would indicate that the ultimate tensile strengths measured from this alloy at room temperature in the screening program are high by about 10 percent while the yield strength values are reasonable.

5.2.4 Comparison of OP 30°R Test Results To Other Cryogenic Data

There are low temperature mechanical properties test data from outside sources for many of the materials tested in the screening program and most of these data appear in the Cryogenic Materials Data Handbook[1] which is a compilation of data from various sources as indicated earlier, in Section 2. In addition there are data supplied by the Aluminum Company of America on certain of the aluminum alloys.[17]

In all instances the data are from specimens of different size and shape from those used in the screening program and it is assumed that various test conditions such as strain rate are also different. Therefore, the comparisons of data which have been made will not be described in the same detail as the comparisons with the pedigree data.

Even when there are known differences in technique, room temperature and cryogenic data from a particular material from an outside laboratory have been used for comparison when the room temperature data are in agreement with either the screening program or pedigree data. In certain instances when the room temperature data are not in good agreement with the screening program data but are in fair agreement with the pedigree data, the absolute changes due to the cryogenic environment are compared. This is on the assumption that the differences due to environment are less sensitive to many experimental variables than the absolute values.

Tensile yield and tensile ultimate strength values at 30°R for twenty-three (23) of the materials tested in the screening program are compared with results from similar materials from various laboratories measured at a slightly higher temperature (≈36°R). Elongation values generally are not noted except where differences are very large, because this function is known to be sensitive to specimen shape and strain rates.

It is assumed that the data are of a quality similar to the screening program data with respect to scatter in the test values.

In general, agreement is good, with differences in the absolute values at cryogenic temperatures rarely greater than 10 percent of the values or the differences due to cryogenic environment rarely differing by more than a few percent.

The following alloys are not compared because there are not readily accessable cryogenic data from similar material stocks at similar test conditions:

Aluminum Alloys, 1099, 5083, 5086, X-250, B-750
Titanium 55A
Stainless Steels, A-286 (AMS 5737), AM 350, 440C

Aluminum 7079 was not compared. Although there are data from material of nominally the same composition, the strength values are so much lower than the screening program values at both temperatures that it must be concluded that the materials and/or test conditions are not equivalent.

The following alloys show good agreement (within ten percent) between cryogenic strength values obtained in the screening program and values obtained elsewhere:

Aluminum Alloys, 2014, 2024, 2219, 7178, A-356

Titanium Alloys, Ti 5% Al-2.5% Sn (ELI), Ti 8% Al-1% Mo-1% V

Inconel X

Stainless Steel A-286 (AMS 5735)

The following alloys show good agreement (within ten percent) between differences due to cryogenic environment obtained in the screening program and values obtained elsewhere:

Aluminum 5456

Nickel Alloys, René 41 and Inconel (cold drawn)

Austenitic Manganese Steel T-450

Nickel Alloy Steel ASTM A-353

The screening program test values from the following alloys at cryogenic temperature show minor discrepencies with other data as noted:

Aluminum 6061, F_{tu} from the screening program about ten percent below the other values

Titanium 6% Al - 4% V (annealed) and Ti 6% Al - 4% V (aged) F_{tu} and F_{ty} low

Nickel Alloy K Monel, elongation value low

The following alloys show large discrepencies between at least one of the cryogenic strength values obtained in the screening program and values obtained elsewhere as noted:

Titanium 5% Al - 2.5% Sn (Std. I), difference from the screening program due to cryogenic temperature in F_{tu} and F_{ty} are more than twenty percent below other values.

Stainless Steels 304 and 347, F_{ty} values appear to be about twenty percent low

Stainless Steel 310, F_{tu} and F_{ty} values both high

Stainless Steel 17-7 PH, F_{tu} values unusually low ($\approx$ 100 ksi)

5.2.5 Comparison of In-Pile 30°R Test Results To Other Nuclear Cryogenics Data

Nuclear cryogenic data from other sources similar to that obtained in the screening program is very fragmentary. And as numerous writers have pointed out comparison of results from irradiation effects experiments by different investigators is difficult, in general, due to significant differences in irradiation and test conditions such as neutron spectrum.

However, there are nuclear cryogenic data from another source[18] for five materials at the same nominal composition as five of those tested in the screening program. These data have been compared although there are known differences in irradiation and test temperatures, material stocks, specimen shapes, strain rates and methods of strain measurement that can affect the results. The five materials are:

Aluminum 6061
Aluminum A-356
Titanium 5% Al - 2.5% Sn (ELI)
Inconel X
Stainless Steel A 286

There are no serious discrepencies between the two sets of data. In fact, there is remarkably good agreement in certain cases. Both sets of data show significant irradiation induced increases in the yield strengths of Aluminum 6061 and Aluminum A-356 which are nearly equal and neither set shows significant irradiation effects on the yield strengths of the other three alloys.

Also in agreement with these test results, other observers[19] have noted a decrease in the tensile strength of copper bearing aluminum alloys resulting from cryogenic irradiation.

6 ANALYSIS OF TEST RESULTS

The program objectives, as described in Section 1, were principally oriented towards obtaining engineering data rather than theoretical model formulation. For this reason, the materials selected for testing are, in general, the fairly complex structural polycrystalline aggregates in a variety of tempers normally used in structural application rather than the pure metals or simple binary alloys generally used for solid state mechanism studies. However, the test results may be analyzed with respect to the compositions and structures of the materials and do present some opportunity for interpretation with the possibility of yielding fundamental conclusions generally applicable to nuclear cryogenic effects in alloys.

A summary of the test results, presented in detail in Appendix B, has been given in Section 5 of this report. Analysis of the test results is given for each alloy group in the following sections.

Metallographic and, to a lesser extent, X-ray diffraction studies were undertaken to supplement the mechanical properties test data in an effort to provide additional information for analysis of the irradiation effects. Variations in metallographic techniques between irradiated and non-irradiated specimens, presented in Appendix C, sometimes cause apparent structural differences which are not actually present in the material. Each instance of actual structural alteration considered to be of real significance is discussed in the section describing the individual alloy. Other apparent differences in structure observable in the figures in Appendix C are considered to be ascribable to polishing and etching techniques rather than to structural anomalies resulting from either cryogenic or irradiation environments.

A qualitative interpretation of certain test results in terms of generally accepted cryogenic and nuclear irradiation phenomena in metals and alloys is presented in Section 7.

6.1 ALUMINUM ALLOYS

Aluminum does not exhibit the isothermal allotropic crystallographic phase transformation present in some other metals; therefore, a face centered cubic crystal structure is stable at all temperatures below the solidus temperature for the aluminum alloys tested in this program. The aluminum alloys tested fall naturally into two

separate categories: wrought alloys and cast alloys. The wrought alloys are those which receive mechanical forming at elevated temperatures after final solidification. The preheating of the ingots prior to mechanical working and the working itself have profound metallurgical effects on the material. During these operations, the initial cast structure of the ingot, dendritic or cored as the photomicrographs of the three casting alloys in Appendix C illustrate, is mechanically broken up, the material composition is homogenized by diffusion at elevated temperature and any casting voids or porosity generated by shrinkage during solidification are welded closed. Since these treatments may alter mechanical properties to as great a degree as changes in chemical composition, the 10 wrought aluminum alloys tested in this program are treated separately from the three casting alloys.

An additional distinction, response to heat treatment, is present in the wrought alloys which provides a basis of classification for these materials. Aluminum alloys are essentially substitutional solid solution type alloys, but in some compositions deliberate additions of metals are included which have a limited solubility in aluminum at room temperature and a tendency to form inter-metallic compounds with aluminum or with each other. The solid solubility of these inter-metallics in aluminum is a temperature dependent function; therefore, the distribution and size of precipitates of the inter-metallics can be controlled by appropriate thermal treatment. This program included six heat treatable wrought aluminum alloys: three in which copper (as $CuAl_2$ and Al_2CuMg) is the principal hardening agent, the 2000 series alloys; one in which a complex system of Al-Cu-Mg-Si inter-metallic compounds provides the precipitate, Aluminum 6061; and two in which the additives cause the formation of $MgZn_2$ and complex Al-Zn-Mg compounds as the principal hardening agents, the 7000 series alloys. The hardening effect of these inter-metallics depends on their precipitation after a solution heat treatment. This can be accomplished by several methods and the various heat treat conditions, together with their standard designations, are given below:

Solution treatment followed by strain hardening - T3

Solution treatment followed by natural (room temperature) aging - T4

Artificial aging after rapid cooling during processing - T5

Solution treatment followed by artificial aging - T6

Solution treatment followed by strain hardening followed by artificial aging - T7

Solution treatment followed by artificial aging followed by strain hardening - T8

Sometimes, additional digits are used to designate exact material histories. Alloys were tested in several of the above conditions during this test program.

Pure aluminum, Aluminum 1099, and aluminum alloys containing alloying additions (such as magnesium) with moderate solid solubility in aluminum, the 5000 series, will not respond to thermal hardening due to the absence of inter-metallics and the presence of a stable terminal substitutional solid solution in the system equilibrium (phase) diagram.[20] These alloys are hardenable only by cold work.

The alloy temper designations indicate the degree of strain hardening the material has received. The letter - O - after the alloy designation indicates that the material has been fully annealed after the final cold work and is in a dead soft condition. The designation - H 1 - indicates that the alloy has been cold worked for strain hardening after the final anneal. A second digit from two through nine indicates the degree of cold work, -H 19 - indicating extra hard, - H 18 - indicating full-hard, commercial grade and - H 14 - indicating a tensile strength approximately midway between the - O - and - H 18 - conditions. If the alloy has been partially annealed after strain hardening, the one that forms the initial digit is changed to two. For alloys requiring and receiving a stabilizing thermal treatment after cold work, the initial digit is changed to three. Sometimes a third digit is used to indicate slight variations from these standard treatments.

Examination of the test results as shown in Figure 21 indicate that irradiation environments have a greater over-all effect on the mechanical properties of the strain hardening materials but a more pronounced deleterious effect on the precipitation hardening alloys.

Changes in the values of several functions due to cryogenic environment and due to irradiation are presented in Figures 21 and 24 and the arithmetic means of these test values are presented in Table 4. The magnitude of these changes is shown in Figure 21 and the ratios of the environmentally altered test value to the initial values are shown in Figure 24.

The aluminum alloys may be grouped for discussion of both their cryogenic and irradiation effects according to their nominal compositions.

The high purity Aluminum, 1099, shows real and sizable effects due to cryogenic environment, and also to the combined nuclear-cryogenic environments, which are not similar to effects in the alloyed aluminums.

The alloys 2014, 2024 and 2219, which are similar in composition and strength, behave similarily, with 2024 and 2219, being most alike in their behavior in the cryogenic environment; the ranges of their biases due to the cryogenic environment in the functions shown overlap.

Similarities between the alloys 5083, 5086 and 5456 are most remarkable, with their changes in ultimate strength due to the cryogenic environment and their changes in ultimate strength and yield strength due to irradiation being approximately the same. The changes in their yield strengths due to cryogenic environment are apparently dependent on their proportional content of magnesium, as might be expected.

Alloys 7079 and 7178 are somewhat similar in their cryogenic behavior but not in their behavior under irradiation. The only significant change due to irradiation in these two alloys is the increase in the tensile yield strength for alloy 7178.

The casting alloys do not have much in common except that B-750 and A-356 show similar cryogenic changes in the ultimate tensile and tensile yield strengths. This would appear to be coincidental since there is no similarity in their compositions.

In evaluating the radiation induced changes in the mechanical properties of these alloys, it should be kept in mind that the accumulated dose received by each specimen was 1×10^{17} nvt ($E > 0.5$ Mev). This may well be below the threshold level for some significant effects in these materials, which are therefore undetectable at this relatively low irradiation exposure.

More detailed discussions of the aluminum alloys follow.

6.1.1 Aluminum 1099 -H 14

This alloy is a high purity commercial grade of aluminum in which solid state effects are relatively unaffected by the presence of "foreign" solute atoms or second phase constituents.

The behavior of this material at cryogenic temperature was unique among the materials tested in the screening program. A major (x 2.56) increase in ultimate tensile strength and in elongation (from 23 percent to 61 percent) was accompanied with a reduction in the absolute value for the tensile yield strength (x 0.56) at 30°R, unirradiated, compared with room temperature test results. The F_{ty}/F_{tu} ratio decreased from 0.94 to 0.22 as a result of the 30°R environments.

Photomicrographs of this material are shown in Figure C 1 of Appendix C. Comparison of the fracture areas of the room temperature and the 30°R, unirradiated specimens offers confirming evidence of a change in strain pattern at cryogenic temperatures. The grain distortion during plastic flow at room temperature consisted of longitudinal elongation of the individual grains; at 30°R planes of mechanical twinning at 45° to the axis of loading were observed. Mechanical twinning of face centered cubic lattice metals, while not observed during room temperature testing, has been reported during cryogenic straining of single crystals.(21)

Although three specimens were tested at 30°R after irradiation to 1×10^{17} nvt, inadvertent variations in test conditions in two instances influenced the data to a degree which precluded direct comparison of test results among the three specimens. One test specimen was prestressed prior to irradiation which added an unknown degree of cold work in the specimen at the time of initial application of the monitored stress. A second test specimen obtained an unknown quantity of self-annealing after receiving approximately eighty percent of the desired irradiation when a temporary refrigeration system malfunction allowed the specimen temperature to increase to about 70°R. The temperature was restabilized at 30°R after ten minutes and the irradiation period was completed. One specimen was tested in the non-prestressed condition after a complete irradiation exposure to 1×10^{17} nvt at 30°R. The test results from this single specimen showed radiation induced effects of an increase by a factor of 1.46 in ultimate tensile strength accompanied by a factor of 6.21 increase in tensile yield strength and a decrease in elongation from sixty-one percent to forty-six percent. The F_{ty}/F_{tu} ratio increased to 0.88, indicating an almost complete recovery to the room temperature value.

The change in tensile yield strength values due to irradiation is mitigated by either prestressing or low temperature self-annealing. The specimen tested at 30°R, irradiated to 1×10^{17} nvt after prestressing and the one which obtained a degree of self-annealing at $\approx$70°R, reported in Table B-1, Appendix B, gave similar test results with an increase in ultimate tensile strength by a factor of 1.31. The tensile yield increased by a factor of 3.5 and the F_{ty}/F_{tu} ratio increased to approximately 0.70.

Comparison of the photomicrographs of the fracture area shown in Figure C 1, Appendix C, shows the presence of mechanical twinning only in the specimen tested at 30°R with no irradiation exposure. This confirms a radiation induced increase in critical shear stress to above the level required for macroscopic strain of the material.

X-ray diffraction patterns for the material after testing under the three sets of test conditions are shown in Figure 27. They tend to confirm the presence of twinning only in the specimen tested at 30°R without irradiation.

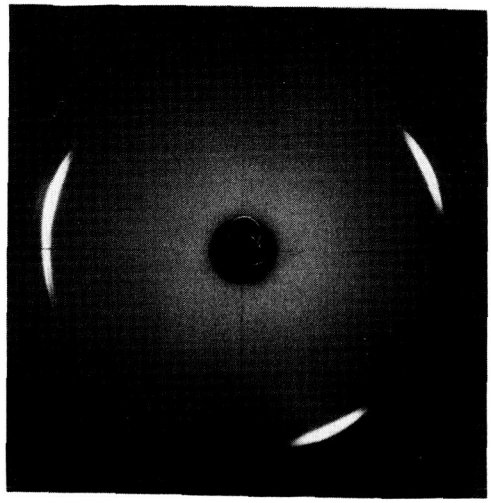

(a) Back reflection from deformed region of specimen failed at room temperature, showing preferred orientation with considerable grain distortion

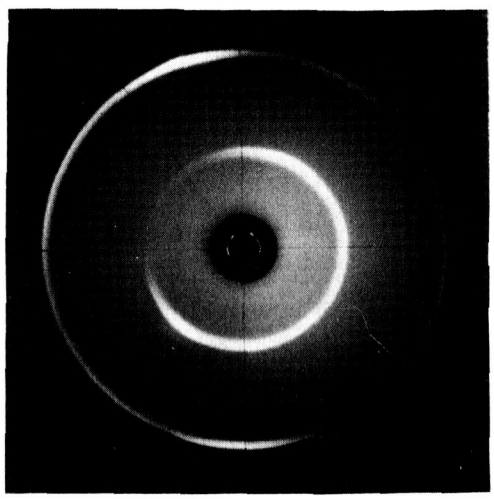

(b) Back reflection from deformed region of specimen failed at 30°R without irradiation, showing less preferred orientation than in (a) but somewhat higher degree of grain distortion

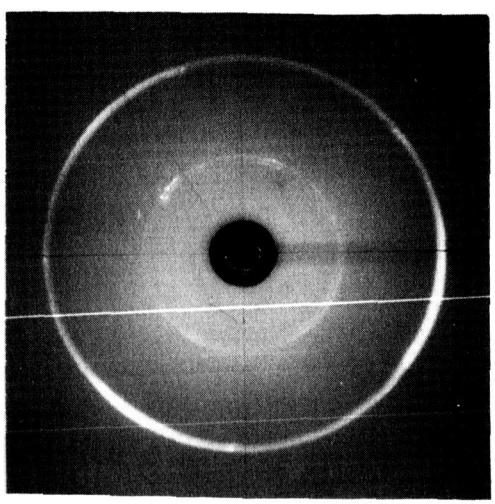

(c) Back reflection from deformed region of specimen failed at 30°R after irradiation of 10^{17}nvt, showing preferred orientation as in (b) but very limited grain distortion

FIGURE 27 X-RAY DIFFRACTION PATTERNS FROM ALUMINUM 1099

6.1.2 Aluminum-Copper Alloys

The copper bearing aluminum alloys have a hardening response to thermal treatment caused by the temperature dependence of the solubility limit of copper intermetallic compounds in solid solution with aluminum as the solvent. The intentional addition of two or three atomic percent of solute atoms or alien precipitates with greater mass and smaller atomic radii than the matrix atoms influences both the cryogenic and irradiation behavior of these alloys.

A reduction in the arithmetic mean of the ultimate tensile strength is shown in Figure 21 for all of the aluminum-copper alloys after irradiation at 30°R.

Additional experimental work at higher irradiation levels might be desirable for the aluminum-copper alloys due to the indication of deleterious irradiation effects with a threshold as low as 1×10^{17} nvt.

6.1.2.1 Aluminum 2014 - T651

This alloy was tested in the solution heat treated and thermally aged condition. The cryogenic effect in this alloy was significant. The ultimate tensile strength was increased by a factor of 1.39, accompanied by an increase by 1.13 in tensile yield. The F_{ty}/F_{tu} ratio decreased from 0.92 to 0.75 with a resultant significant increase in elongation from twelve percent to eighteen percent.

The specimens tested at 30°R after an accumulated fast neutron exposure of 1×10^{17} nvt showed a slight decrease in the mean ultimate tensile strength (x 0.93) with no statistically significant (at the ninety percent confidence level) change in tensile yield strength, compared with unirradiated specimens tested at 30°R. The elongation reverted to the room temperature values and the F_{ty}/F_{tu} ratio showed almost complete recovery to the room temperature values. The reduction in mean ultimate tensile strength resulting from irradiation is of questionable practical significance due to the scatter of the test data as indicated by the range of the bias.

Photomicrographs of this material are shown in Figure C 2 of Appendix C. Comparison of the fracture areas of the room temperature and the 30°R, unirradiated, microstructures shows a diminution in strain hardening during stressing to failure evidenced by the reduction of grain elongation parallel to the axial loading direction. This confirms the observed reduction in F_{ty}/F_{tu} ratio and the increase in reported elongation.

6.1.2.2 Aluminum Alloy 2024 - T 351

This alloy material received its hardening treatment by strain hardening rather than by aging after solution heat treatment. The cryogenic effect in this alloy increased the 30°R ultimate tensile strength by a factor of 1.59 and the tensile yield strength by a factor of 1.53, causing only a minor, and probably not significant change in the F_{ty}/F_{tu} ratio. The elongation was not significantly affected.

The mean ultimate tensile value decreased after irradiation, but the magnitude of test data scatter, indicated by the range of the bias in Figure 21 , exceeds the difference and the validity of the apparent reduction in F_{tu} is not statistically significant at the chosen confidence level (ninety percent). A slight (x 1.03) but statistically significant increase in the F_{ty} resulted from the irradiation; elongation dropped from 22.3 percent to 16.3 percent as a result of irradiation. The photomicrographs shown in Figure C 3 of Appendix C show no significant structural difference between the unirradiated specimen tested at room temperature and at 30°R. Any apparent difference is attributable to variations in polishing and etching techniques.

Any possible change in strain hardening rate, such as was observed in Aluminum 2014 - T 651, is obscured in metallographic examination by the prior cold work of the material required to produce the -T 351 condition.

6.1.2.3 Aluminum 2219 - T 87

This copper bearing alloy, incorporating additions of several minor constituents to increase the mechanical properties at elevated temperature, received combined strain and precipitation hardening treatments (aging) after solution heat treatment prior to testing. The cryogenic effect in this alloy increased the 30°R ultimate tensile strength by a factor of 1.62 and the tensile yield strength by 1.42. The drop in F_{ty}/F_{tu} ratio from 0.81 to 0.71 was accompanied by a very slight increase in elongation.

A slight decrease (x 0.98) apparent in F_{tu} due to irradiation is not significant at the ninety percent confidence level. A slight increase (x 1.09) in F_{ty} due to irradiation is significant. The elongation was virtually unchanged.

No significant structural changes were observed in the photomicrographs shown in Figure C 4, Appendix C. Any structural variation would appear to be masked by the prior cold work of -T 87 temper material; any apparent variation is attributable to variations in polishing and etching techniques.

6.1.3 Aluminum-Magnesium Alloys

This series of aluminum alloys does not show a hardening response to thermal treatments. The temper of these materials is controlled by the degree of cold work received after the final anneal.

These alloys appear to have a significant irradiation induced increase in tensile yield strength accompanied by a reduction of elongation. However, the irradiation induced reduction of ductility should not be considered as indicative of serious embrittlement since the elongation values obtained at 30°R, x 10^{17} nvt remained larger than the room temperature, unirradiated, values.

6.1.3.1 Aluminum 5083 - H 321

This alloy showed large cryogenic effects. The increase in the ultimate tensile strength is about by a factor of 2.06. The factor of 1.35 increase in tensile yield caused a diminution in F_{ty}/F_{tu} ratio from 0.69 to 0.45 with an increase of elongation from eleven percent to twenty-one percent.

No tests had been run on this material after irradiation at the termination of the screening program.

6.1.3.2 Aluminum 5086 - H 32

This alloy has a cryogenic behavior quite similar to that of Aluminum 5083. The principal observable difference between the two materials is the smaller increase in tensile yield strength of 5086 at 30°R (x 1.13). The ultimate tensile strength of 5086 was increased by approximately a factor of two. The F_{ty}/F_{tu} ratio was reduced from 0.70 to 0.39 with an accompaning increase of elongation from eleven percent to thirty percent.

Test results obtained at 30°R after an integrated exposure of 1×10^{17} nvt (fast) indicated a negligible change in the ultimate tensile strength accompanied by an increase (x 1.64) in tensile yield strength. The F_{ty}/F_{tu} ratio increased from 0.39 to 0.63 but the material retained an elongation of about twice its room temperature value.

Examination of the photomicrographs shown in Figure C 6 of Appendix C show no significant structural change; any such change would appear to be masked by the prior cold work of the material. The enlarged etch pits in the irradiated condition are attributable to variation in the etching technique.

6.1.3.3 Aluminum 5456 - H 321

The irradiation and cryogenic effects in this alloy are similar to those of the other two magnesium containing alloys. The cryogenically induced increase in ultimate tensile strength was by a factor of 1.85; in tensile yield, x 1.29. The decrease in F_{ty}/F_{tu} ratio from 0.68 to 0.48 was accompanied by an increase of about fifty percent in elongation.

The specimens tested at 30°R after irradiation to 1×10^{17} nvt (fast) showed a negligible increase in ultimate tensile strength and an increase in tensile yield strength by a factor of 1.52. The F_{ty}/F_{tu} ratio, therefore, increased to 0.72 but the elongation remained above room temperature values. Only two specimens of this material had been tested after irradiation at the termination of the screening program.

The photomicrographs shown in Figure C 7, Appendix C, show no significant structural change, with the exception that the fracture at 30°R appears to be more brittle than the fracture at room temperature. Any other apparent differences are attributable to variations in polishing and etching techniques.

6.1.4 Aluminum-Magnesium-Silicon Alloys-Aluminum 6061 - T 6

This alloy was hardened by thermal treatment through age hardening after solution heat treating. The cryogenic environment increased the ultimate tensile strength (x 1.57) and the tensile yield strength (x 1.26) in this alloy. The resultant F_{ty}/F_{tu} ratio decreased from 0.92 to 0.74, accompanied by an increase in elongation from eighteen percent to thirty percent.

The test results obtained at 30°R after irradiation to 1×10^{17} nvt (fast) indicated a slight drop (to 0.95 of OP value) in ultimate tensile strength and a significant increase (x 1.18) in tensile yield strength. The recovery of the F_{ty}/F_{tu} to 0.92, suprisingly, was not accompanied with a significant change in elongation.

The photomicrographs in Figure C 8, Appendix C, show no significant irradiation induced changes. Photomicrographs of the 30°R, unirradiated, specimens are not available.

6.1.5 Aluminum-Zinc Alloys

This series of alloys is hardenable by solution heat treatment followed by artificial aging.

6.1.5.1 Aluminum 7079 - T 6

The cryogenic environment increased the ultimate tensile strength value by a factor of 1.53 and the tensile yield by 1.46 at 30°R in this alloy. The F_{ty}/F_{tu} ratio showed a moderate reduction from 0.94 to 0.89 while elongation was reduced from eleven percent to six percent.

The test results for the specimens tested at 30°R after an exposure of 1×10^{17} nvt (fast) showed a slight reduction in both ultimate tensile strength and tensile yield strength (x 0.92 and x 0.98 respectively) with little change in elongation as a result of irradiation. However, the scatter in test data indicated by the bias range in Figure 21 makes the validity of these reductions in mean value questionable.

The photomicrographs shown in Figure C 9 show no significant structural changes. The surface recrystallization observed in the material pedigree sample was removed during specimen fabrication and thus had no effect on test results. Any apparent difference is attributable to variations in polishing and etching techniques.

6.1.5.2 Aluminum 7178 - T 651

The cryogenic effect on this alloy resulted in an increase of ultimate tensile strength by a factor of 1.47 and of tensile yield by 1.34. The drop in F_{ty}/F_{tu} ratio from 0.92 to

0.83 was not accompanied by an appreciable change in elongation.

Tests on the specimens at 30°R after irradiation to 1×10^{17} nvt (fast) showed a probable increase in mean ultimate tensile strength (x 1.04) and a significant increase in tensile yield strength (x 1.12). The increase in F_{ty}/F_{tu} ratio from 0.83 to 0.90 was accompanied by a decrease from twelve percent to six percent in elongation. The increase in mean ultimate tensile strength is smaller than the scatter in test data, as Figure 21 shows, and therefore of questionable significance. However, the increase in tensile yield strength shown in Figure 21 is statistically significant.

The photomicrographs shown in Figure C 10 show no significant change in microstructure. Any apparent difference is attributable to variations in polishing and etching technique.

6.1.6 Casting Alloys

Although there is no particular relationship of chemical composition among the three casting alloys tested, they are grouped together because of the structural resemblance of castings in general.

All three aluminum casting alloys were gravity-feed cast either in sand molds or cast iron permanent molds. This casting technique frequently results in the production of microscopic voids with a random distribution or of inter-dendritic shrinkage cavities. Both types of discontinuities were observed in the cast materials and are shown in the photomicrographs in Appendix C, Figures C 11, C 12 and C 13.

Although the presence of discontinuities of these types has an adverse and non-reproducible effect on the mechanical properties, their presence is common in gravity-feed castings and the test data for these materials can be considered typical for these alloys produced using these techniques.

6.1.6.1 Aluminum X 250 - T 4

This material is primarily an aluminum-magnesium-zinc alloy, sand cast. At 30°R, the tensile yield strength increased by a factor of 1.5 while the ultimate tensile

strength was reduced (x 0.88). This increased the F_{ty}/F_{tu} ratio by about one third. The material exhibited nil ductility at 30°R, contrasted with twenty-one percent elongation at room temperature.

The specimens tested after irradiation at 30°R to 1×10^{17} nvt (fast) showed a slight decrease (x 0.95) in ultimate tensile strength. No yield was obtainable as the specimens failed with less than 0.2 percent permanent set.

Photomicrographs shown in Figure C 11 show no structural changes, but provide evidence of micro-porosity.

6.1.6.2 Aluminum B750 - T5

This material is primarily an aluminum-tin-nickel alloy cast in permanent molds. The cryogenic effect increased the ultimate tensile strength (x 1.44) and the tensile yield (x 1.29). The slight (from 0.66 to 0.59) ratio change in the F_{ty}/F_{tu} ratio was accompanied by a change in elongation from nine percent to seven percent.

Exposure to an irradiation of 1×10^{17} nvt prior to testing increased the tensile yield strength by a factor of 1.73 while causing only a modest (x 1.08) increase in ultimate tensile strength. The increase in the F_{ty}/F_{tu} ratios from 0.59 to 0.94 was accompanied by a drop in elongation from seven percent to three percent.

The photomicrographs shown in Figure C12, Appendix C, show no significant structural changes, but do provide evidence of the presence of micro-porosity in the test specimens.

6.1.6.3 Aluminum A356 - T61

This material is an aluminum-silicon alloy cast in permanent molds. The cryogenic effects include an increase in ultimate tensile strength (x 1.46) and in tensile yield strength (x 1.24). The reduction of the F_{ty}/F_{tu} ratio was accompanied by a slight drop in elongation, from fifteen percent to twelve percent.

The specimens tested after irradiation at 30°R showed slight decreases in ultimate tensile strength (x 0.96) and elongation (to nine percent) coupled with an increase by a factor of 1.23 in tensile yield strength.

The photomicrographs shown in Figure C 13, Appendix C, show no structural change due to irradiation but do reveal inter-dendritic shrinkage.

6.2 TITANIUM ALLOYS

Unlike aluminum, titanium has an isothermal crystallographic phase transformation. In the pure metal below 1600°F the stable crystallographic form is hexagonal close packed structure called alpha titanium. Between 1600°F and the melting point at 3130°F, the thermodynamically stable crystallographic structure is body centered cubic, called beta titanium. The addition of alloying elements will move this alpha-beta transition to either higher or lower temperatures depending on the addition elements. Examination of the equilibrium (phase) diagrams for titanium alloys[20] shows that of the alloying additions in the titanium alloys tested in this program, aluminum promotes alpha stability and molybdinum, tin and vanadium promote beta stability.

In many titanium alloy systems, the transformation from the beta phase to alpha on cooling is accompanied by an eutectoid decomposition with the resultant formation of inter-metallic compounds. This eutectoid reaction is absent in the Ti-Al, Ti-Sn, Ti-Mo and Ti-V alloy systems and, therefore, inter-metallics are not a significant component of any of the alloys included in the screening program. It is common practice, both in the United States and in other countries[22] to make a balanced alloy containing both alpha and beta stabilizing elements.

Titanium 55A is a commercially pure titanium grade, Titanium 5% Al-2.5% Sn contains about twice as much alpha stabilizer as beta stabilizer and the Titanium 8% Al-1% Mo-1% V is heavily alpha stabilized. Therefore, the only material tested in the program which would be expected to contain a significant beta content is the annealed Titanium 6% Al-4% V alloy. In practice in the titanium industry annealing is usually conducted at temperatures considerably below full solution temperature, so the tendency for retained beta is less in this annealed material than it would be in the solution treated material prior to aging; however, almost complete beta transformation should have occurred in the aged 6-4 alloy during the aging cycle. Therefore, the quantity of retained beta in these materials, including the Titanium 6% Al-4% V, would be expected to be small. Still, the rather sharp drop in elongation encountered at 30°R, unirradiated, for all the alloys except 55A might be indicative of the presence of some bcc beta phase. Metallographic evaluation of the materials by the manufacturer also indicated

small amounts of retained beta phase.

One of the alloys, Titanium 5% Al-2.5% Sn, was tested at two levels of interstitial content: one produced by normal titanium vacuum melting practice and one with controlled maxima for carbon, nitrogen, hydrogen and oxygen. Although oxygen is not truly an interstitial in the sense used by the physicist,[23] its tendency to cause room temperature brittleness in titanium has been shown and it is grouped with the actual interstitials in titanium technology.

All the titanium alloys included in the screening program are similar in certain aspects of their nuclear cryogenic behavior, even though they are of various compositions and structure and have divergent mechanical properties at room temperature. Both absolute and percentage changes in the titanium alloys show less divergency than similar changes in the other three groups of materials.

As is seen in Figures 22 and 25 and Table 5, actual changes due to the cryogenic or the combined nuclear-cryogenic environment in ultimate tensile stress are essentially the same, with the exception of the Titanium 5% Al-2.5% Sn alloy with the extra low interstitial content, indicating an interstitial-neutron interaction as a contributing factor in irradiation behavior in titanium alloys. The F_{ty}/F_{tu} ratio, rather high in most cases in the titanium alloys, remains essentially constant for the three environmental conditions. This function shows some reduction due to cryogenic and irradiation environments in unalloyed titanium (55A). With a few exceptions, changes in the other strength functions are also essentially the same for all these alloys.

The photomicrographs of the titanium alloys do not show any effects that can be related to the few small differences between alloys or test conditions that do exist.

6.2.1 Titanium 55A

This material, commercially pure titanium, was tested in the annealed condition. Figures 22 and 25 indicate that at 30°R this material exhibits large cryogenic increases in the strength functions, with the F_{tu} and F_{ty} increasing by factors of 2.53 and 2.28 respectively. These changes were accompanied by a slight increase in ductility - from an elongation of thirty percent at room temperature to thirty-three percent at 30°R.

Irradiation at 30°R caused small additional increases in strength properties - F_{tu} increased by a factor of 1.14, F_{ty} by a factor of 1.08 - with an increase in ductility, as measured by elongation, to 34 percent.

Titanium 55A is the only one of the titanium alloys tested with a F_{ty}/F_{tu} ratio at room temperature less than 0.9. It is also the only titanium to show significant temperature or irradiation effects on this property; the ratio was 0.80 at room temperature , 0.72 at 30°R, unirradiated and 0.69 at 30°R after irradiation.

6.2.2 Titanium 5% Al - 2.5% Sn (Standard and Extra Low Interstitial)

This alloy was tested in the annealed condition in both standard commercial grade and with a controlled level of interstitial and oxygen content. The cryogenic behavior of the two grades of this alloy is similar. Both the F_{tu} and F_{ty} for the two grades are increased by factors ranging from 1.78 to 1.89. The apparent difference in the elongation values is of dubious significance due to experimental scatter and the presence of outliers in the two samples with opposite effects on the arithmetic mean. The interstitial and oxygen content seemed to have a greater influence on the nuclear cryogenic behavior. The absolute changes induced by irradiation in Ti 5% Al - 2.5% Sn (Std. I) are more similar to the changes in the other titanium alloys (with standard interstitial content) than to Ti 5% Al-2.5% Sn (ELI). The F_{tu} and F_{ty} showed moderate increases, by a factor of 1.06.

The F_{tu} value of the Ti 5% Al-2.5% Sn (ELI) showed a real, but very slight, reduction after irradiation at 30°R, (x 0.98). The reduction in F_{ty} (x 0.99) is not significant at the 90 percent confidence level. The apparent increase in elongation after cryogenic irradiation is based on one specimen, the value of which falls within the scatter band for the 30°R, unirradiated, sample and is not of significance. These test results of this alloy indicate that interstitials play some effect in irradiation hardening of the titanium alloys.

6.2.3 Titanium 6% Al - 4% V

This alloy, a heat treatable alpha-beta alloy, was tested in the annealed and in the solution-treated-and-aged conditions. The cryogenic effects were similar on materials of both heat treatments. The F_{ty} and F_{tu} were increased by factors in the range from 1.68 to 1.81 in both cases. This was accompanied by reductions of elongation from 14 percent to 8 percent in the annealed material and from 16 percent to 6 percent in the aged material.

The irradiation effect on these two materials was similar to most of the other titanium alloys, moderate increases by factors ranging from 1.04 to 1.07 in F_{tu} and F_{ty} coupled with a small, and possibly not significant, reduction in elongation.

The scatter evident, in Figure 22, in the annealed material makes the changes due to irradiation not statistically significant at the ninety percent confidence level. However, at least some of this scatter could be a measure of random, non-uniform precipitation of a vanadium rich secondary alpha from a primary solution of retained beta phase, induced by irradiation. Comparison of the similarities between the mechanical properties of the aged material at 30°R without irradiation and the annealed material at 30°R after irradiation show a similarity in arithmetic mean which might indicate irradiation effects similar to aging. It should be borne in mind that annealing and solution treating are not identical in titanium technology. The difference between the two conditions is more complex than aging alone. Therefore, a similarity between irradiation aging and thermal aging may be obscured by other specimen variables.

6.2.4 Titanium 8% Al - 1% Mo - 1% V

This alloy, duplex annealed to prevent beta retention, exhibited behavior similar to the other alpha titanium standard interstitial materials. The cryogenic strengthening was of the same order of magnitude (F_{tu} x 1.73, F_{ty} x 1.70) as in the other alloys. Ductility measurements were not obtained after testing at 30°R, unirradiated.

The effect of irradiation at 30°R was, as might have been anticipated from the other standard alpha alloys, to mildly (x 1.09 and x 1.08) increase the F_{tu} and F_{ty} values.

6.3 NICKEL ALLOYS

Nickel, occurring near the center of the first long period of the Periodic Chart of the Elements, has a favorable atomic size for the formation of numerous alloy systems of both the substitutional and interstitial solid solution type.(23) It is a face centered cubic metal with no allotropic crystallographic transformation.

One of the nickel alloys tested, Inconel, is a Cr-Fe-Ni alloy which is not hardenable by heat treatment and was tested in the cold worked condition. One of the

other nickel alloys, René 41 (a Ni-Cr-Co-Mo alloy) is precipitation hardenable due to addition of Ti-Al-Fe to form inter-metallic compounds but was tested in the solution treated condition. K Monel (a Cu-Ni alloy) and Inconel X (another Cr-Ni-Fe alloy) also are hardenable through the formation of Ti-Al-Fe inter-metallics and were tested in the age hardened condition.

Examination of the family of nickel equilibrium (phase) diagrams[20] shows the major alloying element to have broad solubility bands - indeed Cu and Co are completely isomorphorous - in the nickel rich end. This should provide good structural stability at cryogenic temperatures. However, the fairly high inter-metallic compound content, in super-saturated solution in one case and appearing as precipitates in the others, might be expected to influence both cryogenic and irradiation behavior.

The nickel alloys investigated have much higher percentages and a greater variety of alloying elements than the titanium alloys investigated in the screening program and consequently show a wider divergence in their nuclear-cryogenic behavior. The aged alloys (K Monel and Inconel X) show less effect of the cryogenic environment on the yield strength than is shown by the other two alloys but do not show a corresponding difference due to irradiation.

The photomicrographs from these alloys show no differences that can be related to the differences in mechanical properties.

A summary of the test data is shown in Figures 22 and 25 and in Table 5 .

6.3.1 René 41

René 41 showed the largest cryogenically induced changes in both absolute and relative values for the strength functions among the nickel alloys; F_{tu} was increased by a factor of 1.49 and F_{ty} by 1.70. This was accompanied by an increase in elongation from fifty-five percent to sixty percent.

This material, tested in the solution treated condition, might be expected to show the effects of irradiation induced precipitation of the Ti-Al-Fe inter-metallic compounds.

6.3.2 K Monel

This alloy, tested in the age hardened condition, showed cryogenic effects on strength factors generally similar to René 41, solution treated, but of a somewhat smaller magnitude. F_{tu} increased by a factor of 1.21, and F_{ty} by a factor of 1.24. The elongation increased from twenty-eight percent to thirty-two percent.

The increase in F_{ty} (x 1.14) due to irradiation at 30°R is significant. The ductility parameters were not significantly changed by irradiation.

6.3.3 Inconel

This material, a cold-worked non-heat-treatable alloy, showed absolute and relative cryogenically induced changes of a magnitude between those of the solution treated alloy and the precipitation hardened alloys. At 30°R in unirradiated specimens, F_{tu} was increased by a factor of 1.35, and F_{ty} by 1.34. Elongation increased from fourteen percent to twenty percent.

Any irradiation induced effects on F_{tu} and F_{ty} at 30°R, if present, were very small and obscured by the experimental scatter.

6.3.4 Inconel X

This material, tested in the aged condition, showed a considerably smaller cryogenic effect on F_{ty} than the other nickel alloys while the other cryogenic values remained consistent with the pattern of behavior predictable from the test results of the other nickel alloys. F_{tu} increased by a factor of 1.21 while the increase in F_{ty} was only a factor of 1.06. There is one rather low outlier in yield strength (126 Ksi as opposed to 4 specimens between 156 Ksi and 160 Ksi) in the five specimen sample tested at 30°R; however, even if this value were arbitrarially discarded, this function would be appreciably lower than anticipated. Elongation increased from twenty-five percent to thirty-three percent.

As in the other nickel alloys, scatter affects the statistical significance of the observed changes due to irradiation at 30°R.

6.4 FERROUS ALLOYS

Iron, like nickel, is a transition element located near the center of the first long period of the Periodic Table. It also has an atomic size favorable to the formation of numerous alloy systems.[23] Additionally, elemental iron has two allotropic crystallographic changes. Between the temperatures of 1670°F and 2550°F a face centered cubic lattice is thermodynamically stable. Below 1670°F and above 2550°F the stable structure is a body centered cubic lattice. The room temperature stable bcc lattice is called the alpha phase, the intermediate phase is called gamma, and the phase with high temperature stability is called delta. (The designation beta was given to the body centered alpha phase at temperatures above the curie point at a time before the true nature of phase transformations was understood, and is no longer used.) The lower temperature gamma-alpha transformation is accompanied by eutectoid decomposition in many iron binary systems and the presence of small amounts of carbon causes this type of reaction in many cases where it would not occur under actual binary conditions. This combination of circumstances make the ferrous alloys among the more complex of the commonly used alloy systems.

Massive additions of some alloying elements - notably nickel and manganese - depress the alpha-gamma transformation temperature so that an essentially gamma structure, metallographically termed austenite, can be retained at room temperature. These austenitic steels form a separate group of materials with properties and property mechanisms not similar to other ferrous alloys since the physical and structural changes associated with the crystallographic transformation do not normally occur. However, the stability of the austenite is temperature dependent and decreases in cryogenic environments. Some austenitic steels, through the addition of small quantities of alloying elements selected to form desired intermetallic compounds, are age hardenable by mechanisms similar to those of the aluminum and nickel alloys.

Additions of other alloying elements - and of the gamma stabilizers in smaller quantities - cause major alteration in the nature of the eutectoid reaction during the gamma-alpha transformation. The alpha iron phase of the dual phase eutectoid can be altered from body centered cubic (ferrite) to hexagonal close packed or tetragonal (martensite)

with a great many intermediate structures obtainable. By appropriate thermal treatment, the distribution of the inter-metallic compound phase of the eutectoid can be varied from the lamellar or spheroidal pearlites through accicular supersaturated or intra-lattice precipitates structures.

For the purposes of this discussion, the materials have been grouped with those alloys in which the austenitic structure is normally retained at room temperature in one group and those where a non-austenitic structure is desired at normal temperatures in another.

A summary of the test data is given in Figures 23 and 26 and Table 6.

6.4.1 Austenitic Steels

The austenitic steels fall naturally into two classes: those which are not heat treatable, and those which - through the addition of relatively small but significant quantities of alloying elements - can be thermally hardened by the precipitation of inter-metallic compounds. The testing program included four materials of the first class; AISI Type 304, AISI Type 310, AISI Type 347 and Austenitic Manganese Steel T-450. The first three of this class are high chromium-nickel stainless steels. T-450 contains less than 4 percent chromium and is not a stainless grade; it was developed especially for cryogenic applications. All four of these alloys were tested in the annealed condition. The program also included one steel of the second class; Type A 286 which contains titanium, vanadium and aluminum to provide the precipitating action. This material was tested in two heat treated conditions, the significant varient being in the temperature of solution treatment.

The mechanical properties of austenitic steels at cryogenic temperatures are governed by two structural configurations; the original austenitic face-centered cubic lattice and martensite formed from that lattice during deformation at cryogenic temperatures through the absorption of transformation energy from the applied load. The major cryogenic hardening effect in the original austenitic grains is due to the change in energy required to produce stacking faults during deformation. In face-centered cubic materials, a stacking fault may be considered as a sub-microscopic region bounded by partial dislocations and acting as an extended dislocation. The width of the sub-structure, a function of stacking fault energy, influences the rate of strain hardening. The second hardening effect is a function of the transformation of austenite, meta-stable at cryogenic temperatures, to martensite. The initial martensite transformation product seems to be a hexagonal close packed structure which, with the absorption of additional energy, is transformed in part to a body-centered tetragonal structure.[24] The principal locus of transformation

would be expected to occur in the grain boundary area where the transition layer of atoms have less thermodynamic stability. This cryogenic hardening effect is reduced in the age hardenable austenites by the initial lattice distortion caused by the presence of inter-metallic precipitates. Otherwise, it bears a direct relationship to low temperature austenitic stability.

The rather violent stress fluctuations frequently reported(1) for these materials during plastic behavior were observed but, unfortunately, could not be recorded as functions of strain due to equipment limitations discussed in Section 4.

The effects induced on these materials at exposures of 1×10^{17} nvt ($E > 0.5$ Mev), except for changes in F_{ty}, were minor compared to the effects of cryogenic temperatures alone. Effects observed were not sufficiently uniform enough for inclusion in a general discussion and are mentioned in the individual discussion of each class of alloy.

6.4.1.1 Chromium-Nickel Austenitic Stainless Steels, AISI Type 304, 310 and 347

These materials are structurally very similar. They were all tested in the annealed condition, water quenched from 1900°F to insure maximum austenitic retention at room temperature. The structure in each steel is, essentially, a interstitial solid solution of carbon in highly alloyed gamma iron. On the basis of chemical analysis, 310 would be expected to have the greatest low temperature austenitic stability, 304 the least.

The cryogenic effect on the F_{tu} of these alloys is practically identical. Reference to Figures 16 and 19 shows that both absolute and ratio changes are in good agreement, with changes in F_{tu} by factors of about 2.5. This change seems to be independent of austenitic stability.

The cryogenic effect on F_{ty}, on the other hand, is not nearly as uniform within the group. The increase in F_{ty} of 304 (x 1.07*) was very slight. The increase in F_{ty} of 347 (x 1.19) was more pronounced and the increase in this function in 310 (x 2.2) approaches the magnitude of the cryogenic effect on the F_{tu} for this material. The increase in austenitic stability, in 347 over 304 is predictably slight, being based on an increased nickel content of less than 2 percent (by weight) and an increased

---

* The sample lot of five specimens tested at 30°R contained one abnormally low value included in the average. Four F_{ty} values fell between 40 ksi and 47 ksi and one specimen was reported at 25.4 ksi. However, even if this specimen were arbitrarily excluded this ratio would be 1.17 and the same general reasoning would apply.

manganese content of less than 1 percent. The austenitic stability of 310, however, should be greatly increased over that of 304 since the 310 contains 20.7 percent nickel, over twice as much as the 304. Thus, the cryogenic effect on the F_{ty} is clearly dependent on austenitic stability.

In the relatively unstable austenites, the major portion of the cryogenic hardening effect occurs during plastic deformation. This is substantiated by the curves in Figure 28. This figure shows the elastic and early plastic portions of the stress-strain curves for 304 at the three environmental conditions. As the difference of slope of the curved segment from the linear modulus slope curve to the 0.2 percent offset strain line shows, the stress required to impart a given strain in this area increases at 30°R by about a factor of 3. This indicates that the increase in yield strength as determined by the 0.2 percent offset method is largely a product of strain hardening during plastic, not elastic, deformation. This is borne out by other parameters. The elongation in 304 dropped from 76 percent to 34 percent at 30°R, 347 from 60 percent to 41 percent, 310 remained constant at 43 percent. The F_{ty}/F_{tu} ratio of 304 went from 0.39 to 0.16, 347 from 0.46 to 0.22, 310 from 0.74 to 0.65. The observed very small cryogenic effect on the elastic behavior of the chromium-nickel austenites indicates that the phase transformation hardening mechanisms earlier discussed provides a major contribution to the total cryogenic hardening of these alloys. With increased austenitic stability, the change in energy required to produce stacking faults in the fcc lattice would appear to be of greater importance in the total effect.

All three alloys show increases in F_{tu} as a result of irradiation at 30°R; 304 by a factor of 1.07, 347 by 1.06, 310 by 1.03. However, scatter in the test data, as shown in Figure 16, make this effect of questionable validity. Both 304 and 347 show "real" increases in F_{ty} after irradiation at 30°R, by factors of 1.31 and 1.23 respectively but 310 does not show a similar increase. There was no change of elongation due to irradiation for any of the chromium-nickel austenites observable within the limits of experimental accuracy. The irradiation induced changes in the F_{ty} in 304 and 347, greater both as absolute values and as ratios than the cryogenic changes in that function, appear to be of real significance. This, coupled with increases in the F_{ty}/F_{tu} ratio, in 304 from 0.16 to 0.20 and in 347 from 0.22 to 0.26, indicate an important change in behavior in the late elastic, early plastic region of the stress-strain curve. Examination of Figure 28 verifies this. The slope of the curve for 30°R, irradiated material, is much greater at the onset of plastic flow, but after about .004 in/in. total strain, the stress-strain ratios for the two curves appear to be approaching equality. This would indicate the possibility of some irradiation induced phase transformation with a hardening effect similar to that described above as a model of cryogenic hardening.

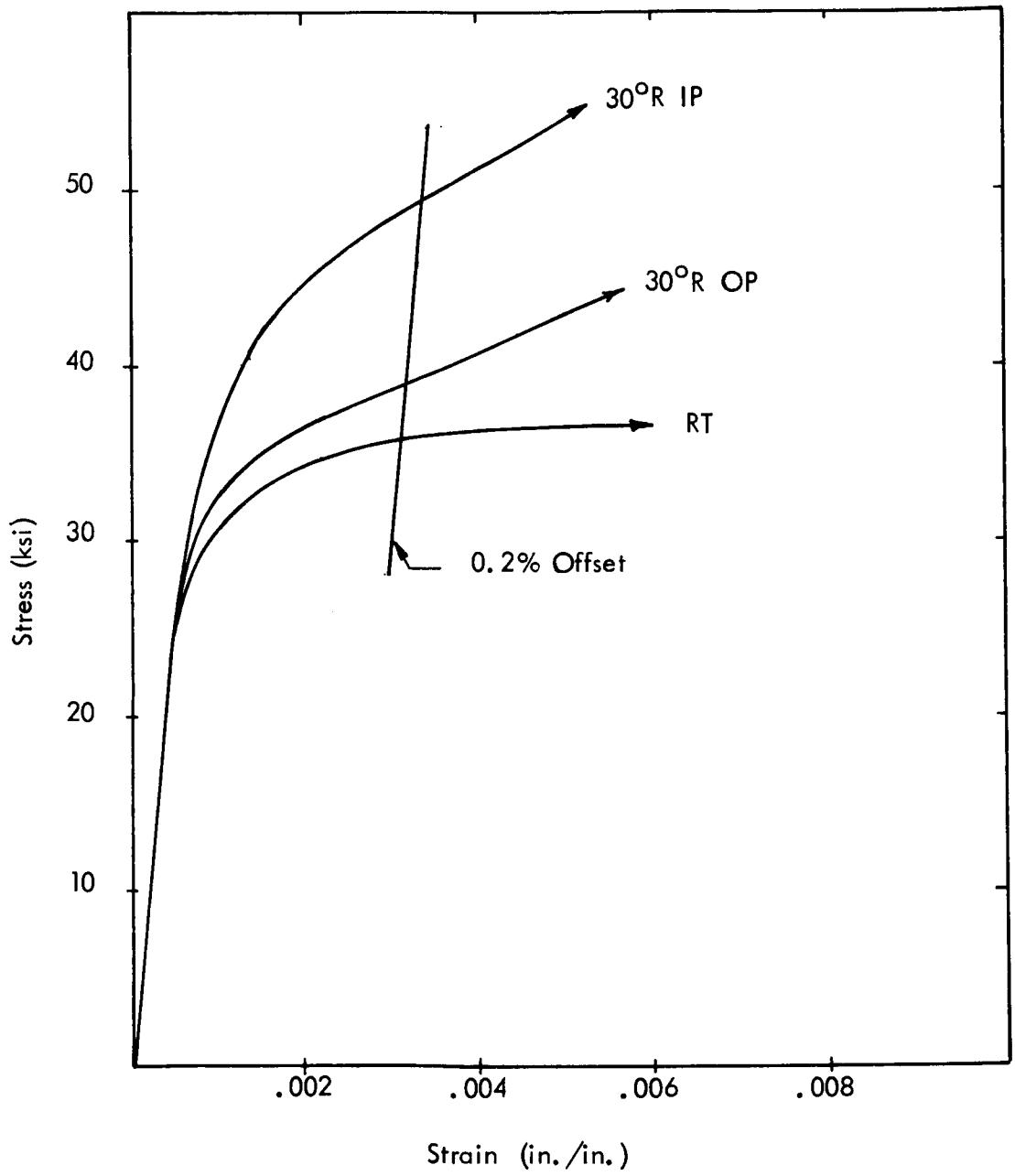

FIGURE 28 ELASTIC AND EARLY PLASTIC PORTION OF TYPICAL STRESS STRAIN CURVES, TYPE 304 STAINLESS STEEL

No metallographic changes attributable either to cryogenic or nuclear-cryogenic exposure were observed in the photomicrographs presented in Appendix C.

6.4.1.2 Austenitic Manganese Steel T-450

This steel contains manganese (nominally 19 percent) as the primary austenizing agent with minor additions of nickel, copper, chromium and nitrogen to increase the low temperature austenitic stability. This material was tested in the annealed condition, water quenched from 1850°F to ensure maximum austenite retention at room temperature. The structure is essentially an interstitial solid solution of carbon (0.15 percent by weight) and nitrogen in a gamma iron-manganese solid solution containing appreciable substitutional solute atoms of chromium, nickel and copper. It is an experimental alloy, devised for cryogenic applications, and has no broad testing or engineering history. Unlike the other austenitic steels tested in this program, it is not a corrosion resisting grade.

The cryogenic effect on the F_{tu}, both absolute and as a ratio, was less than for the chromium-nickel austenites. However, the cryogenic effect on the F_{tu}, an increase by a factor of 1.65 is not negligible. A marked difference in cryogenic behavior between T-450 and the 300 series stainless steels, discussed in Section 6.4.1.1, is the change in the F_{ty}. In T-450 the yield strength increased some 78 ksi in absolute units and by a factor of 2.36 of the room temperature value. The F_{ty}/F_{tu} ratio jumped from 0.32 to 0.46 and the elongation dropped from 70 percent to 31 percent. T-450, alone among the austenitic steels tested, shows an increase of the F_{ty}/F_{tu} ratio at 30°R. This indicates a different mode of cryogenic hardening. It seems probable that the manganese austenite undergoes major transformation hardening during elastic straining. This model is confirmed metallographically in Figure C29, Appendix C. The specimens tested at 30°R, both unirradiated and irradiated, show a much greater degree of grain distortion indicative of the generation of hexagonal and tetragonal martensite along the austenitic lattice planes, than in the material tested at room temperature. The evidence of this transformation is as great at the gage mark as at the fracture, indicating that it occurred at relatively low strain rates.

No significant radiation induced changes either in mechanical properties or microstructure were observed.

6.4.1.3 Type A 286 Stainless Steel

The structure of this age hardening super alloy is dependent on thermal history. It was tested in two different heat treatment conditions; in conformance with AMS 5735 and AMS 5737.[25] The difference in the heat treatments is best shown by quotation from the applicable specifications:

- AMS 5735 D, Section 6.1.1

  "Heat Treatment: The product shall be solution heat treated by heating to 1800°F ± 25, holding at heat for 1 hr, and quenching in oil or water, and shall then be precipitation heat treated by heating to no lower than 1300°F but not higher than 1400°F, holding at heat for 16 hr, and air cooling."

- AMS 5737 B, Section 6.1.1

  "Heat Treatment: The product shall be annealed by heating to 1650°F ± 25, holding at heat for 2 hr, and quenching in oil, or water, and shall then be precipitation heat treated by heating to 1325°F ± 25, holding at heat for 16 hr, and air cooling."

The original heat treatment, AMS 5735 was altered by AMS 5737 in an effort to improve high temperature properties, particularly creep at around 1000°F. The structure after either heat treatment is austenite with precipitated inter-metallics, but the distribution and size of the precipitates may vary between heat treatment methods.

At 30°R, the AMS 5735 material shows an increase in F_{tu} (x 1.51) and in F_{ty} (x 1.33). This is accompanied by an increase in elongation from 26 percent to 34 percent. The F_{ty}/F_{tu} ratio drops from 0.72 to 0.64. Under the same conditions, the AMS 5737 material shows increases in F_{tu} (x 1.39) and in F_{ty} (x 1.17) and an increase in elongation from 24 percent to 32 percent and the F_{ty}/F_{tu} ratio dropped from 0.78 to 0.66. While the absolute values of the strength functions are somewhat higher for the AMS 5737, the difference decreases at low temperatures. For example, the F_{ty} of AMS

5737 is about 20 percent higher at room temperature, the difference is only about 5 percent at 30°R. It would appear that the heat treatment of AMS 5737 has less effect on low temperature properties than on high temperature properties.

No significant metallographic changes were observed in the photomicrographs shown in Appendix C.

6.4.2 Non-Austenitic Steels

As may be expected when materials are grouped on the basis of not being something else, there is not much in common structurally or chemically among the non-austenitic steels. The structures of these alloys are all more complex than the austenites.

At first glance, AM 350 and 17-7 PH appear clearly related due to the similarity of mechanical properties and chemical composition. They are both proprietary stainless steels capable of developing high tensile strengths through heat treatment and are sometimes classified as super alloys. Both contain about 16 1/2 percent Cr and about 7 percent other major alloy additions. However, 17-7 PH contains 7 percent Ni, a strong gamma stabilizer. AM 350 has a nominal 4.3 percent Ni balanced with a nominal 2.75 percent Mo, which has a gamma loop type equilibrium (phase) system with iron. There is sufficient structural dissimilarity between these materials to warrant separate discussions.

ASTM A 353 steel has a high nickel ferrite-pearlite structure with no particular similarity to any other material in the test program.

Type 440C stainless is a fully martensitic structure with massive undissolved carbides, and is dissimilar structurally to the other materials.

6.4.2.1 AM 350 Stainless Steel (SCT)

This material is a proprietary alloy, developed by the Allegheny-Ludlum Steel Corporation. The chemical composition has been carefully balanced with constituents to stabilize each crystallographic phase of iron. This was done to allow precise crystallographic control through heat treatment. Since the thermal history of AM 350 is of great structural significance, that received by this lot of material will be

reviewed in some detail. In the as-rolled condition, AM 350 contains about 10 percent delta ferrite (the bcc phase stable in elemental iron only above 1400°C) finely dispersed in an austenitic matrix. The initial stage in the final heat treatment cycle consisted of holding at 1750°F for one hour to cause the precipitation of carbides at the austenite-ferrite interfaces. The material was water quenched from 1750°F and the austenite-ferrite structure was retained. Since AM 350 has a M_s temperature (the temperature at which the austenite-martensite transformation begins) near room temperature, the material was then held at -100°F for three hours to ensure maximum martensite formation. The martensite was tempered for three hours at 850°F to provide the maximum strength consistent with adequate ductility. Tempering martensite at this temperature range forms a supersaturated solid solution of carbon in alpha iron of non-uniform concentration. As the concentration of carbon atoms in the martensite structure is reduced, the tetragonal distortion of the structure is reduced and the crystal more nearly approaches the bcc cubic form of alpha iron. The final structure of tempered martensite is complex, consisting of mixed tetragonal and cubic lattice, both body centered, of differing degrees of distortion, randomally dispersed interstitial carbon atoms and highly dispersed complex chromium-iron carbides, such as $[(Cr, Fe)_7 C_3]$ and $[(Cr, Fe)_{23} C_6]$.

AM 350 showed increases in F_{tu} and F_{ty} at 30°R, by factors of 1.71 and 1.78 respectively. It developed a degree of cryogenic embrittlement shown by the reduction of elongation from 19 percent to 11 percent. A sharp reduction of stress level, similar in appearance to an upper yield point, is observable in the stress-strain curves of this material tested at 30°R, presented as Figure D 5 of Appendix D.

Irradiation at cryogenic temperatures has an adverse effect on this material. As can be seen from Figure 46 and Table 5, most functions are reduced by exposure to 1×10^{17} nvt ($E > 0.5$ Mev) at 30°R. The net changes in F_{tu} (x 0.92) and F_{ty} (x 0.93) seem minor and the change in F_{ty} is not of statistical significance at the chosen confidence level (90 percent). However, the elongation dropped from 11 percent to 7 percent and the F_{tun}/F_{tu} ratio dropped from 0.79 to 0.47 and there was a large and significant reduction in absolute tensile notch strength. The apparent "upper yield" is observable in the stress-strain curve at this environment also.

The photomicrographs shown in Figure C 30 of Appendix C confirm the presence of radiation damage through the shape of the fracture and its transgrannular nature but offer no clue to the mechanism.

6.4.2.2 Type 17-7 PH Steel (RH 950)

This material is a proprietary alloy developed by the Armco Steel Company. The composition is near that of the austenitic stainless steels and it is sometimes referred to as "semi-austenitic." The RH 950 heat treatment consists of rapid cooling from 1750°F, holding at -100°F and reheating to 950°F. The resultant micro-structure is accicular and resembles martensite metallographically. The manufacturer's literature(26) states that its nature as a true martensite has not been confirmed by X-ray diffraction methods. This pseudo-martensite contains submicroscopic precipitates of complex chromium-iron-carbides and chromium-aluminum inter-metallic compounds, such as $CrAl_7$ and Cr_2Al_{11}.

Type 17-7 PH showed severe cryogenic embrittlement. The elongation dropped from 14 percent to an unmeasurable low figure. However, a small degree of plastic behavior is observable on the stress-strain curve, presented in Figure D 5 of Appendix D, by the deviation of the curve from the modulus slope. The F_{tun}/F_{tu} ratio dropped from above unity to 0.55, and there was a reduction in the absolute F_{tun} value by a factor of 0.68. The F_{tu} and F_{ty} both increased by factors of 1.43 and 1.46 respectively.

Type 17-7 PH Steel also showed a serious reduction in mechanical properties due to irradiation at 30°R. After exposure to 1×10^{17} nvt ($E > 0.5$ Mev), both the F_{tu} and the F_{ty} were reduced about 0.75. Elongation was again unmeasurably small but observable on the stress-strain curve.

6.4.2.3 ASTM A 353 Steel

This material, a standard ASTM low carbon nickel alloy steel used principally for the construction of ASME Code Pressure Vessels, was tested in the normalized condition. The post-fabrication heat treatment consisted of austenizing at 1650°F, cooling in still air, reheating to 1450°F and cooling in cool air. This treatment results in eutectoid decomposition. The eutectoid, fine lamallar pearlite, consists of alternate layers of Fe_3C and a high nickel substitutional solid solution in alpha iron ferrite. Since nickel is not a carbide forming alloying element in steel, all the nickel atoms are randomly dispersed in both the eutectoid ferrite and in the free ferrite. Due to the inherent lack of close control of cooling rates during air cooling, the inter-lamallar spacing and the free ferrite distribution are non-uniform.

The presence of an appreciable population of solute nickel atoms improves the cryogenic behavior of the bcc iron structure. This is shown by the cryogenic increase in F_{tu} (x 1.82) and in F_{ty} (x 1.97). The elongation dropped from 25 percent to 18 percent. However, nothing similar to the catastrophic loss of ductility frequently observed[1] in alpha phase steels occurred.

Test specimens irradiated to 1×10^{17} nvt ($E > 0.5$ Mev) showed moderate increases in F_{tu} and F_{ty}, by factors of 1.07 and 1.09 respectively. This was accompanied by a small (from 18 percent to 16 percent) reduction in the mean of the elongation after irradiation but the range of test values for the two conditions overlap.

6.4.2.4 AISI Type 440C Stainless Steel

This material, a high-chromium high-carbon grade, was tested in the fully hardened condition. The heat treatment consisted, after mill annealing, of austenizing in a neutral salt bath at 1925°C, oil quenching, cooling to -100°F and tempering at 350°F. Although the range of the major alloying constituent, Chromium, in 440C is of the same order as in AM 350 and 17-7 PH, the structural formation is governed by a somewhat different mechanism. The chromium-iron equilibrium (phase) diagram, [20] naturally, has a profound influence on the equilibrium structure of all three alloys. This system is a relatively simple gamma loop. However, the addition of appreciable carbon content considerably complicates the phase behavior of chromium-iron alloys. Since chromium has strong carbide forming tendencies and also seriously limits the solubility of carbon in austenite, even the equilibrium behavior of chromium-iron-carbon alloys is complex. This is demonstrated by the 1.0 percent carbon section of the chromium-iron-carbon ternary system. [20]

The structure of 440C after the hardening treatment received by the test specimens is martensitic with randomly dispersed massive complex chromium carbides containing dissolved iron, such as $[(Cr, Fe)_7 C_3]$ and $[(Cr, Fe)_{23} C_6]$. Due to the low tempering temperature, probably little of the body centered tetragonal martensite has reverted to the cubic structure. It is extremely hard (R_c 60). This structure is rather brittle at room temperature and the ductility, as measured by elongation, was nil in all three test conditions. However, both cryogenic and nuclear-cryogenic environments appear to increase the already severe brittle behavior. Although the plastic deformation was not large enough to measure on the failed specimens, the stress-strain curve shown in Figure 29, indicates plastic behavior at room temperature by deviation from linearity. The curves for specimens tested at 30°R, unirradiated

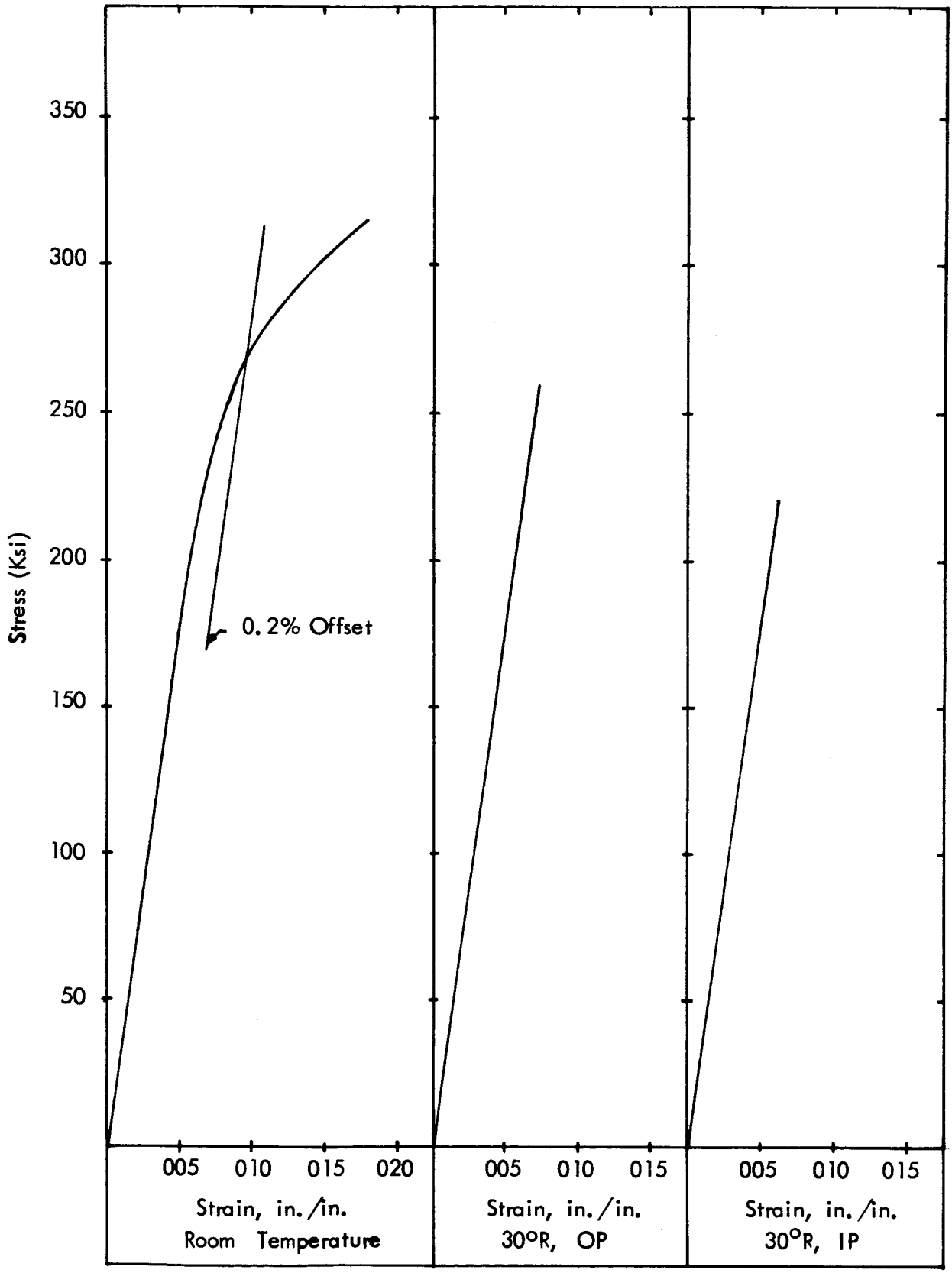

FIGURE 29 STRESS-STRAIN CURVES FOR AISI TYPE 440 C STAINLESS STEEL

and irradiated, do not show any indication of plasticity. The embrittlement due to cryogenic environment is confirmed metallographically. Metallographic examination also indicates a further embrittlement caused by irradiation at cryogenic temperatures. The photomicrographs, shown in Figure C 33, Appendix C, show the extreme brittleness of this material at all test conditions by the presence of independent systems of small cracks in the fracture zone and by branching of the fracture face. However, an increase in brittleness is indicated in the photomicrograph of the fracture area in the 30°R, unirradiated, specimen by the more highly transgrannular path of crack propagation. In the photomicrograph of the 30°R, 1×10^{17} nvt specimen showing the fracture face, it can be seen in the upper right corner that the crack propagated transgrannularly through carbide particles, indicating an extremely brittle matrix. This photograph is a composite to show, in one print, both carbide banding, typical of materials with low carbon solubility in the austenitic phase, and the fracture path through the carbide constituent. The white division between the two segments represents a physical separation of about 0.002 inch.

The scatter in the test data, indicated in Figure 23, is not unexpected in extremely brittle materials. Localized high stresses, caused by inhomogeneties in the material, cannot be relieved by energy absorption through localized plastic flow before the stress level approaches the cohesive strength of the material. If the cohesive strength is exceeded, a sub-microscopic crack is initiated. Since the energy required for crack propagation is somewhat less than that required for crack formation, failure would occur at a load level less than the anticipated macroscopic F_{tu}.

All tensile functions deteriorate in a cryogenic environment, the F_{tu} dropped by a factor of 0.83. A reduction in F_{tun}/F_{tu} from 0.69 to 0.41 was accompanied by a reduction in the absolute value of the F_{tun} by a factor of 0.50.

Irradiation at 30°R caused further deterioration in mechanical properties. The specimens tested after irradiation showed an additional reduction of ultimate tensile strength of the same order of magnitude as the cryogenic effect.

7 QUALITATIVE INTERPRETATION OF CERTAIN TEST RESULTS

Some of the test results may be interpreted in view of the physical metallurgy of the tested alloys discussed in Section 6 and known plastic deformation, cryogenic, nuclear and nuclear cryogenic effects that occur in metals and alloys generally.

The purpose of such an interpretation would be to help meet the secondary objective of the screening program, as mentioned in the introduction, which was to formulate models of low temperature irradiation effects in the more simple materials and to allow prediction of such effects in various structural alloys at other test conditions.

A possible approach is to indicate any correspondence that exists between the fundamental physical characteristics of the alloys and the real cryogenic and nuclear cryogenic effects that are seen in the test results (Section 5). Such correspondence even at the low integrated flux (10^{17} nvt >0.5 Mev neutrons) would increase the opportunity to extrapolate these results to higher fluxes, to other alloy compositions, or to other test or alloy conditions. This correspondence has been pointed out for various cases in Section 6.

The scope of any further interpretation must be limited to discussion in terms of the generally accepted cryogenic and nuclear irradiation phenomena in metals and alloys and to the discussion of real changes in the strength values and appreciable changes in the elongation (ductility) of the more simple materials.

For the most part the structure and composition of the alloys investigated in the program are much more complex than those that have yielded the widely accepted views of plastic deformation and cryogenic and irradiation effects and there is danger of too liberally interpretating the test results, even those from the relatively simple materials (Aluminum 1099 and Titanium 55A).

7.1 BACKGROUND

Fundamental to any explanation of plastic deformation is the dislocation, which may be thought of in its simplest form (an edge dislocation) as an extrapartial plane of atoms between two full planes of atoms in a crystal lattice. Dislocations actually take many forms within a crystallite (grain) and exist in abundance. The grain boundaries may be considered as arrays of dislocations. Dislocations can be generated in the process of plastic deformation; they also can be annihilated.

The degree to which a dislocation or groups of dislocations can overcome obstacles and move within a crystallite, the degree to which the motion can be transferred to dislocations in adjoining planes, and the degree to which a crystallite (grain) can slip on more than one plane all combine to determine the mechanical properties of a material. An obstacle for dislocation motion is any thing that causes a stress field in the lattice such as a "foreign" atom (interstitial or substitutional), a vacancy, a precipitate of "foreign" atoms or inter-metallics.

The complexity of dislocation arrays in most metals and alloys requires that moving dislocations intersect with other dislocations. This presents an obstacle which must be overcome by the generation of vacancies or interstitials by the moving dislocation. In most cases there would be a preference for generating vacancies since less energy is required to form a vacancy than to form an interstitial. The total number of planes on which dislocations can move is dependent on the lattice structure and the crystallite orientations. There is more choice in a cubic lattice than in a hexagonal lattice. Because of this, slip in hexagonal lattices is more laminar (less turbulent) than in cubic lattices. Fcc lattices and bcc lattices also show different characteristics due to relative ease with which interstitials and vacancies can be formed in the lattice. Furthermore the type of dislocation and stacking fault and the transfer of energy from one slip plane to adjoining planes will vary from fcc to bcc structure.

The yield strength of a material depends primarily on the ease of initiating dislocation motion by overcoming obstacles such as impurity atoms or precipitates. It should be noted that the 0.2 percent offset yield strength is an arbitrary engineering parameter and is not a true measure of the initiation of slip and therefore is not the most desirable measurement for the purpose of interpretation.

As deformation proceeds the array of dislocations and generated defects becomes more dense and more complex, and the grain boundaries become less important as obstacles to dislocation motion. The ultimate strength depends on the work hardenability of the material, which is the rate at which resistance to dislocation motion (slip) develops. Ductility as measured by elongation is related to the ease of dislocation motion as well as the number of dislocation sources.

A notch in the tensile specimen surface changes the loading at the base of the notch from uniaxial to triaxial. Fundamentally, an increase in notch strength would be an indication of the ability of the crystallites to slip on a number of planes simultaneously.

Fast neutron irradiation of a metal or alloy lattice knocks atoms (knock-ons) out of the lattice. These knock-ons in turn knock other atoms out of the lattice with a resulting distribution of vacancies and interstitials.[27] At room temperature these vacancies and interstitials have sufficient energy to diffuse. Within a crystal they may diffuse to a dislocation and act as deterrents to dislocation motion, and the vacancies can coagulate to form dislocation loops[28] which may act as new sources of dislocations on the application of stress.

The presence of vacancies and interstitials within a alloy lattice can aid any phase change or precipitation that tends to occur.

Not so well understood are other phenomena which may occur in alloy lattices under fast neutron irradiation. The existance of a thermal spike has been postulated[29] at the end of every primary knock-on path in materials (depending on atomic masses and ionic radii) where the mean free path of the knock-on is of the same order of magnitude as the unit lattice and where the energy dissipated is concentrated in a region small enough to raise the temperature above the melting point of the material. This results in regions within the irradiated crystallite which have been effectively melted (under pressure of the surrounding lattice) and quenched leaving a complex array of vacancies, interstitials and probably more complex defects. Similarly, and more generally accepted, at least for metals, is the concept of a displacement spike[30] consisting of a heavily damaged region with a central region from which many atoms have been displaced, resulting in a cluster of vacancies surrounded by a volume containing many interstitials.

Long range displacements of atoms within irradiated crystallites have also been postulated[31] as focusing collisions resulting from an atom being struck at such an angle that its momentum is transferred along the lattice in a preferred crystallographic direction without actual atomic displacement. A distortion in the lattice in the form of dislocations, foreign atoms and grain boundaries interrupts the propogation of movement and causes a displacement many atomic distances from the initial impact. Similarly, an extra atom in a row of atoms can be generated and displaced in certain crystallographic directions.

Channeling of knocked-on atoms at relatively low energies (in the ionized state) has also been postulated,[32] and in an alloy such channeling would occur more often with the atoms of small ionic radius than with those of large radius. Light atoms generally would be preferentially displaced, conceivably being thus concentrated in regions of high lattice distortions - as near an existing precipitate, dislocation, grain boundary or vacancy cluster. They may, in such a way, accelerate[33] precipitation phenomena or retard such phenomena[34] depending on the precipitation process involved, the atom which is preferentially displaced, etc.

Interstitials already existing in a lattice may be assumed to be preferentially displaced and coagulated to some degree by irradiation. Since they already exist they do not require energy for formation and in the case of certain interstitials like carbon (small ionic radii) have low activation energies for motion.

Data from various[35] experiments on irradiation effects in metals and alloys at room temperatures yield the following conclusions that might be applied to interpretation of the screening program data:

> F_{ty} and F_{tu} increase in annealed materials and increase to a lesser degree in cold worked materials. Percentage increases in F_{tu} are generally lower than in F_{ty}.
>
> Elongation decreases in annealed materials and decreases somewhat less in cold worked materials.
>
> Work hardenability decreases.
>
> Nil-ductility transition temperatures of non-austenitic steel materials increase.
>
> All results are affected by grain size and impurity concentration.

Irradiating a material at cryogenic temperatures obviously will alter the effects of neutron irradiation as well as change the deformation characteristics on deforming prior to warm up. Some of the phenomena associated with neutron irradiation will occur at any temperature because the energy available from the incident neutron is large with respect to the thermal energy of the atoms in the lattice. The more obvious differences in such phenomena are caused by limited energy available for diffusion processes, and therefore an altogether different distribution of vacancies and interstitials is to be expected after irradiation at cryogenic temperatures from that resulting from irradiation at room temperature. The number of vacancies and interstitials generated by a neutron hit can be assumed to be independent of temperature, whereas the diffusion of these defects is temperature dependent.

Any such phenomenon as a thermal spike, displacement spike, focusing collision, channeling or preferential displacement resulting from neutron hits would depend to some extent on the temperature. The reduced compressibility of the lattice at low temperatures would alter a thermal spike, and reduced thermal agitation of the atoms would obviously improve the chances for focusing, channeling and preferential displacement.

7.2 INTERPRETATION

Discussion of certain of the unexpected cryogenic and nuclear effects observed in the screening program which are of fundamental interest, rather than of interest to design engineers follows.

The decrease in F_{ty} of Aluminum 1099 at 30°R was unexpected. Even though the material is cold worked to some extent it can be assumed that dislocations are relatively free to move in this material. It can be pointed out that in a pure metal face centered cubic single crystal, the yield strength is not dependent on temperature. Also, the 0.2 percent offset method of determining the yield stress gives values that are only approximately in proportion to the strain at which deviation from the linear portion of the stress-strain curve occurs. Aluminum 1099 showed a real increase in F_{tu} with irradiation. The effects of annealing during tests on F_{tu} and F_{ty} indicate that the radiation induced defects diffused to grain boundaries rather than to dislocations or into clusters in such a manner as to act as barriers to dislocation motion. The effects of pre-stressing indicate that the increase in dislocation density or deformation induced defects effectively reduces the ability of radiation induced defects to pin the dislocations, possibly due to some mutual annihilation. The presence of mechanical twinning in the specimens tested at 30°R, OP indicate that the intragranular critical shear stress has been exceeded at stress levels below that required for macroscopic plastic behavior. The absence of twinning in the 30°R, IP specimens indicates sufficient neutron and knock-on interaction with atoms to cause a significant increase in intragranular critical shear stress.

Aluminum 7178 and 7079 are remarkably different in their changes due to irradiation. The 7178 alloy has a higher concentration of copper and zinc, which are both precipitates. It appears that the 7079 alloy is possibly reduced in ultimate tensile strength while the Aluminum 7178 is probably increased. Aluminum 7178 exhibits a real increase in tensile yield strength while there is no effect on the yield strength in Aluminum 7079. In this respect, 7178 is more like the 5000 series Aluminum alloys (non heat treatable) than it is like 7079. Large decreases in elongation in 7178 with irradiation even with respect to other aluminum alloys is similar to Aluminum B 750 in

this respect. Precipitation phenomena are involved here and the higher concentration of the inter-metallic precipitates in Aluminum 7178 can account for these differences.

The differences in behavior of Titanium 5% Al - 2.5% Sn (ELI) and (Std. I) deserve particular attention. The standard interstitial is more similar to other titanium alloys (with standard interstitial content) than to the Titanium 5% Al - 2.5% Sn (ELI). The only statistically significant difference between these two groups of materials is in the tensile notch strength; the extra low interstitial materials having a higher notch strength at 30°R than the standard interstitial material and less effect of irradiation than the standard interstitial material. Also, there is probably less total effect on the strength values in the extra low interstitial material than in the standard material. It must be concluded that the removal of interstitials, including oxygen as well as carbon, hydrogen and nitrogen, reduced the effect of irradiation at cryogenic temperatures. This can be interpreted in terms of the preferential displacements described earlier (Section 7.1).

René 41 and Inconel X exhibit similar irradiation effects with real decreases in F_{tun} and possible increases in F_{ty}. The K Monel showed real increases in F_{ty} and less than a probable change in F_{tu}. It is possible that material fully aged by thermal treatment would show further increases in strength functions due to irradiation. The net irradiation effect on the precipitate distribution is unpredictable, and the irradiation induced point defects act to restrain dislocation motion between the precipitates. Inconel X showed only a probable increase in F_{ty} at cryogenic temperatures, which is conceivably associated with an over-aging phenomena with the precipitate phase being incoherent with the parent lattice. It should be noted that this is essentially a high temperature material being tested in a low temperature environment.

Two A 286 stainless steel precipitate type alloys with differing heat treatments (AMS 5735 and AMS 5737) show a difference in sign in changes of F_{tun} due to irradiation. The differences in heat treatment are described in Section 6.4.1.3. Regardless of how particle size distribution will effect the tensile notch strength, there is undoubtedly a difference between the two heat treatments with respect to precipitate particle size and distribution of particles as indicated by the higher strengths in the A 286 (AMS 5737). It is conceivable that there is a critical precipitate particle size above which neutron irradiation might cause an additional growth and below which irradiation would cause resolution since this is the aging process believed to occur naturally in some precipitate alloys.

8 EVALUATION OF TEST RESULTS AS DESIGN CRITERIA

The changes in strength functions resulting from cryogenic and nuclear-cryogenic environments are shown in the figures presented in Section 5.1. Figures 21, 22 and 23 show the changes in absolute values; Figures 24, 25 and 26 show the net changes as indicated by the 30° out-of-pile/30° in-pile ratios and initial room temperature values. A tabular review of all test results, based on the arithmetic means of sample lots is given in Tables 4, 5 and 6, also appearing in Section 5.1. The raw data obtained in the testing program is presented as Appendix B.

Since achieving the required structural strength with a minimum weight is one of the major problems of designers of aerospace equipment, the materials in this testing program have been listed in Figure 30 using an order of merit based on the strength to weight ratio.

Since the ratio between the yield and ultimate tensile strengths (F_{ty}/F_{tu}) ranges from less than 0.20 to over 0.95 in the materials tested in this program, it was felt that a strength-weight ratio based on yield strength would be of more practical design use than one based on ultimate tensile strength.

Therefore, the figure of merit used as the basis for Figure 30 is the tensile yield strength at 30°R after irradiation to 1×10^{17} nvt ($E > 0.5$ Mev), divided by the density of the alloy in lbs/in^3 at room temperature. Values are also given for the yield strength divided by density (F_{ty}/d) for each material at the other test conditions.

Due to the non-homogeneous nature of materials manufactured by commercial methods, the relative positions of the several alloys are not absolute. The ranges of values of this function might be expected to overlap for materials in adjacent locations, and these materials, for practical purposes, may be considered equivalent. A difference of several numbers in order of merit, however, indicates a significant incremental variation between the two materials.

Order of Merit	Alloy	Density (d)	Test Condition	F_{ty}(ksi)/d(lb/in^3) x 10^{-2}
1	Titanium 6 Al - 4V (Aged)	0.160	RT 30°R OP 30°R IP	9.9 17.2 18.3
2	Titanium 6 Al - 4V (Annealed)	0.160	RT 30°R OP 30°R IP	8.6 15.2 15.9
3	Titanium 8Al-1Mo-1V	0.158	RT 30°R OP 30°R IP	8.3 14.2 15.4
4	Titanium 5 Al-2.5 Sn (Std.)	0.161	RT 30°R OP 30°R IP	7.1 12.8 13.5
5	Titanium 5 Al-2.5 Sn (ELI)	0.161	RT 30°R OP 30°R IP	7.0 13.3 13.2
6	Aluminum 7079	0.099	RT 30°R OP 30°R IP	9.0 13.1 12.9
7	Aluminum 7178	0.10	RT 30°R OP 30°R IP	8.0 10.8 12.1
8	Steel AM-350	0.282	RT 30°R OP 30°R IP	6.6 11.8 (1) 10.9 (1)
9	Steel 17-7 PH	0.276	RT 30°R OP 30°R IP	8.2 12.0 (1) 9.1 (1)
10	Titanium 55A	0.163	RT 30°R OP 30°R IP	3.3 7.5 8.1
11	Aluminum 2024	0.100	RT 30°R OP 30°R IP	5.0 7.7 7.9
12	Steel 440C	0.28	RT 30°R OP 30°R IP	9.6 9.3 (1) (2) 7.8 (1) (2)
13	Aluminum 2219	0.102	RT 30°R OP 30°R IP	4.7 6.7 7.3
14	Aluminum 2014	0.101	RT 30°R OP 30°R IP	6.0 6.8 7.1
15	Aluminum 5456	0.096	RT 30°R OP 30°R IP	3.5 4.6 6.9
16	Steel A353	0.28	RT 30°R OP 30°R IP	3.2 6.2 6.8
17	Aluminum 5086	0.096	RT 30°R OP 30°R IP	3.3 3.8 6.2
18	Aluminum 5083	0.096	RT 30°R OP 30°R IP	3.4 4.5 - (3)
19	Aluminum 6061	0.097	RT 30°R OP 30°R IP	4.1 5.2 6.1
20	Inconel	0.304	RT 30°R OP 30°R IP	4.3 5.8 5.9
21	Steel A 286 (5737)	0.286	RT 30°R OP 30°R IP	4.7 5.5 5.8
22	Inconel X	0.30	RT 30°R OP 30°R IP	4.7 5.0 5.4
23	Steel A 286 (5735)	0.286	RT 30°R OP 30°R IP	3.9 5.2 5.3
24	Aluminum X250	0.097	RT 30°R OP 30°R IP	3.4 5.1 4.8 (2)
25	Aluminum A 356	0.096	RT 30°R OP 30°R IP	3.2 3.9 4.8
26	Steel 310	0.29	RT 30°R OP 30°R IP	2.2 4.8 4.7
27	K Monel	0.306	RT 30°R OP 30°R IP	3.2 4.0 4.5
28	Aluminum 1099	0.097	RT 30°R OP 30°R IP	1.3 0.7 (4) 4.5
29	Aluminum B 750	0.104	RT 30°R OP 30°R IP	1.9 2.4 4.2
30	René 41	0.30	RT 30°R OP 30°R IP	2.1 3.6 3.8
31	Steel T 450	0.28	RT 30°R OP 30°R IP	1.4 3.3 3.3
32	Steel 347	0.29	RT 30°R OP 30°R IP	1.5 1.8 2.2
33	Steel 304	0.29	RT 30°R OP 30°R IP	1.3 1.4 1.8

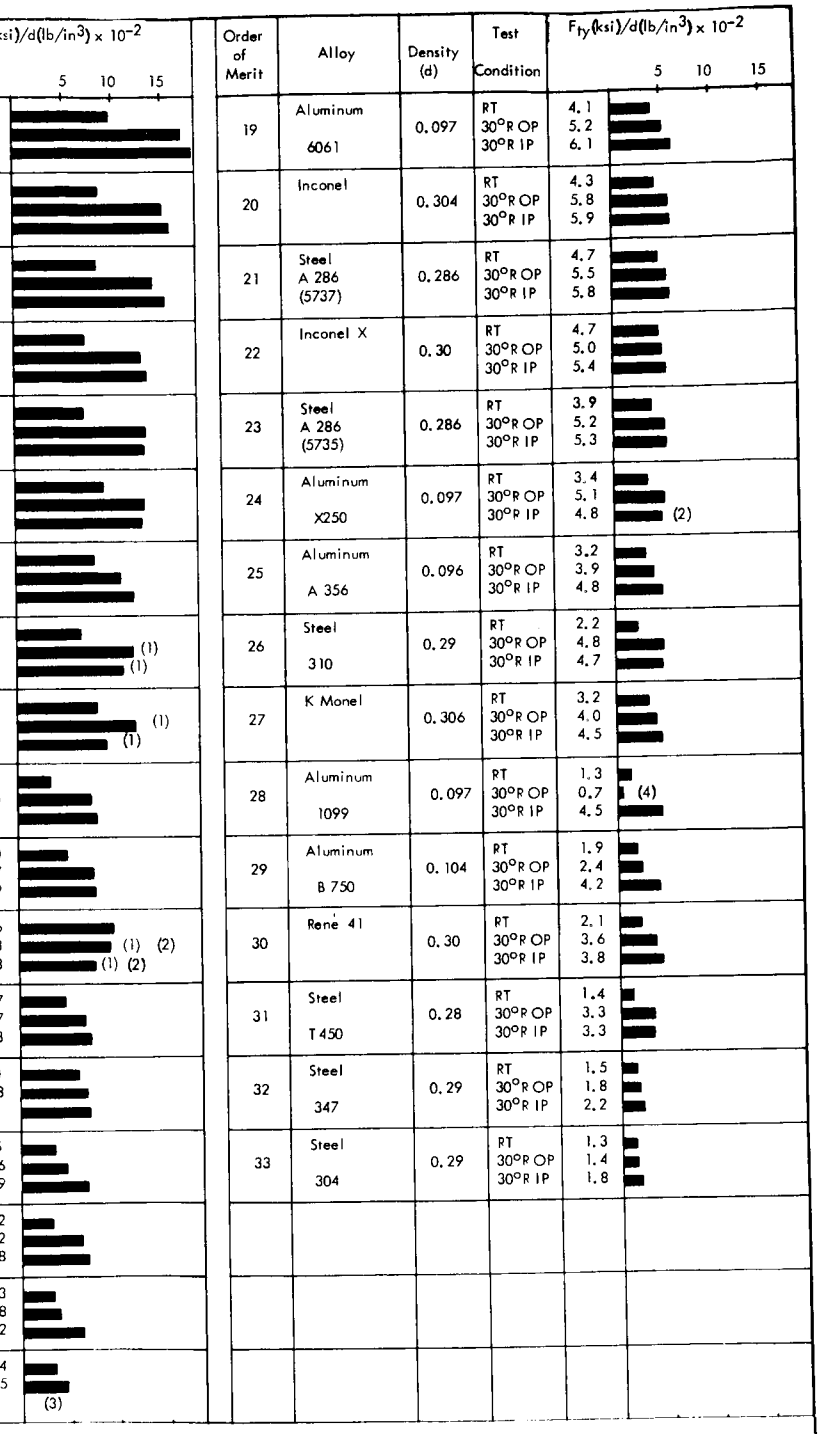

1 Ductility parameters indicate severe embrittlement.

2 Specimens failed at less than 0.2% offset. Reported value is F_{tu}/d.

3 Aluminum 5083 not tested after irradiation. This alloy placed arbitrarily in this relative position due to similarity of composition and non-irradiated behavior with 5086 and 5456.

4 The low strength-weight ratio of Aluminum 1099 at 30°R, unirradiated, should be noted.

FIGURE 30 TENSILE YIELD STRENGTH TO WEIGHT RATIOS FOR 33 ALLOYS AT VARIOUS TEST CONDITIONS IN ORDER OF DECREASING VALUE IN-PILE AT 30°R

9 CONCLUSIONS AND RECOMMENDATIONS

In general, cryogenic temperatures enhance the strength functions, F_{tu} and F_{ty}, in materials not subject to a low-temperature nil-ductility transformation. This fact has been used by the designers of liquified gas handling equipment to reduce the weight of this type of hardware.

In several instances, fast neutron irradiation also increased the strength values. However, this effect is of less use to the designer than the cryogenic effect since the neutron dose sensitivity makes it a time dependent function. The principal interest of designers in irradiation effects is in the avoidance of "radiation damage" which might compromise the integrity of the design. Again, it should be noted that the accumulated dose of 1×10^{17} nvt ($E > 0.5$ Mev) received by the specimens tested in this program may be well below the threshold levels of some materials and the observed changes might increase in magnitude or reverse in sign with increased exposures to a fast neutron environment.

9.1 CONCLUSIONS

In the following paragraphs, the nature of the observed effects are noted for all the materials tested in this program. The alloys were evaluated using the statistical method briefly described in Section 4.2.6. In the following paragraphs, "real" indicates statistically significant with a confidence level of 90 percent, "probable" indicates statistically significant with a confidence level of about 50 percent and "no observable" means with no statistical significance at the 50 percent confidence level. All the changes discussed in the following paragraphs are based on absolute values.

9.1.1 Materials Exhibiting "Real" Adverse Cryogenic Effects In Strength Functions

The following alloys showed "real" degradation in one or more strength functions as a result of exposure to 30°R, unirradiated. They should be used in cryogenic environments only after evaluation for a specific application on the basis of all available cryogenic test data. The figure in parenthesis indicates the ratio of the test

value for the designated function at 30°R to its test value at room temperature or states both values.

Aluminum 1099 ($F_{ty} \times 0.56$)

Stainless Steel 17-7 PH ($F_{tun} \times 0.68$)

Stainless Steel 440C ($F_{tu} \times 0.83$; $F_{tun} \times 0.50$)

9.1.2 Materials Exhibiting "Real" Adverse Cryogenic-Irradiation Effects On Strength Functions

The following alloys showed "real" degradation in one or more strength functions as a result of irradiation to 1×10^{17} nvt ($E > 0.5$ Mev) at 30°R.*

The numerical values in parenthesis after each alloy indicate the ratio of the test values after irradiation to values from unirradiated samples tested at 30°R. In several cases, these changes are of such minor magnitude that their practical significance is dubious. However, the existance of any adverse effect in mechanical properties of statistical significance at the 90 percent confidence level after this relatively low irradiation exposure level indicates a possible susceptibility to more serious damage at higher irradiation levels. Caution should be exercised in the application of these materials in nuclear-cryogenic environments.

Aluminum 2014 ($F_{tu} \times 0.93$)

Titanium 5Al-2 1/2 Sn, ELI ($F_{tu} \times 0.98$)

René 41 ($F_{tun} \times 0.95$)

Inconel X ($F_{tun} \times 0.92$)

Stainless Steel A-286 (AMS 5737) ($F_{tun} \times 0.94$)

Stainless Steel AM 350 ($F_{tu} \times 0.92$; $F_{tun} \times 0.55$)

Stainless Steel 17-7 PH ($F_{tu} \times 0.75$; $F_{ty} \times 0.76$)

Stainless Steel 440C ($F_{tu} \times 0.83$)

---

* Aluminum 5083 was not tested after irradiation.

Testing of these alloys after exposures to high levels of irradiation would appear to be of interest.

9.1.3 Materials Exhibiting "Probable" Adverse Cryogenic Effects On Strength Functions

Aluminum X-250 is the only material which showed "probable" degradation in one or more strength functions as a result of exposure to 30°R without irradiation with no observed real change in any strength function. However, the test coupons of this alloy contained considerable micro-porosity from the casting process. This introduction of a random uncontrolled variable introduces a degree of uncertainty in statistical analyses.

9.1.4 Materials Exhibiting "Probable" Adverse Cryogenic-Irradiation Effects On Strength Functions

The following alloys showed "probable" adverse irradiation effects on some strength functions, but none with a statistical confidence level of 90 percent. Due to the fairly low irradiation level of this experiment, further testing would be desirable on these materials before evaluation of these effects.

Aluminum 2024 ($F_{tu} \times 0.95$)

Aluminum 2219 ($F_{tu} \times 0.98$)

Aluminum 6061 ($F_{tu} \times 0.95$)

Aluminum 7079 ($F_{tu} \times 0.92$)

Stainless Steel 304 ($F_{tun} \times 0.90$)

Stainless Steel A-286 (AMS 5735) ($F_{tu} \times 0.97$)

Austenitic Manganese Steel T-450 ($F_{tu} \times 0.98$)

Although, in some instances, these effects are equal to or greater in magnitude than those listed in Section 9.1.2, but the scatter in these values reduces their statistical significance, as discussed in Section 4.2.6.

9.1.5 Materials Exhibiting "No Observable" Adverse Cryogenic Or Irradiation Effects On Strength Functions

The following materials showed no statistically significant (at the 50 percent confidence level) deterioration of any strength function. Within the limitation of the irradiation level of this experiment, the strength criteria of these materials appears suitable for nuclear-cryogenic applications.

Aluminum 5086
Aluminum 5456
Aluminum 7178
Aluminum B-750
Aluminum A-356
Titanium 55A
Titanium 5% Al - 2 1/2% Sn - Std.
Titanium 6% Al - 4% V - both aged and annealed
Titanium 8% Al - 1% Mo - 1% V
K Monel
Inconel
Stainless Steel 310
Stainless Steel 347
Stainless Steel A 286 (AMS 5735)
ASTM A 353 Steel

9.1.6 Materials Exhibiting Appreciable And Serious Cryogenic Effects In Ductility Functions

The following alloys show an appreciable loss in ductility in the cryogenic environment, the reduction being sufficient to suggest a significant cryogenic embrittlement.*

Aluminum 7079 (Elongation from 11.4 percent to 5.8 percent)
Aluminum X-250 (Elongation from 20.6 percent to nil)

* Ductility parameters for Titanium 8% Al - 1% Mo - 1% V not available.

Titanium 6Al-4V, Annealed (Elongation from 13.8 percent to 7.6 percent)

Titanium 6Al-4V, Aged (Elongation from 16.5 percent to 6.4 percent)

Stainless Steel 17-7 PH (Elongation from 13.8 percent to nil)

Stainless Steel 440C does not appear in the above listing since this material shows very slight ductility on the basis of elongation and reduction of area measurements at room temperature.

9.1.7 Materials Exhibiting Appreciable Cryogenic Reduction in Ductility Functions While Retaining Reasonable Ductility

The following materials showed significant reduction of ductility as a result of cryogenic exposure but retained elongation values of at least 10 percent, rounded off to the nearest percent.

Titanium 5Al-2 1/2 Sn, Std. I (Elongation from 23.3 percent to 13.8 percent)

Titanium 5% Al-2 1/2 % Sn - ELI (Elongation from 16 percent to 9.7 percent)

Stainless Steel 304 (Elongation from 76.5 percent to 34.4 percent)

Stainless Steel 347 (Elongation from 60.3 percent to 41.3 percent)

Austenitic Manganese Steel T-450 (Elongation from 70.2 percent to 31.2 percent)

Stainless Steel AM 350 (Elongation from 19.3 percent to 11.0 percent)

ASTM A 353 Steel (Elongation from 25.2 percent to 18.0 percent)

9.1.8 Materials Exhibiting Appreciable And Serious Cryogenic Irradiation Effects In Ductility Functions

The following materials showed a significant reduction of ductility as a result of irradiation

at a level which might suggest significant embrittlement through irradiation.

Aluminum 7178 (Elongation from 12.4 percent to 6.3 percent)

Aluminum B-750 (Elongation from 7.0 percent to 3.3 percent)

Aluminum A-356 (Elongation from 11.6 percent to 8.7 percent)

Titanium 6Al-4V-Annealed (Elongation from 7.6 percent to 5.7 percent)

Titanium 6Al-4V-Aged (Elongation from 6.4 percent to 5 percent)

Titanium 8Al-1Mo-1V*

Stainless Steel AM 350 (Elongation from 11 percent to 7.3 percent)

The following materials exhibited nil ductility at 30°R, unirradiated. An increase in the severity of their brittle behavior from irradiation embrittlement might be observable if they were tested using criteria other than elongation and reduction of area.

Aluminum X-250

Stainless Steel 17-7 PH

Stainless Steel 440C

9.1.9 Materials Exhibiting Appreciable Cryogenic-Irradiation Induced Reduction In Ductility Functions While Retaining Reasonable Ductility

The following alloys showed a considerable reduction in ductility at 30°R after irradiation in comparison with specimens tested at 30°R, out-of-pile. In most cases, due to a cryogenic increase in ductility, the irradiated test specimens showed as great or greater ductility than the room temperature specimens. In all cases, the ductility as measured by elongation is 10 percent or greater. However, the tendency for radiation embrittlement might be expected to increase with higher irradiation levels.

Aluminum 1099 (Elongation from 61.4 percent to 46 percent)

Aluminum 2014 (Elongation from 17.7 percent to 12.7 percent)

Aluminum 2024 (Elongation from 22.3 percent to 16.3 percent)

Aluminum 5086 (Elongation from 30.0 percent to 22.3 percent)

Aluminum 5456 (Elongation from 18.2 percent to 14 percent)

---

* Ductility parameters for specimens tested at 30°R, unirradiated not available. Elongation at 30°R, 1×10^{17}nvt was 5.7 percent; room temperature value was 22.7 percent.

Titanium 5Al-2 1/2 Sn-Std. 1 (Elongation from 13.8 percent to 11.5 percent)

René 41 (Elongation from 60.5 percent to 55.0 percent)

Inconel X (Elongation from 33 percent to 29 percent)

Stainless Steel 347 (Elongation from 41.3 percent to 37 percent)

9.2 RECOMMENDATIONS REGARDING USE OF TEST RESULTS AS DESIGN CRITERIA

The following alloys - due to drastic reductions in one or more of the strength or ductility functions - seem unsuitable for most engineering applications at 30°R.

Aluminum 1099
Aluminum 7079
Titanium 6% Al - 4% V - Annealed
Titanium 6% Al - 4% V - Aged
Stainless Steel 17-7 PH
Stainless Steel 440C

The changes in ductility functions in Aluminum 7079 and Titanium 6-4 might not have adverse effects for many specific uses. However, materials are available with superior cryogenic properties for most applications at liquid hydrogen temperatures.

In all cases except Aluminum 1099, the undesirable cryogenic effect on one or more functions is increased by irradiation at 30°R. Thus, these materials seem even less suitable for nuclear-cryogenic environments than for simple low temperature service.

In the case of Aluminum 1099, the yield strength loss at 30°R is recovered after exposure to a fast neutron field. This effect, discussed in Section 6.1, is of interest but would seem of little practical application to the designer.

The following materials - due to small but statistically significant reductions after irradiation in one or more of the strength or ductility functions or to scatter of test

data which might obscure significant effects - should be the subject of additional investigation before extensive use in nuclear-cryogenic applications:

Aluminum Alloys	2014, 2024, 2219, 5086, 5456, 6061 and 7178
Titanium Alloys	5 Al-2 1/2 Sn, Std. I, 5 Al-2 1/2 Sn, ELI and 8 Al - 1 Mo - 1V
Nickel Alloys	René 41 and Inconel X
Stainless Steels	304, 347, A-286 (AMS 5735), A-286 (AMS 5737) and AM-350
Austenitic Manganese Steel	T-450
ASTM Steel	A 353

Although further study is indicated prior to a general recommendation for use, many of these materials may prove suitable for specific applications and none showed drastic reductions in strength or ductility functions.

The analyses of test results for each alloy, given in Section 6, as well as the data presented in Section 5 and Appendix B of this report may prove of assistance in the evaluation of any individual alloy for a specific application.

The following materials appear to have satisfactory tensile properties after irradiation to 1×10^{17}nvt ($E > 0.5$ Mev) at 30°R:

Titanium	55A
Nickel Alloys	K Monel and Inconel
Stainless Steel	310

The aluminum casting alloys have not been included in this discussion as the previously noted internal micro-porosity introduced during casting solidification introduces statistical uncertainty of the dependence of the observed change in strength functions on the environmental effects.

Aluminum 5083, while possessing satisfactory cryogenic properties, was not tested after irradiation.

9.3 RECOMMENDATIONS FOR FUNDAMENTALLY ORIENTED TESTS

There is an obvious need for better understanding of the fundamental mechanisms involved in the nuclear cryogenic effects in structural materials. Strictly engineering effect studies are limited in that it is physically impossible to test all potentially useful materials under all anticipated conditions. Also, there can be unforeseen changes in both anticipated operating conditions and in material production techniques and there will be unforeseen new structural alloy developments.

Carefully designed tests on the tensile properties of the more simple polycrystalline materials, when considered in relation to cryogenic-irradiation data on numerous material properties being generated at various laboratories from pure metals and simple alloy single crystals, might yield criteria which would be generally applicable to a wide variety of complex structural materials.

Probably of most importance and of particular value to nuclear-propulsion engineers would be annealing experiments which would allow extrapolation or interpolation of test results obtained at a few temperatures to anticipated operating temperatures. Initial annealing experiments should be on the simple materials, such as Aluminum 1099 with the intent to extend these to increasingly complex alloys, if necessary.

Actual operating integrated fluxes will be orders of magnitude higher in many applications than 10^{17} nvt so it would also be desirable to have results from some of the simple materials irradiated to at least 10^{18} nvt.

10 REFERENCES

1. Cryogenics Materials Data Handbook, Technical Document Report No. ML-TDR-64-280, August 1964.

2. Radiation Effects Information Center, Battelle Memorial Institute, Dual Coordinate Indices and Monthly Accession Lists, Published Serially.

3. Din, F.; and Dockett, A.H.: Low-Temperature Techniques, Interscience Publishers, Inc., 1960.

4. Private Correspondence, Aluminum Company of America and F.W. Thomas, Lockheed-Georgia Company, 1959.

5. McDonald, J.C. : Lockheed Missiles and Space Company, Private Communication, 1961.

6. Cryogenic Materials Data Handbook, PB 171 809 - 1962.

7. Menard, J.; and Weil, L. : Gamma to Alpha Transformations In Austenitic Stainless Steels Under Stress (Single and Repeated) Down to 20°K, U of Greenoble, France: Presented at Cryogenic Engineering Conf. (University of Colorado), 1960.

8. Death, F.S.; and Long, H.M. : Low Temperature Properties of Some Selected Austenitic Manganese Steels, Presented at Cryogenic Engineering Conference (University of California), 1959.

9. Anon. : ASTM Standards, The American Society For Testing Materials, 1958, Part 3.

10. Peterson, R.E. : Stress Concentration Design Factors, John Wiley & Sons, Inc. NY 1953.

11. Low, J.R. Jr. et. al. : Screening Tests For High Strength Alloys Using Sharply Notched Cylindrical Specimens, Materials Research and Standards, ASTM Vol. 2, No. 3, March 1962, pp. 196.

    Strawley, J.E. and Brown, W.F., Jr. : Fracture Toughness Testing, NASA Technical Note NASA TN D-2599, National Aeronautics and Space Administration, Washington, D.C. January 1965.

12. Coltman, R.R.; Klabunde, C.G.; McDonald, D.C. and Redman, J.K. : Reactor Damage in Pure Metals, J. Appl. Phys., Vol. 33, No. 12, December 1962.

13. Coltman, R.R. : ORNL, Private Communication, 1962.

14. Dixon, Wilfrid J.; and Massey, Frank J. Jr. : Introduction to Statistical Analysis, McGraw-Hill Book Co., Inc. 1951.

15. Hoel, P.G. : Introduction to Mathematical Statistics, 2nd Edition, John Wiley and Sons, Inc.

16. Joseph, J.W. Jr. : Stress Relaxation in Stainless Steel During Irradiation, USAEC Report DP-369, 1959, pp. 29.

17. Typical Physical and Mechanical Properties Data of Aluminum Alloys Supplied to Lockheed-Georgia Company by the Aluminum Company of America (not released for publication) January 1961.

18. Thornton, H.G. : Report No. FZK-263-1 to Space Nuclear Propulsion Office of NASA, General Dynamics, Fort Worth, 20 October 1965.

19. Watson, J.F.; and Christian, J.L.; and Allen, J.W. : A Study of the Effects of Nuclear Radiation on High-Strength Aerospace Vehicle Materials at the Boiling Point of Hydrogen (-423°F), ERR - AN - 085 General Dynamics/Astronautics and General Dynamics/Fort Worth. September 27, 1961.

20. Smithells, C.J. : Metals Reference Book, Butterworths (London), 1962, Vol. 1.

21. Blewitt, T.H.; Coltman, R.R.; and Redman, J.K. : Low Temperature Deformation of Copper Single Crystals, J. Appl. Phys., Vol. 28, No. 6, June 1957, pp. 651-660.

22. Lakatin, Y. (N. Weinstein, trans.) : Engineering Physical Metallurgy. Foreign Languages Publishing House (Moscow) 1959.

23. Seitz, Frederick: The Physics of Metals, McGraw-Hill, 1943.

24. Watson, J.F.; and Christian, J.L. : Low Temperature Properties of Cold Rolled AISI Types 301, 302, 304 ELI and 310 Stainless Steel Sheet. ASTM Special Technical Publication No. 287, pp. 170-193; Discussion by Reed, R.P., pp. 194-195.

25. Anon. : Aeronautical Materials Specification, The American Society of Automobile Engineers, 1959.

26. Anon. : Armco Steel Company, Bull. No. TDM 562.

27. Dienes, G.J. and Vineyard, G.H. : Radiation Effects in Solids, Interscience Publishers, 1957.

28. Beevers, C.J. and Nelson, R.S. : Properties of Reactor Materials and the Effects of Radiation Damage, pp. 127, Butterworths (London), 1962.

29. Seitz, F. : Disc. Faraday Soc., Vol. 5, 1949, pp. 271.

30. Brinkman, J.A. : Production of Atomic Displacements by High Energy Particles, Am. J. Phys., Vol. 24, 1956, pp. 246.

31. Silsbee, R.H. : Focusing and Collision Problems in Solids, J. Appl. Phys. 28, 1957, pp. 1246.

32. Jamison, R.E. : Theory of Irradiation Effects in Alloys, Bull. Am. Phys. Soc., Ser. II, Vol. 3, 1958, pp. 118.

33. Tucker, C.W. and Treaftis, H. : Effect of Electron Irradiation on Cluster Formation in Al - 2 At. % Cu Alloy, Bull. Am. Phys. Soc. Series II, Vol. 3, 1958, pp. 118.

34. Jamison, R.E. : Retardation of Zone Growth in An Al-Ag Precipitate Alloy By Previous Fast Neutron Irradiation, Bull. Am. Phys. Soc., Ser. II, Vol. 2, 1957, pp. 151.

35. Radiation Effects Information Center, Battelle Memorial Institute, REIC Report No. 20, Sept. 15, 1961.

APPENDIX A

MATERIAL PEDIGREE DATA

The pedigree data, supplied by the vendors of the test specimen materials for NASw-114, are summarized in Tables A 1 through A 3.

Complete pedigree data is available in the pedigree report, ER-5542 of February, 1962, and its Addendum of September 1963. Minor errors of transcription in ER-5542 have been corrected in the tables in this Appendix.

TABLE A 1 a

PHYSICAL CHARACTERISTICS OF ALUMINUM ALLOYS (PEDIGREE DATA)

Alloy	Temper	Lock-heed Code	Form	Specifi-cation	Vendor		F_{tu} (ksi)	F_{ty} (ksi)	Elonga-tion (% in 4D)	Hardness	Grain Size	
											Grains /mm^2	ASTM No. (E112-58T)
						Vendor Code	Longitud-inal	Longitud-inal	Longitud-inal	Test	Longi-tudinal	
						Vendor Lot No.	Trans-verse	Trans-verse	Trans-verse	Value	Trans-verse	
1099	H-14	8 Ba	0.5" Plate	Vendor	Alcoa*	199352 199352	13.50 14.25	12.90 13.95	20.5 19.5	Brinell 26	**	
2014	T-651	1 Ba	0.5" Plate	AMS-4029	Alcoa*	251757 747-461	69.10 69.45	64.55 62.65	11.7 10.3	Brinell 137	880 990	6.0 to 6.5
2024	T-351	7 Ba	0.5" Plate	AMS-4037 E	Alcoa*	251758 747-441	70.00 68.45	54.45 47.00	21.1 19.7	Brinell 128	345 515	5.0
2219	T-87	2 Ba	0.5" Plate	Vendor	Alcoa*	251776 124-481	67.15 67.55	55.25 55.25	12.0 10.9	Brinell 128	280 560	5.0
5083	H-321	3 Ba	0.5" Plate	Mil-A-17358B	Alcoa*	251941 124-461	50.45 50.05	35.75 31.90	14.0 19.7	Brinell 86	**	
5086	H-32	11 Ba	0.5" Plate	Mil-A-19070A	Reynolds	RK-7948 RK-7948	44.90 43.70	32.60 31.10	16.0 17.5	Rockwell-15T 76	**	
5456	H-321	5 Ba	0.5" Plate	Mil-A-19842 B	Alcoa*	251779 124-351	54.05 53.40	38.00 33.90	13.7 17.7	Brinell 93	**	
6061	T-6	12 Ba	0.5" Plate	QQ-A-327B	Reynolds	75762A 75762A	49.40 49.50	43.50 44.40	17.5 15.0	Rockwell-15T 84	**	
7079	T-6	13 Ba	0.5" Rod	Vendor	Alcoa*	ARL-281577	91.40 -	86.70 -	10.8 -	Brinell 152	**	
7178	T-651	10 Bb	0.5" Plate	Mil-A-9180A	Alcoa*	251780 747-711	90.30 89.30	83.90 81.00	10.0 10.3	Brinell 164	40 400	3.0
X-250	T-4	4 Ba	Sand Casting	Vendor	Alcoa*	251801 E-2464A-D	60.30 -	33.10 -	21.0 -	Brinell 91	**	
B-750	T-5	6 Ba	P.M. Casting	Vendor	Alcoa*	251951 Bar-301	30.80 -	22.40 -	4.0 -	Brinell 64	**	
A 356	T-61	14 Ba	P.M. Casting	Vendor	Alcoa*	ARL-281682	42.15 -	27.55 -	18.0	Brinell 80	**	

* The Aluminum Company of America

** not measured

TABLE A 1 b

CHEMICAL ANALYSES OF ALUMINUM ALLOYS (PEDIGREE DATA)

Alloy	Lock-heed Code	ELEMENT, WEIGHT PERCENT													
		Al	Cu	Fe	Si	Mn	Mg	Zn	Ni	Cr	Ti	V	Zr	Sn	Other
1099	8 Ba	99.99	0.003	0.001	0.001	-	-	-	-	-	-	-	-	-	-
2014	1 Ba	(1)	4.35	0.43	0.86	0.66	0.56	0.18	0.01	0.03	0.04	-	-	-	-
2024	7 Ba	(1)	4.45	0.29	0.12	0.57	1.46	0.07	0.01	0.03	0.02	-	-	-	-
2219	2 Ba	(1)	6.11	0.21	0.08	0.29	0.01	0.00	0.02	0.00	0.07	0.11	0.16	-	-
5083	3 Ba	(1)	0.06	0.22	0.13	0.77	4.26	0.01	0.00	0.09	0.01	-	-	-	-
5086	11 Ba	(1)	0.08	0.33	0.18	0.35	3.59	0.08	(2)	0.16	0.02	-	-	-	(2)
5456	5 Ba	(1)	0.05	0.18	0.10	0.82	5.13	0.03	0.00	0.11	0.03	-	-	-	-
6061	12 Ba	(1)	0.32	0.40	0.69	0.05	0.88	0.06	(2)	0.27	0.02	-	-	-	(2)
7079	13 Ba	(1)	0.74	0.17	0.10	0.15	3.42	4.50	0.00	0.16	0.01	-	-	-	-
7178	10 Bb	(1)	1.78	0.23	0.10	0.05	2.59	6.72	0.00	0.20	0.04	-	-	-	-
X-250	4 Ba	(1)	0.17	0.10	0.09	0.23	8.41	1.56	0.00	0.00	0.09	-	-	-	-
B 750	6 Ba	(1)	1.87	0.29	0.25	0.03	0.88	-	1.15	-	0.03	-	-	6.48	-
A-356	14 Ba	(1)	0.01	0.15	6.86	0.01	0.38	0.02	0.02	0.00	0.13	-	-	-	-

(1). balance

(2). less than 0.02 wt. % each of seven common impurities

TABLE A 2 a

PHYSICAL CHARACTERISTICS OF TITANIUM AND NICKEL ALLOYS (PEDIGREE DATA)

	Temper	Lock-heed Code	Form	Specifi-cation	Vendor	Vendor Code / Heat Number	F_{tu} (ksi)	F_{ty} (ksi)	Elonga-tion (% in 4D)	Hardness Test / Value	Grain Size ASTM No. (E112-58T)
TITANIUM ALLOYS											
Ti 55A	Annealed	1 Aa	0.5' Round Bar	Mil-T-7993A Class II	TMCA*	-- / M-9186	70.5	60.5	35	Rockwell B 87	5
Ti-5Al-2.5 Sn (Std. I)	Annealed	3 Aa	0.5" Round Bar	AMS-4910	TMCA*	-- / M-7888	131.0	127.0	22	Rockwell C 31-33	8
Ti-5Al-2.5 Sn (ELI)	Annealed	8 Aa	0.5" Round Bar	TMCA 49021-1	TMCA*	-- / V-2402	119.3	101.2	17	Rockwell C 24.9	-
Ti-6Al-4V (Annealed)	Annealed	2 Ac	0.5" Round Bar	Mil-T-9047C	TMCA*	-- / M8574	146.0	138.0	15.5	Rockwell C	-
Ti-6Al-4V (Aged)	Solution Treated & Aged	2 Aa	0.5" Round Bar	Mil-T-9047C	TMCA*	-- / M-9812	173.0	165.0	13	Rockwell C 33-36	-
Ti-8Al-1Mo-1V	Annealed	4 Aa	0.5" Round Bar	Vendor	TMCA*	A-4506 / V-1306	143.0	139.5	19	Rockwell C	9
NICKEL ALLOYS											
René 41	Solution Treated	7 Ca	0.5" Round Bar	Vendor	General Electric	VM-5155 / R-144	140.2	68.5	48.4	(BHN) 248	4-6
K Monel	Drawn, Annealed & Aged	1 Fb	0.5" Round Bar	QQ-N-286A	INCO**	HK48080 / M8759K	156.0	105.0	29	Rockwell C 31	9
Inconel	Cold Drawn	2 Fb	0.5" Round Bar	Mil-N-6710	INCO**	HK48081 / NX2774	137.0	130.5	12	Rockwell C 27	7
Inconel X	Aged	3 Fa	0.5" Round Bar	AMS 5667	INCO**	45745 / 2645	188.9	128.3	26.4	Rockwell C 38	8 or finer

* The Titanium Metals Corporation of America

** The International Nickel Company

TABLE A 2 b

CHEMICAL ANALYSES OF TITANIUM AND NICKEL ALLOYS (PEDIGREE DATA)

TITANIUM ALLOYS	Lock-heed Code	ELEMENT, WEIGHT PERCENT											
		C	Fe	Al	Sn	V	Mo				N_2	H_2	O_2
Ti 55A	1 Aa	0.032	0.19								0.023	0.006	0.218
Ti-5Al-2.5 Sn (Std. I)	3 Aa	0.032	0.110	5.10	2.5						0.019	0.012	0.116
Ti-5Al-2.5 Sn (ELI)	8 Aa	0.033	0.028	5.43	2.41						0.011	0.0056	0.053
Ti-6Al-4V (Annealed)	2 Ac	0.010	0.170	5.95		4.00					0.022	0.006	0.065
Ti-6Al-4V (Aged)	2 Aa	0.010	0.15	5.80		3.90					0.035	0.010	0.102
Ti-8Al-1Mo-1V	4 Aa	0.030	0.12	8.02		1.14	1.0				0.013	0.009	0.091
NICKEL ALLOYS		C	S	Si	Mn	Cr	Cu	Mo	Co	Ti	Al	Fe	Cb & Ta
René 41	7 Ca	0.11	0.006	0.06	0.07	19.05		9.91	10.93	3.10	1.48	0.71	
K Monel	1 Fb	0.15	0.005	0.22	0.55		30.45			0.48	2.79	1.02	
Inconel	2 Fb	0.03	0.007	0.23	0.18	15.37						6.89	
Inconel X	3 Fa	0.07		0.05	0.14	15.42	0.01	0.09	0.05	2.68	0.68	7.68	0.88

TABLE A 3 a

PHYSICAL CHARACTERISTICS OF FERROUS ALLOYS (PEDIGREE DATA)

Alloy	Temper	Lock-heed	Form	Specifi-cation	Vendor	Vendor Code / Heat Number	F_{tu} (ksi)	F_{ty} (ksi)	Elonga-tion (% in 4D)	Hardness Test / Value	Grain Size ASTM No. (E112-58T) Longitud-inal / Trans-verse
304	Annealed	2 Cb	1.0" Round Bar	ASTM-A 167-58	Carpenter	W73659 801904	88.8	42.80	57.2	Rockwell B 82.5	5.0-6.0 5.0-6.0
310	Annealed	3 Cb	0.5" Round Bar	ASTM-A 167-58	Carpenter	W73661 X-48576	91.1	75.0	23.8	Rockwell B 92	4.0-5.0 5.0-6.0
347	Annealed	4 Cb	0.5" Round Bar	ASTM-A 167-58	Carpenter	W73663 X-45779	91.0	50.6	42.0	Rockwell B 88	9.5-10.0 9.5-10.0
A286 (AMS-5735)	Solution Treated, Aged	6 Ca	0.5" Round Bar	AMS5735-E (Mod.)	Carpenter	W80763 K-46419	159.8	125.1	22.8	Rockwell C 31	7.5-10.0 7.0-8.0
A286 (AMS-5737)	Solution Treated, Aged	8 Ca	0.5" Round Bar	AMS5737	Allegheny-Ludlum	-- W-23742	159.0	127.0	20	Brinell (1000 Kg) 302	7.0-8.0 7.0-8.0
T-450 *	Annealed	1 Eb	0.484" Round Bar	Lockheed	Carpenter	W-73664 B-03116	93.4	34.5	58.6	Rockwell B 80	4.5-5.5 4.5-5.5
AM 350 **	SCT	10 Ca	0.5" Round Bar	Vendor	Allegheny-Ludlum	-- 28579-H	207.0	184.0	14	Rockwell C 46	- -
17-7 PH ***	RH-950	11 Ca	0.5" Round Bar	Vendor	Republic	-- 3331411	209.0	185.0	12	Rockwell C 47	- -
A-353	Normalized, Air Cooled	5 Ca	0.5" Plate	Grade B ASTM-A 353-58	Lukens	2757 16156	133.6	101.9	28	Rockwell B 96	8.0 or finer finer
440C	Quenched & Drawn	9 Ca	0.5" Round Bar	ASTM-A 276-57T	Carpenter	W44461 805931	285.0 ****	275.0 ****	2 ****	Rockwell C 60	- -

* Developed by the Union Carbide Corporation, Linde Division

** Proprietary alloy of the Allegheny-Ludlum Steel Corporation

*** Proprietary alloy of the Armco Steel Corporation

**** Typical values from manufacturers literature

" Stress relieved specimens

TABLE A 3 b

CHEMICAL ANALYSES OF FERROUS ALLOYS (PEDIGREE DATA)

Alloy	Lock-heed Code	ELEMENT, WEIGHT PERCENT														
		C	Mn	Si	P	S	Cr	Ni	Mo	Cu	Co	N	Nb	Ti	V	Al
304	2 Cb	0.062	0.81	0.52	0.016	0.018	18.36	9.22	0.07	0.14	0.055	0.027				
310	3 Cb	0.038	1.62	0.67	0.018	0.007	25.06	20.70	0.19	0.19	0.077	0.041				
347	4 Cb	0.058	1.48	0.70	0.022	0.008	18.18	11.03	0.14	0.15	0.064	0.033	0.81	0.02		
A 286 (AMS-5735)	6 Ca	0.047	1.71	0.82	0.017	0.003	14.52	25.95	1.22	0.12		0.005		2.27	0.26	0.15
A 286 (AMS-5737)	8 Ca	0.053	1.20	0.55	0.012	0.001	14.77	25.90	1.22					2.19	0.21	0.16
T-450	1 Eb	0.15	18.39	0.23	0.005	0.008	3.12	2.11	0.02	1.55	0.011	0.036				
AM350	10 Ca	0.099	0.95	0.41	0.028	0.011	16.49	4.31	2.76	0.10		0.087				
17-7 PH	11 Ca	0.062	0.55	0.28	0.023	0.008	16.70	6.98								1.26
A 353	5 Ca	0.08	0.48	0.21	0.02	0.024		8.58								
440C	9 Ca	1.09	0.37	0.21	0.014	0.010	17.44	0.30	0.51	0.11	0.02	0.021			0.05	

APPENDIX B

TEST RESULTS

The complete test data generated in each specimen tested in the screening program are given in Tables B 1 through B 33 with certain self-explanatory statistical evaluation.

The data herein reported is discussed in Sections 4, 5, 6 and 7 of the body of this report.

TABLE B 1 a

TEST RESULTS, ALUMINUM 1099 (H-14)

Specimen Number	Test Temp	Total Fast Flux[a] (nvt)	F_{tu} (ksi) Test Value		Bias[b]	Bias Range[c]	F_{ty} (ksi) Test Value		Bias[b]	Bias Range[c]
TENSILE TESTS										
8 Ba 1	RT	None	11.7				11.0			
8 Ba 2	RT	None	13.3				12.6			
8 Ba 17	RT	None	14.0				13.4			
8 Ba 27	RT	None	12.6				11.9			
8 Ba 34	RT	None	14.3				13.5			
Arith. Mean				13.18				12.48		
Std. Deviation				1.06				1.05		
8 Ba 36	30°R	None	33.0				8.19			
8 Ba 39	30°R	None	30.0				6.03			
8 Ba 40	30°R	None	30.0				8.04			
8 Ba 82	30°R	None	39.3				6.67			
8 Ba 86	30°R	None	36.6				7.13			
Arith. Mean				33.78	+20.6	+17.1		6.97	- 5.5	-4.3
Std. Deviation				4.11		+24.1		0.95		-6.7
8 Ba 87	30°R	10^{17}	49.2		+15.4		43.3		+36.3	
8 Ba 84[i]	30°R	10^{17}	45.9		+12.1		33.5		+26.5	
8 Ba 80[k]	30°R	10^{17}	45.8		+12.0		31.0		+24.0	
Arith. Mean				(l)	(l)	(l)		(l)	(l)	(l)
Std. Deviation				(l)		(l)		(l)		(l)
TENSILE NOTCH TESTS			F_{tun} (ksi)				F_{tun}/F_{tu}			
8 Ba 3	RT	None	16.2				1.38			
8 Ba 7	RT	None	16.4				1.23			
8 Ba 14	RT	None	15.2				1.09			
8 Ba 18	RT	None	16.0				1.27			
8 Ba 26	RT	None	16.8				1.17			
Arith. Mean				16.12				1.228		
Std. Deviation				0.59				0.110		
8 Ba 28	30°R	None	47.2				1.43			
8 Ba 42	30°R	None	45.8				1.53			
8 Ba 44	30°R	None	47.8				1.59			
8 Ba 45	30°R	None	47.2				1.20			
8 Ba 57	30°R	None	47.8				1.31			
Arith. Mean				47.16	+31.0	+30.2		1.412	+ 0.18	+0.02
Std. Deviation				0.82		+31.9		0.158		+0.34
(q)	30°R	10^{17}					(q)			
(q)	30°R	10^{17}					(q)			
(q)	30°R	10^{17}					(q)			
Arith. Mean										
Std. Deviation										

TABLE B 1 b

TEST RESULTS, ALUMINUM 1099 (H-14)

F_{ty}/F_{tu}	Elongation (%)	Reduction of Area (%)	Fracture Stress (ksi)	Total Fast Flux[a] (nvt)	Test Temp	Specimen Number
				TENSILE TESTS		
0.94	22	74	(e)	None	RT	8 Ba 1
0.94	26	83	(e)	None	RT	8 Ba 2
0.95	25	78	(e)	None	RT	8 Ba 17
0.94	21	79	(e)	None	RT	8 Ba 27
0.94	20	81	(e)	None	RT	8 Ba 34
0.942	22.8	79.0	(e)	. . . . .	Arith. Mean	
0.25	62	62	(e)	None	30°R	8 Ba 36
0.20	61	61	(e)	None	30°R	8 Ba 39
0.27	63	76	(e)	None	30°R	8 Ba 40
0.17	60	71	110.0	None	30°R	8 Ba 82
0.19	61	76	110.0	None	30°R	8 Ba 86
0.216	61.4	69.2	110.0	. . . . .	Arith. Mean	
0.88	46	54	87.4	10^{17}	30°R	8 Ba 87
0.73	43	56	89.5	10^{17}	30°R	8 Ba 84 (i)
0.68	41	67	107.0	10^{17}	30°R	8 Ba 80 (k)
(l)	(l)	(l)	(l)	. . . . .	Arith. Mean	

(e). not recorded

(i). interruption of refrigeration at 80% of total accumulated dose caused specimen temperature to increase to about 70°R for about 10 minutes

(k). apparently strained, before irradiation, to about one-half of total elongation

(l). not averaged due to non-identical test conditions

(a). of neutrons with >.5 mev energy

(b). change in mean of test value with respect to previous test condition

(c). with 90% confidence

TABLE B 2 a

TEST RESULTS, ALUMINUM 2014 (T-651)

Specimen Number	Test Temp	Total Fast Flux[a] (nvt)	F_{tu} (ksi) Test Value		Bias[b]	Bias Range[c]	F_{ty} (ksi) Test Value		Bias[b]	Bias Range[c]
TENSILE TESTS										
1 Ba 13	RT	None	71.1				63.8			
1 Ba 35	RT	None	62.4				57.5			
1 Ba 46	RT	None	64.5				59.8			
1 Ba 47	RT	None	64.8				59.7			
1 Ba 48	RT	None	65.4				60.9			
Arith. Mean				65.64			.....	60.34		
Std. Deviation				3.25			.....	2.29		
1 Ba 49	30°R	None	91.6				56.7			
1 Ba 63	30°R	None	92.9				63.1			
1 Ba 67	30°R	None	87.1				71.2			
1 Ba 68	30°R	None	89.1				72.3			
1 Ba 70	30°R	None	94.8				78.1			
Arith. Mean				91.10	+25.5	+21.8	.....	68.28	+7.9	+ 0.7
Std. Deviation				3.05		+29.2	.....	8.40		+15.2
1 Ba 65	30°R	10^{17}	81.3				64.9			
1 Ba 71	30°R	10^{17}	90.6				78.2			
1 Ba 72	30°R	10^{17}	81.9				72.2			
Arith. Mean				84.60	- 6.5	- 0.1	.....	71.77	+3.5	- 7.0
Std. Deviation				5.20		-12.9	.....	6.66		+13.9
TENSILE NOTCH TESTS			F_{tun} (ksi)				F_{tun}/F_{tu}			
1 Ba 15	RT	None	80.6				1.13			
1 Ba 16	RT	None	76.7				1.23			
1 Ba 18	RT	None	80.8				1.25			
1 Ba 19	RT	None	79.3				1.22			
1 Ba 27	RT	None	80.1				1.22			
Arith. Mean				79.50			.....	1.21		
Std. Deviation				1.67			.....	0.04		
1 Ba 54	30°R	None	101.0				1.10			
1 Ba 55	30°R	None	98.8				1.06			
1 Ba 57	30°R	None	102.0				1.17			
1 Ba 58	30°R	None	102.0				1.14			
1 Ba 61	30°R	None	102.0				1.08			
Arith. Mean				101.16	+21.7	+19.9	.....	1.11	-0.10	- 0.05
Std. Deviation				1.39		+23.5	.....	0.05		- 0.15
(q)	30°R	10^{17}								
(q)	30°R	10^{17}								
(q)	30°R	10^{17}								
Arith. Mean							.....			
Std. Deviation							.....			

TABLE B 2 b

TEST RESULTS, ALUMINUM 2014 (T-651)

F_{ty}/F_{tu}	Elongation (%)	Reduction of Area (%)	Fracture Stress (ksi)	Total Fast Flux[a] (nvt)	Test Temp	Specimen Number
				TENSILE TESTS		
0.90	13	34	69.3	None	RT	1 Ba 13
0.92	13	36	(e)	None	RT	1 Ba 35
0.93	13	34	(e)	None	RT	1 Ba 46
0.92	11	36	(e)	None	RT	1 Ba 47
0.93	11	35	(e)	None	RT	1 Ba 48
0.920	12.2	35.0	69.3	. . . . .	Arith. Mean	
0.62	(d)	(d)	(e)	None	30°R	1 Ba 49
0.68	(d)	(d)	(e)	None	30°R	1 Ba 63
0.82	16	28	114.0	None	30°R	1 Ba 67
0.81	19	26	115.0	None	30°R	1 Ba 68
0.82	18	25	122.0	None	30°R	1 Ba 70
0.750	17.7	26.3	117.0	. . . . .	Arith. Mean	
0.80	13	13	93.4	10^{17}	30°R	1 Ba 65
0.86	12	21	108.3	10^{17}	30°R	1 Ba 71
0.88	13	21	103.0	10^{17}	30°R	1 Ba 72
0.847	12.7	18.3	101.6	. . . . .	Arith. Mean	

(d). not available

(e). not recorded

(q). test deleted from screening program

(a). of neutrons with >.5 mev energy

(b). change in mean of test value with respect to previous test condition

(c). with 90% confidence

TABLE B 3 a

TEST RESULTS, ALUMINUM 2024 (T-351)

Specimen Number	Test Temp	Total Fast Flux[a] (nvt)	F_{tu} (ksi) Test Value		Bias[b]	Bias Range[c]	F_{ty} (ksi) Test Value		Bias[b]	B R
TENSILE TESTS										
7 Ba 1	RT	None	67.4				50.7			
7 Ba 7	RT	None	67.0				50.4			
7 Ba 17	RT	None	68.1				50.4			
7 Ba 23	RT	None	66.1				49.7			
7 Ba 40	RT	None	66.8				50.3			
Arith. Mean				67.08				50.30		
Std. Deviation				0.74				0.37		
7 Ba 14	30°R	None	111.0				79.5			
7 Ba 28	30°R	None	106.0				76.8			
7 Ba 32	30°R	None	105.0				75.9			
7 Ba 36	30°R	None	106.0				77.3			
7 Ba 39	30°R	None	105.0				76.5			
Arith. Mean				106.6	+39.5	+37.3		77.20	+26.9	+
Std. Deviation				2.5		+41.7		1.38		+
7 Ba 6	30°R	10^{17}	111.4				(e)			
7 Ba 9	30°R	10^{17}	90.6				79.2			
7 Ba 25	30°R	10^{17}	100.3				79.6			
Arith. Mean				100.8	- 5.8	+ 6.0		79.40	+ 2.2	+
Std. Deviation				10.4		-17.7		0.28		+
TENSILE NOTCH TESTS			F_{tun} (ksi)				F_{tun}/F_{tu}			
7 Ba 4	RT	None	69.8				1.04			
7 Ba 5	RT	None	71.7				1.07			
7 Ba 8	RT	None	74.2				1.09			
7 Ba 10	RT	None	74.6				1.13			
7 Ba 11	RT	None	73.8				1.10			
Arith. Mean				72.82				1.086		
Std. Deviation				2.03				.033		
7 Ba 12	30°R	None	97.9				0.88			
7 Ba 20	30°R	None	99.1				0.93			
7 Ba 24	30°R	None	97.0				0.92			
7 Ba 38	30°R	None	101.0				0.95			
7 Ba 42	30°R	None	83.2				0.79			
Arith. Mean				95.64	+17.8	+11.7		0.894	- 0.19	-
Std. Deviation				7.11		+24.0		0.632		-
(q)	30°R	10^{17}								
(q)	30°R	10^{17}								
(q)	30°R	10^{17}								
Arith. Mean										
Std. Deviation										

TABLE B 3 b

TEST RESULTS, ALUMINUM 2024 (T-351)

F_{ty}/F_{tu}	Elongation (%)	Reduction of Area (%)	Fracture Stress (ksi)	Total Fast Flux[a] (nvt)	Test Temp	Specimen Number
				TENSILE TESTS		
0.75	21	23	(e)	None	RT	7 Ba 1
0.75	20	25	(e)	None	RT	7 Ba 7
0.74	22	32	(e)	None	RT	7 Ba 17
0.75	22	30	(e)	None	RT	7 Ba 23
0.75	23	31	(e)	None	RT	7 Ba 40
0.748	21.6	28.2	(e)	. . . . .	Arith. Mean	
0.72	20	21	(e)	None	30°R	7 Ba 14
0.72	(d)	(d)	(e)	None	30°R	7 Ba 28
0.72	17	20	(e)	None	30°R	7 Ba 32
0.73	31	18	(e)	None	30°R	7 Ba 36
0.73	21	22	(e)	None	30°R	7 Ba 39
0.724	22.3	20.3	(e)	. . . . .	Arith. Mean	
(e)	18	16	133.0	10^{17}	30°R	7 Ba 6
0.87	15	14	105.0	10^{17}	30°R	7 Ba 9
0.79	16	24	133.0	10^{17}	30°R	7 Ba 25
0.830	16.3	18.0	123.7	. . . . .	Arith. Mean	

(d). not available

(e). not recorded

(q). test deleted from screening program

(a). of neutrons with >.5 mev energy

(b). change in mean of test value with respect to previous test condition

(c). with 90% confidence

TABLE B 4 a

TEST RESULTS, ALUMINUM 2219 (T-87)

Specimen Number	Test Temp	Total Fast Flux[a] (nvt)	F_{tu} (ksi) Test Value		Bias[b]	Bias Range[c]	F_{ty} (ksi) Test Value		Bias[b]	Bias Range[c]
TENSILE TESTS										
2 Ba 41	RT	None	63.1				51.4			
2 Ba 45	RT	None	62.7				51.7			
2 Ba 50	RT	None	63.1				51.0			
2 Ba 53	RT	None	62.6				50.8			
2 Ba 60	RT	None	43.7				35.2			
Arith. Mean				59.04				48.02		
Std. Deviation				8.58				7.18		
2 Ba 30	30°R	None	95.9				67.6			
2 Ba 32	30°R	None	96.5				68.4			
2 Ba 34	30°R	None	95.2				66.9			
2 Ba 35	30°R	None	95.3				68.0			
2 Ba 36	30°R	None	96.4				70.0			
Arith. Mean				95.86	+36.8	+29.7		68.18	+20.2	+14.1
Std. Deviation				0.59		+44.0		1.16		+26.2
2 Ba 58	30°R	10^{17}	93.5				76.2			
2 Ba 61	30°R	10^{17}	96.0				77.2			
2 Ba 70	30°R	10^{17}	91.7				68.8			
Arith. Mean				93.73	- 2.1	+ 0.3		74.07	+ 5.9	+ 0.6
Std. Deviation				2.16		- 4.6		4.59		+11.1
TENSILE NOTCH TESTS			F_{tun} (ksi)				F_{tun}/F_{tu}			
2 Ba 31	RT	None	76.1				1.21			
2 Ba 37	RT	None	73.4				1.17			
2 Ba 38	RT	None	73.9				1.17			
2 Ba 40	RT	None	75.4				1.20			
2 Ba 42	RT	None	74.6				1.71			
Arith. Mean				74.68				1.29		
Std. Deviation				1.09				0.23		
2 Ba 43	30°R	None	99.3				1.04			
2 Ba 44	30°R	None	102.0				1.06			
2 Ba 49	30°R	None	89.4				0.94			
2 Ba 52	30°R	None	98.8				1.04			
2 Ba 54	30°R	None	101.0				1.05			
Arith. Mean				98.10	+23.4	+19.1		1.03	- 0.26	- 0.06
Std. Deviation				5.03		+27.7		0.05		- 0.46
(q)	30°R	10^{17}								
(q)	30°R	10^{17}								
(q)	30°R	10^{17}								
Arith. Mean										
Std. Deviation										

TABLE B 4 b

TEST RESULTS, ALUMINUM 2219 (T-87)

F_{ty}/F_{tu}	Elongation (%)	Reduction of Area (%)	Fracture Stress (ksi)	Total Fast Flux[a] (nvt)	Test Temp	Specimen Number
				TENSILE TESTS		
0.81	14	31	(e)	None	RT	2 Ba 41
0.82	16	34	(e)	None	RT	2 Ba 45
0.81	13	31	(e)	None	RT	2 Ba 50
0.81	16	37	(e)	None	RT	2 Ba 53
0.81	12	28	52.4	None	RT	2 Ba 60
0.812	14.2	32.2	52.4	. . . . .	Arith. Mean	
0.70	16	23	(e)	None	30°R	2 Ba 30
0.71	18	31	(e)	None	30°R	2 Ba 32
0.70	15	27	(e)	None	30°R	2 Ba 34
0.71	15	28	(e)	None	30°R	2 Ba 35
0.73	18	27	(e)	None	30°R	2 Ba 36
0.710	16.4	27.2	(e)	. . . . .	Arith. Mean	
0.81	15	15	109.0	10^{17}	30°R	2 Ba 58
0.80	15	19	113.0	10^{17}	30°R	2 Ba 61
0.75	16	21	112.0	10^{17}	30°R	2 Ba 70
0.787	15.3	18.3	111.3	. . . . .	Arith. Mean	

(e). not recorded

(q). test deleted from screening program

(a). of neutrons with >.5 mev energy

(b). change in mean of test value with respect to previous test condition

(c). with 90% confidence

TABLE B 5 a

TEST RESULTS, ALUMINUM 5083 (H-321)

Specimen Number	Test Temp	Total Fast Flux[a] (nvt)	F_{tu} (ksi) Test Value		Bias[b]	Bias Range[c]	F_{ty} (ksi) Test Value		Bias[b]	Bias Range[c]
TENSILE TESTS										
3 Ba 4	RT	None	47.0				31.7			
3 Ba 5	RT	None	46.0				31.5			
3 Ba 6	RT	None	45.5				31.8			
3 Ba 7	RT	None	46.5				33.1			
3 Ba 8	RT	None	46.8				32.7			
Arith. Mean				46.36				32.16		
Std. Deviation				.61				.70		
3 Ba 12	30°R	None	93.6				43.7			
3 Ba 31	30°R	None	101.0				43.4			
3 Ba 38	30°R	None	88.7				41.7			
3 Ba 39	30°R	None	93.0				42.0			
3 Ba 40	30°R	None	101.0				45.8			
Arith. Mean				95.46	+49.1	+44.6 +53.6		43.32	+11.2	+10.4 +11.9
Std. Deviation				5.40				1.63		
(f)	30°R	10^{17}								
(f)	30°R	10^{17}								
(f)	30°R	10^{17}								
Arith. Mean										
Std. Deviation										
TENSILE NOTCH TESTS			F_{tun} (ksi)				F_{tun}/F_{tu}			
3 Ba 15	RT	None	54.6				1.16			
3 Ba 16	RT	None	55.0				1.20			
3 Ba 17	RT	None	54.8				1.20			
3 Ba 18	RT	None	55.9				1.20			
3 Ba 19	RT	None	55.1				1.18			
Arith. Mean				55.08				1.19		
Std. Deviation				0.50				0.02		
3 Ba 1	30°R	None	74.5				.80			
3 Ba 20	30°R	None	75.0				.74			
3 Ba 21	30°R	None	69.8				.79			
3 Ba 22	30°R	None	74.3				.80			
3 Ba 32	30°R	None	89.9				.89			
Arith. Mean				76.70	+21.6	+15.2 +28.0		0.804	- 0.39	- 0.34 - 0.43
Std. Deviation				7.67				0.055		
(q)	30°R	10^{17}								
(q)	30°R	10^{17}								
(q)	30°R	10^{17}								
Arith. Mean										
Std. Deviation										

TABLE B 5 b

TEST RESULTS, ALUMINUM 5083 (H-321)

F_{ty}/F_{tu}	Elongation (%)	Reduction of Area (%)	Fracture Stress (ksi)	Total Fast Flux[a] (nvt)	Test Temp	Specimen Number
				TENSILE TESTS		
0.67	11	21	(d)	None	RT	3 Ba 4
0.68	11	25	(d)	None	RT	3 Ba 5
0.70	12	18	(d)	None	RT	3 Ba 6
0.71	12	27	(d)	None	RT	3 Ba 7
0.70	11	28	(d)	None	RT	3 Ba 8
0.692	11.4	23.8	(d)	. . . . .	Arith. Mean	
0.47	25	23	(e)	None	30°R	3 Ba 12
0.43	12	25	132.0	None	30°R	3 Ba 31
0.47	20	20	(e)	None	30°R	3 Ba 38
0.45	26	30	(e)	None	30°R	3 Ba 39
0.45	22	22	128.0	None	30°R	3 Ba 40
0.454	21.0	24.0	130.0	. . . . .	Arith. Mean	
				10^{17}	30°R	(f)
				10^{17}	30°R	(f)
				10^{17}	30°R	(f)
				. . . . .	Arith. Mean	

(d). not available

(e). not recorded

(f). screening program ended before completion of this test

(q). test deleted from screening program

(a). of neutrons with >.5 mev energy

(b). change in mean of test value with respect to previous test condition

(c). with 90% confidence

TABLE B 6 a

TEST RESULTS, ALUMINUM 5086 (H-32)

Specimen Number	Test Temp	Total Fast Flux[a] (nvt)	F_{tu} (ksi) Test Value		Bias[b]	Bias Range[c]	F_{ty} (ksi) Test Value		Bias[b]	Bias Range[c]
TENSILE TESTS										
11 Ba 31	RT	None	45.9				32.8			
11 Ba 32	RT	None	44.5				32.1			
11 Ba 61	RT	None	43.7				29.3			
11 Ba 63	RT	None	49.1				35.7			
11 Ba 71	RT	None	43.5				30.1			
Arith. Mean				45.34			.....	32.00		
Std. Deviation				2.30			.....	2.51		
11 Ba 50	30°R	None	88.4				31.8			
11 Ba 51	30°R	None	91.7				39.3			
11 Ba 64	30°R	None	97.2				37.0			
11 Ba 66	30°R	None	91.8				36.6			
11 Ba 73	30°R	None	90.7				36.2			
Arith. Mean				91.96	+46.6	+43.3	.....	36.18	+ 4.2	+ 1.1
Std. Deviation				3.23		+49.9	.....	2.73		+ 7.3
11 Ba 40	30°R	10^{17}	92.5				61.1			
11 Ba 68	30°R	10^{17}	98.6				60.4			
11 Ba 72	30°R	10^{17}	91.6				56.9			
Arith. Mean				94.23	+ 2.27	- 2.8	.....	59.47	+23.3	+19.8
Std. Deviation				3.81		+ 7.4	.....	2.25		+26.8
TENSILE NOTCH TESTS			F_{tun} (ksi)				F_{tun}/F_{tu}			
11 Ba 15	RT	None	52.6				1.15			
11 Ba 16	RT	None	53.6				1.20			
11 Ba 17	RT	None	53.3				1.22			
11 Ba 18	RT	None	52.6				1.07			
11 Ba 19	RT	None	52.3				1.20			
Arith. Mean				52.88			.....	1.17		
Std. Deviation				0.54			.....	0.06		
11 Ba 20	30°R	None	70.6				0.80			
11 Ba 21	30°R	None	58.6				0.64			
11 Ba 22	30°R	None	75.7				0.78			
11 Ba 23	30°R	None	68.4				0.75			
11 Ba 24	30°R	None	68.7				0.76			
Arith. Mean				68.40	+15.5	+10.3	.....	0.75	- 0.42	- 0.33
Std. Deviation				6.21		+20.7	.....	0.09		- 0.51
(q)	30°R	10^{17}								
(q)	30°R	10^{17}								
(q)	30°R	10^{17}								
Arith. Mean							.....			
Std. Deviation							.....			

TABLE B 6 b

TEST RESULTS, ALUMINUM 5086 (H-32)

F_{ty}/F_{tu}	Elongation (%)	Reduction of Area (%)	Fracture Stress (ksi)	Total Fast Flux[a] (nvt)	Test Temp	Specimen Number
				TENSILE TESTS		
0.71	8	29	(e)	None	RT	11 Ba 31
0.72	10	24	(e)	None	RT	11 Ba 32
0.67	12	15	50.6	None	RT	11 Ba 61
0.73	12	20	59.0	None	RT	11 Ba 63
0.69	11	22	53.0	None	RT	11 Ba 71
0.704	10.6	22.0	54.2	. . . . .	Arith. Mean	
0.36	30	29	125.0	None	30°R	11 Ba 50
0.43	(d)	(d)	(e)	None	30°R	11 Ba 51
0.38	28	24	128.0	None	30°R	11 Ba 64
0.40	31	25	122.0	None	30°R	11 Ba 66
0.40	31	22	116.0	None	30°R	11 Ba 73
0.394	30.0	25.0	122.7	. . . . .	Arith. Mean	
0.66	21	18	112.0	10^{17}	30°R	11 Ba 40
0.61	24	22	127.0	10^{17}	30°R	11 Ba 68
0.62	22	20	115.0	10^{17}	30°R	11 Ba 72
0.630	22.3	20.0	118.0	. . . . .	Arith. Mean	

(d). not available

(e). not recorded

(q). test deleted from screening program

(a). of neutrons with >.5 mev energy

(b). change in mean of test value with respect to previous test condition

(c). with 90% confidence

TABLE B 7 a

TEST RESULTS, ALUMINUM 5456 (H-321)

Specimen Number	Test Temp	Total Fast Flux[a] (nvt)	F_{tu} (ksi) Test Value		Bias[b]	Bias Range[c]	F_{ty} (ksi) Test Value		Bias[b]	Bias Range[c]
TENSILE TESTS										
5 Ba 10	RT	None	51.4				34.9			
5 Ba 11	RT	None	49.2				34.1			
5 Ba 14	RT	None	49.5				34.1			
5 Ba 30	RT	None	49.7				34.2			
5 Ba 31	RT	None	49.7				32.7			
Arith. Mean				49.90			.....	34.00		
Std. Deviation				0.86			.....	0.80		
5 Ba 1	30°R	None	90.2				45.1			
5 Ba 3	30°R	None	91.2				44.7			
5 Ba 6	30°R	None	94.2				44.8			
5 Ba 7	30°R	None	92.3				45.1			
5 Ba 38	30°R	None	93.1				39.6			
Arith. Mean				92.20	+42.3	+40.8	.....	43.86	+ 9.9	+ 7.8
Std. Deviation				1.57		+43.8	.....	2.39		+12.0
5 Ba 39	30°R	10^{17}	90.9				68.9			
5 Ba 47	30°R	10^{17}	95.4				64.5			
(f)	30°R	10^{17}								
Arith. Mean				93.15	+ 1.0	- 3.8	.....	66.70	+22.8	+17.9
Std. Deviation				3.18		+ 5.7	.....	3.10		+27.8
TENSILE NOTCH TESTS			F_{tun} (ksi)				F_{tun}/F_{tu}			
5 Ba 15	RT	None	59.7				1.16			
5 Ba 16	RT	None	59.6				1.21			
5 Ba 17	RT	None	58.4				1.18			
5 Ba 19	RT	None	60.4				1.22			
5 Ba 20	RT	None	59.8				1.20			
Arith. Mean				59.58			.....	1.19		
Std. Deviation				0.73			.....	0.02		
5 Ba 22	30°R	None	70.3				0.78			
5 Ba 25	30°R	None	67.4				0.74			
5 Ba 26	30°R	None	69.0				0.73			
5 Ba 27	30°R	None	70.4				0.76			
5 Ba 28	30°R	None	56.8				0.61			
Arith. Mean				66.78	+ 7.2	+ 2.4	.....	0.72	- 0.47	- 0.41
Std. Deviation				5.71		+12.0	.....	0.07		- 0.53
(q)	30°R	10^{17}								
(q)	30°R	10^{17}								
(q)	30°R	10^{17}								
Arith. Mean							.....			
Std. Deviation							.....			

TABLE B 7 b

TEST RESULTS, ALUMINUM 5456 (H-321)

F_{ty}/F_{tu}	Elongation (%)	Reduction of Area (%)	Fracture Stress (ksi)	Total Fast Flux[a] (nvt)	Test Temp	Specimen Number
				TENSILE TESTS		
0.68	11	7	(e)	None	RT	5 Ba 10
0.69	13	10	(e)	None	RT	5 Ba 11
0.69	13	10	(e)	None	RT	5 Ba 14
0.69	14	11	(e)	None	RT	5 Ba 30
0.66	13	14	(e)	None	RT	5 Ba 31
0.682	12.8	10.4	(e)	. . . . .	Arith. Mean	
0.50	17	15	(e)	None	30°R	5 Ba 1
0.49	18	18	(e)	None	30°R	5 Ba 3
0.48	21	15	(e)	None	30°R	5 Ba 6
0.49	21	18	(e)	None	30°R	5 Ba 7
0.43	14	18	113.0	None	30°R	5 Ba 38
0.478	18.2	16.8	113.0	. . . . .	Arith. Mean	
0.76	14	15	107.0	10^{17}	30°R	5 Ba 39
0.68	14	18	116.0	10^{17}	30°R	5 Ba 47
				10^{17}	30°R	(f)
0.720	14.0	16.5	111.5	. . . . .	Arith. Mean	

(e). not recorded

(f). screening program ended before completion of this test

(q). test deleted from screening program

(a). of neutrons with >.5 mev energy

(b). change in mean of test value with respect to previous test condition

(c). with 90% confidence

TABLE B 8 a

TEST RESULTS, ALUMINUM 6061 (T-6)

Specimen Number	Test Temp	Total Fast Flux[a] (nvt)	F_{tu} (ksi) Test Value		Bias[b]	Bias Range[c]	F_{ty} (ksi) Test Value		Bias[b]	Bias Range[c]
TENSILE TESTS										
12 Ba 6	RT	None	43.1				40.0			
12 Ba 8	RT	None	41.6				38.5			
12 Ba 10	RT	None	44.5				40.6			
12 Ba 11	RT	None	44.1				40.3			
12 Ba 12	RT	None	43.5				40.6			
Arith. Mean				43.36				40.00		
Std. Deviation				1.12				0.88		
12 Ba 1	30°R	None	72.4				55.6			
12 Ba 2	30°R	None	68.3				51.2			
12 Ba 3	30°R	None	67.8				51.0			
12 Ba 4	30°R	None	66.2				49.7			
12 Ba 5	30°R	None	66.0				44.6			
Arith. Mean				68.14	+24.8	+22.4		50.42	+10.4	+ 7.1
Std. Deviation				2.58		+27.1		3.94		+13.8
12 Ba 61	30°R	10^{17}	68.1				62.0			
12 Ba 66	30°R	10^{17}	64.4				63.7			
12 Ba 69	30°R	10^{17}	61.2				52.4			
Arith. Mean				64.57	- 3.6	+ 0.9		59.37	+ 9.0	+ 1.3
Std. Deviation				3.45		- 8.0		6.09		+16.6
TENSILE NOTCH TESTS			F_{tun} (ksi)				F_{tun}/F_{tu}			
12 Ba 55	RT	None	57.3				1.33			
12 Ba 58	RT	None	54.3				1.31			
12 Ba 59	RT	None	58.3				1.31			
12 Ba 63	RT	None	54.8				1.24			
12 Ba 64	RT	None	57.9				1.33			
Arith. Mean				56.52				1.30		
Std. Deviation				1.84				0.01		
12 Ba 67	30°R	None	74.6				1.03			
12 Ba 68	30°R	None	71.2				1.04			
12 Ba 72	30°R	None	73.8				1.09			
12 Ba 74	30°R	None	72.3				1.09			
12 Ba 77	30°R	None	72.9				1.10			
Arith. Mean				72.96	+16.4	+14.6		1.07	- 0.2	- 0.19
Std. Deviation				1.32		+18.3		0.03		- 0.27
(q)	30°R	10^{17}								
(q)	30°R	10^{17}								
(q)	30°R	10^{17}								
Arith. Mean										
Std. Deviation										

TABLE B 8 b

TEST RESULTS, ALUMINUM 6061 (T-6)

F_{ty}/F_{tu}	Elongation (%)	Reduction of Area (%)	Fracture Stress (ksi)	Total Fast Flux[a] (nvt)	Test Temp	Specimen Number
				TENSILE TESTS		
0.93	16	36	(e)	None	RT	12 Ba 6
0.93	18	52	(e)	None	RT	12 Ba 8
0.91	20	52	(e)	None	RT	12 Ba 10
0.91	20	53	(e)	None	RT	12 Ba 11
0.93	(d)	(d)	(e)	None	RT	12 Ba 12
0.922	18.5	48.3	(e)	. . . . .	Arith. Mean	
0.77	30	36	(e)	None	30°R	12 Ba 1
0.74	29	44	(e)	None	30°R	12 Ba 2
0.75	33	41	(e)	None	30°R	12 Ba 3
0.75	28	45	(e)	None	30°R	12 Ba 4
0.68	30	41	(e)	None	30°R	12 Ba 5
0.738	30.0	41.4	(e)	. . . . .	Arith. Mean	
0.91	(d)	(d)	(d)	10^{17}	30°R	12 Ba 61
0.99	30	36	100.2	10^{17}	30°R	12 Ba 66
0.86	30	32	88.6	10^{17}	30°R	12 Ba 69
0.920	30.0	34.0	95.4	. . . . .	Arith. Mean	

(d). not available

(e). not recorded

(q). test deleted from screening program

(a). of neutrons with >.5 mev energy

(b). change in mean of test value with respect to previous test condition

(c). with 90% confidence

TABLE B 9 a

TEST RESULTS, ALUMINUM 7079 (T-6)

Specimen Number	Test Temp	Total Fast Flux[a] (nvt)	F_{tu} (ksi) Test Value		Bias[b]	Bias Range[c]	F_{ty} (ksi) Test Value		Bias[b]	Bias Range[c]
TENSILE TESTS										
13 Ba 1	RT	None	97.7				90.8			
13 Ba 4	RT	None	97.8				91.8			
13 Ba 6	RT	None	98.4				91.8			
13 Ba 20	RT	None	92.4				86.4			
13 Ba 30	RT	None	89.3				84.0			
Arith. Mean				95.12				88.96		
Std. Deviation				4.06				3.56		
13 Ba 10	30°R	None	145.0				127.0			
13 Ba 11	30°R	None	143.0				128.0			
13 Ba 15	30°R	None	150.0				135.0			
13 Ba 18	30°R	None	147.0				130.0			
13 Ba 27	30°R	None	141.0				129.0			
Arith. Mean				145.20	+50.1	+45.6		129.80	+40.8	+37.5
Std. Deviation				3.49		+54.5		1.90		+44.2
13 Ba 22	30°R	10^{17}	145.0				138.0			
13 Ba 25	30°R	10^{17}	128.0				123.0			
13 Ba 36	30°R	10^{17}	128.0				122.0			
Arith. Mean				133.70	-11.5	- 0.1		127.70	- 2.1	+ 8.1
Std. Deviation				9.82		-22.9		8.96		-12.3
TENSILE NOTCH TESTS			F_{tun} (ksi)				F_{tun}/F_{tu}			
13 Ba 48	RT	None	111.0				1.14			
13 Ba 49	RT	None	111.0				1.13			
13 Ba 51	RT	None	110.0				1.12			
13 Ba 57	RT	None	105.0				1.14			
13 Ba 60	RT	None	104.0				1.16			
Arith. Mean				108.20				1.14		
Std. Deviation				3.42				0.01		
13 Ba 31	30°R	None	142.0				0.98			
13 Ba 58	30°R	None	156.0				1.09			
13 Ba 59	30°R	None	149.0				0.99			
13 Ba 62	30°R	None	161.0				1.10			
13 Ba 65	30°R	None	151.0				1.07			
Arith. Mean				151.80	+43.6	+37.0		1.05	- 0.09	- 0.04
Std. Deviation				7.19		+50.2		0.06		- 0.14
(q)	30°R	10^{17}								
(q)	30°R	10^{17}								
(q)	30°R	10^{17}								
Arith. Mean										
Std. Deviation										

TABLE B 9 b

TEST RESULTS, ALUMINUM 7079 (T-6)

F_{ty}/F_{tu}	Elongation (%)	Reduction of Area (%)	Fracture Stress (ksi)	Total Fast Flux[a] (nvt)	Test Temp	Specimen Number
				TENSILE TESTS		
0.93	12	29	(e)	None	RT	13 Ba 1
0.94	13	26	(e)	None	RT	13 Ba 4
0.93	12	30	(e)	None	RT	13 Ba 6
0.94	10	19	105.0	None	RT	13 Ba 20
0.94	10	22	102.0	None	RT	13 Ba 30
0.936	11.4	25.2	103.5	. . . . .	Arith. Mean	
0.88	9	7	155.0	None	30°R	13 Ba 10
0.90	8	6	152.0	None	30°R	13 Ba 11
0.90	7	5	158.0	None	30°R	13 Ba 15
0.88	2	5	155.0	None	30°R	13 Ba 18
0.91	3	6	147.0	None	30°R	13 Ba 27
0.894	5.8	5.8	153.4	. . . . .	Arith. Mean	
0.95	5	3	150.0	10^{17}	30°R	13 Ba 22
0.96	5	6	137.0	10^{17}	30°R	13 Ba 25
0.95	6	4	133.0	10^{17}	30°R	13 Ba 36
0.953	5.3	4.3	140.0	. . . . .	Arith. Mean	

(e). not recorded

(q). test deleted from screening program

(a). of neutrons with >.5 mev energy

(b). change in mean of test value with respect to previous test condition

(c). with 90% confidence

TABLE B 10 a

TEST RESULTS, ALUMINUM 7178 (T-651)

Specimen Number	Test Temp	Total Fast Flux[a] (nvt)	F_{tu} (ksi) Test Value		Bias[b]	Bias Range[c]	F_{ty} (ksi) Test Value		Bias[b]	Bias Range[c]
TENSILE TESTS										
10 Bb 134	RT	None	88.0				80.8			
10 Bb 138	RT	None	87.8				79.6			
10 Bb 152	RT	None	85.8				80.1			
10 Bb 153	RT	None	88.2				81.0			
10 Bb 154	RT	None	88.6				80.9			
Arith. Mean				87.68				80.48		
Std. Deviation				1.09				0.61		
10 Bb 157	30°R	None	132.0				110.0			
10 Bb 158	30°R	None	128.0				108.0			
10 Bb 159	30°R	None	129.0				107.0			
10 Bb 161	30°R	None	129.0				109.0			
10 Bb 162	30°R	None	127.0				106.0			
Arith. Mean				129.00	+41.3	+39.5		108.00	+27.5	+26.1
Std. Deviation				1.87		+43.1		1.58		+28.9
10 Bb 135	30°R	10^{17}	138.0				127.0			
10 Bb 141	30°R	10^{17}	130.0				118.0			
10 Bb 143	30°R	10^{17}	135.0				119.0			
Arith. Mean				134.30	+ 5.3	- 1.6		121.30	+13.3	+ 7.7
Std. Deviation				4.04		+12.2		4.88		+18.9
TENSILE NOTCH TESTS			F_{tun} (ksi)				F_{tun}/F_{tu}			
10 Bb 137	RT	None	99.5				1.13			
10 Bb 142	RT	None	100.0				1.14			
10 Bb 144	RT	None	100.0				1.17			
10 Bb 145	RT	None	101.0				1.15			
10 Bb 148	RT	None	101.0				1.14			
Arith. Mean				100.30				1.146		
Std. Deviation				0.67				0.005		
10 Bb 62	30°R	None	117.0				0.89			
10 Bb 64	30°R	None	135.0				1.05			
10 Bb 65	30°R	None	120.0				0.93			
10 Bb 149	30°R	None	133.0				1.03			
10 Bb 169	30°R	None	136.0				1.07			
Arith. Mean				128.20	+27.9	+20.4		0.994	- 0.15	- 0.08
Std. Deviation				8.98		+35.4		0.081		- 0.22
(q)	30°R	10^{17}								
(q)	30°R	10^{17}								
(q)	30°R	10^{17}								
Arith. Mean										
Std. Deviation										

TABLE B 10 b

TEST RESULTS, ALUMINUM 7178 (T-651)

F_{ty}/F_{tu}	Elongation (%)	Reduction of Area (%)	Fracture Stress (ksi)	Total Fast Flux[a] (nvt)	Test Temp	Specimen Number
				TENSILE TESTS		
0.92	13	23	(e)	None	RT	10 Bb 134
0.91	12	21	(e)	None	RT	10 Bb 138
0.93	13	25	(e)	None	RT	10 Bb 152
0.92	10	21	(e)	None	RT	10 Bb 153
0.91	12	24	(e)	None	RT	10 Bb 154
0.918	12.0	22.8	(e)	. . . . .	Arith. Mean	
0.83	16	15	(e)	None	30°R	10 Bb 157
0.84	12	13	(e)	None	30°R	10 Bb 158
0.83	12	13	(e)	None	30°R	10 Bb 159
0.84	11	12	(e)	None	30°R	10 Bb 161
0.83	11	12	(e)	None	30°R	10 Bb 162
0.834	12.4	13.0	(e)	. . . . .	Arith. Mean	
0.92	7	1	140.0	10^{17}	30°R	10 Bb 135
0.91	6	6	139.0	10^{17}	30°R	10 Bb 141
0.88	6	6	136.0	10^{17}	30°R	10 Bb 143
0.903	6.3	4.3	138.3	. . . . .	Arith. Mean	

(e). not recorded

(q). test deleted from screening program

(a). of neutrons with >.5 mev energy

(b). change in mean of test value with respect to previous test condition

(c). with 90% confidence

TABLE B 11 a

TEST RESULTS, ALUMINUM X-250 (T-4)

Specimen Number	Test Temp	Total Fast Flux[a] (nvt)	F_{tu} (ksi) Test Value		Bias[b]	Bias Range[c]	F_{ty} (ksi) Test Value		Bias[b]	Bias Range[c]
TENSILE TESTS										
4 Ba 8	RT	None	58.7				32.5			
4 Ba 9	RT	None	60.5				33.7			
4 Ba 10	RT	None	59.8				33.4			
4 Ba 25	RT	None	43.5				30.9			
4 Ba 26	RT	None	58.8				33.4			
Arith. Mean				56.26				32.78		
Std. Deviation				7.17				1.14		
4 Ba 16	30°R	None	35.9				(g)			
4 Ba 27	30°R	None	55.8				49.5			
4 Ba 29	30°R	None	54.4				47.3			
4 Ba 40	30°R	None	57.4				50.3			
4 Ba 41	30°R	None	44.2				(h, i)			
Arith. Mean				49.54	-6.7	+ 3.4		49.03	+16.2	+14.2
Std. Deviation				9.21		-16.9		1.55		+18.3
4 Ba 12	30°R	10^{17}	52.3				(g)			
4 Ba 14	30°R	10^{17}	42.7				(g)			
4 Ba 23	30°R	10^{17}	45.8				(g)			
Arith. Mean				46.93	-2.6	+ 6.4		(e)	(e)	(e)
Std. Deviation				4.90		-11.7		(e)		(e)
TENSILE NOTCH TESTS			F_{tun} (ksi)				F_{tun}/F_{tu}			
4 Ba 6[p]	RT	None	54.0				0.92			
4 Ba 15	RT	None	66.7				1.10			
4 Ba 17	RT	None	65.3				1.09			
4 Ba 19[p]	RT	None	52.7				1.21			
4 Ba 20[p]	RT	None	54.0				0.92			
Arith. Mean				58.54				1.048		
Std. Deviation				6.85				0.127		
4 Ba 3	30°R	None	51.4				1.43			
4 Ba 4	30°R	None	53.2				0.95			
4 Ba 5	30°R	None	51.0				0.94			
4 Ba 22	30°R	None	54.7				0.95			
4 Ba 30	30°R	None	53.9				1.22			
Arith. Mean				52.84	-5.7	+ 0.2		1.098	+ 0.05	- 0.50
Std. Deviation				1.59		-11.6		0.646		+ 0.60
(q)	30°R	10^{17}								
(q)	30°R	10^{17}								
(q)	30°R	10^{17}								
Arith. Mean										
Std. Deviation										

TABLE B 11 b

TEST RESULTS, ALUMINUM X-250 (T-4)

F_{ty}/F_{tu}	Elongation (%)	Reduction of Area (%)	Fracture Stress (ksi)	Total Fast Flux[a] (nvt)	Test Temp	Specimen Number
				TENSILE TESTS		
0.55	20	15	(e)	None	RT	4 Ba 8
0.56	23	22	(e)	None	RT	4 Ba 9
0.56	19	22	(e)	None	RT	4 Ba 10
0.71	(d)	(d)	(e)	None	RT	4 Ba 25
0.57	(d)	(d)	(e)	None	RT	4 Ba 26
.590	20.6	19.6		. . . . .	Arith. Mean	
0.89	nil	nil	35.9	None	30°R	4 Ba 16
0.87	nil	nil	55.8	None	30°R	4 Ba 27
0.88	nil	nil	54.4	None	30°R	4 Ba 29
	nil	nil	57.4	None	30°R	4 Ba 40
	nil	nil	44.2	None	30°R	4 Ba 41
.880	nil	nil	49.54	. . . . .	Arith. Mean	
(e)	nil	nil	52.3	10^{17}	30°R	4 Ba 12
(e)	nil	nil	42.7	10^{17}	30°R	4 Ba 14
(e)	nil	nil	45.8	10^{17}	30°R	4 Ba 23
	nil	nil	46.93	. . . . .	Arith. Mean	

(d). not available

(e). not recorded

(g). failed at less than .2% plastic strain

(h). failed outside of gage length

(i). casting defect at fracture

(p). failed outside notch

(q). test deleted from screening program

(a). of neutrons with >.5 mev energy

(b). change in mean of test value with respect to previous test condition

(c). with 90% confidence

TABLE B 12 a

TEST RESULTS , ALUMINUM B-750 (T-5)

Specimen Number	Test Temp	Total Fast Flux[a] (nvt)	F_{tu} (ksi) Test Value		Bias[b]	Bias Range[c]	F_{ty} (ksi) Test Value		Bias[b]	Bias Range[c]
TENSILE TESTS										
6 Ba 50	RT	None	30.6				20.4			
6 Ba 64	RT	None	29.8				19.3			
6 Ba 65	RT	None	28.4				18.7			
6 Ba 67	RT	None	28.8				17.7			
6 Ba 68	RT	None	30.1				21.2			
Arith. Mean				29.54				19.46		
Std. Deviation				0.89				1.38		
6 Ba 69	30°R	None	42.2				24.6			
6 Ba 71	30°R	None	38.4				23.6			
6 Ba 72	30°R	None	45.4				27.7			
6 Ba 73	30°R	None	44.5				26.1			
6 Ba 76	30°R	None	42.4				23.9			
Arith. Mean				42.58	+13.0	+10.7		25.18	+ 5.7	+ 3.9
Std. Deviation				2.72		+15.4		1.71		+ 7.6
6 Ba 51	30°R	10^{17}	44.3				40.8			
6 Ba 79	30°R	10^{17}	49.3				47.4			
6 Ba 81	30°R	10^{17}	45.0				42.4			
Arith. Mean				46.20	+ 3.6	- 0.2		43.53	+18.3	+14.2
Std. Deviation				2.71		+ 7.5		3.44		+22.5
TENSILE NOTCH TESTS			F_{tun} (ksi)				F_{tun}/F_{tu}			
6 Ba 5	RT	None	30.9				1.01			
6 Ba 14	RT	None	29.5				0.99			
6 Ba 16	RT	None	31.7				1.12			
6 Ba 33	RT	None	(o)				(o)			
6 Ba 43	RT	None	32.3				1.07			
Arith. Mean				31.10				1.048		
Std. Deviation				1.21				0.070		
6 Ba 34	30°R	None	30.8				0.730			
6 Ba 44	30°R	None	33.8				0.880			
6 Ba 48	30°R	None	29.0				0.639			
6 Ba 49	30°R	None	(o)				(o)			
6 Ba 53	30°R	None	31.0				0.731			
Arith. Mean				31.15	+ 0.05	- 2.2		0.745	- 0.30	- 0.18
Std. Deviation				1.98		+ 2.3		0.100		- 0.42
(q)	30°R	10^{17}								
(q)	30°R	10^{17}								
(q)	30°R	10^{17}								
Arith. Mean										
Std. Deviation										

TABLE B 12 b

TEST RESULTS, ALUMINUM B-750 (T-5)

F_{ty}/F_{tu}	Elongation (%)	Reduction of Area (%)	Fracture Stress (ksi)	Total Fast Flux[a] (nvt)	Test Temp	Specimen Number
				TENSILE TESTS		
0.67	8	10	(e)	None	RT	6 Ba 50
0.65	9	9	(e)	None	RT	6 Ba 64
0.66	9	16	(e)	None	RT	6 Ba 65
0.61	10	9	(e)	None	RT	6 Ba 67
0.70	8	10	(e)	None	RT	6 Ba 68
0.658	8.8	10.8	(e)	. . . . .	Arith. Mean	
0.58	(d)	(d)	(e)	None	30°R	6 Ba 69
0.61	(d)	3	(e)	None	30°R	6 Ba 71
0.61	7	2	(e)	None	30°R	6 Ba 72
0.59	7	6	(e)	None	30°R	6 Ba 73
0.56	7	5	(e)	None	30°R	6 Ba 76
0.590	7.0	4.0	(e)	. . . . .	Arith. Mean	
0.92	4	nil	44.3	10^{17}	30°R	6 Ba 51
0.96	3	2	50.4	10^{17}	30°R	6 Ba 79
0.94	3	1	45.6	10^{17}	30°R	6 Ba 81
0.940	3.3	1.0	46.8	. . . . .	Arith. Mean	

(d). not available

(e). not recorded

(o). test results voided

(q). test deleted from screening program

(a). of neutrons with >.5 mev energy

(b). change in mean of test value with respect to previous test condition

(c). with 90% confidence

TABLE B 13 a

TEST RESULTS, ALUMINUM A 356 (T-61)

Specimen Number	Test Temp	Total Fast Flux[a] (nvt)	F_{tu} (ksi) Test Value		Bias[b]	Bias Range[c]	F_{ty} (ksi) Test Value		Bias[b]	Bias Range[c]
TENSILE TESTS										
14 Ba 13	RT	None	42.7				28.0			
14 Ba 70	RT	None	44.5				29.3			
14 Ba 85	RT	None	42.9				31.5			
14 Ba 92	RT	None	45.7				31.2			
14 Ba 95	RT	None	44.7				31.6			
Arith. Mean				44.10				30.32		
Std. Deviation				1.27				1.60		
14 Ba 15	30°R	None	59.7				31.2			
14 Ba 74	30°R	None	67.5				37.2			
14 Ba 77	30°R	None	75.6				43.1			
14 Ba 90	30°R	None	65.3				40.5			
14 Ba 93	30°R	None	54.6				35.9			
Arith. Mean				64.54	+20.4	+13.7		37.58	+7.3	+ 3.3
Std. Deviation				7.97		+27.2		4.55		+11.3
14 Ba 10	30°R	10^{17}	61.2				47.0			
14 Ba 48	30°R	10^{17}	63.3				46.0			
14 Ba 69	30°R	10^{17}	61.8				45.4			
Arith. Mean				62.10	- 2.4	+ 4.6		46.13	+8.6	+ 4.5
Std. Deviation				1.08		- 9.5		0.81		+12.6
TENSILE NOTCH TESTS			F_{tun} (ksi)				F_{tun}/F_{tu}			
14 Ba 1	RT	None	58.2				1.36			
14 Ba 4	RT	None	53.3				1.20			
14 Ba 16	RT	None	51.4				1.20			
14 Ba 20	RT	None	49.1				1.07			
14 Ba 30	RT	None	44.8				1.00			
Arith. Mean				51.36				1.166		
Std. Deviation				4.97				0.139		
14 Ba 32	30°R	None	76.7				1.28			
14 Ba 35	30°R	None	61.8				0.92			
14 Ba 43	30°R	None	58.9				0.78			
14 Ba 46	30°R	None	67.8				1.04			
14 Ba 68	30°R	None	64.1				1.17			
Arith. Mean				65.86	+14.5	+10.0		1.038	-0.13	+ 0.07
Std. Deviation				6.88		+19.0		0.197		- 0.33
(q)	30°R	10^{17}								
(q)	30°R	10^{17}								
(q)	30°R	10^{17}								
Arith. Mean										
Std. Deviation										

TABLE B 13 b

TEST RESULTS, ALUMINUM A 356 (T-61)

F_{ty}/F_{tu}	Elongation (%)	Reduction of Area (%)	Fracture Stress (ksi)	Total Fast Flux[a] (nvt)	Test Temp	Specimen Number
				TENSILE TESTS		
0.66	14	14	49.5	None	RT	14 Ba 13
0.66	15	18	54.1	None	RT	14 Ba 70
0.73	12	10	47.9	None	RT	14 Ba 85
0.68	17	29	64.5	None	RT	14 Ba 92
0.71	15	21	56.6	None	RT	14 Ba 95
0.688	14.6	18.4	54.52	. . . . .	Arith. Mean	
0.52	12	16	71.1	None	30°R	14 Ba 15
0.55	12	10	75.1	None	30°R	14 Ba 74
0.57	15	12	86.0	None	30°R	14 Ba 77
0.62	12	7	70.5	None	30°R	14 Ba 90
0.66	7	2	55.6	None	30°R	14 Ba 93
0.584	11.6	9.4	71.66	. . . . .	Arith. Mean	
0.77	9	8	66.4	10^{17}	30°R	14 Ba 10
0.73	7	6	68.1	10^{17}	30°R	14 Ba 48
0.73	10	10	68.4	10^{17}	30°R	14 Ba 69
0.743	8.7	8.0	67.63	. . . . .	Arith. Mean	

(q). test deleted from screening program

(a). of neutrons with >.5 mev energy

(b). change in mean of test value with respect to previous test condition

(c). with 90% confidence

TABLE B 14 a

TEST RESULTS, TITANIUM ALLOY 55A (ANNEALED)

Specimen Number	Test Temp	Total Fast Flux[a] (nvt)	F_{tu} (ksi) Test Value		Bias[b]	Bias Range[c]	F_{ty} (ksi) Test Value		Bias[b]	Bias Range[c]
TENSILE TESTS										
1 Aa 126	RT	None	66.8				55.3			
1 Aa 139	RT	None	69.4				63.3			
1 Aa 155	RT	None	67.0				51.2			
1 Aa 157	RT	None	65.1				47.5			
1 Aa 158	RT	None	66.7				50.4			
Arith. Mean				67.00				53.50		
Std. Deviation				1.54				6.13		
1 Aa 160	30°R	None	172.0				124.0			
1 Aa 191	30°R	None	167.0				118.0			
1 Aa 192	30°R	None	171.0				124.0			
1 Aa 193	30°R	None	167.0				120.0			
1 Aa 194	30°R	None	170.0				124.0			
Arith. Mean				169.40	+102.4	+100.1		122.00	+68.5	+62.9
Std. Deviation				2.30		+104.7		2.83		+74.1
1 Aa 138	30°R	10^{17}	181.0				128.0			
1 Aa 144	30°R	10^{17}	216.0				136.0			
1 Aa 148	30°R	10^{17}	180.0				131.0			
Arith. Mean				192.30	+ 22.9	- 0.2		131.70	+ 9.7	+ 4.5
Std. Deviation				20.50		+ 46.0		4.04		+14.9
TENSILE NOTCH TESTS			F_{tun} (ksi)				F_{tun}/F_{tu}			
1 Aa 130	RT	None	81.9				1.23			
1 Aa 131	RT	None	82.7				1.19			
1 Aa 133	RT	None	83.3				1.24			
1 Aa 134	RT	None	86.4				1.33			
1 Aa 135	RT	None	87.1				1.31			
Arith. Mean				84.28				1.26		
Std. Deviation				2.32				0.06		
1 Aa 137	30°R	None	161.0				0.94			
1 Aa 140	30°R	None	169.0				1.01			
1 Aa 141	30°R	None	158.0				0.92			
1 Aa 146	30°R	None	168.0				1.01			
1 Aa 147	30°R	None	180.0				1.06			
Arith. Mean				167.20	+ 82.9	+ 75.6		0.99	- 0.27	- 0.20
Std. Deviation				8.53		+ 90.3		0.06		- 0.34
1 Aa 94	30°R	10^{17}	195.0				1.08			
1 Aa 183	30°R	10^{17}	172.0				0.80			
1 Aa 98	30°R	10^{17}	195.0				1.08			
Arith. Mean				187.30	+ 20.1	- 2.2		0.99	0.00	+ 0.26
Std. Deviation				13.28		+ 42.4		0.16		- 0.26

TABLE B 14 b

TEST RESULTS, TITANIUM ALLOY 55A (ANNEALED)

F_{ty}/F_{tu}	Elongation (%)	Reduction of Area (%)	Fracture Stress (ksi)	Total Fast Flux[a] (nvt)	Test Temp	Specimen Number
				TENSILE TESTS		
0.83	31	62	(e)	None	RT	1 Aa 126
0.91	25	59	(e)	None	RT	1 Aa 139
0.76	31	63	(e)	None	RT	1 Aa 155
0.73	33	65	(e)	None	RT	1 Aa 157
0.76	(d)	(d)	(e)	None	RT	1 Aa 158
0.798	30.0	62.3	(e)	. . . . .	Arith. Mean	
0.72	(d)	(d)	(e)	None	30°R	1 Aa 160
0.71	33	54	(e)	None	30°R	1 Aa 191
0.73	(d)	(d)	(e)	None	30°R	1 Aa 192
0.72	34	51	(e)	None	30°R	1 Aa 193
0.73	33	54	(e)	None	30°R	1 Aa 194
0.722	33.3	53.0	(e)	. . . . .	Arith. Mean	
0.71	(d)	(d)	(e)	10^{17}	30°R	1 Aa 138
0.63	32	52	(e)	10^{17}	30°R	1 Aa 144
0.73	36	54	(e)	10^{17}	30°R	1 Aa 148
0.690	34.0	53.0	(e)	. . . . .	Arith. Mean	

(d). not available

(e). not recorded

(a). of neutrons with >.5 mev energy

(b). change in mean of test value with respect to previous test condition

(c). with 90% confidence

TABLE B 15 a

TEST RESULTS, TITANIUM - 5 AL - 2.5 SN (ANNEALED)

Specimen Number	Test Temp	Total Fast Flux[a] (nvt)	F_{tu} (ksi) Test Value		Bias[b]	Bias Range[c]	F_{ty} (ksi) Test Value		Bias[b]	Bias Range[c]
TENSILE TESTS										
3 Aa 15	RT	None	124.0				121.0			
3 Aa 16	RT	None	125.0				114.0			
3 Aa 17	RT	None	127.0				115.0			
3 Aa 18	RT	None	125.0				112.0			
3 Aa 19	RT	None	125.0				112.0			
Arith. Mean				125.20			.....	114.80		
Std. Deviation				1.10			.....	3.70		
3 Aa 21	30°R	None	229.0				205.0			
3 Aa 29	30°R	None	226.0				215.0			
3 Aa 30	30°R	None	225.0				(e)			
3 Aa 54	30°R	None	213.0				201.0			
3 Aa 55	30°R	None	231.0				200.0			
Arith. Mean				224.80	+99.6	+ 93.7	.....	205.25	+90.4	+83.2
Std. Deviation				7.01		+105.5	.....	6.85		+97.6
3 Aa 52	30°R	10^{17}	222.0				212.0			
3 Aa 57	30°R	10^{17}	238.0				231.0			
3 Aa 58	30°R	10^{17}	257.0				211.0			
Arith. Mean				239.00	+14.2	- 6.4	.....	218.00	+12.7	- 2.1
Std. Deviation				17.52		+34.8	.....	11.27		+27.5
TENSILE NOTCH TESTS			F_{tun} (ksi)				F_{tun}/F_{tu}			
3 Aa 1	RT	None	168.0				1.35			
3 Aa 2	RT	None	169.0				1.35			
3 Aa 3	RT	None	166.0				1.31			
3 Aa 4	RT	None	164.0				1.31			
3 Aa 5	RT	None	167.0				1.34			
Arith. Mean				166.80			.....	1.33		
Std. Deviation				1.92			.....	0.02		
3 Aa 7	30°R	None	257.0				1.12			
3 Aa 8	30°R	None	254.0				1.12			
3 Aa 9	30°R	None	247.0				1.10			
3 Aa 10	30°R	None	247.0				1.16			
3 Aa 11	30°R	None	243.0				1.05			
Arith. Mean				249.60	+82.8	+77.8	.....	1.11	- 0.22	- 0.18
Std. Deviation				5.73		+87.8	.....	0.04		- 0.26
3 Aa 13	30°R	10^{17}	278.0				1.25			
3 Aa 40	30°R	10^{17}	266.0				1.12			
3 Aa 47	30°R	10^{17}	275.0				1.07			
Arith. Mean				273.00	+23.4	+14.8	.....	1.15	+ 0.04	- 0.07
Std. Deviation				6.25		+32.0	.....	0.09		+ 0.15

TABLE B 15 b

TEST RESULTS, TITANIUM - 5 AL - 2.5 SN (ANNEALED)

F_{ty}/F_{tu}	Elongation (%)	Reduction of Area (%)	Fracture Stress (ksi)	Total Fast Flux[a] (nvt)	Test Temp	Specimen Number
				TENSILE TESTS		
0.98	(d)	(d)	(e)	None	RT	3 Aa 15
0.91	23	52	(e)	None	RT	3 Aa 16
0.91	(d)	(d)	(e)	None	RT	3 Aa 17
0.90	24	52	(e)	None	RT	3 Aa 18
0.90	23	48	(e)	None	RT	3 Aa 19
0.920	23.3	50.7	(e)	. . . . .	Arith. Mean	
0.90	13	34	(e)	None	30°R	3 Aa 21
0.95	(d)	(d)	(e)	None	30°R	3 Aa 29
(e)	12	35	(e)	None	30°R	3 Aa 30
0.94	12	30	298.0	None	30°R	3 Aa 54
0.87	18	21	(e)	None	30°R	3 Aa 55
0.915	13.8	30.0	298.0	. . . . .	Arith. Mean	
0.95	9	(e)	(e)	10^{17}	30°R	3 Aa 52
0.97	14	36	(e)	10^{17}	30°R	3 Aa 57
0.82	(d)	(d)	(e)	10^{17}	30°R	3 Aa 58
0.913	11.5	36.0	(e)	. . . . .	Arith. Mean	

(d). not available

(e). not recorded

(a). of neutrons with >.5 mev energy

(b). change in mean of test value with respect to previous test condition

(c). with 90% confidence

TABLE B 16 a

TEST RESULTS, TITANIUM - 5 AL - 2.5 SN (ELI, ANNEALED)

Specimen Number	Test Temp	Total Fast Flux[a] (nvt)	F_{tu} (ksi) Test Value		Bias[b]	Bias Range[c]	F_{ty} (ksi) Test Value		Bias[b]	Bias Range[c]
TENSILE TESTS										
8 Aa 4	RT	None	133.0				119.0			
8 Aa 9	RT	None	130.0				118.0			
8 Aa 11	RT	None	130.0				118.0			
8 Aa 30	RT	None	121.0				108.0			
8 Aa 36	RT	None	118.0				104.0			
Arith. Mean				126.40				113.40		
Std. Deviation				6.50				6.91		
8 Aa 18	30°R	None	231.0				203.0			
8 Aa 27	30°R	None	236.0				225.0			
8 Aa 32	30°R	None	223.0				213.0			
8 Aa 34	30°R	None	227.0				217.0			
8 Aa 35	30°R	None	225.0				213.0			
Arith. Mean				228.40	+102.0	+ 95.1		214.20	+100.8	+ 92.0
Std. Deviation				5.18		+108.9		7.95		+109.6
8 Aa 12	30°R	10^{17}	223.0				215.0			
8 Aa 24	30°R	10^{17}	225.0				213.0			
8 Aa 25	30°R	10^{17}	222.0				211.0			
Arith. Mean				223.30	- 5.1	- 0.3		213.00	- 1.2	+ 6.1
Std. Deviation				1.53		- 9.9		2.00		- 8.5
TENSILE NOTCH TESTS			F_{tun} (ksi)				F_{tun}/F_{tu}			
8 Aa 3	RT	None	165.0				1.24			
8 Aa 5	RT	None	154.0				1.18			
8 Aa 20	RT	None	149.0				1.15			
8 Aa 41	RT	None	145.0				1.20			
8 Aa 42	RT	None	154.0				1.31			
Arith. Mean				153.40				1.220		
Std. Deviation				7.50				0.063		
8 Aa 13	30°R	None	272.0				1.18			
8 Aa 43	30°R	None	261.0				1.11			
8 Aa 44	30°R	None	267.0				1.20			
8 Aa 45	30°R	None	263.0				1.16			
8 Aa 50	30°R	None	273.0				1.21			
Arith. Mean				267.20	+113.8	+106.2		1.170	- 0.05	+ 0.01
Std. Deviation				5.31		+121.4		0.040		- 0.11
8 Aa 10	30°R	10^{17}	266.0				1.19			
8 Aa 16	30°R	10^{17}	277.0				1.23			
8 Aa 21	30°R	10^{17}	268.0				1.21			
Arith. Mean				270.00	+ 2.8	- 5.2		1.210	+ 0.04	+ 0.00
Std. Deviation				5.87		+ 10.8		0.020		+ 0.08

TABLE B 16 b

TEST RESULTS, TITANIUM - 5AL - 2.5 SN (ELI, ANNEALED)

F_{ty}/F_{tu}	Elongation (%)	Reduction of Area (%)	Fracture Stress (ksi)	Total Fast Flux[a] (nvt)	Test Temp	Specimen Number
				TENSILE TESTS		
0.89	12	40	(e)	None	RT	8 Aa 4
0.91	19	46	(e)	None	RT	8 Aa 9
0.91	13	43	(e)	None	RT	8 Aa 11
0.89	18	39	169.0	None	RT	8 Aa 30
0.88	18	43	171.0	None	RT	8 Aa 36
0.896	16.0	42.2	170.0	. . . . .	Arith. Mean	
0.92	(d)	(d)	(e)	None	30°R	8 Aa 18
0.95	(r)	(r)	(e)	None	30°R	8 Aa 27
0.96	8	33	(e)	None	30°R	8 Aa 32
0.96	10	32	(e)	None	30°R	8 Aa 34
0.95	11	32	(e)	None	30°R	8 Aa 35
0.948	9.7	32.3	(e)	. . . . .	Arith. Mean	
0.96	(d)	(d)	(e)	10^{17}	30°R	8 Aa 12
0.95	(d)	(d)	(e)	10^{17}	30°R	8 Aa 24
0.95	11	31	(e)	10^{17}	30°R	8 Aa 25
0.953	11.0	31.0	(e)	. . . . .	Arith. Mean	

(d). not available

(e). not recorded

(r). specimen necked-down but did not fail

(a). of neutrons with >.5 mev energy

(b). change in mean of test value with respect to previous test condition

(c). with 90% confidence

TABLE B 17 a

TEST RESULTS, TITANIUM - 6 AL - 4V (ANNEALED)

Specimen Number	Test Temp	Total Fast Flux[a] (nvt)	F_{tu} (ksi) Test Value		Bias[b]	Bias Range[c]	F_{ty} (ksi) Test Value		Bias[b]	Bias Range[c]
TENSILE TESTS										
2 Ac 2	RT	None	145.0				140.0			
2 Ac 3	RT	None	142.0				135.0			
2 Ac 4	RT	None	143.0				134.0			
2 Ac 5	RT	None	145.0				141.0			
2 Ac 6	RT	None	145.0				139.0			
Arith. Mean				144.00			.....	137.80		
Std. Deviation				1.41			.....	3.12		
2 Ac 1	30°R	None	249.0				228.0			
2 Ac 9	30°R	None	264.0				230.0			
2 Ac 10	30°R	None	261.0				253.0			
2 Ac 12	30°R	None	263.0				255.0			
2 Ac 71	30°R	None	265.0				250.0			
Arith. Mean				260.40	+116.4	+110.8	.....	243.20	+105.4	+ 94.2
Std. Deviation				6.54		+122.0	.....	13.10		+116.6
2 Ac 59	30°R	10^{17}	265.0				(e)			
2 Ac 61	30°R	10^{17}	266.0				254.0			
2 Ac 72	30°R	10^{17}	290.0				(e)			
Arith. Mean				273.70	+ 13.3	- 3.6	.....	254.00	+ 10.8	
Std. Deviation				14.15		+ 30.2	.....	0.00		
TENSILE NOTCH TESTS			F_{tun} (ksi)				F_{tun}/F_{tu}			
2 Ac 15	RT	None	185.0				1.28			
2 Ac 16	RT	None	183.0				1.29			
2 Ac 17	RT	None	184.0				1.29			
2 Ac 18	RT	None	183.0				1.26			
2 Ac 19	RT	None	187.0				1.29			
Arith. Mean				184.40			.....	1.28		
Std. Deviation				1.67			.....	0.01		
2 Ac 21	30°R	None	277.0				1.11			
2 Ac 22	30°R	None	289.0				1.28			
2 Ac 23	30°R	None	272.0				1.03			
2 Ac 26	30°R	None	283.0				1.07			
2 Ac 27	30°R	None	287.0				1.10			
Arith. Mean				281.60	+ 97.2	+ 91.2	.....	1.12	- 0.16	- 0.08
Std. Deviation				7.06		+103.2	.....	0.10		- 0.24
2 Ac 58	30°R	10^{17}	265.0				1.00			
2 Ac 63	30°R	10^{17}	301.0				1.13			
2 Ac 65	30°R	10^{17}	285.0				0.98			
Arith. Mean				283.67	+ 2.1	- 19.1	.....	1.04	- 0.08	+ 0.04
Std. Deviation				18.04		+ 23.2	.....	0.08		- 0.20

TABLE B 17 b

TEST RESULTS, TITANIUM - 6 AL - 4V (ANNEALED)

F_{ty}/F_{tu}	Elongation (%)	Reduction of Area (%)	Fracture Stress (ksi)	Total Fast Flux[a] (nvt)	Test Temp	Specimen Number
				TENSILE TESTS		
0.96	13	48	(e)	None	RT	2 Ac 2
0.95	14	43	(e)	None	RT	2 Ac 3
0.94	14	42	(e)	None	RT	2 Ac 4
0.97	14	47	(e)	None	RT	2 Ac 5
0.96	(d)	(d)	(e)	None	RT	2 Ac 6
0.957	13.8	45.0	(e)	. . . . .	Arith. Mean	
0.92	10	30	(e)	None	30°R	2 Ac 1
0.87	7	30	(e)	None	30°R	2 Ac 9
0.97	7	27	(e)	None	30°R	2 Ac 10
0.97	7	29	(e)	None	30°R	2 Ac 12
0.94	7	36	(e)	None	30°R	2 Ac 71
0.934	7.6	30.4	(e)	. . . . .	Arith. Mean	
	6	37	(e)	10^{17}	30°R	2 Ac 59
0.95	5	37	(e)	10^{17}	30°R	2 Ac 61
	6	38	(e)	10^{17}	30°R	2 Ac 72
0.950	5.7	37.3	(e)	. . . . .	Arith. Mean	

(d). not available

(e). not recorded

(a). of neutrons with >.5 mev energy

(b). change in mean of test value with respect to previous test condition

(c). with 90% confidence

TABLE B 18 a

TEST RESULTS, TITANIUM - 6 AL - 4V (AGED)

Specimen Number	Test Temp	Total Fast Flux[a] (nvt)	F_{tu} (ksi) Test Value		Bias[b]	Bias Range[c]	F_{ty} (ksi) Test Value		Bias[b]	Bias Range[c]
TENSILE TESTS										
2 Aa 2	RT	None	170.0				161.0			
2 Aa 3	RT	None	169.0				161.0			
2 Aa 4	RT	None	168.0				155.0			
2 Aa 5	RT	None	170.0				160.0			
2 Aa 7	RT	None	161.0				156.0			
Arith. Mean				167.60				158.60		
Std. Deviation				3.78				2.88		
2 Aa 10	30°R	None	284.0				275.0			
2 Aa 11	30°R	None	277.0				274.0			
2 Aa 13	30°R	None	283.0				279.0			
2 Aa 29	30°R	None	281.0				274.0			
2 Aa 30	30°R	None	286.0				273.0			
Arith. Mean				282.20	+114.6	+110.4		275.00	+116.4	+113.3
Std. Deviation				3.42		+118.8		2.35		+119.5
2 Aa 43	30°R	10^{17}	296.0				281.0			
2 Aa 44	30°R	10^{17}	303.0				294.0			
2 Aa 77	30°R	10^{17}	308.0				305.0			
Arith. Mean				302.30	+ 20.1	+ 12.7		293.30	+ 18.3	+ 4.7
Std. Deviation				6.03		+ 27.5		12.01		+ 31.9
TENSILE NOTCH TESTS			F_{tun} (ksi)				F_{tun}/F_{tu}			
2 Aa 60	RT	None	202.0				1.19			
2 Aa 61	RT	None	199.0				1.18			
2 Aa 62	RT	None	201.0				1.20			
2 Aa 63	RT	None	204.0				1.20			
2 Aa 64	RT	None	203.0				1.26			
Arith. Mean				201.80				1.21		
Std. Deviation				1.92				0.03		
2 Aa 67	30°R	None	283.0				1.00			
2 Aa 68	30°R	None	288.0				1.04			
2 Aa 69	30°R	None	291.0				1.03			
2 Aa 70	30°R	None	291.0				1.04			
2 Aa 71	30°R	None	291.0				1.02			
Arith. Mean				288.80	+ 87.0	+ 83.7		1.03	- 0.18	- 0.15
Std. Deviation				3.49		+ 90.3		0.02		- 0.21
2 Aa 54	30°R	10^{17}	292.0				0.99			
2 Aa 56	30°R	10^{17}	297.0				0.98			
2 Aa 72	30°R	10^{17}	296.0				0.96			
Arith. Mean				295.00	+ 6.2	+ 2.5		0.98	- 0.05	- 0.03
Std. Deviation				1.87		+ 9.9		0.02		- 0.07

TABLE B 18 b

TEST RESULTS, TITANIUM - 6 AL - 4V (AGED)

F_{ty}/F_{tu}	Elongation (%)	Reduction of Area (%)	Fracture Stress (ksi)	Total Fast Flux[a] (nvt)	Test Temp	Specimen Number
				TENSILE TESTS		
0.95	16	54	(e)	None	RT	2 Aa 2
0.95	19	54	(e)	None	RT	2 Aa 3
0.92	13	55	(e)	None	RT	2 Aa 4
0.94	(d)	(d)	(e)	None	RT	2 Aa 5
0.97	18	53	(e)	None	RT	2 Aa 7
0.946	16.5	54.0	(e)	. . . . .	Arith. Mean	
0.97	7	31	(e)	None	30°R	2 Aa 10
0.99	7	28	(e)	None	30°R	2 Aa 11
0.99	5	22	(e)	None	30°R	2 Aa 13
0.98	7	24	(e)	None	30°R	2 Aa 29
0.95	6	22	(e)	None	30°R	2 Aa 30
0.976	6.4	25.4	(e)	. . . . .	Arith. Mean	
0.95	5	24	(e)	10^{17}	30°R	2 Aa 43
0.97	(d)	(d)	(e)	10^{17}	30°R	2 Aa 44
0.99	5	21	(e)	10^{17}	30°R	2 Aa 77
0.970	5.0	22.5	(e)	. . . . .	Arith. Mean	

(d). not available

(e). not recorded

(a). of neutrons with >.5 mev energy

(b). change in mean of test value with respect to previous test condition

(c). with 90% confidence

TABLE B 19 a

TEST RESULTS, TITANIUM - 8 AL - 1 MO- 1V (ANNEALED)

Specimen Number	Test Temp	Total Fast Flux[a] (nvt)	F_{tu} (ksi) Test Value		Bias[b]	Bias Range[c]	F_{ty} (ksi) Test Value		Bias[b]	Bias Range[c]
TENSILE TESTS										
4 Aa 6	RT	None	134.0				130.0			
4 Aa 7	RT	None	141.0				135.0			
4 Aa 8	RT	None	140.0				136.0			
4 Aa 51	RT	None	136.0				128.0			
4 Aa 52	RT	None	139.0				130.0			
Arith. Mean				138.00				131.80		
Std. Deviation				2.92				3.49		
4 Aa 1	30°R	None	242.0				220.0			
4 Aa 2	30°R	None	243.0				236.0			
4 Aa 3	30°R	None	236.0				217.0			
4 Aa 4	30°R	None	236.0				224.0			
4 Aa 5	30°R	None	238.0				224.0			
Arith. Mean				239.00	+101.0	+ 97.3		224.20	+ 92.4	+ 85.7
Std. Deviation				3.32		+104.7		7.22		+ 99.1
4 Aa 34	30°R	10^{17}	264.0				238.0			
4 Aa 38	30°R	10^{17}	259.0				247.0			
4 Aa 43	30°R	10^{17}	262.0				243.0			
Arith. Mean				261.70	+ 22.7	+ 18.7		242.70	+ 18.5	+ 10.4
Std. Deviation				2.52		+ 26.7		4.51		+ 26.6
TENSILE NOTCH TESTS			F_{tun} (ksi)				F_{tun}/F_{tu}			
4 Aa 17	RT	None	173.0				1.29			
4 Aa 19	RT	None	176.0				1.25			
4 Aa 20	RT	None	178.0				1.27			
4 Aa 21	RT	None	174.0				1.28			
4 Aa 22	RT	None	174.0				1.25			
Arith. Mean				175.00				1.27		
Std. Deviation				2.00				0.02		
4 Aa 23	30°R	None	256.0				1.06			
4 Aa 25	30°R	None	280.0				1.15			
4 Aa 27	30°R	None	258.0				1.09			
4 Aa 28	30°R	None	270.0				1.14			
4 Aa 29	30°R	None	272.0				1.14			
Arith. Mean				267.20	+ 92.2	+ 83.7		1.12	- 0.15	- 0.12
Std. Deviation				10.06		+100.7		0.01		- 0.19
4 Aa 33	30°R	10^{17}	277.0				1.05			
4 Aa 67	30°R	10^{17}	292.0				1.27			
4 Aa 68	30°R	10^{17}	277.0				1.06			
Arith. Mean				282.00	+ 14.8	+ 1.7		1.13	+ 0.01	- 0.13
Std. Deviation				8.66		+ 27.9		0.12		+ 0.15

TABLE B 19 b

TEST RESULTS, TITANIUM - 8 AL - 1 MO - 1V (ANNEALED)

F_{ty}/F_{tu}	Elongation (%)	Reduction of Area (%)	Fracture Stress (ksi)	Total Fast Flux[a] (nvt)	Test Temp	Specimen Number
				TENSILE TESTS		
0.97	23	49	(e)	None	RT	4 Aa 6
0.96	23	53	(e)	None	RT	4 Aa 7
0.97	(d)	(d)	(e)	None	RT	4 Aa 8
0.94	22	56	(e)	None	RT	4 Aa 51
0.94	(d)	(d)	(e)	None	RT	4 Aa 52
0.956	22.7	52.6	(e)	. . . . .	Arith. Mean	
0.91	(d)	(d)	(e)	None	30°R	4 Aa 1
0.97	(d)	(d)	(e)	None	30°R	4 Aa 2
0.92	(d)	(d)	(e)	None	30°R	4 Aa 3
0.95	(d)	(d)	(e)	None	30°R	4 Aa 4
0.94	(d)	(d)	(e)	None	30°R	4 Aa 5
0.938	(e)	(e)	(e)	. . . . .	Arith. Mean	
0.90	6	31	(e)	10^{17}	30°R	4 Aa 34
0.95	6	30	(e)	10^{17}	30°R	4 Aa 38
0.93	5	26	(e)	10^{17}	30°R	4 Aa 43
0.927	5.7	29.0	(e)	. . . . .	Arith. Mean	

(d). not available

(e). not recorded

(a). of neutrons with >.5 mev energy

(b). change in mean of test value with respect to previous test condition

(c). with 90% confidence

TABLE B 20 a

TEST RESULTS, NICKEL ALLOY RENE 41 (SOLUTION TREATED)

Specimen Number	Test Temp	Total Fast Flux[a] (nvt)	F_{tu} (ksi) Test Value		Bias[b]	Bias Range[c]	F_{ty} (ksi) Test Value		Bias[b]	Bias Range[c]
TENSILE TESTS										
7 Ca 1	RT	None	132.0				63.3			
7 Ca 3	RT	None	130.0				(e)			
7 Ca 4	RT	None	130.0				62.6			
7 Ca 5	RT	None	128.0				62.2			
7 Ca 6	RT	None	131.0				64.7			
Arith. Mean				130.20				63.20		
Std. Deviation				1.48				1.10		
7 Ca 10	30°R	None	187.0				96.8			
7 Ca 11	30°R	None	195.0				115.0			
7 Ca 12	30°R	None	198.0				111.0			
7 Ca 13	30°R	None	198.0				112.0			
7 Ca 14	30°R	None	194.0				103.0			
Arith. Mean				194.40	+64.2	+60.3		107.60	+44.4	+38.0
Std. Deviation				4.51		+68.1		7.47		+50.8
7 Ca 8	30°R	10^{17}	197.0				114.0			
7 Ca 36	30°R	10^{17}	197.0				115.0			
7 Ca 40	30°R	10^{17}	190.0				111.0			
Arith. Mean				194.70	+ 0.3	- 5.7		113.30	+ 5.7	- 1.2
Std. Deviation				4.04		+ 6.3		2.08		+12.6
TENSILE NOTCH TESTS			F_{tun} (ksi)				F_{tun}/F_{tu}			
7 Ca 44	RT	None	145.0				1.10			
7 Ca 45	RT	None	143.0				1.10			
7 Ca 46	RT	None	141.0				1.08			
7 Ca 49	RT	None	141.0				1.10			
7 Ca 50	RT	None	144.0				1.10			
Arith. Mean				142.80				1.10		
Std. Deviation				1.79				0.01		
7 Ca 52	30°R	None	208.0				1.11			
7 Ca 53	30°R	None	202.0				1.04			
7 Ca 54	30°R	None	207.0				1.05			
7 Ca 55	30°R	None	204.0				1.03			
7 Ca 56	30°R	None	203.0				1.05			
Arith. Mean				204.80	+62.0	+59.4		1.06	- 0.04	- 0.01
Std. Deviation				2.59		+64.6		0.03		- 0.07
7 Ca 29	30°R	10^{17}	195.0				.99			
7 Ca 31	30°R	10^{17}	199.0				1.01			
7 Ca 37	30°R	10^{17}	188.0				.99			
Arith. Mean				194.00	-10.8	- 4.2		1.00	- 0.06	- 0.03
Std. Deviation				5.57		-17.4		0.01		- 0.09

TABLE B 20 b

TEST RESULTS, NICKEL ALLOY RENE 41 (SOLUTION TREATED)

F_{ty}/F_{tu}	Elongation (%)	Reduction of Area (%)	Fracture Stress (ksi)	Total Fast Flux[a] (nvt)	Test Temp	Specimen Number
				TENSILE TESTS		
0.48	(d)	(d)	(e)	None	RT	7 Ca 1
(e)	52	62	(e)	None	RT	7 Ca 3
0.48	55	59	(e)	None	RT	7 Ca 4
0.49	55	62	(e)	None	RT	7 Ca 5
0.49	57	60	(e)	None	RT	7 Ca 6
0.485	54.8	60.8	(e)	. . . . .	Arith. Mean	
0.52	(d)	(d)	(e)	None	30°R	7 Ca 10
0.59	(d)	(d)	(e)	None	30°R	7 Ca 11
0.56	59	49	(e)	None	30°R	7 Ca 12
0.57	(d)	(d)	(e)	None	30°R	7 Ca 13
0.53	62	52	(e)	None	30°R	7 Ca 14
0.554	60.5	50.5	(e)	. . . . .	Arith. Mean	
0.58	57	51	401.0	10^{17}	30°R	7 Ca 8
0.58	53	45	(e)	10^{17}	30°R	7 Ca 36
0.58	(d)	(d)	(e)	10^{17}	30°R	7 Ca 40
0.580	55.0	48.0	401.0	. . . . .	Arith. Mean	

(d). not available

(e). not recorded

(a). of neutrons with >.5 mev energy

(b). change in mean of test value with respect to previous test condition

(c). with 90% confidence

TABLE B 21 a

TEST RESULTS, NICKEL ALLOY K MONEL (AGED)

Specimen Number	Test Temp	Total Fast Flux[a] (nvt)	F_{tu} (ksi) Test Value		Bias[b]	Bias Range[c]	F_{ty} (ksi) Test Value		Bias[b]	Bias Range[c]
TENSILE TESTS										
1 Fb 1	RT	None	154.0				97.5			
1 Fb 2	RT	None	155.0				97.1			
1 Fb 3	RT	None	154.0				98.0			
1 Fb 4	RT	None	154.0				99.8			
1 Fb 5	RT	None	154.0				96.6			
Arith. Mean				154.20				97.80		
Std. Deviation				0.45				1.23		
1 Fb 6	30°R	None	184.0				121.0			
1 Fb 7	30°R	None	191.0				124.0			
1 Fb 8	30°R	None	192.0				123.0			
1 Fb 9	30°R	None	184.0				118.0			
1 Fb 11	30°R	None	185.0				121.0			
Arith. Mean				187.20	+33.0	+29.7		121.40	+23.6	+21.4
Std. Deviation				3.96		+36.3		2.30		+25.8
1 Fb 12	30°R	10^{17}	188.0				141.0			
1 Fb 30	30°R	10^{17}	189.0				138.0			
1 Fb 38	30°R	10^{17}	188.0				137.0			
Arith. Mean				188.30	+ 1.1	- 2.4		138.67	+17.3	+14.2
Std. Deviation				0.58		+ 4.6		2.08		+20.3
TENSILE NOTCH TESTS			F_{tun} (ksi)				F_{tun}/F_{tu}			
1 Fb 15	RT	None	178.0				1.16			
1 Fb 17	RT	None	177.0				1.14			
1 Fb 18	RT	None	179.0				1.16			
1 Fb 19	RT	None	179.0				1.16			
1 Fb 20	RT	None	189.0				1.23			
Arith. Mean				180.40				1.17		
Std. Deviation				4.88				0.03		
1 Fb 22	30°R	None	210.0				1.14			
1 Fb 23	30°R	None	211.0				1.10			
1 Fb 24	30°R	None	212.0				1.10			
1 Fb 25	30°R	None	207.0				1.13			
1 Fb 26	30°R	None	210.0				1.14			
Arith. Mean				210.00	+29.6	+25.3		1.12	- 0.05	- 0.02
Std. Deviation				1.87		+33.9		0.02		- 0.08
1 Fb 27	30°R	10^{17}	207.0				1.10			
1 Fb 40	30°R	10^{17}	210.0				1.11			
1 Fb 45	30°R	10^{17}	217.0				1.15			
Arith. Mean				211.30	+ 1.3	- 4.7		1.12	0.00	- 0.04
Std. Deviation				5.13		+ 7.3		0.03		+ 0.04

TABLE B 21 b

TEST RESULTS, NICKEL ALLOY K MONEL (AGED)

F_{ty}/F_{tu}	Elongation (%)	Reduction of Area (%)	Fracture Stress (ksi)	Total Fast Flux[a] (nvt)	Test Temp	Specimen Number
				TENSILE TESTS		
0.63	(d)	(d)	(e)	None	RT	1 Fb 1
0.63	27	55	(e)	None	RT	1 Fb 2
0.64	27	55	(e)	None	RT	1 Fb 3
0.65	30	56	(e)	None	RT	1 Fb 4
0.63	28	51	(e)	None	RT	1 Fb 5
0.636	28.0	54.3	(e)	. . . . .	Arith. Mean	
0.66	34	55	(e)	None	30°R	1 Fb 6
0.65	28	55	(e)	None	30°R	1 Fb 7
0.64	(d)	(d)	(e)	None	30°R	1 Fb 8
0.64	32	54	(e)	None	30°R	1 Fb 9
0.65	34	55	(e)	None	30°R	1 Fb 11
0.648	32.0	54.8	(e)	. . . . .	Arith. Mean	
0.75	34	50	329.0	10^{17}	30°R	1 Fb 12
0.73	32	52	365.0	10^{17}	30°R	1 Fb 30
0.73	33	52	323.0	10^{17}	30°R	1 Fb 38
0.737	33.0	51.3	339.0	. . . . .	Arith. Mean	

(d). not available

(e). not recorded

(a). of neutrons with >.5 mev energy

(b). change in mean of test value with respect to previous test condition

(c). with 90% confidence

TABLE B 22 a

TEST RESULTS, NICKEL ALLOY INCONEL (COLD DRAWN)

Specimen Number	Test Temp	Total Fast Flux[a] (nvt)	F_{tu} (ksi) Test Value		Bias[b]	Bias Range[c]	F_{ty} (ksi) Test Value		Bias[b]	Bias Range[c]
TENSILE TESTS										
2 Fb 1	RT	None	139.0				134.0			
2 Fb 2	RT	None	139.0				130.0			
2 Fb 3	RT	None	137.0				(e)			
2 Fb 4	RT	None	137.0				130.0			
2 Fb 5	RT	None	139.0				132.0			
Arith. Mean				138.20				131.50		
Std. Deviation				1.10				1.91		
2 Fb 7	30°R	None	190.0				181.0			
2 Fb 8	30°R	None	191.0				180.0			
2 Fb 10	30°R	None	184.0				172.0			
2 Fb 77	30°R	None	185.0				176.0			
2 Fb 78	30°R	None	182.0				170.0			
Arith. Mean				186.40	+48.2	+44.8		175.80	+44.3	+39.9
Std. Deviation				3.91		+51.6		4.82		+48.7
2 Fb 68	30°R	10^{17}	186.0				174.0			
2 Fb 69	30°R	10^{17}	204.0				189.0			
2 Fb 84	30°R	10^{17}	183.0				174.0			
Arith. Mean				191.00	+ 4.6	- 8.6		179.00	+ 3.2	- 7.4
Std. Deviation				11.36		+17.8		8.66		+13.8
TENSILE NOTCH TESTS			F_{tun} (ksi)				F_{tun}/F_{tu}			
2 Fb 30	RT	None	181.0				1.30			
2 Fb 31	RT	None	179.0				1.29			
2 Fb 32	RT	None	181.0				1.32			
2 Fb 33	RT	None	176.0				1.28			
2 Fb 34	RT	None	178.0				1.28			
Arith. Mean				179.00				1.29		
Std. Deviation				2.12				0.02		
2 Fb 70	30°R	None	223.0				1.17			
2 Fb 71	30°R	None	213.0				1.12			
2 Fb 72	30°R	None	227.0				1.23			
2 Fb 73	30°R	None	224.0				1.21			
2 Fb 74	30°R	None	225.0				1.24			
Arith. Mean				222.40	+43.4	+38.5		1.19	- 0.10	- 0.06
Std. Deviation				5.46		+48.3		0.05		- 0.14
2 Fb 11	30°R	10^{17}	233.0				1.25			
2 Fb 14	30°R	10^{17}	238.0				1.17			
2 Fb 37	30°R	10^{17}	241.0				1.32			
Arith. Mean				237.30	+14.9	+ 8.3		1.25	+ 0.06	- 0.04
Std. Deviation				4.04		+21.5		0.08		+ 0.16

TABLE B 22 b

TEST RESULTS, NICKEL ALLOY INCONEL (COLD DRAWN)

F_{ty}/F_{tu}	Elongation (%)	Reduction of Area (%)	Fracture Stress (ksi)	Total Fast Flux[a] (nvt)	Test Temp	Specimen Number
				TENSILE TESTS		
0.96	(d)	(d)	(e)	None	RT	2 Fb 1
0.94	15	55	(e)	None	RT	2 Fb 2
(e)	13	56	(e)	None	RT	2 Fb 3
0.95	13	53	(e)	None	RT	2 Fb 4
0.95	14	55	(e)	None	RT	2 Fb 5
0.950	13.8	54.8	(e)	. . . . .	Arith. Mean	
0.95	15	57	(e)	None	30°R	2 Fb 7
0.94	24	57	(e)	None	30°R	2 Fb 8
0.93	22	56	(e)	None	30°R	2 Fb 10
0.95	19	54	(e)	None	30°R	2 Fb 77
0.93	(d)	(d)	(e)	None	30°R	2 Fb 78
0.940	20.0	56.0	(e)	. . . . .	Arith. Mean	
0.94	27	52	356.0	10^{17}	30°R	2 Fb 68
0.93	25	52	371.0	10^{17}	30°R	2 Fb 69
0.95	23	49	331.0	10^{17}	30°R	2 Fb 84
0.940	25.0	51.0	352.7	. . . . .	Arith. Mean	

(d). not available

(e). not recorded

(a). of neutrons with >.5 mev energy

(b). change in mean of test value with respect to previous test condition

(c). with 90% confidence

TABLE B 23 a

TEST RESULTS, NICKEL ALLOY INCONEL X (AGED)

Specimen Number	Test Temp	Total Fast Flux[a] (nvt)	F_{tu} (ksi) Test Value		Bias[b]	Bias Range[c]	F_{ty} (ksi) Test Value		Bias[b]	Bias Range[c]
TENSILE TESTS										
3 Fa 9	RT	None	198.0				144.0			
3 Fa 21	RT	None	199.0				143.0			
3 Fa 18	RT	None	199.0				144.0			
3 Fa 20	RT	None	205.0				139.0			
3 Fa 24	RT	None	202.0				141.0			
Arith. Mean				200.60				142.20		
Std. Deviation				2.89				2.17		
3 Fa 5	30°R	None	251.0				160.0			
3 Fa 10	30°R	None	248.0				156.0			
3 Fa 14	30°R	None	248.0				156.0			
3 Fa 17	30°R	None	250.0				156.0			
3 Fa 19	30°R	None	219.0				126.0			
Arith. Mean				243.20	+42.6	+31.1		150.80	+ 8.6	- 3.1
Std. Deviation				13.59		+54.1		13.97		+20.3
3 Fa 22	30°R	10^{17}	236.0				159.0			
3 Fa 38	30°R	10^{17}	253.0				163.0			
3 Fa 42	30°R	10^{17}	234.0				162.0			
Arith. Mean				241.00	- 2.2	+14.4		161.30	+10.5	- 1.9
Std. Deviation				10.44		-18.8		2.08		+22.9
TENSILE NOTCH TESTS			F_{tun} (ksi)				F_{tun}/F_{tu}			
3 Fa 49	RT	None	198.0				1.00			
3 Fa 50	RT	None	196.0				0.98			
3 Fa 51	RT	None	196.0				0.98			
3 Fa 54	RT	None	209.0				1.02			
	RT	None								
Arith. Mean				199.75				0.99		
Std. Deviation				6.23				0.02		
3 Fa 46	30°R	None	241.0				0.96			
3 Fa 47	30°R	None	261.0				1.05			
3 Fa 48	30°R	None	248.0				1.00			
3 Fa 53	30°R	None	259.0				1.04			
3 Fa 56	30°R	None	240.0				1.10			
Arith. Mean				249.80	+50.1	+39.8		1.03	+ 0.05	+ 0.00
Std. Deviation				9.83		+60.3		0.05		+ 0.10
3 Fa 43	30°R	10^{17}	232.0				0.98			
3 Fa 52	30°R	10^{17}	229.0				0.91			
3 Fa 55	30°R	10^{17}	230.0				0.98			
Arith. Mean				230.30	-19.5	-10.8		0.96	- 0.07	- 0.01
Std. Deviation				1.53		-28.2		0.04		- 0.13

TABLE B 23 b

TEST RESULTS, NICKEL ALLOY INCONEL X (AGED)

F_{ty}/F_{tu}	Elongation (%)	Reduction of Area (%)	Fracture Stress (ksi)	Total Fast Flux[a] (nvt)	Test Temp	Specimen Number
				TENSILE TESTS		
0.73	(d)	(d)	(e)	None	RT	3 Fa 9
0.72	26	52	328.0	None	RT	3 Fa 21
0.72	(d)	(d)	(e)	None	RT	3 Fa 18
0.68	25	52	(e)	None	RT	3 Fa 20
0.70	25	53	(e)	None	RT	3 Fa 24
0.710	25.3	52.3	328.0	. . . . .	Arith. Mean	
0.64	32	44	432.0	None	30°R	3 Fa 5
0.63	32	45	406.0	None	30°R	3 Fa 10
0.63	31	46	448.0	None	30°R	3 Fa 14
0.62	38	47	428.0	None	30°R	3 Fa 17
0.58	32	46	395.0	None	30°R	3 Fa 19
0.620	33.0	45.6	421.8	. . . . .	Arith. Mean	
0.67	30	43	400.0	10^{17}	30°R	3 Fa 22
0.64	29	36	383.0	10^{17}	30°R	3 Fa 38
0.69	28	33	350.0	10^{17}	30°R	3 Fa 42
0.667	29.0	37.3	377.7	. . . . .	Arith. Mean	

(d). not available

(e). not recorded

(a). of neutrons with >.5 mev energy

(b). change in mean of test value with respect to previous test condition

(c). with 90% confidence

TABLE B 24 a

TEST RESULTS, 304 STAINLESS STEEL (ANNEALED)

Specimen Number	Test Temp	Total Fast Flux[a] (nvt)	F_{tu} (ksi) Test Value		Bias[b]	Bias Range[c]	F_{ty} (ksi) Test Value		Bias[b]	Bias Range[c]
TENSILE TESTS										
2 Cb 97	RT	None	96.3				37.5			
2 Cb 207	RT	None	94.9				35.7			
2 Cb 212	RT	None	95.3				36.4			
2 Cb 214	RT	None	93.5				37.6			
2 Cb 241	RT	None	95.7				36.6			
Arith. Mean				95.14				36.76		
Std. Deviation				1.05				0.83		
2 Cb 215	30°R	None	244.0				40.4			
2 Cb 218	30°R	None	270.0				46.5			
2 Cb 220	30°R	None	215.0				25.4			
2 Cb 234	30°R	None	232.0				43.1			
2 Cb 238	30°R	None	249.0				42.7			
Arith. Mean				242.00	+146.9	+129.9		39.62	+ 2.9	- 4.0
Std. Deviation				20.41		+163.9		8.24		+ 9.8
2 Cb 229	30°R	10^{17}	254.0				50.0			
2 Cb 265	30°R	10^{17}	260.0				52.4			
2 Cb 245	30°R	10^{17}	267.0				53.3			
Arith. Mean				260.33	+ 18.3	- 0.8		51.90	+12.3	+ 4.9
Std. Deviation				6.51		+ 37.5		1.71		+19.7
TENSILE NOTCH TESTS			F_{tun} (ksi)				F_{tun}/F_{tu}			
2 Cb 95	RT	None	99.4				1.03			
2 Cb 211	RT	None	103.0				1.09			
2 Cb 216	RT	None	109.0				1.14			
2 Cb 222	RT	None	92.7				0.99			
2 Cb 231	RT	None	110.0				1.15			
Arith. Mean				102.82				1.08		
Std. Deviation				7.14				0.07		
2 Cb 233	30°R	None	163.0				0.67			
2 Cb 235	30°R	None	189.0				0.70			
2 Cb 244	30°R	None	208.0				0.97			
2 Cb 246	30°R	None	150.0				0.65			
2 Cb 247	30°R	None	257.0				1.03			
Arith. Mean				193.40	+ 90.6	+ 55.1		0.80	- 0.28	- 0.12
Std. Deviation				42.09		+126.1		0.18		- 0.44
2 Cb 292	30°R	10^{17}	197.0				0.78			
2 Cb 295	30°R	10^{17}	148.0				0.57			
2 Cb 299	30°R	10^{17}	175.0				0.66			
Arith. Mean				173.30	- 20.1	+ 25.7		0.67	- 0.13	+ 0.07
Std. Deviation				24.54		- 65.9		0.11		- 0.33

TABLE B 24 b

TEST RESULTS, 304 STAINLESS STEEL (ANNEALED)

F_{ty}/F_{tu}	Elongation (%)	Reduction of Area (%)	Fracture Stress (ksi)	Total Fast Flux[a] (nvt)	Test Temp	Specimen Number
				TENSILE TESTS		
0.39	80	81	(e)	None	RT	2 Cb 97
0.38	77	81	(e)	None	RT	2 Cb 207
0.38	77	82	(e)	None	RT	2 Cb 212
0.40	(d)	(d)	(e)	None	RT	2 Cb 214
0.38	72	81	(e)	None	RT	2 Cb 241
0.386	76.5	81.3	(e)	. . . . .	Arith. Mean	
0.17	37	27	(e)	None	30°R	2 Cb 215
0.17	36	42	(e)	None	30°R	2 Cb 218
0.12	36	45	(e)	None	30°R	2 Cb 220
0.19	32	57	(e)	None	30°R	2 Cb 234
0.17	31	21	(e)	None	30°R	2 Cb 238
0.164	34.4	38.4	(e)	. . . . .	Arith. Mean	
0.20	(d)	(d)	(e)	10^{17}	30°R	2 Cb 229
0.20	35	35	(e)	10^{17}	30°R	2 Cb 265
0.20	32	22	(e)	10^{17}	30°R	2 Cb 245
0.200	33.5	28.5	(e)	. . . . .	Arith. Mean	

(d). not available

(e). not recorded

(a). of neutrons with >.5 mev energy

(b). change in mean of test value with respect to previous test condition

(c). with 90% confidence

TABLE B 25 a

TEST RESULTS, 310 STAINLESS STEEL (ANNEALED)

Specimen Number	Test Temp	Total Fast Flux[a] (nvt)	F_{tu} (ksi) Test Value		Bias[b]	Bias Range[c]	F_{ty} (ksi) Test Value		Bias[b]	Bias Range[c]
TENSILE TESTS										
3 Cb 4	RT	None	78.6				59.9			
3 Cb 5	RT	None	82.8				61.4			
3 Cb 15	RT	None	84.9				58.8			
3 Cb 32	RT	None	87.0				65.3			
3 Cb 33	RT	None	91.2				67.8			
Arith. Mean				84.90				62.64		
Std. Deviation				4.70				3.79		
3 Cb 34	30°R	None	206.0				132.0			
3 Cb 64	30°R	None	212.0				141.0			
3 Cb 65	30°R	None	217.0				142.0			
3 Cb 67	30°R	None	215.0				138.0			
3 Cb 68	30°R	None	211.0				136.0			
Arith. Mean				212.20	+127.3	+122.1		137.80	+75.2	+70.6
Std. Deviation				4.21		+132.5		4.03		+79.8
3 Cb 37	30°R	10^{17}	202.0				116.0			
3 Cb 39	30°R	10^{17}	208.0				132.0			
3 Cb 66	30°R	10^{17}	246.0				159.0			
Arith. Mean				218.67	+ 6.5	- 20.5		135.67	- 2.1	+22.5
Std. Deviation				23.86		+ 33.5		21.73		-26.8
TENSILE NOTCH TESTS			F_{tun} (ksi)				F_{tun}/F_{tu}			
3 Cb 16	RT	None	110.0				1.40			
3 Cb 17	RT	None	117.0				1.41			
3 Cb 18	RT	None	112.0				1.32			
3 Cb 19	RT	None	112.0				1.29			
3 Cb 20	RT	None	111.0				1.22			
Arith. Mean				112.40				1.33		
Std. Deviation				2.70				0.08		
3 Cb 23	30°R	None	161.2				0.78			
3 Cb 24	30°R	None	158.0				0.75			
3 Cb 26	30°R	None	161.0				0.74			
3 Cb 28	30°R	None	222.0				1.03			
3 Cb 59	30°R	None	241.0				1.14			
Arith. Mean				188.64	+ 76.2	+ 43.1		0.89	- 0.44	- 0.27
Std. Deviation				39.72		+109.3		0.19		- 0.61
3 Cb 51	30°R	10^{17}	204.0				1.01			
3 Cb 58	30°R	10^{17}	222.0				1.07			
3 Cb 62	30°R	10^{17}	228.0				0.93			
Arith. Mean				218.00	+ 29.4	- 7.9		1.00	+ 0.12	- 0.06
Std. Deviation				12.49		+ 66.6		0.07		+ 0.29

TABLE B 25 b

TEST RESULTS, 310 STAINLESS STEEL (ANNEALED)

F_{ty}/F_{tu}	Elongation (%)	Reduction of Area (%)	Fracture Stress (ksi)	Total Fast Flux[a] (nvt)	Test Temp	Specimen Number
				TENSILE TESTS		
0.76	44	79	(e)	None	RT	3 Cb 4
0.74	(d)	(d)	(e)	None	RT	3 Cb 5
0.69	42	80	(e)	None	RT	3 Cb 15
0.75	42	78	(e)	None	RT	3 Cb 32
0.74	43	79	(e)	None	RT	3 Cb 33
0.736	42.8	79.0	(e)	. . . . .	Arith. Mean	
0.64	43	59	501.0	None	30°R	3 Cb 34
0.67	43	57	474.0	None	30°R	3 Cb 64
0.65	44	54	463.0	None	30°R	3 Cb 65
0.64	42	55	445.0	None	30°R	3 Cb 67
0.64	42	56	427.0	None	30°R	3 Cb 68
0.648	42.8	56.2	462.0	. . . . .	Arith. Mean	
0.57	47	28	279.0	10^{17}	30°R	3 Cb 37
0.63	50	17	250.0	10^{17}	30°R	3 Cb 39
0.65	48	20	307.0	10^{17}	30°R	3 Cb 66
0.617	48.3	21.7	278.7	. . . . .	Arith. Mean	

(d). not available

(e). not recorded

(a). of neutrons with >.5 mev energy

(b). change in mean of test value with respect to previous test condition

(c). with 90% confidence

TABLE B 26 a

TEST RESULTS, 347 STAINLESS STEEL (ANNEALED)

Specimen Number	Test Temp	Total Fast Flux[a] (nvt)	F_{tu} (ksi) Test Value		Bias[b]	Bias Range[c]	F_{ty} (ksi) Test Value		Bias[b]	Bias Range[c]
TENSILE TESTS										
4 Cb 2	RT	None	93.9				44.3			
4 Cb 5	RT	None	94.5				43.4			
4 Cb 6	RT	None	95.1				42.7			
4 Cb 7	RT	None	94.6				44.5			
4 Cb 9	RT	None	94.4				43.6			
Arith. Mean				94.50			.....	43.70		
Std. Deviation				0.43			.....	0.73		
4 Cb 30	30°R	None	233.0				57.6			
4 Cb 31	30°R	None	243.0				47.5			
4 Cb 32	30°R	None	234.0				51.2			
4 Cb 33	30°R	None	243.0				51.8			
4 Cb 34	30°R	None	234.0				51.4			
Arith. Mean				237.40	+142.9	+138.6	.....	51.90	+ 8.20	+ 5.1
Std. Deviation				5.13		+147.2	.....	3.63		+11.3
4 Cb 39	30°R	10^{17}	278.0				69.9			
4 Cb 43	30°R	10^{17}	228.0				60.7			
4 Cb 44	30°R	10^{17}	246.0				61.4			
Arith. Mean				250.70	+ 13.3	- 15.5	.....	64.00	+12.10	+ 5.5
Std. Deviation				25.33		+ 42.1	.....	5.12		+18.7
TENSILE NOTCH TESTS			F_{tun} (ksi)				F_{tun}/F_{tu}			
4 Cb 15	RT	None	123.0				1.08			
4 Cb 16	RT	None	108.0				1.14			
4 Cb 17	RT	None	110.0				1.16			
4 Cb 18	RT	None	119.0				1.26			
4 Cb 19	RT	None	109.0				1.15			
Arith. Mean				113.80			.....	1.158		
Std. Deviation				6.76			.....	0.065		
4 Cb 20	30°R	None	163.0				0.70			
4 Cb 21	30°R	None	231.0				0.95			
4 Cb 22	30°R	None	230.0				0.98			
4 Cb 23	30°R	None	220.0				0.91			
4 Cb 24	30°R	None	227.0				0.97			
Arith. Mean				214.20	+100.4	+ 75.7	.....	0.902	- 0.26	- 0.15
Std. Deviation				28.94		+125.1	.....	0.116		- 0.37
4 Cb 27	30°R	10^{17}	224.0				0.81			
4 Cb 54	30°R	10^{17}	248.0				1.09			
4 Cb 56	30°R	10^{17}	242.0				0.98			
Arith. Mean				238.00	+ 23.8	- 5.0	.....	0.960	+ 0.06	- 0.04
Std. Deviation				12.49		+ 52.6	.....	0.141		+ 0.15

TABLE B 26 b

TEST RESULTS, 347 STAINLESS STEEL (ANNEALED)

F_{ty}/F_{tu}	Elongation (%)	Reduction of Area (%)	Fracture Stress (ksi)	Total Fast Flux[a] (nvt)	Test Temp	Specimen Number
				TENSILE TESTS		
0.47	60	76	(e)	None	RT	4 Cb 2
0.46	(d)	(d)	(e)	None	RT	4 Cb 5
0.45	60	77	(e)	None	RT	4 Cb 6
0.47	61	75	(e)	None	RT	4 Cb 7
0.46	60	78	(e)	None	RT	4 Cb 9
0.462	60.3	76.5	(e)	. . . . .	Arith. Mean	
0.25	43	28	(e)	None	30°R	4 Cb 30
0.20	42	46	(e)	None	30°R	4 Cb 31
0.22	36	52	(e)	None	30°R	4 Cb 32
0.21	(d)	(d)	(e)	None	30°R	4 Cb 33
0.22	44	49	(e)	None	30°R	4 Cb 34
0.220	41.3	43.8	(e)	. . . . .	Arith. Mean	
0.25	(d)	(d)	(e)	10^{17}	30°R	4 Cb 39
0.27	37	55	(e)	10^{17}	30°R	4 Cb 43
0.25	(d)	(d)	(e)	10^{17}	30°R	4 Cb 44
0.257	37.0	55.0	(e)	. . . . .	Arith. Mean	

(d). not available

(e). not recorded

(a). of neutrons with >.5 mev energy

(b). change in mean of test value with respect to previous test condition

(c). with 90% confidence

TABLE B 27 a

TEST RESULTS, A286 STAINLESS STEEL (AMS 5735)

Specimen Number	Test Temp	Total Fast Flux[a] (nvt)	F_{tu} (ksi) Test Value		Bias[b]	Bias Range[c]	F_{ty} (ksi) Test Value		Bias[b]	Bias Range[c]
TENSILE TESTS										
6 Ca 1	RT	None	157.0				116.0			
6 Ca 2	RT	None	158.0				111.0			
6 Ca 3	RT	None	157.0				113.0			
6 Ca 4	RT	None	153.0				111.0			
6 Ca 5	RT	None	155.0				110.0			
Arith. Mean				156.00				112.20		
Std. Deviation				2.00				2.39		
6 Ca 6	30°R	None	248.0				152.0			
6 Ca 7	30°R	None	230.0				149.0			
6 Ca 8	30°R	None	230.0				148.0			
6 Ca 9	30°R	None	230.0				148.0			
6 Ca 10	30°R	None	237.0				151.0			
Arith. Mean				235.00	+79.0	+72.2		149.60	+37.4	+34.9
Std. Deviation				7.87		+85.8		1.82		+39.9
6 Ca 12	30°R	10^{17}	230.0				157.0			
6 Ca 31	30°R	10^{17}	229.0				149.0			
6 Ca 34	30°R	10^{17}	228.0				150.0			
Arith. Mean				229.00	- 6.0	+ 0.9		152.00	+ 2.4	- 2.7
Std. Deviation				1.00		-12.9		4.36		+ 7.5
TENSILE NOTCH TESTS			F_{tun} (ksi)				F_{tun}/F_{tu}			
6 Ca 33	RT	None	179.0				1.14			
6 Ca 36	RT	None	181.0				1.15			
6 Ca 37	RT	None	182.0				1.16			
6 Ca 38	RT	None	180.0				1.18			
6 Ca 39	RT	None	183.0				1.18			
Arith. Mean				181.00				1.16		
Std. Deviation				1.58				0.02		
6 Ca 51	30°R	None	215.0				0.867			
6 Ca 49	30°R	None	209.0				0.909			
6 Ca 50	30°R	None	203.0				0.883			
6 Ca 52	30°R	None	221.0				0.961			
6 Ca 53	30°R	None	234.0				0.987			
Arith. Mean				216.40	+35.4	+25.4		0.92	- 0.24	- 0.20
Std. Deviation				11.91		+45.4		0.05		- 0.28
6 Ca 44	30°R	10^{17}	228.0				0.991			
6 Ca 46	30°R	10^{17}	258.0				1.127			
6 Ca 47	30°R	10^{17}	251.0				1.101			
Arith. Mean				245.67	+29.3	+ 8.8		1.07	+ 0.15	- 0.66
Std. Deviation				15.70		+49.7		0.72		+ 0.96

TABLE B 27 b

TEST RESULTS, A286 STAINLESS STEEL (AMS 5735)

F_{ty}/F_{tu}	Elongation (%)	Reduction of Area (%)	Fracture Stress (ksi)	Total Fast Flux[a] (nvt)	Test Temp	Specimen Number
				TENSILE TESTS		
0.74	27	50	(e)	None	RT	6 Ca 1
0.70	(d)	(d)	(e)	None	RT	6 Ca 2
0.72	25	55	(e)	None	RT	6 Ca 3
0.73	26	49	(e)	None	RT	6 Ca 4
0.71	27	50	(e)	None	RT	6 Ca 5
0.720	26.3	51.0	(e)	. . . . .	Arith. Mean	
0.61	32	44	(e)	None	30°R	6 Ca 6
0.65	36	51	(e)	None	30°R	6 Ca 7
0.64	(d)	(d)	(e)	None	30°R	6 Ca 8
0.64	35	49	(e)	None	30°R	6 Ca 9
0.64	35	42	(e)	None	30°R	6 Ca 10
0.636	34.5	46.5	(e)	. . . . .	Arith. Mean	
0.68	(d)	(d)	(e)	10^{17}	30°R	6 Ca 12
0.65	33	14	(e)	10^{17}	30°R	6 Ca 31
0.66	34	18	(e)	10^{17}	30°R	6 Ca 34
0.663	33.5	16.0	(e)	. . . . .	Arith. Mean	

(d). not available

(e). not recorded

(a). of neutrons with >.5 mev energy

(b). change in mean of test value with respect to previous test condition

(c). with 90% confidence

TABLE B 28 a

TEST RESULTS, A286 STAINLESS STEEL (AMS 5737)

Specimen Number	Test Temp	Total Fast Flux[a] (nvt)	F_{tu} (ksi) Test Value		Bias[b]	Bias Range[c]	F_{ty} (ksi) Test Value		Bias[b]	Bias Range[c]
TENSILE TESTS										
8 Ca 4	RT	None	179.0				141.0			
8 Ca 7	RT	None	174.0				134.0			
8 Ca 10	RT	None	168.0				129.0			
8 Ca 28	RT	None	166.0				129.0			
8 Ca 31	RT	None	172.0				136.0			
Arith. Mean				171.80				133.80		
Std. Deviation				5.12				5.07		
8 Ca 8	30°R	None	248.0				166.0			
8 Ca 12	30°R	None	250.0				161.0			
8 Ca 18	30°R	None	245.0				162.0			
8 Ca 20	30°R	None	206.0				138.0			
8 Ca 21	30°R	None	242.0				157.0			
Arith. Mean				238.20	+66.4	+50.6		156.80	+23.0	+12.9
Std. Deviation				18.25		+82.2		10.99		+33.1
8 Ca 5	30°R	10^{17}	230.0				158.0			
8 Ca 13	30°R	10^{17}	231.0				164.0			
8 Ca 19	30°R	10^{17}	253.0				175.0			
Arith. Mean				238.00	- 0.2	+21.3		165.70	+ 8.9	- 4.7
Std. Deviation				13.00		-21.7		8.62		+22.5
TENSILE NOTCH TESTS			F_{tun} (ksi)				F_{tun}/F_{tu}			
8 Ca 9	RT	None	200.0				1.12			
8 Ca 11	RT	None	201.0				1.16			
8 Ca 17	RT	None	202.0				1.20			
8 Ca 27	RT	None	195.0				1.17			
8 Ca 34	RT	None	183.0				1.06			
Arith. Mean				196.20				1.14		
Std. Deviation				7.86				0.05		
8 Ca 29	30°R	None	256.0				1.03			
8 Ca 32	30°R	None	251.0				1.00			
8 Ca 35	30°R	None	256.0				1.04			
8 Ca 33	30°R	None	258.0				1.25			
8 Ca 41	30°R	None	254.0				1.05			
Arith. Mean				255.00	+58.8	+51.9		1.07	- 0.07	+ 0.03
Std. Deviation				2.65		+65.7		0.10		- 0.16
8 Ca 25	30°R	10^{17}	234.0				1.02			
8 Ca 39	30°R	10^{17}	254.0				1.10			
8 Ca 40	30°R	10^{17}	229.0				.91			
Arith. Mean				239.00	-16.0	- 2.6		1.01	- 0.06	+ 0.29
Std. Deviation				11.73		-29.4		0.30		- 0.41

TABLE B 28 b

TEST RESULTS, A286 STAINLESS STEEL (AMS 5737)

F_{ty}/F_{tu}	Elongation (%)	Reduction of Area (%)	Fracture Stress (ksi)	Total Fast Flux[a] (nvt)	Test Temp	Specimen Number
				TENSILE TESTS		
0.79	25	50	(e)	None	RT	8 Ca 4
0.77	23	51	(e)	None	RT	8 Ca 7
0.77	24	54	272.0	None	RT	8 Ca 10
0.78	23	55	270.0	None	RT	8 Ca 28
0.79	(d)	(d)	(e)	None	RT	8 Ca 31
0.780	23.8	52.5	271.0	. . . . .	Arith. Mean	
0.67	32	44	434.0	None	30°R	8 Ca 8
0.64	31	45	450.0	None	30°R	8 Ca 12
0.66	31	33	368.0	None	30°R	8 Ca 18
0.67	33	46	369.0	None	30°R	8 Ca 20
0.65	32	43	417.0	None	30°R	8 Ca 21
0.658	31.8	42.2	407.6	. . . . .	Arith. Mean	
0.69	29	29	319.0	10^{17}	30°R	8 Ca 5
0.71	32	45	419.0	10^{17}	30°R	8 Ca 13
0.69	32	45	422.0	10^{17}	30°R	8 Ca 19
0.697	31.0	39.7	386.7	. . . . .	Arith. Mean	

(d). not available

(e). not recorded

(a). of neutrons with >.5 mev energy

(b). change in mean of test value with respect to previous test condition

(c). with 90% confidence

TABLE B 29 a

TEST RESULTS, T-450 AUSTENITIC MANGANESE STEEL (ANNEALED)

Specimen Number	Test Temp	Total Fast Flux[a] (nvt)	F_{tu} (ksi) Test Value		Bias[b]	Bias Range[c]	F_{ty} (ksi) Test Value		Bias[b]	Bias Range[c]
TENSILE TESTS										
1 Eb 6	RT	None	110.0				32.5			
1 Eb 14	RT	None	111.0				41.5			
1 Eb 40	RT	None	112.0				36.2			
1 Eb 43	RT	None	150.0				47.4			
1 Eb 45	RT	None	115.0				35.8			
Arith. Mean				119.60				38.68		
Std. Deviation				17.10				5.84		
1 Eb 4	30°R	None	210.0				105.0			
1 Eb 10	30°R	None	190.0				81.0			
1 Eb 18	30°R	None	194.0				92.4			
1 Eb 31	30°R	None	193.0				89.5			
1 Eb 34	30°R	None	199.0				89.4			
Arith. Mean				197.20	+77.6	+63.1		91.46	+52.8	+44.1
Std. Deviation				7.85		+92.1		8.68		+61.5
1 Eb 24	30°R	10^{17}	193.0				92.4			
1 Eb 28	30°R	10^{17}	194.0				92.4			
1 Eb 49	30°R	10^{17}	191.0				92.0			
Arith. Mean				192.70	- 4.5	+ 2.5		92.27	+ 0.8	- 6.7
Std. Deviation				1.53		-11.5		0.25		+ 8.3
TENSILE NOTCH TESTS			F_{tun} (ksi)				F_{tun}/F_{tu}			
1 Eb 32	RT	None	124.0				1.13			
1 Eb 37	RT	None	127.0				1.14			
1 Eb 39	RT	None	123.0				1.10			
1 Eb 50	RT	None	118.0				0.79			
1 Eb 53	RT	None	109.0				0.95			
Arith. Mean				120.20				1.02		
Std. Deviation				7.05				0.15		
1 Eb 9	30°R	None	222.0				1.06			
1 Eb 13	30°R	None	236.0				1.24			
1 Eb 23	30°R	None	216.0				1.11			
1 Eb 44	30°R	None	191.0				0.99			
1 Eb 46	30°R	None	207.0				1.04			
Arith. Mean				214.40	+94.2	+80.5		1.09	+ 0.07	- 0.08
Std. Deviation				16.26		+107.9		0.10		+ 0.21
(q)	30°R	10^{17}								
(q)	30°R	10^{17}								
(q)	30°R	10^{17}								
Arith. Mean										
Std. Deviation										

TABLE B 29 b

TEST RESULTS, T-450 AUSTENITIC MANGANESE STEEL (ANNEALED)

F_{ty}/F_{tu}	Elongation (%)	Reduction of Area (%)	Fracture Stress (ksi)	Total Fast Flux[a] (nvt)	Test Temp	Specimen Number
				TENSILE TESTS		
0.30	71	70	295.0	None	RT	1 Eb 6
0.37	69	77	476.0	None	RT	1 Eb 14
0.32	70	71	(e)	None	RT	1 Eb 40
0.32	70	67	(e)	None	RT	1 Eb 43
0.31	71	69	(e)	None	RT	1 Eb 45
0.324	70.2	70.8	385.5	. . . . .	Arith. Mean	
0.50	28	24	275.0	None	30°R	1 Eb 4
0.43	30	26	258.0	None	30°R	1 Eb 10
0.48	32	30	277.0	None	30°R	1 Eb 18
0.46	30	29	274.0	None	30°R	1 Eb 31
0.45	36	27	273.0	None	30°R	1 Eb 34
0.464	31.2	27.2	271.4	. . . . .	Arith. Mean	
0.48	32	28	270.0	10^{17}	30°R	1 Eb 24
0.48	30	30	276.0	10^{17}	30°R	1 Eb 28
0.48	29	31	277.0	10^{17}	30°R	1 Eb 49
0.480	30.3	29.7	274.3	. . . . .	Arith. Mean	

(e). not recorded

(q). test deleted from screening program

(a). of neutrons with >.5 mev energy

(b). change in mean of test value with respect to previous test condition

(c). with 90% confidence

TABLE B 30 a

TEST RESULTS, AM350 STAINLESS STEEL (SCT)

Specimen Number	Test Temp	Total Fast Flux[a] (nvt)	F_{tu} (ksi) Test Value		Bias[b]	Bias Range[c]	F_{ty} (ksi) Test Value		Bias[b]	Bias Range[c]
TENSILE TESTS										
10 Ca 18	RT	None	206.0				192.0			
10 Ca 21	RT	None	208.0				193.0			
10 Ca 23	RT	None	194.0				183.0			
10 Ca 40	RT	None	193.0				182.0			
10 Ca 42	RT	None	193.0				182.0			
Arith. Mean				199.00			.....	186.40		
Std. Deviation				7.53			.....	5.60		
10 Ca 9	30°R	None	315.0				314.0			
10 Ca 10	30°R	None	313.0				313.0			
10 Ca 11	30°R	None	322.0				322.0			
10 Ca 15	30°R	None	389.0				380.0			
10 Ca 16	30°R	None	364.0							
Arith. Mean				340.60	+141.6	+127.6	.....	332.30	+145.9	+120.0
Std. Deviation				10.79		+155.6	.....	29.65		+171.7
10 Ca 17	30°R	10^{17}	305.0				303.0			
10 Ca 22	30°R	10^{17}	330.0				323.0			
10 Ca 39	30°R	10^{17}	305.0				299.0			
Arith. Mean				313.30	- 27.3	- 8.6	.....	308.30	- 24.0	+ 6.9
Std. Deviation				14.43		- 46.0	.....	12.86		- 54.9
TENSILE NOTCH TESTS			F_{tun} (ksi)				F_{tun}/F_{tu}			
10 Ca 1	RT	None	229.0				1.11			
10 Ca 12	RT	None	235.0				1.13			
10 Ca 14	RT	None	232.0				1.20			
10 Ca 20	RT	None	250.0				1.30			
10 Ca 35	RT	None	252.0				1.30			
Arith. Mean				239.60			.....	1.21		
Std. Deviation				10.64			.....	0.09		
10 Ca 3	30°R	None	240.0				0.76			
10 Ca 6	30°R	None	281.0				0.90			
10 Ca 13	30°R	None	273.0				0.85			
10 Ca 31	30°R	None	264.0				0.68			
10 Ca 36	30°R	None	284.0				0.78			
Arith. Mean				268.40	+ 28.8	+ 11.6	.....	0.79	- 0.41	- 0.31
Std. Deviation				17.67		+ 46.0	.....	0.04		- 0.51
10 Ca 26	30°R	10^{17}	129.0				0.42			
10 Ca 28	30°R	10^{17}	164.0				0.50			
10 Ca 33	30°R	10^{17}	152.0				0.50			
Arith. Mean				148.30	-120.1	-103.5	.....	0.47	- 0.32	- 0.23
Std. Deviation				17.79		-136.7	.....	0.03		- 0.41

TABLE B 30 b

TEST RESULTS, AM350 STAINLESS STEEL (SCT)

F_{ty}/F_{tu}	Elongation (%)	Reduction of Area (%)	Fracture Stress (ksi)	Total Fast Flux[a] (nvt)	Test Temp	Specimen Number
				TENSILE TESTS		
0.93	19	51	300.0	None	RT	10 Ca 18
0.93	20	53	319.0	None	RT	10 Ca 21
0.94	(d)	(d)	(e)	None	RT	10 Ca 23
0.94	19	57	(e)	None	RT	10 Ca 40
0.94	(d)	(d)	(e)	None	RT	10 Ca 42
0.936	19.3	53.7	309.5	. . . . .	Arith. Mean	
1.00	12	37	(e)	None	30°R	10 Ca 9
1.00	10	37	(e)	None	30°R	10 Ca 10
1.00	10	37	(e)	None	30°R	10 Ca 11
0.98	11	34	591.0	None	30°R	10 Ca 15
	12	35	557.0	None	30°R	10 Ca 16
0.995	11.0	36.0	574.0	. . . . .	Arith. Mean	
0.99	7	18	372.0	10^{17}	30°R	10 Ca 17
0.98	11	30	466.0	10^{17}	30°R	10 Ca 22
0.98	4	14	351.0	10^{17}	30°R	10 Ca 39
0.983	7.3	20.7	396.3	. . . . .	Arith. Mean	

(d). not available

(e). not recorded

(a). of neutrons with >.5 mev energy

(b). change in mean of test value with respect to previous test condition

(c). with 90% confidence

TABLE B 31 a

TEST RESULTS, 17-7 PH STAINLESS STEEL (RH-950)

Specimen Number	Test Temp	Total Fast Flux[a] (nvt)	F_{tu} (ksi) Test Value		Bias[b]	Bias Range[c]	F_{ty} (ksi) Test Value		Bias[b]	Bias Range[c]
TENSILE TESTS										
11 Ca 11	RT	None	240.0				231.0			
11 Ca 17	RT	None	238.0				235.0			
11 Ca 20	RT	None	241.0				228.0			
11 Ca 25	RT	None	228.0				220.0			
11 Ca 27	RT	None	227.0				219.0			
Arith. Mean				234.80				226.60		
Std. Deviation				6.76				6.95		
11 Ca 12	30°R	None	342.0				333.0			
11 Ca 29	30°R	None	340.0				334.0			
11 Ca 30	30°R	None	324.0				319.0			
11 Ca 31	30°R	None	332.0				327.0			
11 Ca 39	30°R	None	339.9				337.0			
Arith. Mean				335.40	+118.6	+110.3		330.00	+103.4	+ 95.1
Std. Deviation				7.40		+126.9		7.14		+111.7
11 Ca 28	30°R	10^{17}	260.0				260.0			
11 Ca 32	30°R	10^{17}	256.0				254.0			
11 Ca 46	30°R	10^{17}	238.0				238.0			
Arith. Mean				251.30	- 84.1	- 69.5		250.70	- 79.3	- 65.1
Std. Deviation				11.72		- 98.7		11.38		- 93.5
TENSILE NOTCH TESTS			F_{tun} (ksi)				F_{tun}/F_{tu}			
11 Ca 2	RT	None	260.0				1.08			
11 Ca 4	RT	None	255.0				1.07			
11 Ca 7	RT	None	254.0				1.05			
11 Ca 13	RT	None	289.0				1.27			
11 Ca 15	RT	None	275.0				1.21			
Arith. Mean				266.60				1.14		
Std. Deviation				15.08				0.10		
11 Ca 10	30°R	None	182.0				0.53			
11 Ca 18	30°R	None	193.0				0.57			
11 Ca 21	30°R	None	220.0				0.68			
11 Ca 33	30°R	None	169.0				0.51			
11 Ca 35	30°R	None	149.0				0.44			
Arith. Mean				182.60	- 84.0	- 69.6		0.55	- 0.59	- 0.48
Std. Deviation				8.40		- 98.4		0.09		- 0.70
(q)	30°R	10^{17}								
(q)	30°R	10^{17}								
(q)	30°R	10^{17}								
Arith. Mean										
Std. Deviation										

TABLE B 31 b

TEST RESULTS, 17-7 PH STAINLESS STEEL (RH-950)

F_{ty}/F_{tu}	Elongation (%)	Reduction of Area (%)	Fracture Stress (ksi)	Total Fast Flux[a] (nvt)	Test Temp	Specimen Number
				TENSILE TESTS		
0.96	15	49	(e)	None	RT	11 Ca 11
0.99	14	49	(e)	None	RT	11 Ca 17
0.95	14	48	(e)	None	RT	11 Ca 20
0.96	13	41	294.0	None	RT	11 Ca 25
0.96	13	38	274.0	None	RT	11 Ca 27
0.964	13.8	45.0	279.0	. . . . .	Arith. Mean	
0.97	nil	nil	(e)	None	30°R	11 Ca 12
0.98	nil	nil	340.0	None	30°R	11 Ca 29
0.98	nil	nil	(e)	None	30°R	11 Ca 30
0.98	nil	nil	(e)	None	30°R	11 Ca 31
0.99	nil	nil	339.9	None	30°R	11 Ca 39
0.980	nil	nil	340.0	. . . . .	Arith. Mean	
1.00	nil	nil	260.0	10^{17}	30°R	11 Ca 28
0.99	nil	nil	256.0	10^{17}	30°R	11 Ca 32
1.00	nil	nil	238.0	10^{17}	30°R	11 Ca 46
0.997	nil	nil	251.3	. . . . .	Arith. Mean	

(e). not recorded

(q). test deleted from screening program

(a). of neutrons with >.5 mev energy

(b). change in mean of test value with respect to previous test condition

(c). with 90% confidence

TABLE B 32 a

TEST RESULTS, A 353 STEEL (NORMALIZED)

Specimen Number	Test Temp	Total Fast Flux[a] (nvt)	F_{tu} (ksi) Test Value		Bias[b]	Bias Range[c]	F_{ty} (ksi) Test Value		Bias[b]	Bias Range[c]
TENSILE TESTS										
5 Ca 1	RT	None	111.0				88.0			
5 Ca 2	RT	None	113.0				91.4			
5 Ca 3	RT	None	110.0				88.6			
5 Ca 4	RT	None	110.0				88.4			
5 Ca 5	RT	None	109.0				86.6			
Arith. Mean				110.60				88.60		
Std. Deviation				1.52				1.75		
5 Ca 7	30°R	None	209.0				171.0			
5 Ca 8	30°R	None	204.0				174.0			
5 Ca 9	30°R	None	199.0				166.0			
5 Ca 10	30°R	None	193.0				181.0			
5 Ca 11	30°R	None	203.0				182.0			
Arith. Mean				201.60	+91.0	+85.9		174.80	+86.2	+80.4
Std. Deviation				5.98		+96.1		6.76		+92.0
5 Ca 29	30°R	10^{17}	209.0				183.0			
5 Ca 36	30°R	10^{17}	220.0				194.0			
5 Ca 45	30°R	10^{17}	218.0				193.0			
Arith. Mean				215.70	+14.1	+ 5.7		190.00	+15.2	+ 6.2
Std. Deviation				5.86		+22.5		6.08		+24.2
TENSILE NOTCH TESTS			F_{tun} (ksi)				F_{tun}/F_{tu}			
5 Ca 49	RT	None	137.0				1.23			
5 Ca 50	RT	None	138.0				1.22			
5 Ca 51	RT	None	137.0				1.25			
5 Ca 52	RT	None	137.0				1.25			
5 Ca 53	RT	None	136.0				1.25			
Arith. Mean				137.00				1.24		
Std. Deviation				0.71				0.01		
5 Ca 55	30°R	None	205.0				0.98			
5 Ca 57	30°R	None	181.0				0.89			
5 Ca 60	30°R	None	183.0				0.92			
5 Ca 61	30°R	None	176.0				0.91			
5 Ca 62	30°R	None	203.0				1.00			
Arith. Mean				189.60	+52.6	+41.4		0.94	- 0.30	- 0.26
Std. Deviation				13.41		+63.8		0.05		- 0.34
(q)	30°R	10^{17}								
(q)	30°R	10^{17}								
(q)	30°R	10^{17}								
Arith. Mean										
Std. Deviation										

TABLE B 32 b

TEST RESULTS, A 353 STEEL (NORMALIZED)

F_{ty}/F_{tu}	Elongation (%)	Reduction of Area (%)	Fracture Stress (ksi)	Total Fast Flux[a] (nvt)	Test Temp	Specimen Number
				TENSILE TESTS		
0.79	27	70	(e)	None	RT	5 Ca 1
0.81	23	66	(e)	None	RT	5 Ca 2
0.81	24	70	(e)	None	RT	5 Ca 3
0.80	28	71	(e)	None	RT	5 Ca 4
0.79	24	70	(e)	None	RT	5 Ca 5
0.800	25.2	69.4	(e)	. . . . .	Arith. Mean	
0.82	19	44	(e)	None	30°R	5 Ca 7
0.85	17	46	(e)	None	30°R	5 Ca 8
0.83	22	49	(e)	None	30°R	5 Ca 9
0.94	23	52	(e)	None	30°R	5 Ca 10
0.90	9	7	(e)	None	30°R	5 Ca 11
0.868	18.0	39.6	(e)	. . . . .	Arith. Mean	
0.88	16	20	255.0	10^{17}	30°R	5 Ca 29
0.88	12	9	241.0	10^{17}	30°R	5 Ca 36
0.89	19	35	285.0	10^{17}	30°R	5 Ca 45
0.883	15.7	21.3	260.3	. . . . .	Arith. Mean	

(e). not recorded

(q). test deleted from screening program

(a). of neutrons with >.5 mev energy

(b). change in mean of test value with respect to previous test condition

(c). with 90% confidence

TABLE B 33 a

TEST RESULTS, 440 C STAINLESS STEEL (QUENCHED & DRAWN)

Specimen Number	Test Temp	Total Fast Flux[a] (nvt)	F_{tu} (ksi) Test Value		Bias[b]	Bias Range[c]	F_{ty} (ksi) Test Value		Bias[b]	Bias Range[c]
TENSILE TESTS										
9 Ca 1	RT	None	320.0				275.0			
9 Ca 2	RT	None	323.0				274.0			
9 Ca 7	RT	None	329.0				302.0			
9 Ca 8	RT	None	304.0				256.0			
9 Ca 13	RT	None	303.0				242.0			
Arith. Mean				315.80				269.80		
Std. Deviation				11.69				22.61		
9 Ca 11	30°R	None	285.0				(g)			
9 Ca 12	30°R	None	251.0				(g)			
9 Ca 16	30°R	None	279.0				(g)			
9 Ca 20	30°R	None	242.0				(g)			
9 Ca 21	30°R	None	249.0				(g)			
Arith. Mean				261.20	- 54.6	- 35.8		(g)		
Std. Deviation				19.40		- 73.4				
9 Ca 18	30°R	10^{17}	234.0				(g)			
9 Ca 19	30°R	10^{17}	221.0				(g)			
9 Ca 23	30°R	10^{17}	198.0				(g)			
Arith. Mean				217.70	- 43.5	- 17.0		(g)		
Std. Deviation				18.23		- 70.0				
TENSILE NOTCH TESTS			F_{tun} (ksi)				F_{tun}/F_{tu}			
9 Ca 33	RT	None	218.0				0.68			
9 Ca 34	RT	None	223.0				0.69			
9 Ca 36	RT	None	222.0				0.67			
9 Ca 38	RT	None	211.0				0.69			
9 Ca 41	RT	None	213.0				0.70			
Arith. Mean				217.40				0.69		
Std. Deviation				5.32				0.01		
9 Ca 25	30°R	None	103.0				0.36			
9 Ca 26	30°R	None	93.5				0.37			
9 Ca 28	30°R	None	130.0				0.47			
9 Ca 29	30°R	None	114.0				0.47			
9 Ca 43	30°R	None	98.1				0.39			
Arith. Mean				107.70	-109.7	- 96.8		0.41	-0.27	-0.23
Std. Deviation				14.60		-122.6		0.05		-0.32
9 Ca 27	30°R	10^{17}	137.0				0.59			
9 Ca 31	30°R	10^{17}	112.0				0.51			
9 Ca 35	30°R	10^{17}	107.0				0.54			
Arith. Mean				118.70	+ 11.0	- 11.0		0.55	+0.14	+0.07
Std. Deviation				16.07		+ 33.0		0.04		+0.20

TABLE B 33 b

TEST RESULTS, 440 C STAINLESS STEEL (QUENCHED & DRAWN)

F_{ty}/F_{tu}	Elongation (%)	Reduction of Area (%)	Fracture Stress (ksi)	Total Fast Flux[a] (nvt)	Test Temp	Specimen Number
				TENSILE TESTS		
0.86	nil	nil	320.0	None	RT	9 Ca 1
0.85	nil	nil	323.0	None	RT	9 Ca 2
0.92	nil	nil	329.0	None	RT	9 Ca 7
0.84	nil	nil	304.0	None	RT	9 Ca 8
0.80	nil	nil	303.0	None	RT	9 Ca 13
0.854	nil	nil	315.8	. . . . .	Arith. Mean	
(g)	nil	nil	285.0	None	30°R	9 Ca 11
(g)	nil	nil	251.0	None	30°R	9 Ca 12
(g)	nil	nil	279.0	None	30°R	9 Ca 16
(g)	nil	nil	242.0	None	30°R	9 Ca 20
(g)	nil	nil	249.0	None	30°R	9 Ca 21
(g)	nil	nil	261.2	. . . . .	Arith. Mean	
(g)	nil	nil	234.0	10^{17}	30°R	9 Ca 18
(g)	nil	nil	221.0	10^{17}	30°R	9 Ca 19
(g)	nil	nil	198.0	10^{17}	30°R	9 Ca 23
(g)	nil	nil	217.7	. . . . .	Arith. Mean	

(g). failed at less than .2% plastic strain

(a). of neutrons with >.5 mev energy

(b). change in mean of test value with respect to previous test condition

(c). with 90% confidence

TABLE B 34

APPROXIMATE MODULUS VALUES* FOR 33 MATERIALS
(Ksi x 10^{-3})

ALLOY	TEST CONDITION			ALLOY	TEST CONDITION		
	RT	OP 30°R	IP 30°R		RT	OP 30°R	IP 30°R
ALUMINUM ALLOYS							
1099	9	11	**	6061	10	11	11
2014	11	11	11	7079	10	12	11
2024	10	10	13	7178	10	11	12
2219	9	10	10	X-250	9	11	12
5083	10	12	(f)	B-750	11	11	12
5086	10	12	12	A356	11	9	11
5456	10	11	12				
TITANIUM ALLOYS							
55A	14	18	18	+6 Al, 4 V	15	17	**
+5 Al, 2.5 Sn	15	18	18	+6 Al, 4 V (t)	16	18	20
+5 Al, 2.5 Sn (s)	15	**	18	+8 Al, 1 Mo, 1 V	16	18	**
NICKEL ALLOYS							
René 41	28	32	34	Inconel	25	32	32
K Monel	24	27	28	Inconel X	32	34	34
FERROUS ALLOYS							
304	28	32	29	T-450	27	29	29
310	30	30	33	AM-350	29	32	31
347	26	30	29	17-7 PH	28	29	25
A 286 (u)	30	31	32	A-353	29	27	29
A 286 (v)	30	30	**	440C	30	33	30

* for qualitative comparison only, extensometer installation does not meet ASTM requirements for modulii determinations

** nondeterminable

(f) screening program ended before completion of this test
(s) extra low interstitial content
(t) aged
(u) AMS 5735
(v) AMS 5737

APPENDIX C

PHOTOMICROGRAPHS OF SPECIMENS

The sets of photomicrographs taken in conjunction with the screening test program under Contract NASw-114 are herein presented as Figures C 1 through C 33.

A complete set of photomicrographs shows the following conditions:

1. As received material; longitudinal section

2. As received material; transverse section

3. Failed tensile specimen; room temperature test, longitudinal section at gage mark

4. Failed tensile specimen; room temperature test, longitudinal section at fracture

5. Failed tensile specimen; 30°R, unirradiated, longitudinal section at gage mark

6. Failed tensile specimen; 30°R, unirradiated, longitudinal section at fracture

7. Failed tensile specimen; 30°R, 1×10^{17} nvt, longitudinal section at gage mark

8. Failed tensile specimen; 30°R, 1×10^{17} nvt, longitudinal section at fracture

In instances where the structure at the gage mark was as would be predicted from the structure at the fracture, numbers 3, 5 or 7 are omitted from this Appendix.

Pedigree data photomicrographs of the as received condition were not available for several alloys at the time of publication.

Photomicrographs of Aluminum Alloy 6061 T-6 and Titanium Alloy 8-1-1 after testing at 30°R, unirradiated, were also unavailable.

Aluminum Alloy 5083 was not tested after irradiation.

Comments on the structures shown in these figures are given in the discussion in Section 6 of the body of this report.

In some instances, apparent variation in specimen structures after irradiation in surface preparation technique differences between remote and direct handling methods.

MATERIAL PEDIGREE SAMPLES

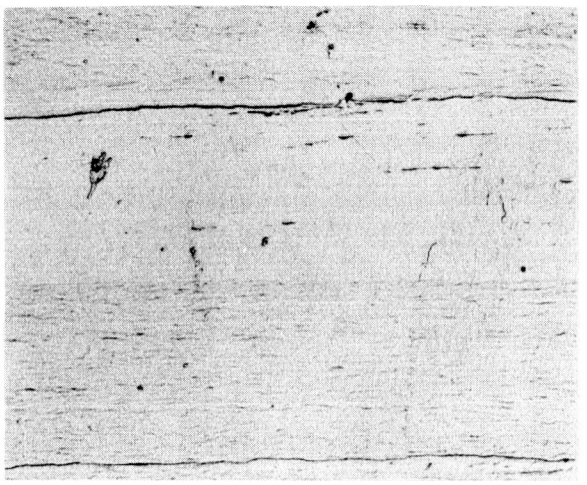

As Received - Longitudinal Section
X 100 Polarized Light

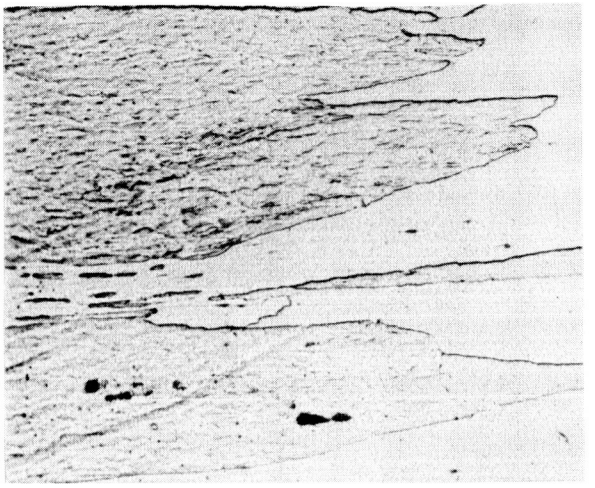

As Received - Transverse Section
X 100 Polarized Light

FAILED TENSILE SPECIMENS
ROOM TEMPERATURE TEST

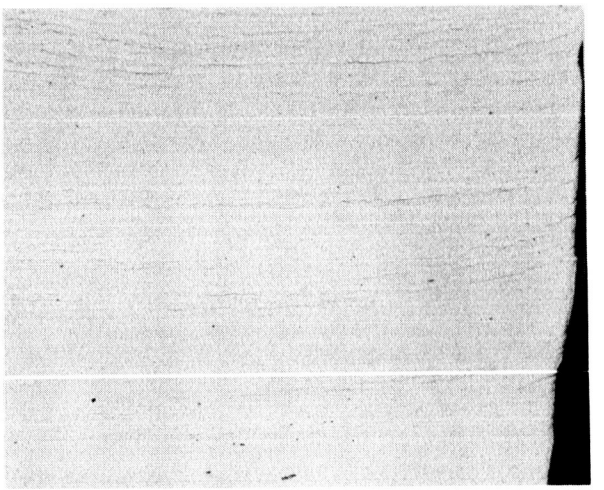

Longitudinal Section at Fracture
250 X Keller's Etch

FIGURE C 1 a PHOTOMICROGRAPHS OF ALUMINUM 1099 (H-14)

FAILED TENSILE SPECIMEN
30°R, UNIRRADIATED TEST

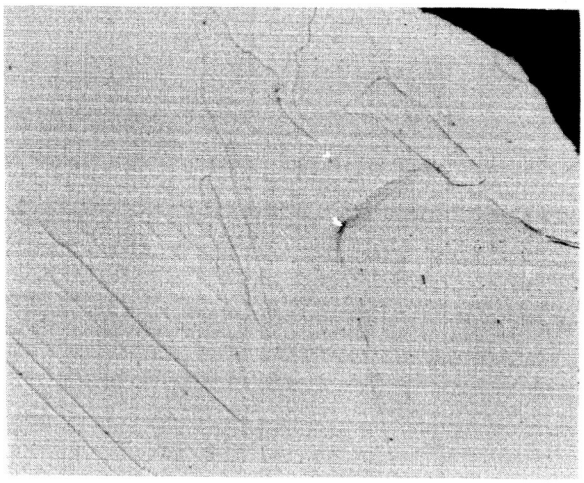

Longitudinal Section at Fracture
X 250 Keller's Etch

FAILED TENSILE SPECIMEN
30°R, 1×10^{17}nvt TEST

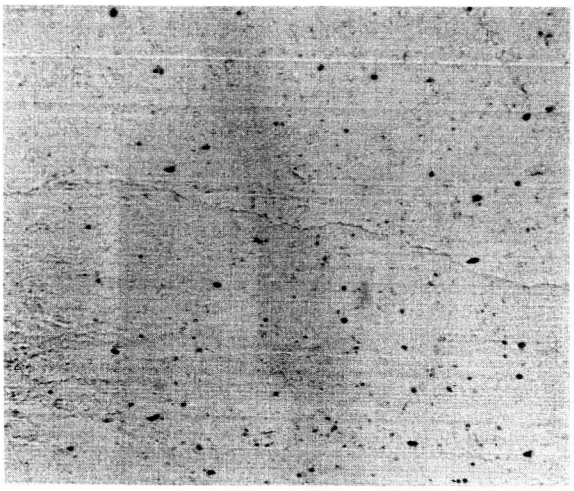

Longitudinal Section at Gage Mark
X 250 Keller's Etch

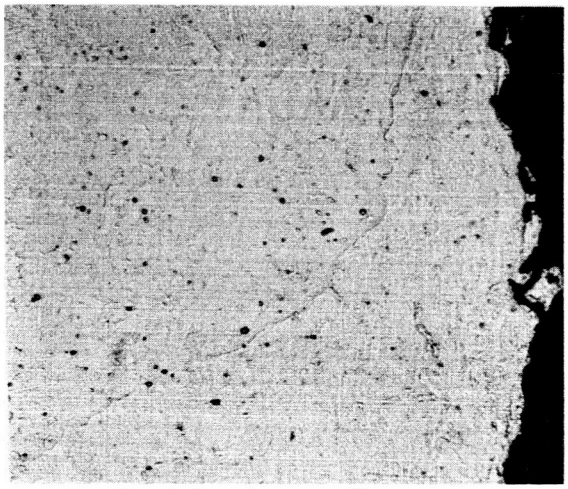

Longitudinal Section at Fracture
X 250 Keller's Etch

FIGURE C 1 b PHOTOMICROGRAPHS OF ALUMINUM 1099 (H-14)

MATERIAL PEDIGREE SAMPLE

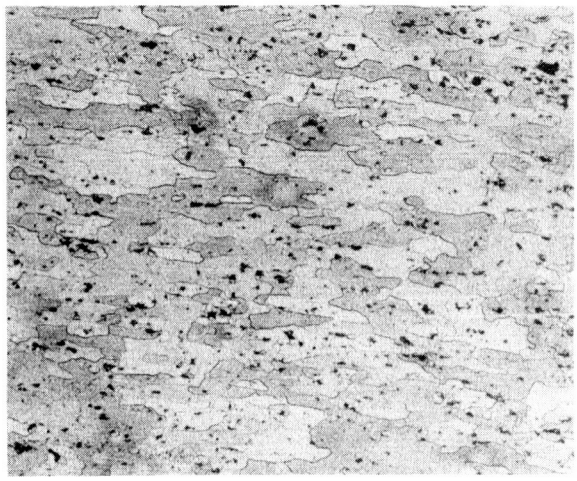

As Received - Transverse Section
X100 Keller's Etch

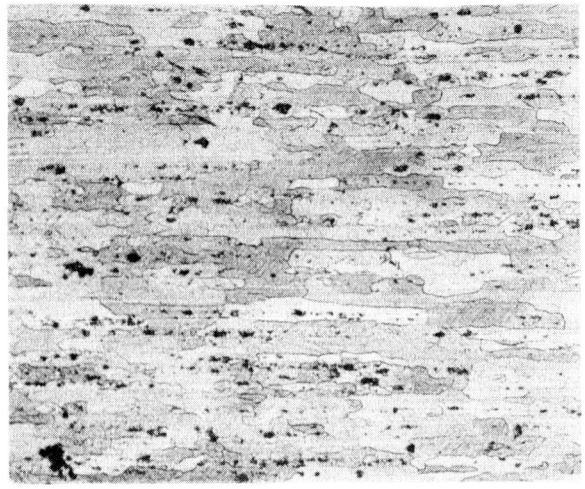

As Received - Longitudinal Section
X 100 Keller's Etch

FAILED TENSILE SPECIMEN
ROOM TEMPERATURE TEST

Longitudinal Section at Fracture
X250 Keller's Etch

FIGURE C 2 a PHOTOMICROGRAPHS OF ALUMINUM 2014 (T-651)

FAILED TENSILE SPECIMEN
30°R, UNIRRADIATED TEST

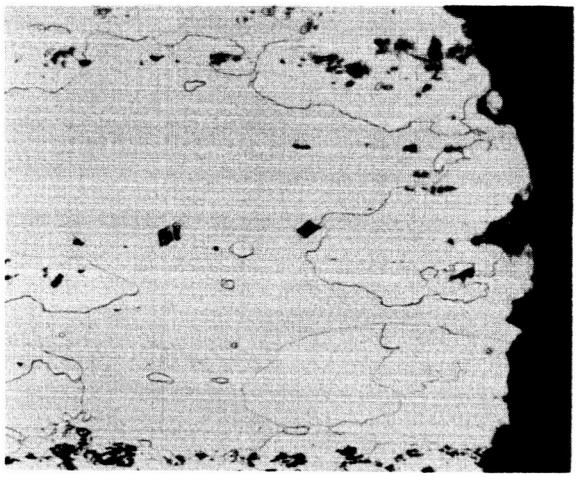

Longitudinal Section at Fracture
X 250 Keller's Etch

FAILED TENSILE SPECIMEN
30°R, 1×10^{17}nvt, TEST

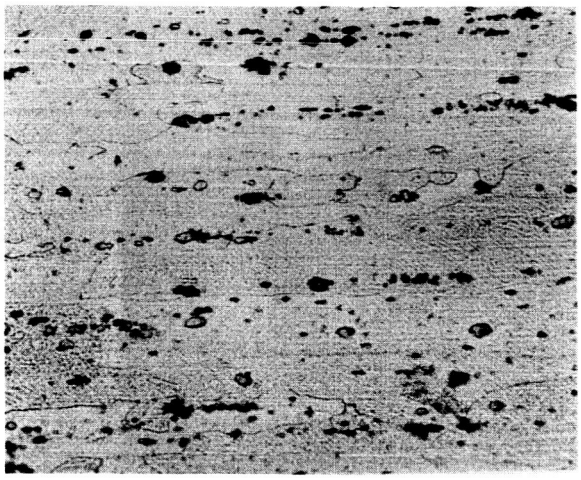

Longitudinal Section at Gage Mark
X 250 Keller's Etch

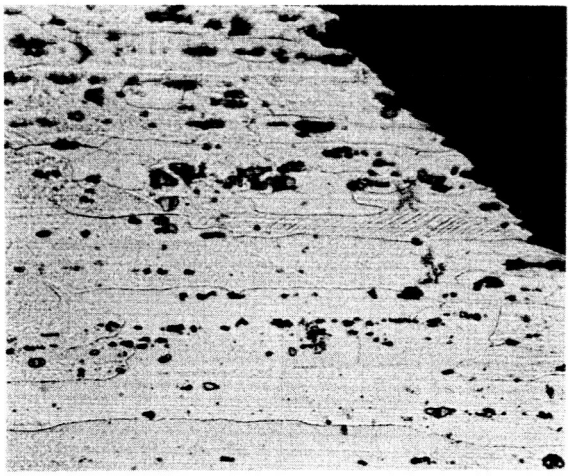

Longitudinal Section at Fracture
X250 Keller's Etch

FIGURE C 2 b PHOTOMICROGRAPHS OF ALUMINUM 2014 (T-651)

MATERIAL PEDIGREE SAMPLE

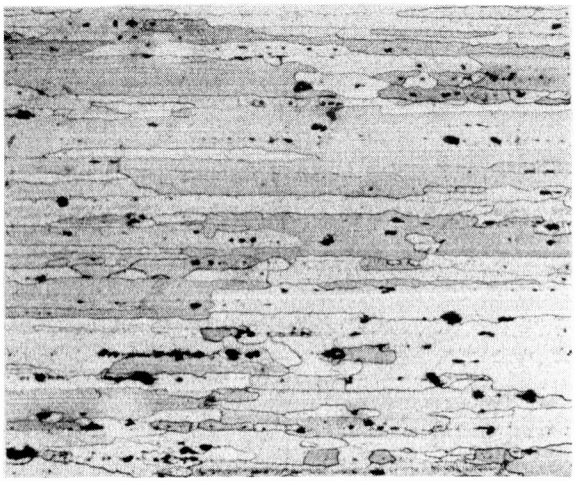

As Received - Longitudinal Section
X 100 Keller's Etch

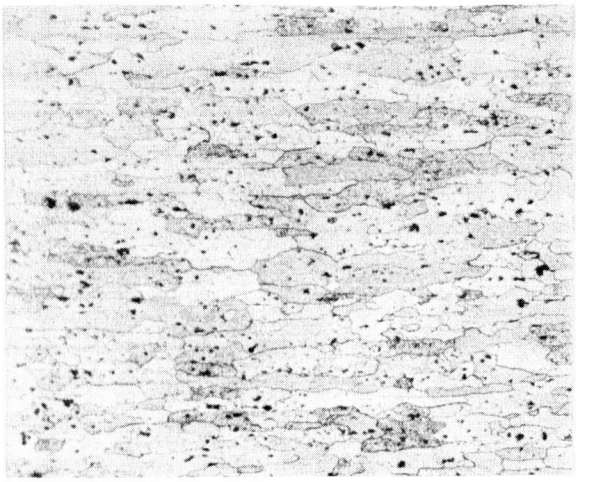

As Received - Transverse Section
X 100 Keller's Etch

FAILED TENSILE SPECIMEN
ROOM TEMPERATURE TEST

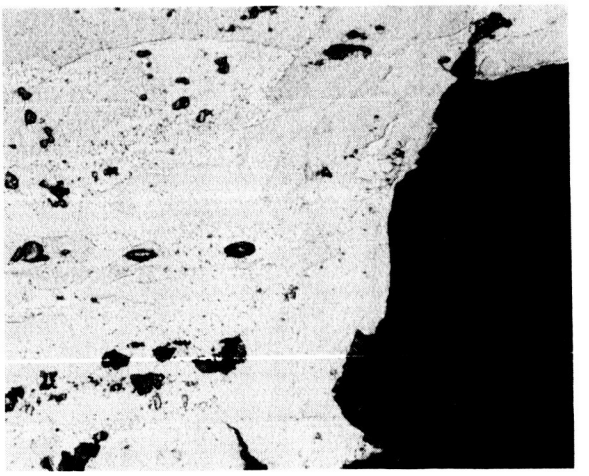

Longitudinal Section at Fracture
X 250 Keller's Etch

FIGURE C 3 a PHOTOMICROGRAPHS OF ALUMINUM 2024 (T-351)

FAILED TENSILE SPECIMEN
30°R, UNIRRADIATED TEST

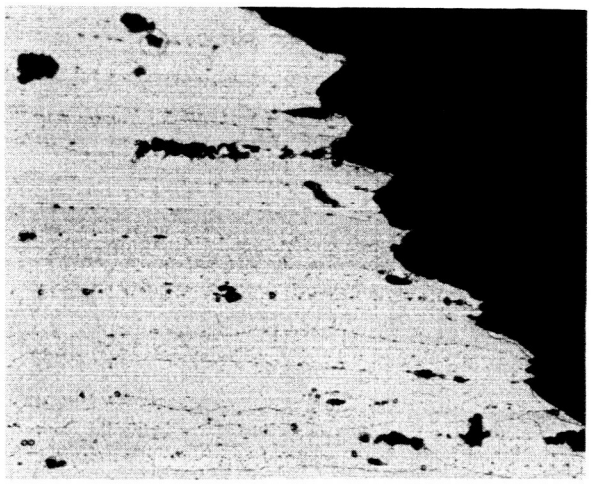

Longitudinal Section at Fracture
X 250 Keller's Etch

FAILED TENSILE SPECIMEN
30°R, 1×10^{17} nvt, TEST

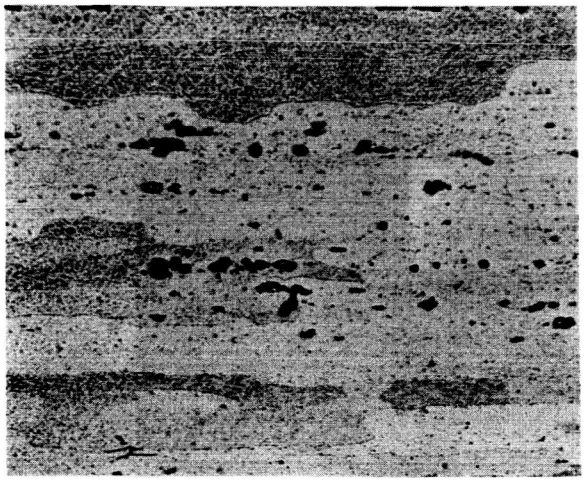

Longitudinal Section at Gage Mark
X 250 Keller's Etch

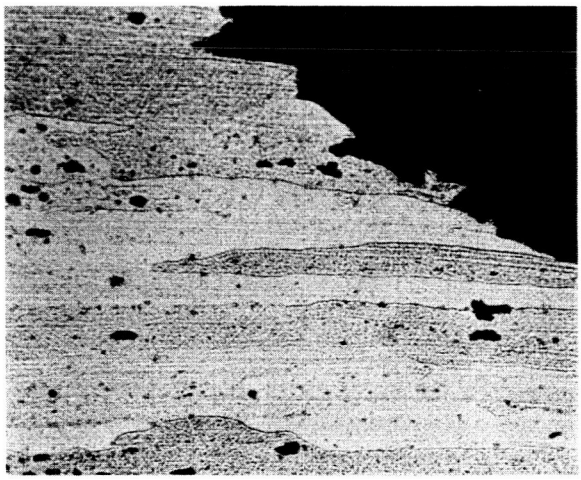

Longitudinal Section at Fracture
X 250 Keller's Etch

FIGURE C 3 b PHOTOMICROGRAPHS OF ALUMINUM 2024 (T-351)

MATERIAL PEDIGREE SAMPLE

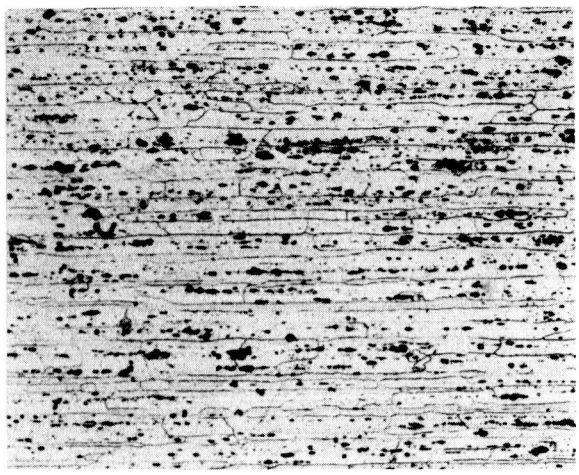

As Received - Longitudinal Section
X 100 Keller's Etch

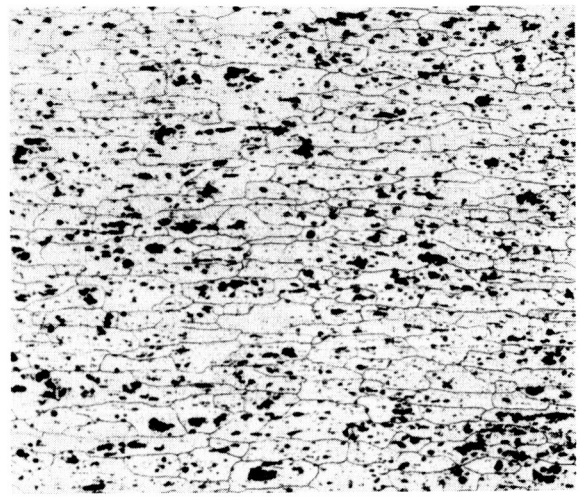

As Received - Transverse Section
X 100 Keller's Etch

FAILED TENSILE SPECIMEN
ROOM TEMPERATURE TEST

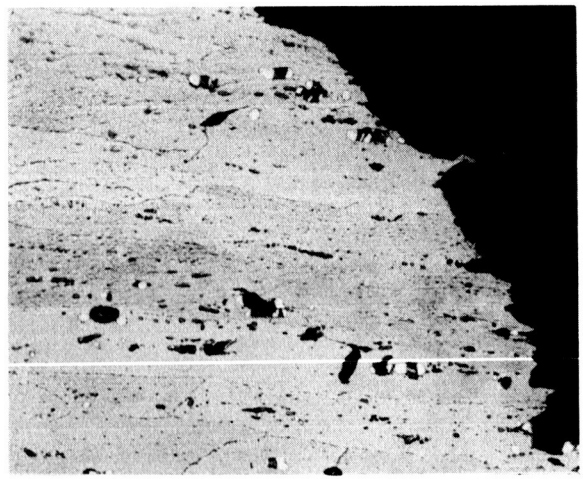

Longitudinal Section at Fracture
X 250 Keller's Etch

FIGURE C 4 a PHOTOMICROGRAPHS OF ALUMINUM 2219 (T87)

FAILED TENSILE SPECIMENS
30°R, UNIRRADIATED TEST

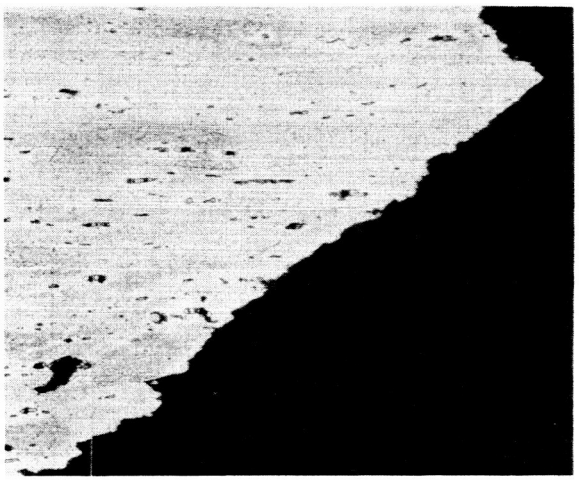

Longitudinal Section at Fracture
X 250 Keller's Etch

FAILED TENSILE SPECIMEN
30°R, 1×10^{17} nvt, TEST

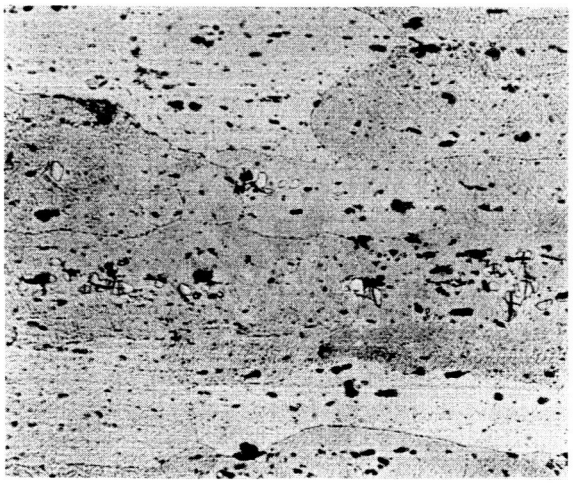

Longitudinal Section at Gage Mark
X 250 Keller's Etch

Longitudinal Section at Fracture
X 250 Keller's Etch

FIGURE C 4 b PHOTOMICROGRAPHS OF ALUMINUM 2219 (T87)

MATERIAL PEDIGREE SAMPLE

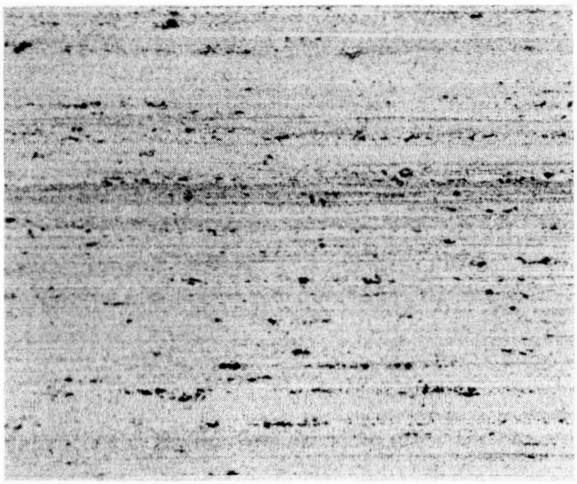

As Received - Longitudinal Section
X 100 Keller's Etch

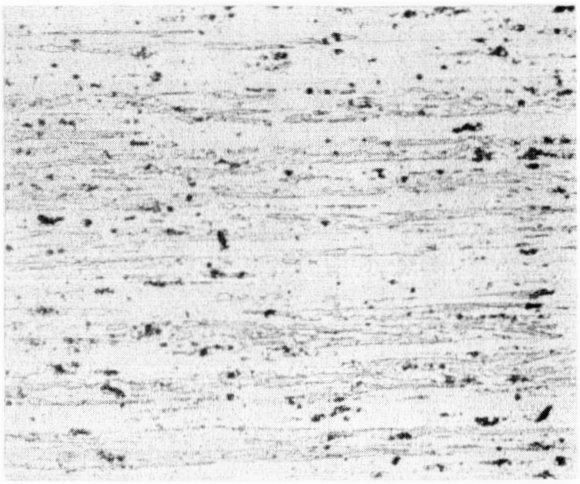

As Received - Transverse Section
X 100 Keller's Etch

FAILED TENSILE SPECIMEN
ROOM TEMPERATURE TEST

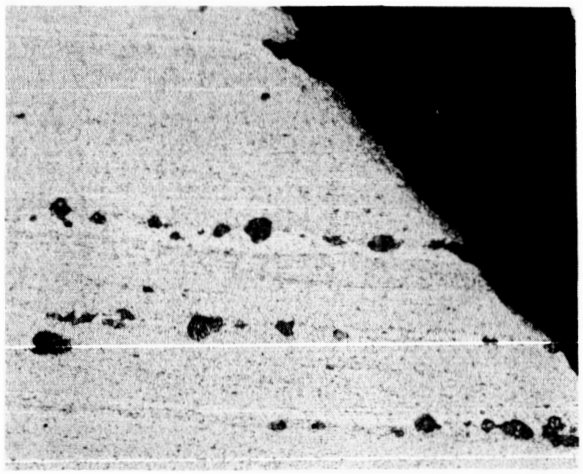

Longitudinal Section at Fracture
X 250 Keller's Etch

FIGURE C 5 a PHOTOMICROGRAPHS OF ALUMINUM 5083 (H-321)

FAILED TENSILE SPECIMENS
30°R, UNIRRADIATED TEST

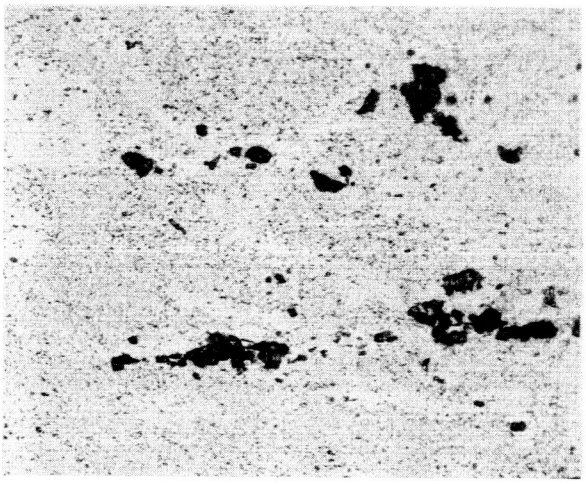

Longitudinal Section at Fracture
X 250 Keller's Etch

FAILED TENSILE SPECIMEN
30°R, 1×10^{17} nvt, TEST

Not Tested

After Irradiation

Not Tested

After Irradiation

FIGURE C 5 b PHOTOMICROGRAPHS OF ALUMINUM 5083 (H-321)

MATERIAL PEDIGREE SAMPLE

As Received - Longitudinal Section
X 250 25% HNO_3

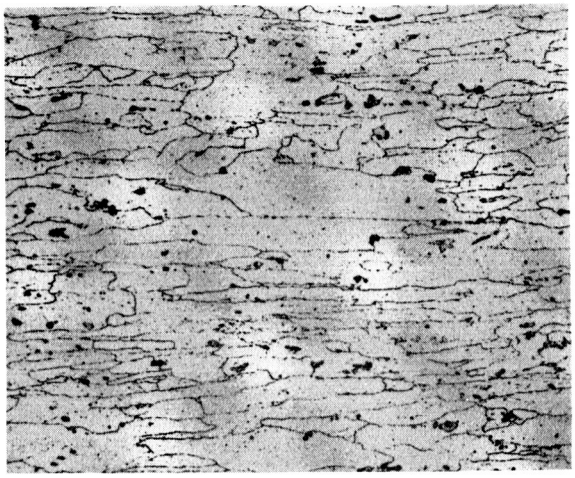

As Received - Transverse Section
X 250 25% HNO_3

FAILED TENSILE SPECIMEN
ROOM TEMPERATURE TEST

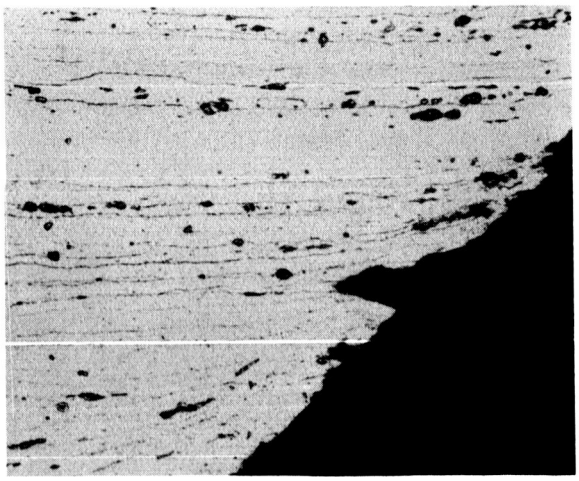

Longitudinal Section at Fracture
X 250 Keller's Etch

FIGURE C 6 a PHOTOMICROGRAPHS OF ALUMINUM 5086 (H-321)

FAILED TENSILE SPECIMENS
30°R, UNIRRADIATED TEST

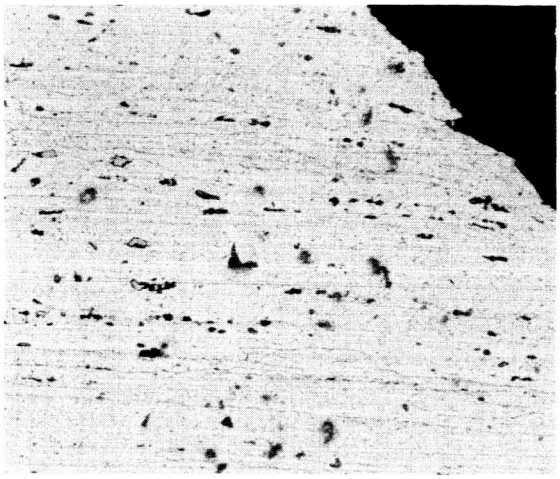

Longitudinal Section at Fracture
X 250 Keller's Etch

FAILED TENSILE SPECIMEN
30°R, 1×10^{17} nvt, TEST

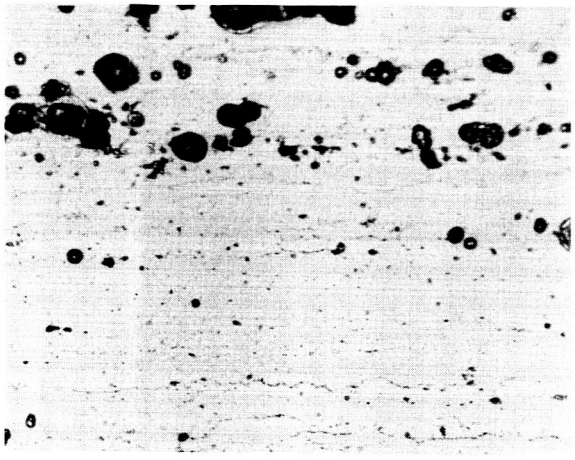

Longitudinal Section at Gage Mark
X 250 Keller's Etch

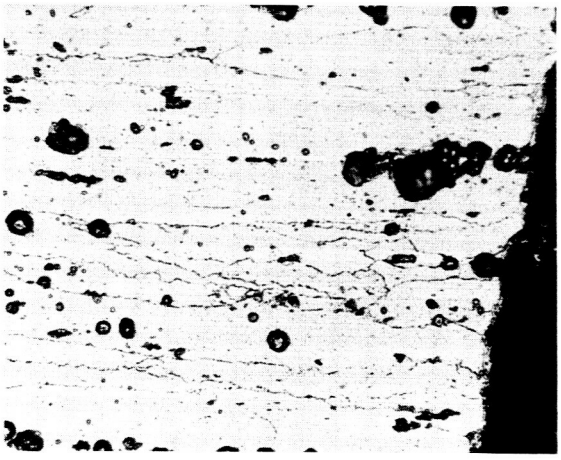

Longitudinal Section at Fracture
X 250 Keller's Etch

FIGURE C 6 b PHOTOMICROGRAPHS OF ALUMINUM 5086 (H-32)

MATERIAL PEDIGREE SAMPLE

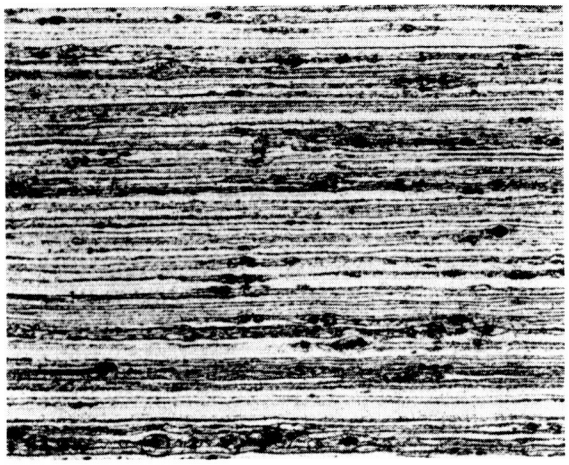

As Received - Longitudinal Section
X 100 Keller's Etch

As Received - Transverse Section
X 100 Keller's Etch

FAILED TENSILE SPECIMEN
ROOM TEMPERATURE TEST

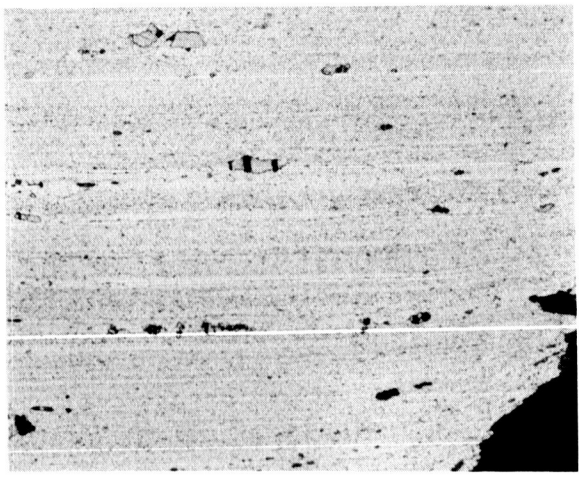

Longitudinal Section at Fracture
X 250 Keller's Etch

FIGURE C 7 a PHOTOMICROGRAPHS OF ALUMINUM 5456 (H-321)

FAILED TENSILE SPECIMENS
30°R, UNIRRADIATED TEST

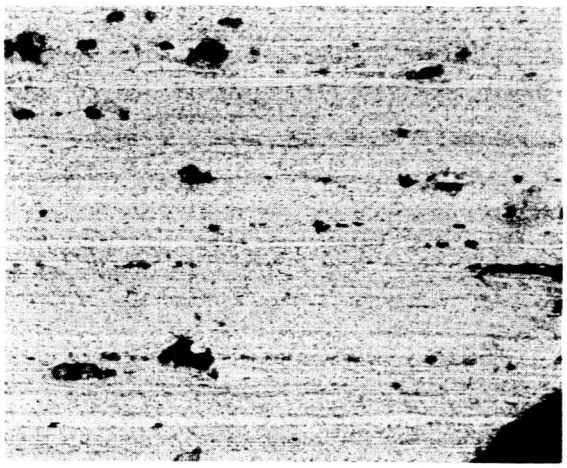

Longitudinal Section at Fracture
X 250 Keller's Etch

FAILED TENSILE SPECIMEN
30°R, 1×10^{17}nvt, TEST

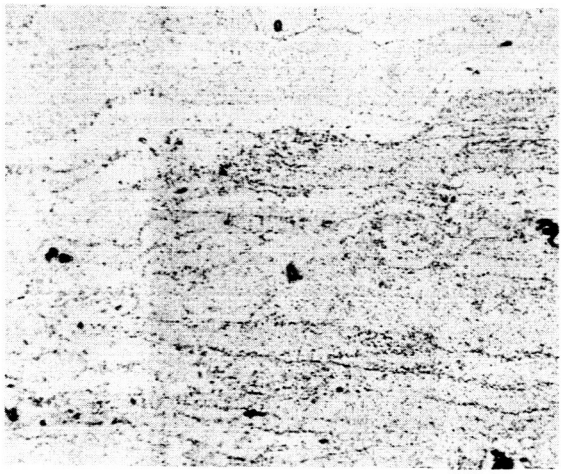

Longitudinal Section at Gage Mark
X 250 Keller's Etch

Longitudinal Section at Fracture
X 250 Keller's Etch

FIGURE C 7 b PHOTOMICROGRAPHS OF ALUMINUM 5456 (H-321)

MATERIAL PEDIGREE SAMPLE

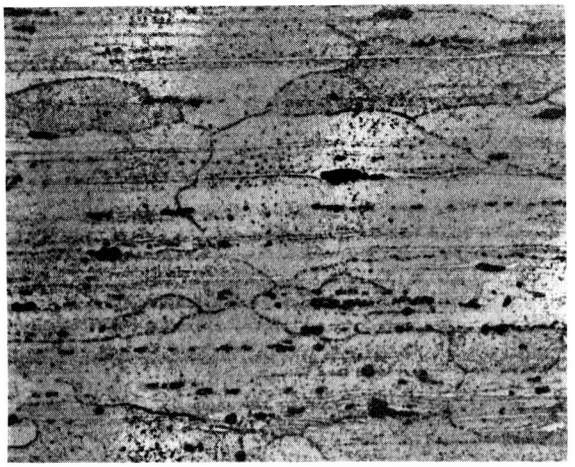

As Received - Longitudinal Section
X 250 0.5% HF

As Received - Transverse Section
X 250 0.5% HF

FAILED TENSILE SPECIMEN
ROOM TEMPERATURE TEST

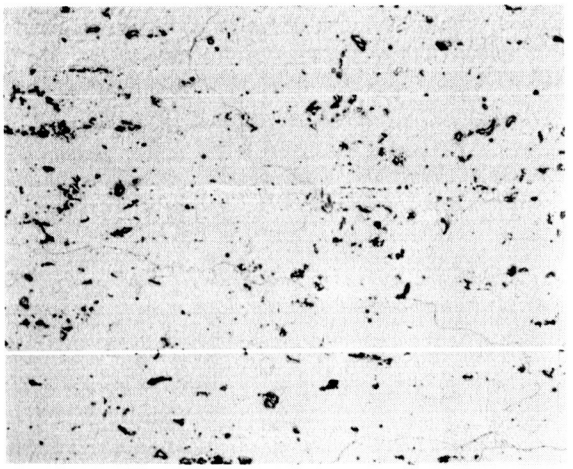

Longitudinal Section at Gage
X 250

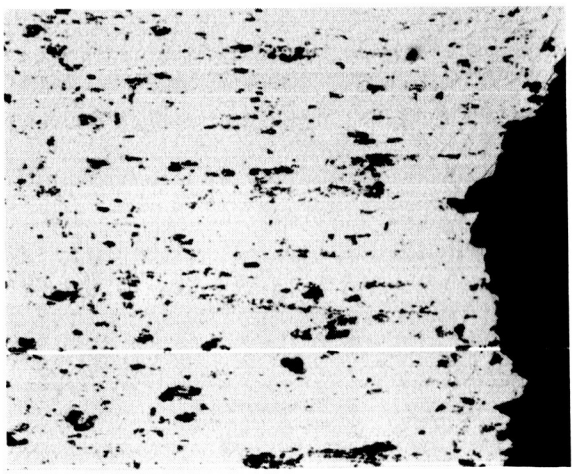

Longitudinal Section at Fracture
X 250 Keller's Etch

FIGURE C 8 a PHOTOMICROGRAPHS OF ALUMINUM 6061 (T-6)

FAILED TENSILE SPECIMENS
30°R, UNIRRADIATED TEST

FAILED TENSILE SPECIMEN
30°R, 1×10^{17} nvt, TEST

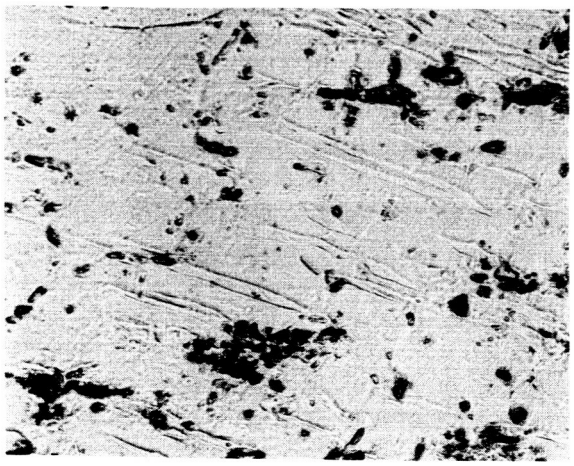

Longitudinal Section at Gage Mark
X 250 Keller's Etch

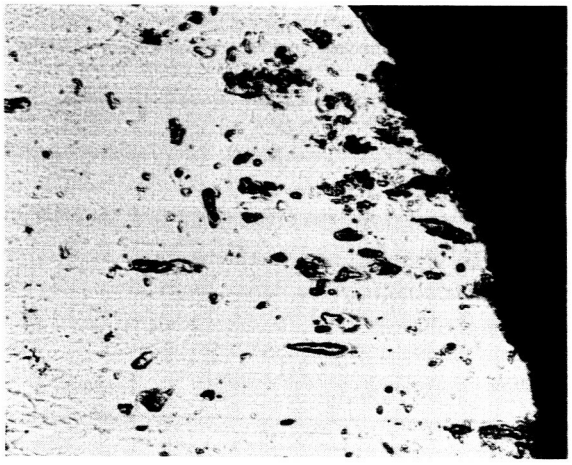

Longitudinal Section at Fracture
X 250 Keller's Etch

FIGURE C 8 b PHOTOMICROGRAPHS OF ALUMINUM 6061 (T-6)

MATERIAL PEDIGREE SAMPLE

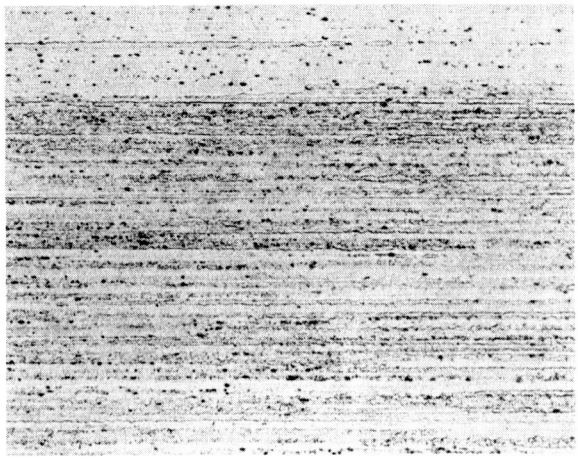

As Received - Longitudinal Section
X100 Keller's Etch

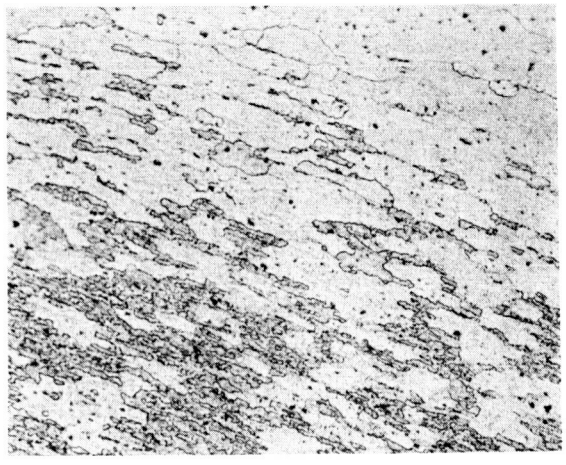

As Received - Transverse Section
X 100 Keller's Etch

FAILED TENSILE SPECIMEN
ROOM TEMPERATURE TEST

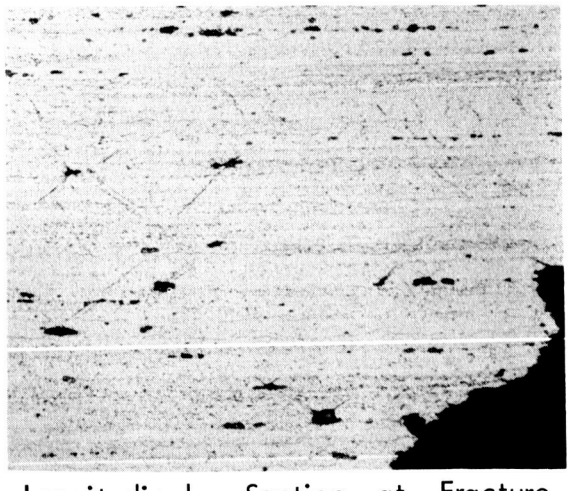

Longitudinal Section at Fracture
X 250 Keller's Etch

FIGURE C 9 a PHOTOMICROGRAPHS OF ALUMINUM 7079 (T-6)

FAILED TENSILE SPECIMENS
30°R, UNIRRADIATED TEST

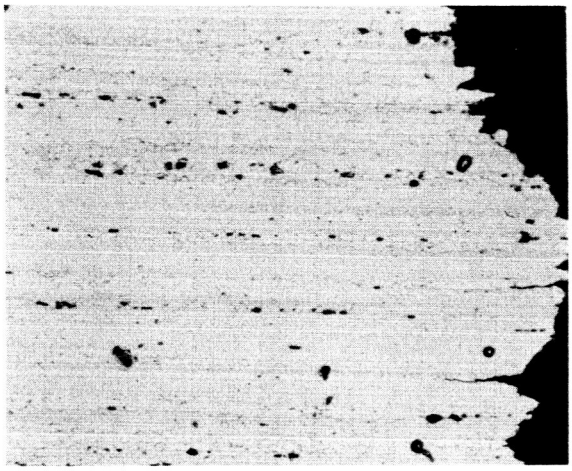

Longitudinal Section at Fracture
X 250 Keller's Etch

FAILED TENSILE SPECIMEN
30°R, 1×10^{17} nvt, TEST

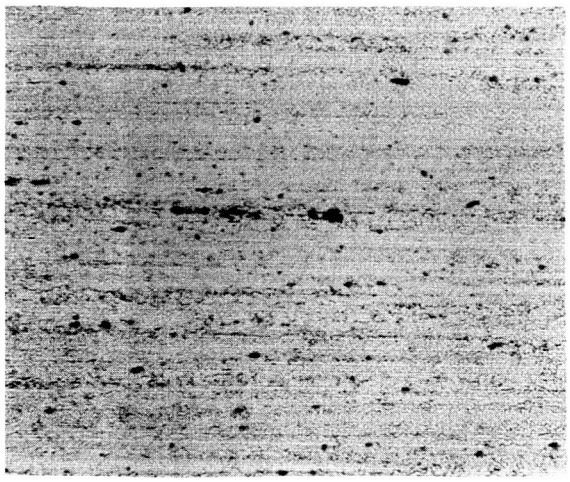

Longitudinal Section at Gage Mark
X 250 Keller's Etch

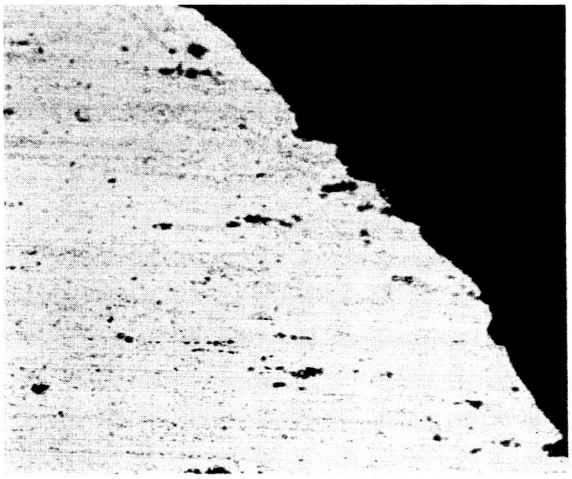

Longitudinal Section at Fracture
X 250 Keller's Etch

FIGURE C 9 b PHOTOMICROGRAPHS OF ALUMINUM 7079 (T-6)

MATERIAL PEDIGREE SAMPLE

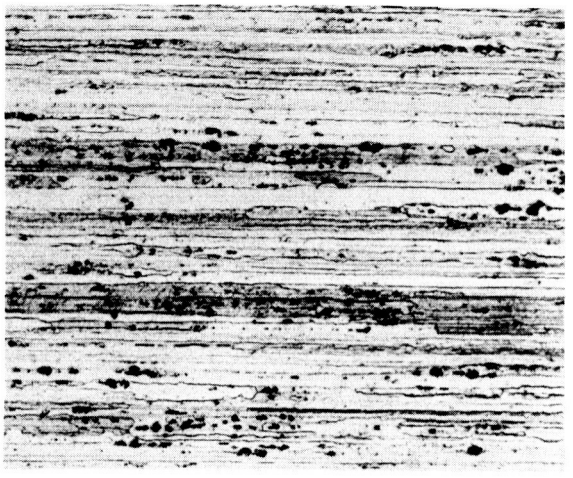

As Received - Longitudinal Section
X 100 Keller's Etch

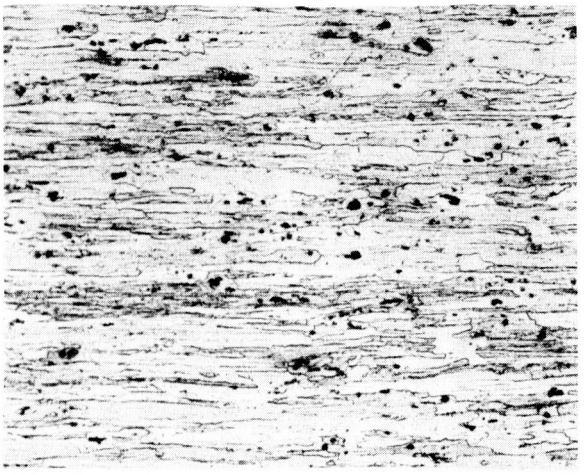

As Received - Transverse Section
X 100 Keller's Etch

FAILED TENSILE SPECIMEN
ROOM TEMPERATURE TEST

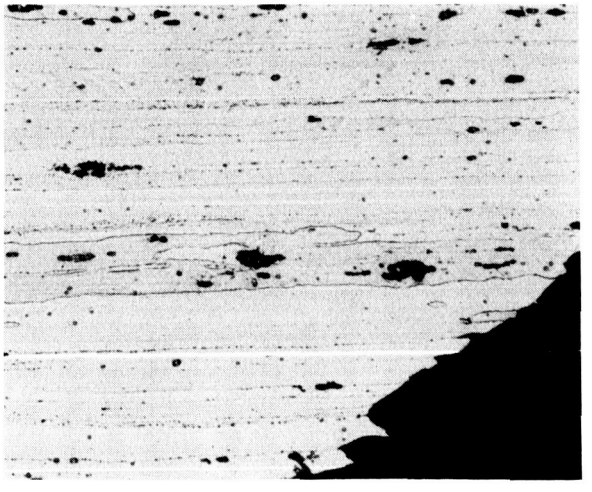

Longitudinal Section at Fracture
X 250 Keller's Etch

FIGURE C 10 a PHOTOMICROGRAPHS OF ALUMINUM 7178 (T-651)

FAILED TENSILE SPECIMENS
30°R, UNIRRADIATED TEST

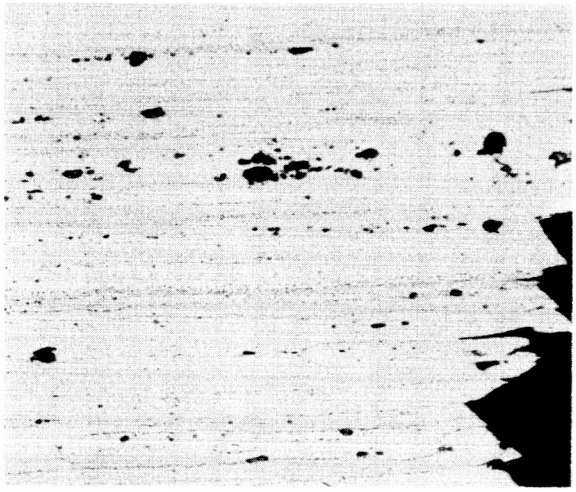

Longitudinal Section at Fracture
X 250 Keller's Etch

FAILED TENSILE SPECIMEN
30°R, 1×10^{17} nvt, TEST

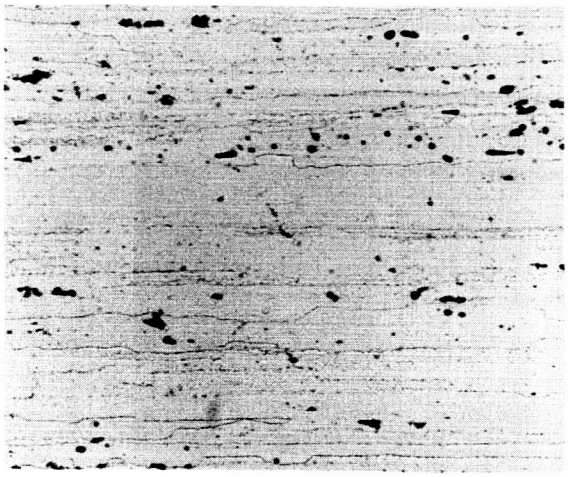

Longitudinal Section at Gage Mark
X 250 Keller's Etch

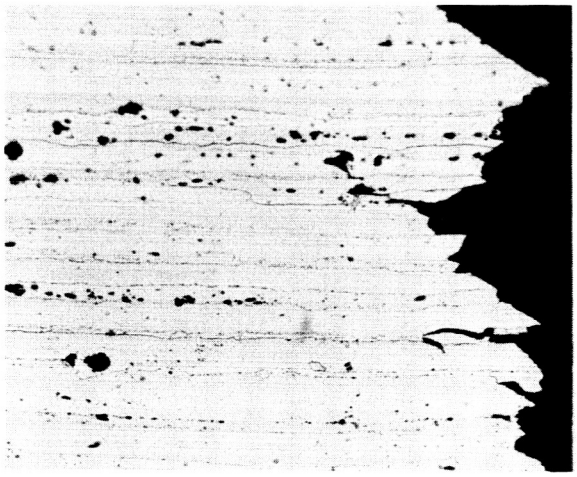

Longitudinal Section at Fracture
X 250 Keller's Etch

FIGURE C 10 b PHOTOMICROGRAPHS OF ALUMINUM 7178 (T-651)

MATERIAL PEDIGREE SAMPLE

As Received - X 100 Transverse Section Keller's Etch

FAILED TENSILE SPECIMEN
ROOM TEMPERATURE TEST

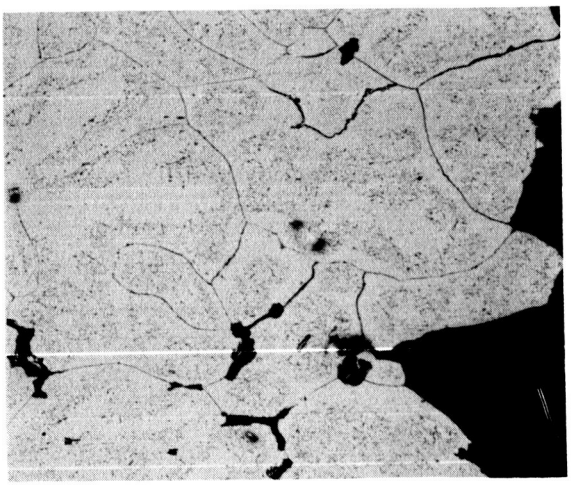

Longitudinal Section at Fracture X 250 Keller's Etch

FIGURE C 11 a PHOTOMICROGRAPHS OF ALUMINUM X 250 (T-4)

FAILED TENSILE SPECIMENS
30°R, UNIRRADIATED TEST

Longitudinal Section at Fracture
X 250 Keller's Etch

FAILED TENSILE SPECIMEN
30°R, 1×10^{17} nvt, TEST

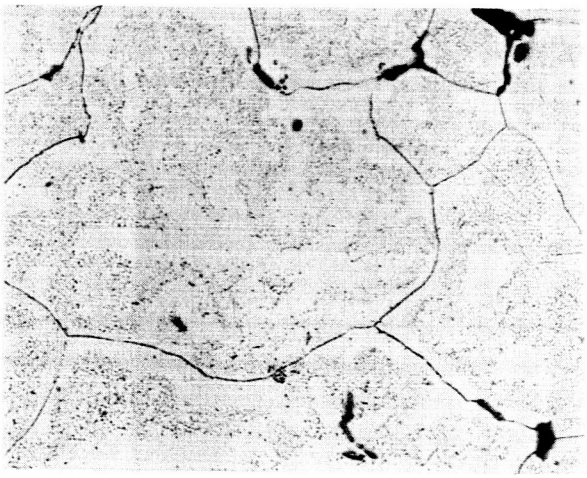

Longitudinal Section at Gage Mark
X 250 Keller's Etch

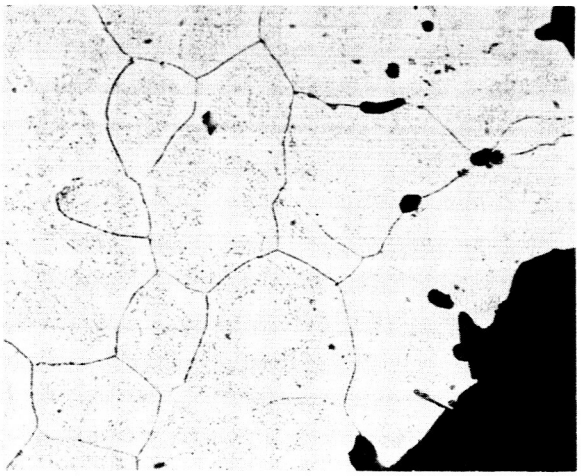

Longitudinal Section at Fracture
X 250 Keller's Etch

FIGURE C 11 b PHOTOMICROGRAPHS OF ALUMINUM X 250 (T-4)

MATERIAL PEDIGREE SAMPLE

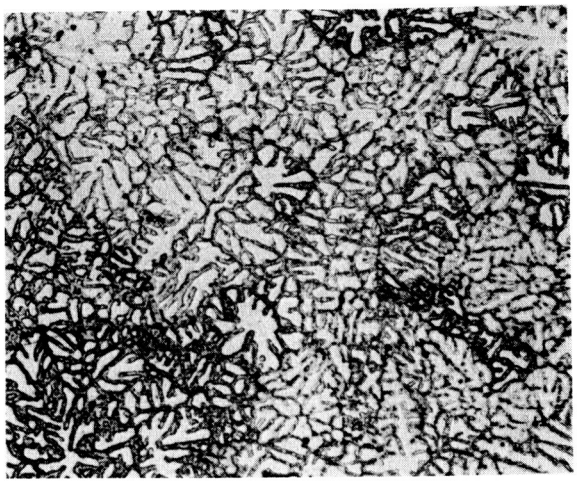

As Received - X 100 Transverse Section Keller's Etch

FAILED TENSILE SPECIMEN
ROOM TEMPERATURE TEST

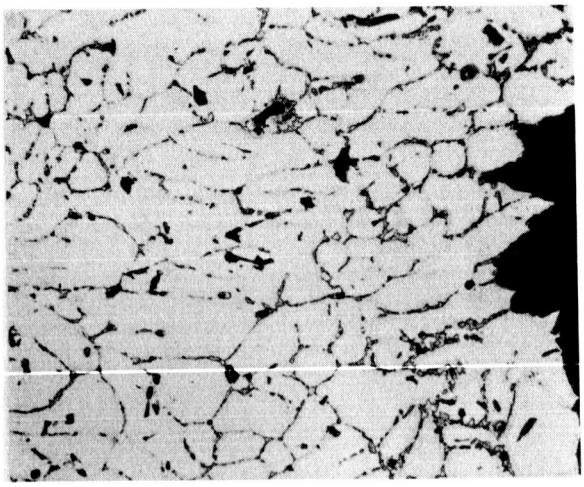

Longitudinal Section at Fracture X 250 Keller's Etch

FIGURE C 12 a PHOTOMICROGRAPHS OF ALUMINUM B-750 (T-5)

FAILED TENSILE SPECIMENS
30°R, UNIRRADIATED TEST

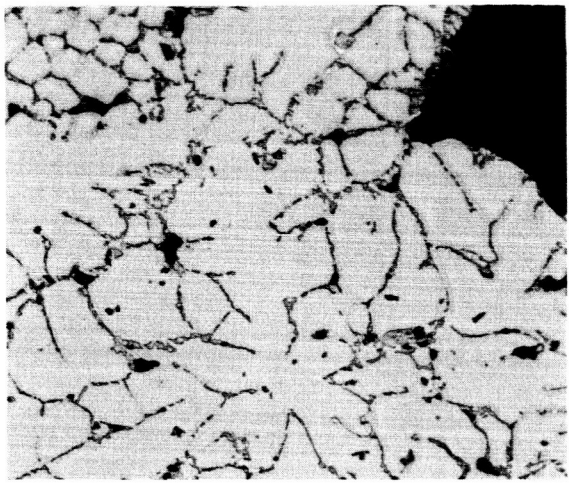

Longitudinal Section at Fracture
X 250 Keller's Etch

FAILED TENSILE SPECIMEN
30°R, 1×10^{17} nvt, TEST

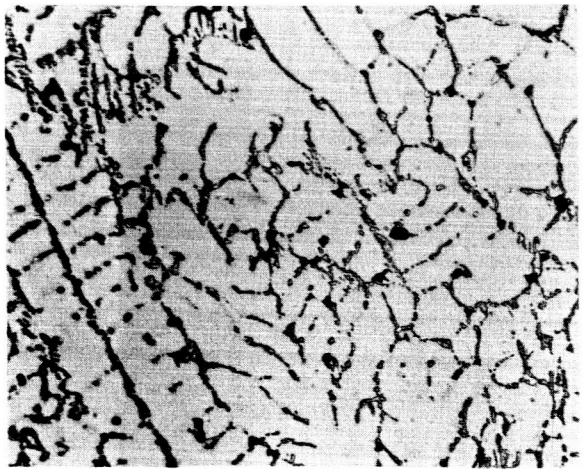

Longitudinal Section at Gage Mark
X 250 Keller's Etch

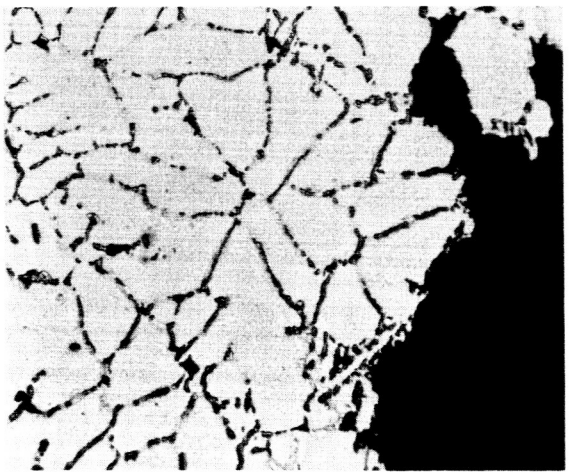

Longitudinal Section at Fracture
X 250 Keller's Etch

FIGURE C 12 b PHOTOMICROGRAPHS OF ALUMINUM B-750 (T-5)

MATERIAL PEDIGREE SAMPLE

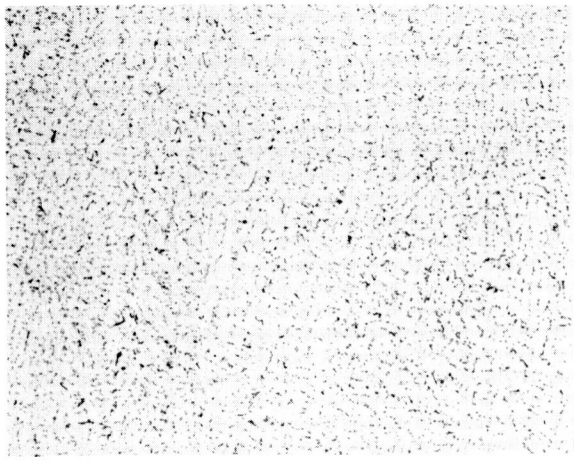

As Received - Longitudinal Section
X 100 Keller's Etch

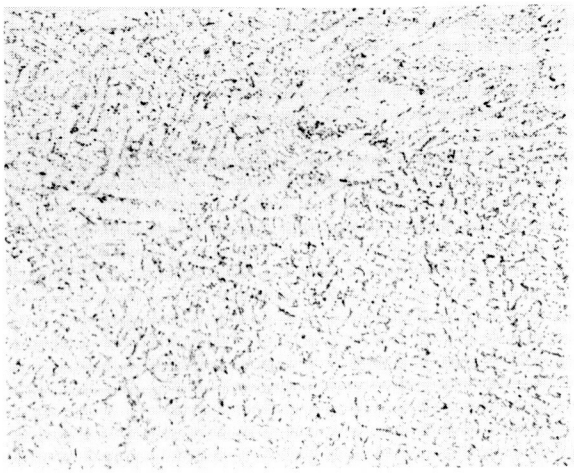

As Received - Transverse Section
X 100 Keller's Etch

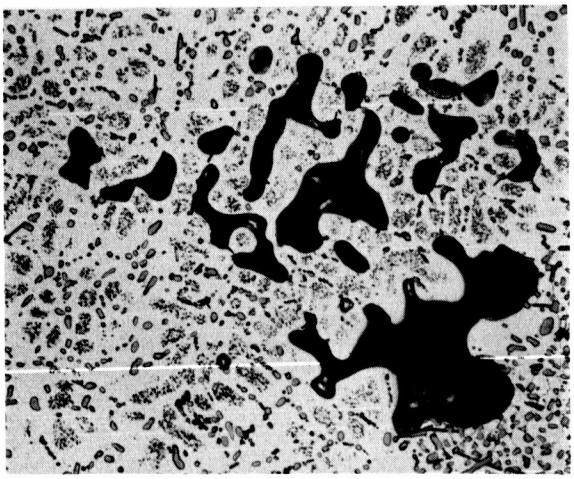

Longitudinal Section at Gage
X 250 Keller's Etch

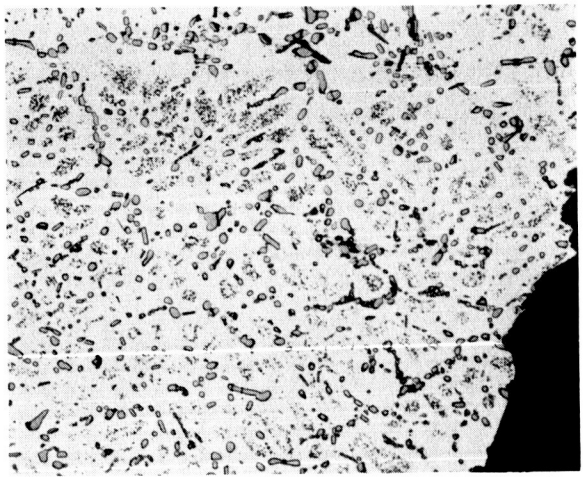

Longitudinal Section at Fracture
Keller's Etch

FIGURE C 13 a PHOTOMICROGRAPHS OF ALUMINUM A 356 (T-61)

FAILED TENSILE SPECIMENS
30°R, UNIRRADIATED TEST

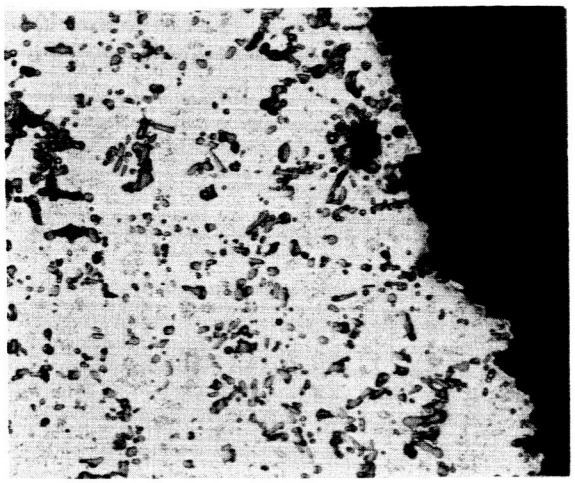

Longitudinal Section at Fracture
X 250 Keller's Etch

FAILED TENSILE SPECIMEN
30°R, 1×10^{17} nvt, TEST

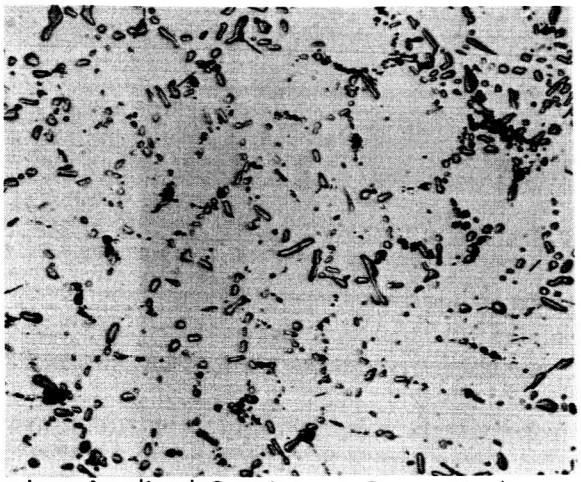

Longitudinal Section at Gage Mark
X 250 Keller's Etch

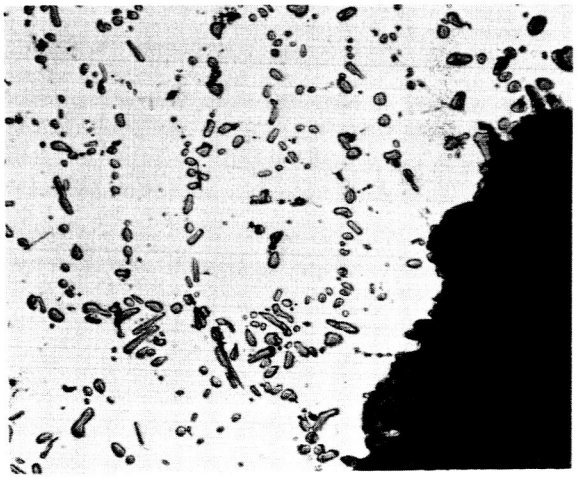

Longitudinal Section at Fracture
X 250 Keller's Etch

FIGURE C 13 b PHOTOMICROGRAPHS OF ALUMINUM A 356 (T-61)

MATERIAL PEDIGREE SAMPLES

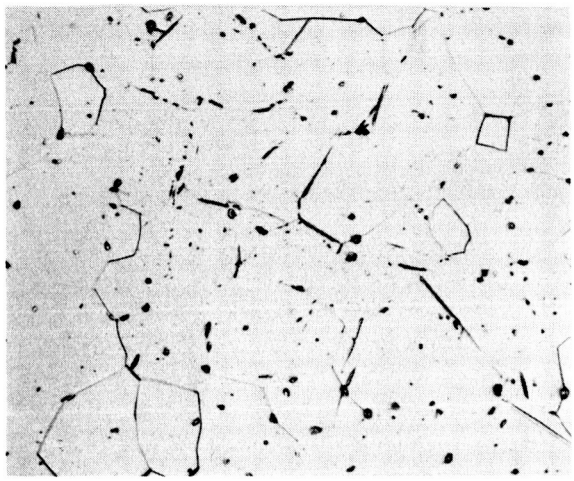

As Received - Longitudinal Section
X 500 Kroll Etch

FAILED TENSILE SPECIMEN
ROOM TEMPERATURE TEST

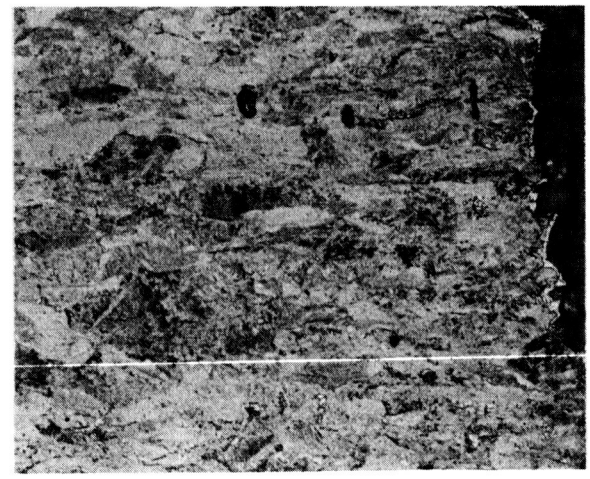

Longitudinal Section at Fracture
X 250 Mixed Acid Etch

FIGURE C 14 a PHOTOMICROGRAPHS OF TITANIUM 55A (ANNEALED)

FAILED TENSILE SPECIMEN
30°R, UNIRRADIATED TEST

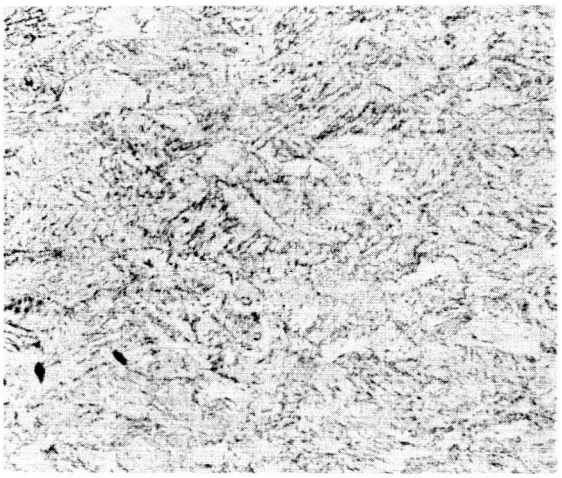

Longitudinal Section at Gage Mark
X 250

FAILED TENSILE SPECIMEN
30°R, 1×10^{17} nvt, TEST

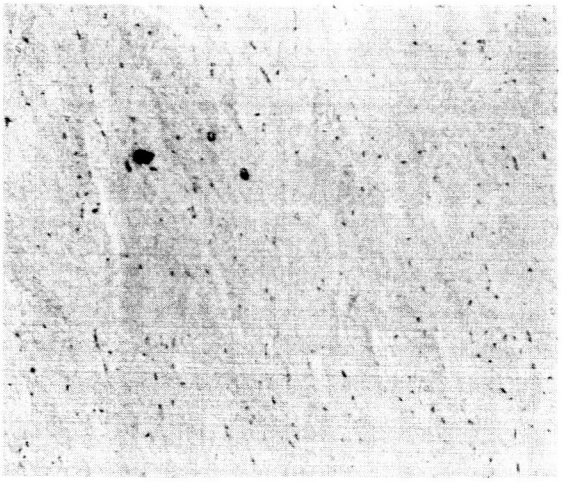

Longitudinal Section at Gage Mark
X250

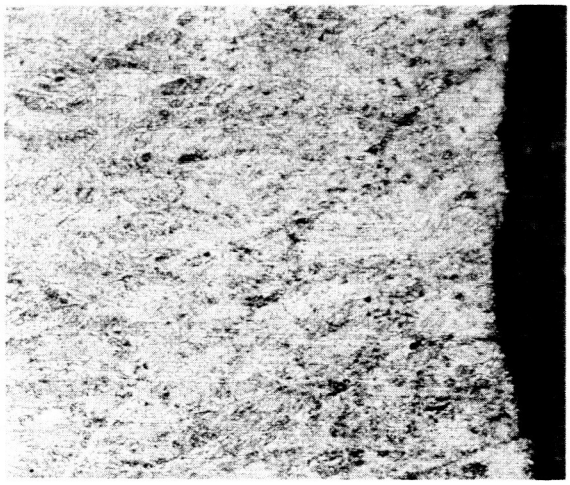

Longitudinal Section at Fracture
X250

FIGURE C 14 b PHOTOMICROGRAPHS OF TITANIUM 55A (ANNEALED)

MATERIAL PEDIGREE SAMPLES

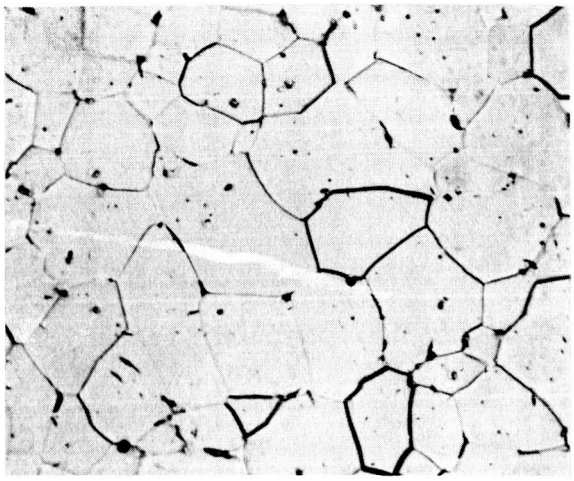

As Received - Longitudinal Section
X 500 Kroll Etch

FAILED TENSILE SPECIMENS
ROOM TEMPERATURE TEST

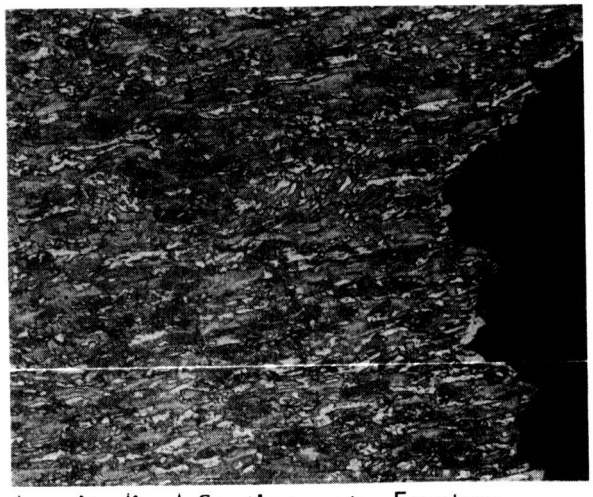

Longitudinal Section at Fracture
X 250

FIGURE C 15 a PHOTOMICROGRAPHS OF TITANIUM-5 AL-2.5 SN (ANNEALED)

FAILED TENSILE SPECIMEN
30°R, UNIRRADIATED TEST

Longitudinal Section at Fracture
X 250 Mixed Acid Etch

FAILED TENSILE SPECIMEN
30°R, 1×10^{17} nvt, TEST

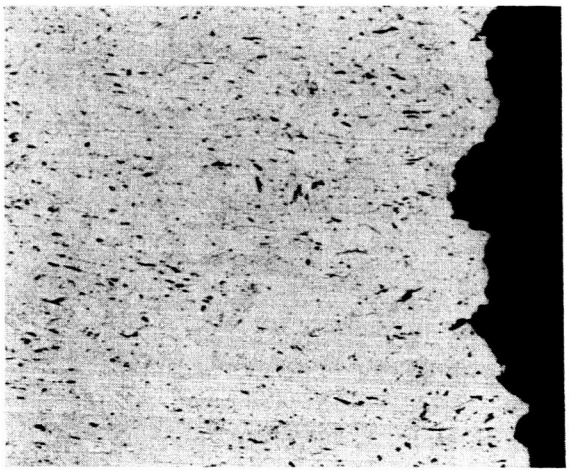

Longitudinal Section at Fracture
X 250

FIGURE C 15 b PHOTOMICROGRAPHS OF TITANIUM-5 AL-2.5 SN (ANNEALED)

MATERIAL PEDIGREE SAMPLES

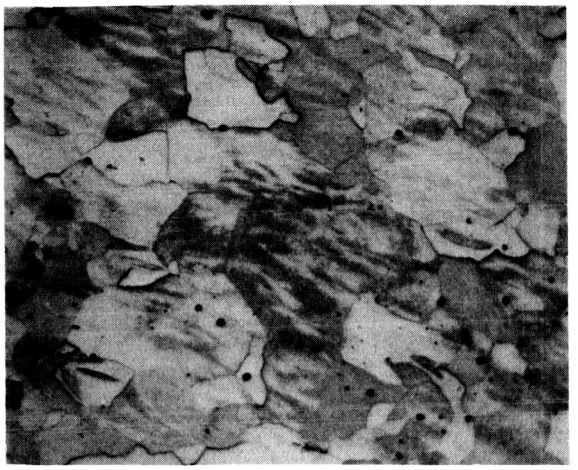

As Received - Longitudinal Section
X 500 Stain Etch

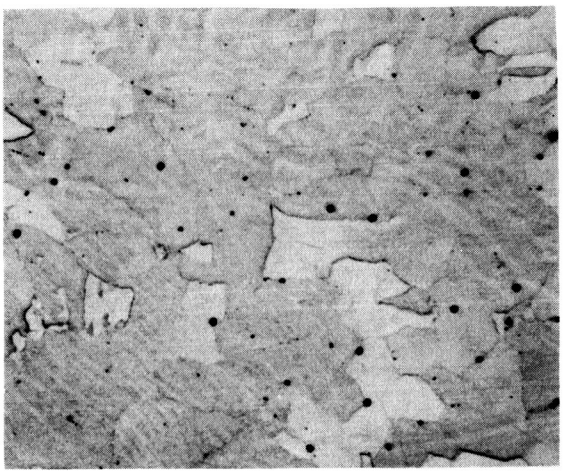

As Received - Transverse Section
X 500 Stain Etch

FAILED TENSILE SPECIMENS
ROOM TEMPERATURE TEST

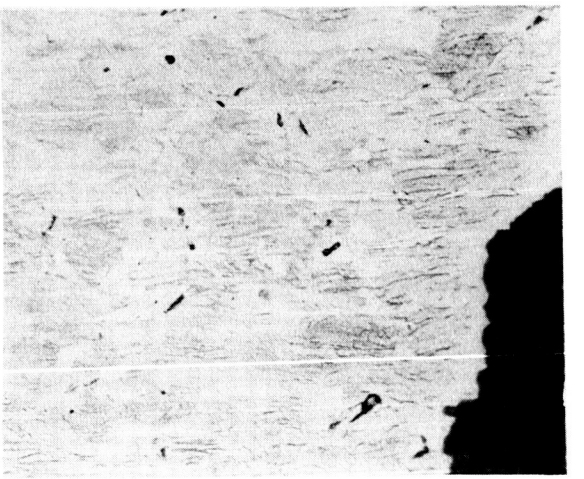

Longitudinal Section at Fracture
X 250

FIGURE C 16 a PHOTOMICROGRAPHS OF TITANIUM-5AL-2.5 SN (ELI, ANNEALED)

FAILED TENSILE SPECIMEN
30°R, UNIRRADIATED TEST

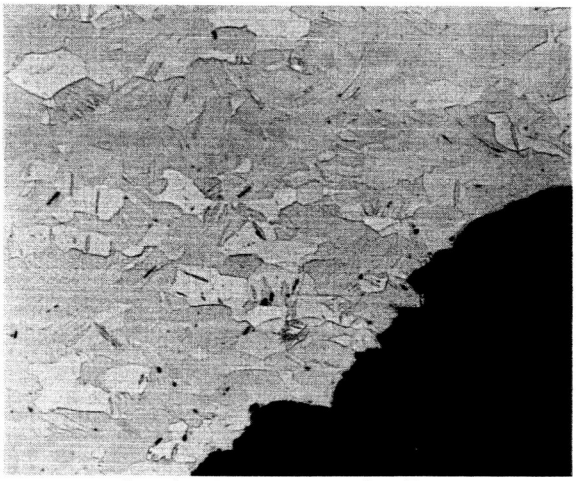

Longitudinal Section of Fracture
X 250

FAILED TENSILE SPECIMEN
30°R, 1×10^{17} nvt, TEST

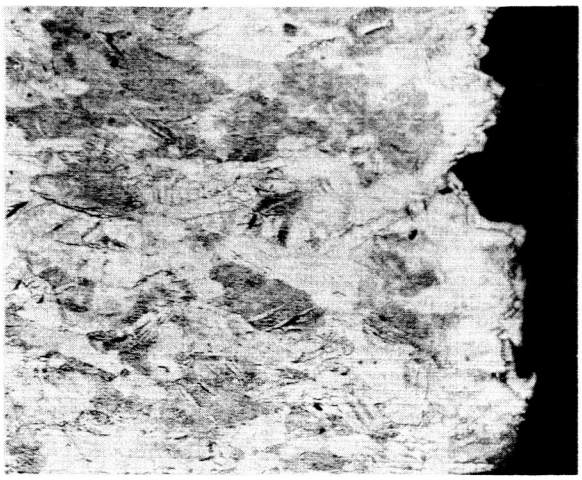

Longitudinal Section at Gage Mark
X 250

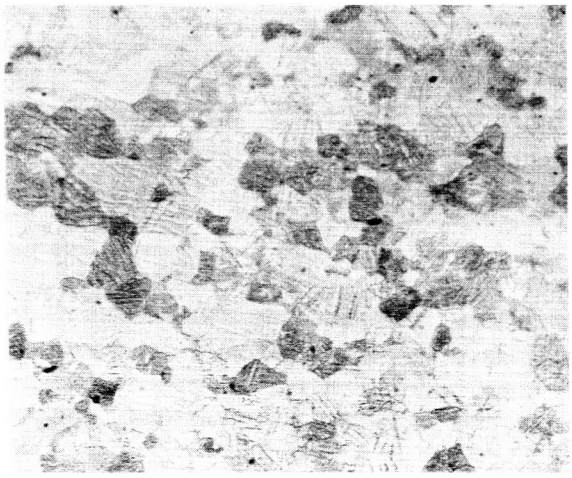

Longitudinal Section at Fracture
X 250 Mixed Acid Etch

FIGURE C. 16 b PHOTOMICROGRAPHS OF TITANIUM - 5AL-2.5 SN (ELI, ANNEALED)

MATERIAL PEDIGREE SAMPLES

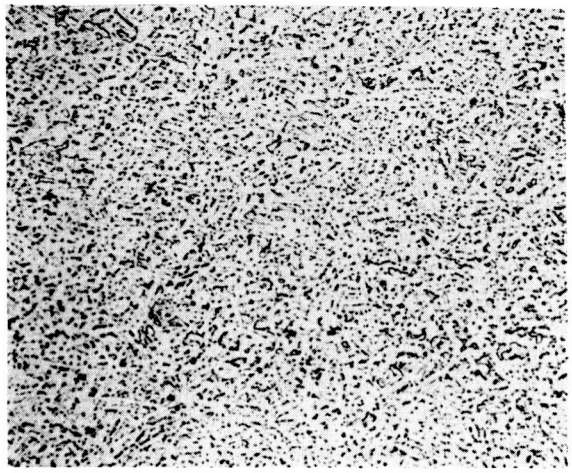

As Received - Longitudinal Section
X 500 Kroll Etch

FAILED TENSILE SPECIMENS
ROOM TEMPERATURE TEST

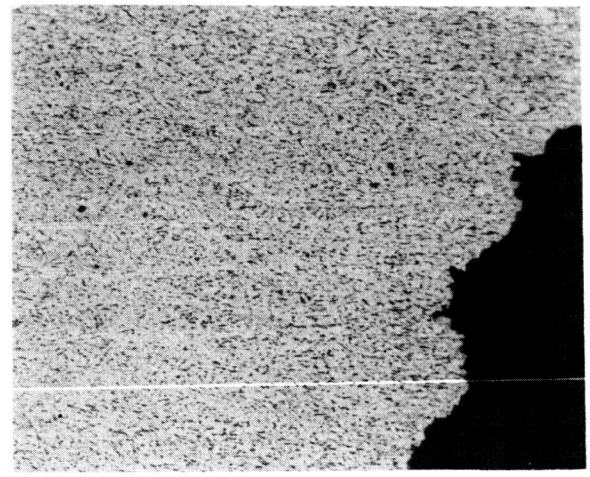

Longitudinal Section at Fracture
X 250

FIGURE C 17 a PHOTOMICROGRAPHS OF TITANIUM - 6 AL-4 V (ANNEALED)

FAILED TENSILE SPECIMEN
30°R, UNIRRADIATED TEST

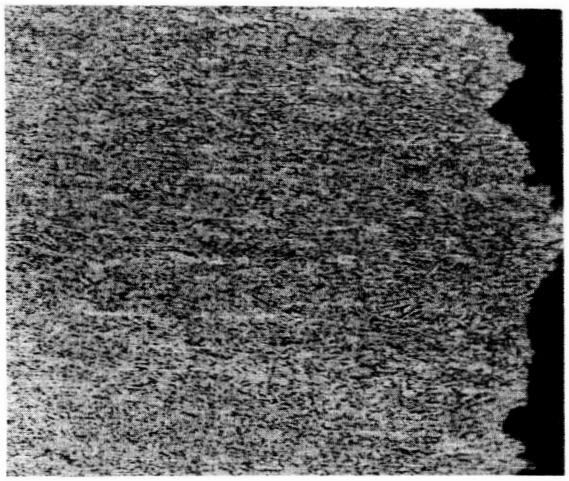

Longitudinal Section at Fracture
X 250

FAILED TENSILE SPECIMEN
30°R, 1×10^{17} nvt, TEST

Longitudinal Section at Fracture
X 250

FIGURE C 17 b PHOTOMICROGRAPHS OF TITANIUM- 6 AL- 4 V (ANNEALED)

MATERIAL PEDIGREE SAMPLES

As Received - Longitudinal Section
X 500 Kroll Etch

FAILED TENSILE SPECIMENS
ROOM TEMPERATURE TEST

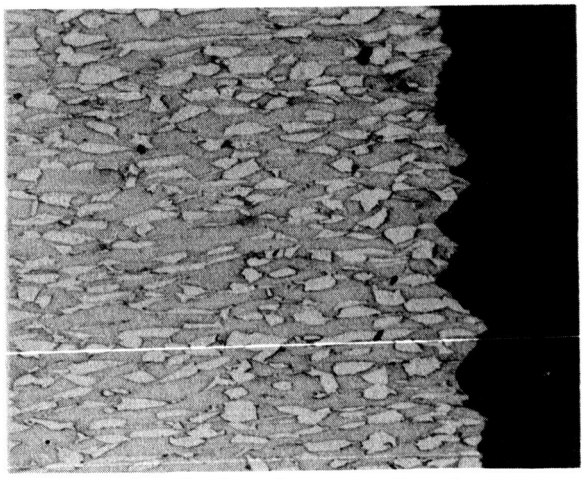

Longitudinal Section at Fracture
X 250

FIGURE C 18 a PHOTOMICROGRAPHS OF TITANIUM - 6 AL - 4V (AGED)

FAILED TENSILE SPECIMEN
30°R, UNIRRADIATED TEST

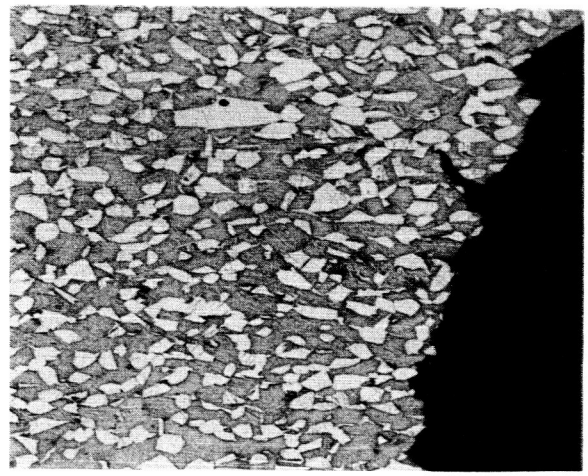

Longitudinal Section at Fracture
X 250

FAILED TENSILE SPECIMEN
30°R, 1×10^{17} nvt, TEST

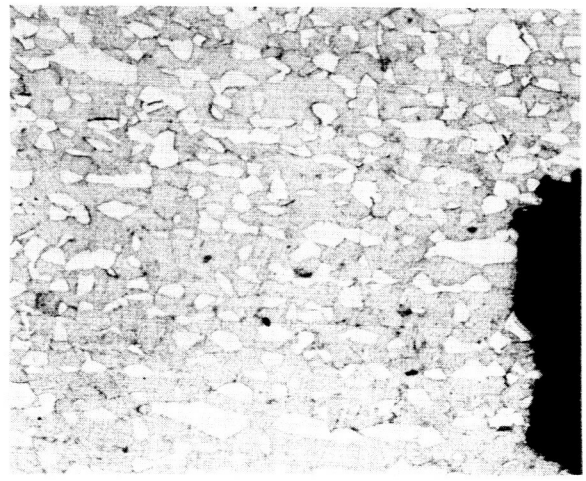

Longitudinal Section at Fracture
X 250

FIGURE C 18 b PHOTOMICROGRAPHS OF TITANIUM-6 AL-4 V (AGED)

MATERIAL PEDIGREE SAMPLES

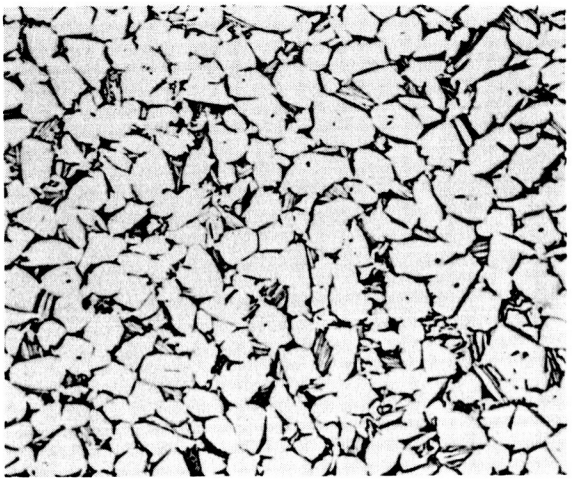

As Received - Longitudinal Section
X 500 Kroll Etch

FAILED TENSILE SPECIMENS
ROOM TEMPERATURE TEST

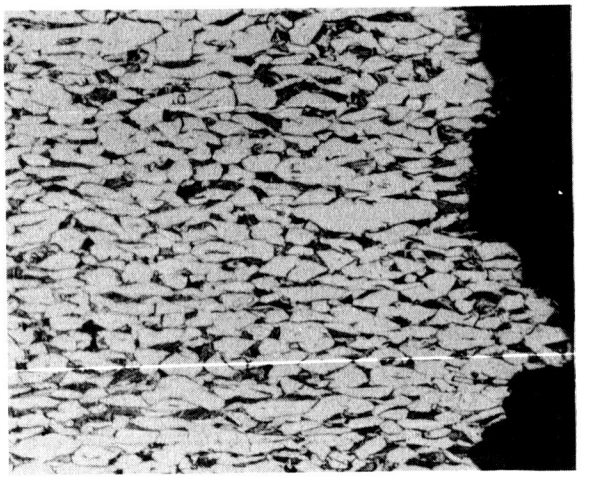

Longitudinal Section at Fracture
X 250

FIGURE C 19 a PHOTOMICROGRAPHS OF TITANIUM - 8 AL-1 MO-1 V (ANNEALED)

FAILED TENSILE SPECIMEN
30°R, UNIRRADIATED TEST

FAILED TENSILE SPECIMEN
30°R, 1×10^{17} nvt, TEST

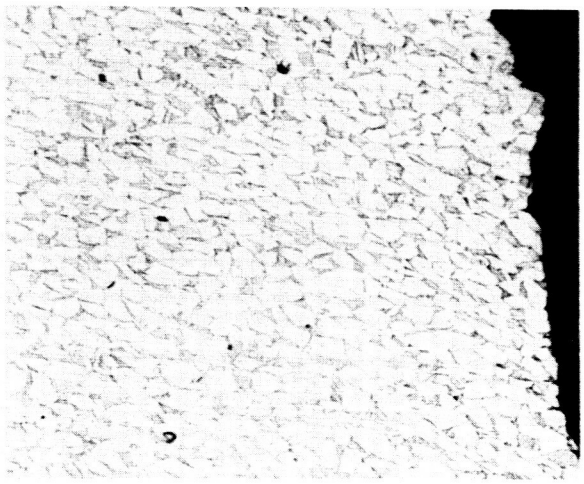

Longitudinal Section at Fracture
X 250

FIGURE C 19 b PHOTOMICROGRAPHS OF TITANIUM - 8AL- 1 MO - 1 V (ANNEALED)

MATERIAL PEDIGREE SAMPLES

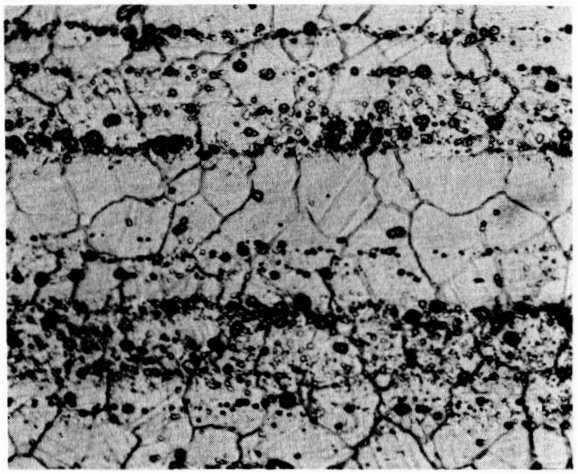

As Received - Longitudinal Section
X 200 Electrolytic Etch

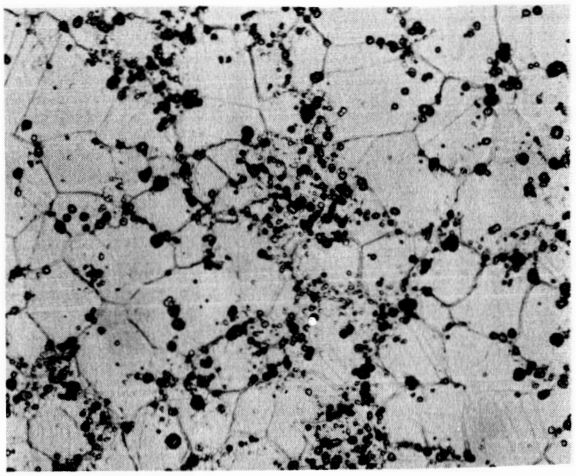

As Received - Transverse Section
X 200 Electrolytic Etch

FAILED TENSILE SPECIMENS
ROOM TEMPERATURE TEST

Longitudinal Section at Fracture
X 250

FIGURE C 20 a PHOTOMICROGRAPHS OF RENE 41 (SOLUTION TREATED)

FAILED TENSILE SPECIMEN
30°R, UNIRRADIATED TEST

Longitudinal Section at Fracture
X 250

FAILED TENSILE SPECIMEN
30°R, 1×10^{17} nvt, TEST

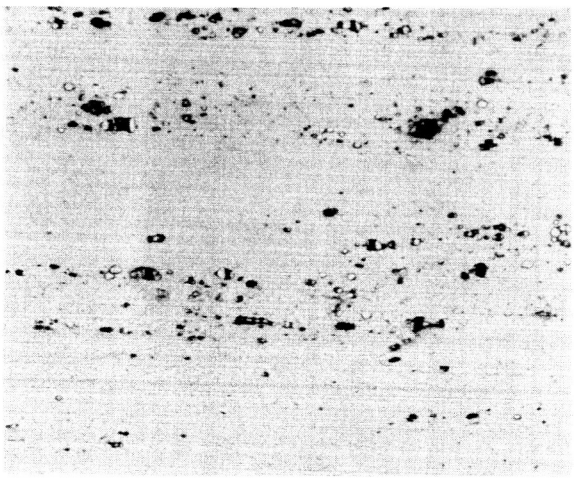

Longitudinal Section at Gage Mark
X 250

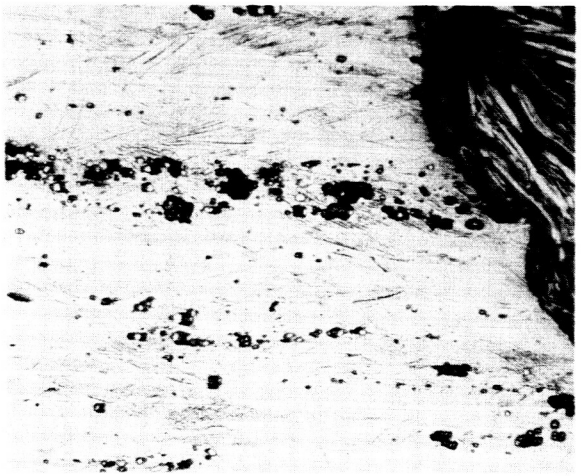

Longitudinal Section at Fracture
X 250

FIGURE C 20 b PHOTOMICROGRAPHS OF RENÉ 41 (SOLUTION TREATED)

MATERIAL PEDIGREE SAMPLES

As Received - Longitudinal Section
X 100 Mixed Acid Etch

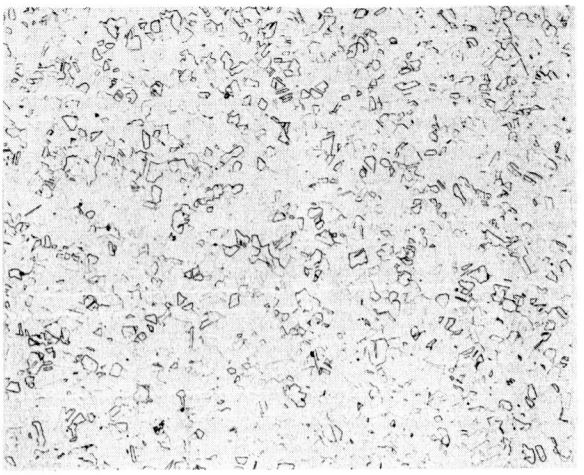

As Received - Transverse Section
X 100 Mixed Acid Etch

FAILED TENSILE SPECIMENS
ROOM TEMPERATURE TEST

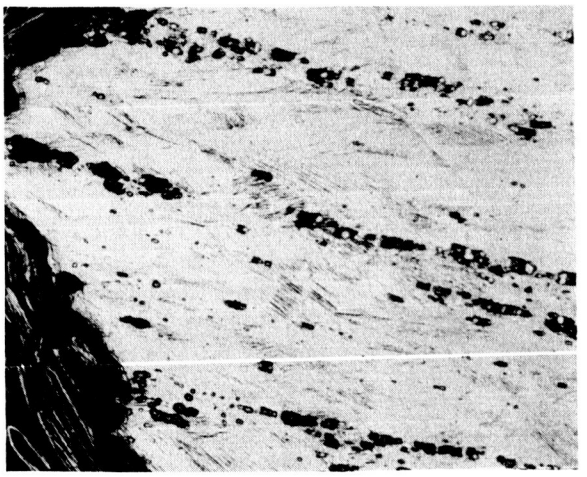

Longitudinal Section at Fracture
X 250

FIGURE C 21 a PHOTOMICROGRAPHS OF
K MONEL (AGED)

FAILED TENSILE SPECIMEN
30°R, UNIRRADIATED TEST

Longitudinal Section at Fracture
X 250

FAILED TENSILE SPECIMEN
30°R, 1×10^{17} nvt, TEST

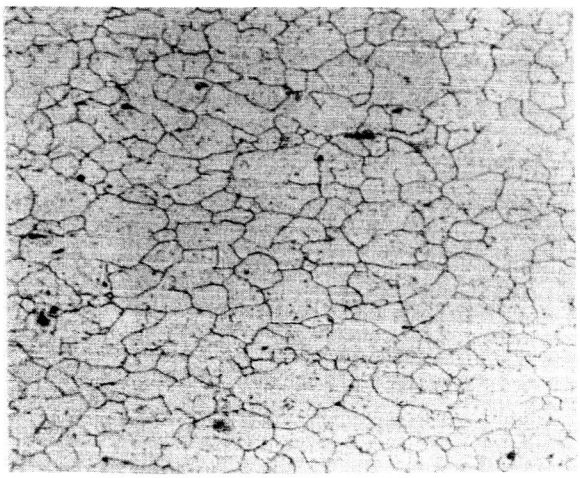

Longitudinal Section at Gage Mark
X 250

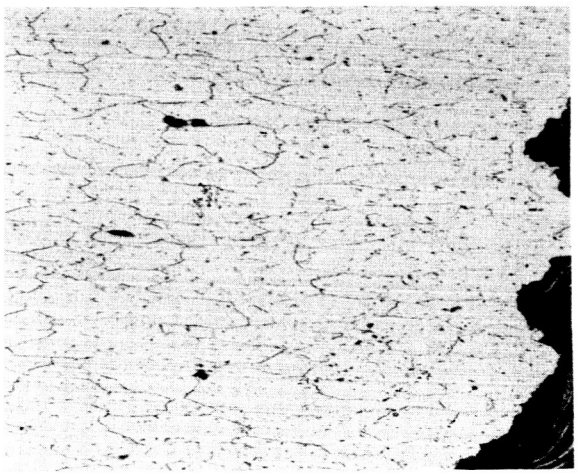

Longitudinal Section at Fracture
X 250

FIGURE C 21 b PHOTOMICROGRAPHS OF K MONEL (AGED)

MATERIAL PEDIGREE SAMPLES

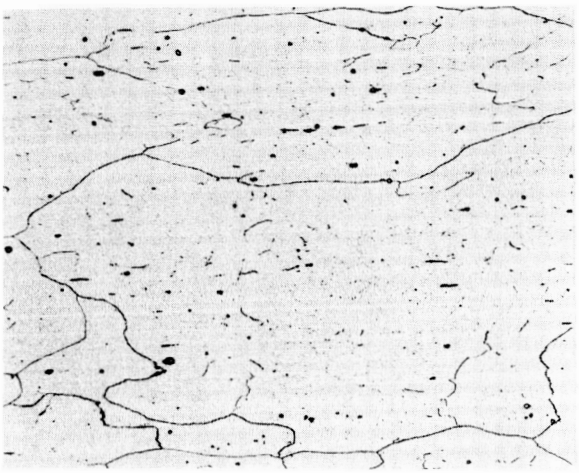

As Received - Longitudinal Section
X 100 5% Nital. Elect. Etch

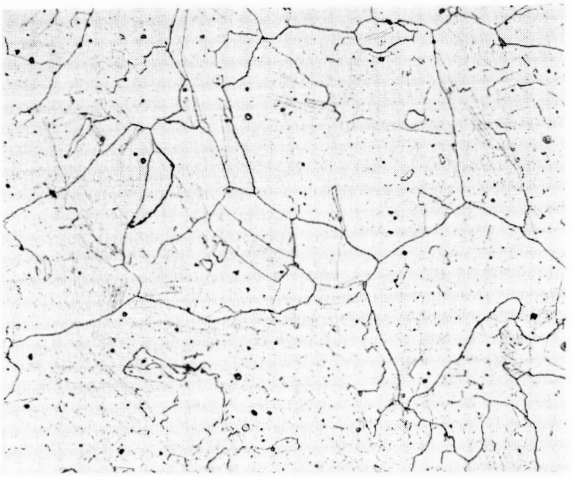

As Received - Transverse Section
X 100 5% Nital. Elect. Etch

FAILED TENSILE SPECIMENS
ROOM TEMPERATURE TEST

Longitudinal Section at Fracture
X 250

FIGURE C 22 a PHOTOMICROGRAPHS OF INCONEL (COLD DRAWN)

FAILED TENSILE SPECIMEN
30°R, UNIRRADIATED TEST

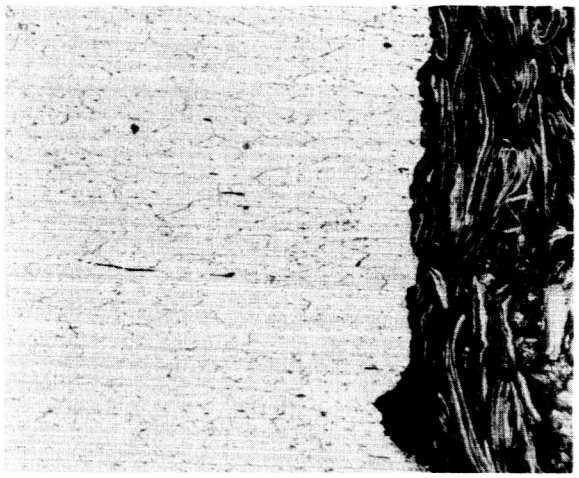

Longitudinal Section at Fracture
X 250

FAILED TENSILE SPECIMEN
30°R, 1×10^{17} nvt, TEST

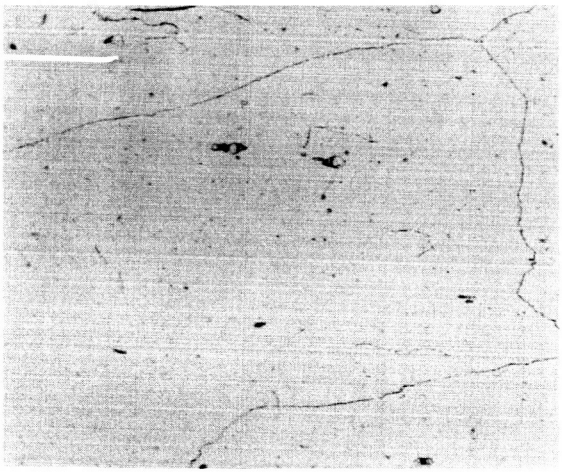

Longitudinal Section at Gage Mark
X 250

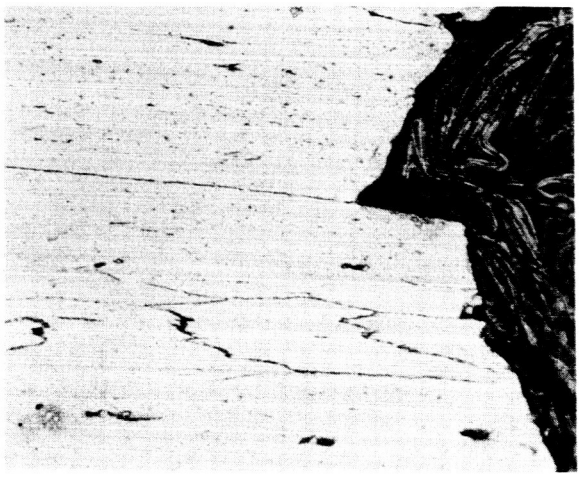

Longitudinal Section at Fracture
X 250

FIGURE C 22 b PHOTOMICROGRAPHS OF INCONEL (COLD DRAWN)

MATERIAL PEDIGREE SAMPLES

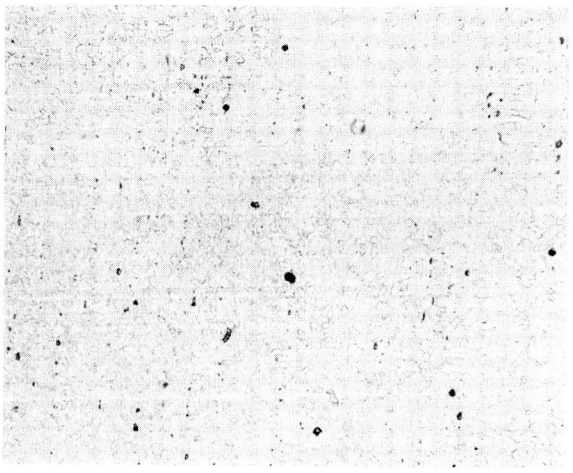

As Received - Longitudinal Section
X 100 Mixed Acid Etch

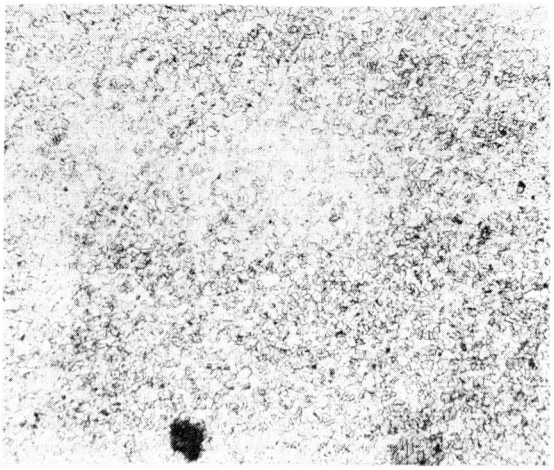

As Received - Transverse Section
X 100 Mixed Acid Etch

FAILED TENSILE SPECIMENS
ROOM TEMPERATURE TEST

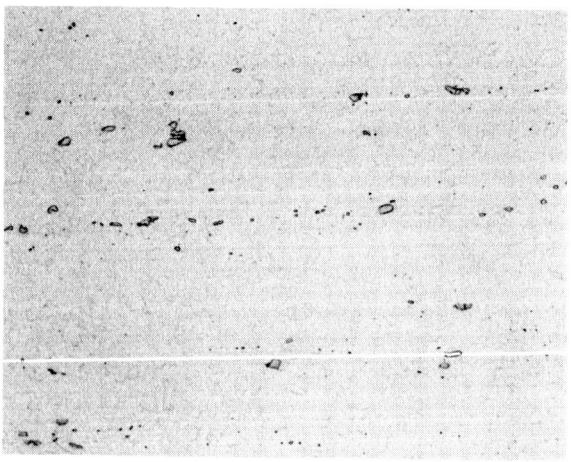

Longitudinal Section at Gage Mark
X 250 Mixed Acid Etch

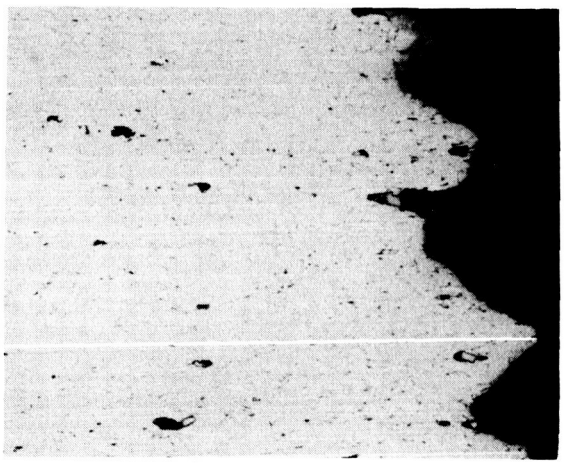

Longitudinal Section at Fracture
X 250 Mixed Acid Etch

FIGURE C 23 a PHOTOMICROGRAPHS OF INCONEL X (AGED)

FAILED TENSILE SPECIMEN
30°R, UNIRRADIATED TEST

Longitudinal Section at Fracture
X 250

FAILED TENSILE SPECIMEN
30°R, 1×10^{17} nvt, TEST

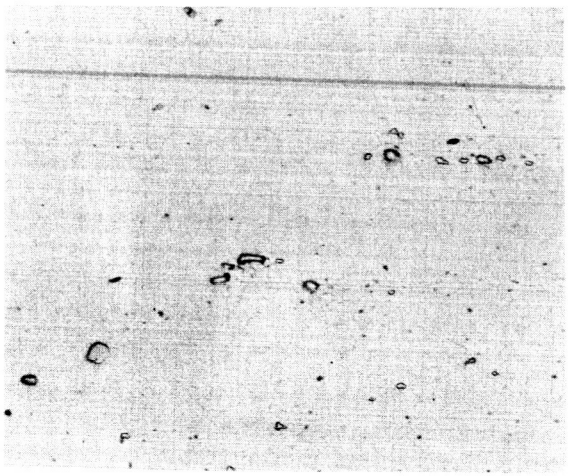

Longitudinal Section at Gage Mark
X 250

Longitudinal Section at Fracture
X 250

FIGURE C 23 b PHOTOMICROGRAPHS OF INCONEL X (AGED)

MATERIAL PEDIGREE SAMPLES

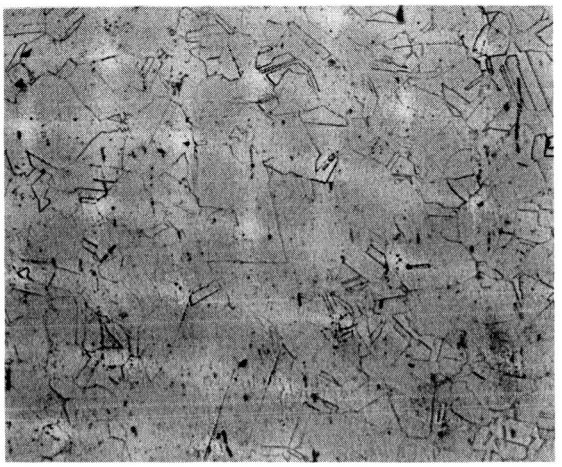

As Received - Longitudinal Section
X 100 Oxalic Acid, Electro

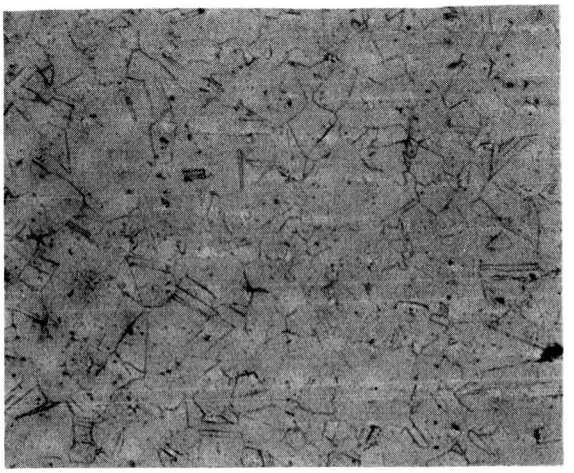

As Received - Transverse Section
X 100 Oxalic Acid, Electro

FAILED TENSILE SPECIMENS
ROOM TEMPERATURE TEST

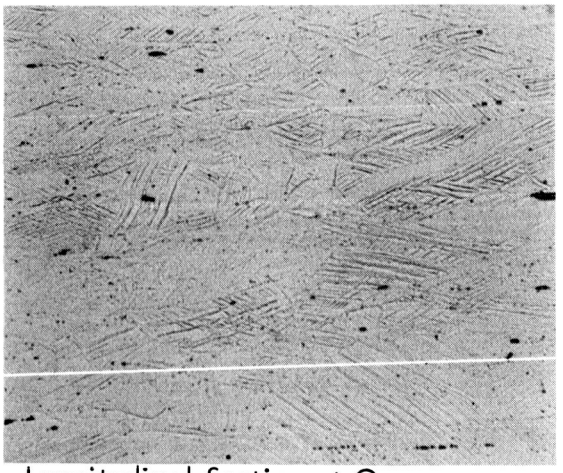

Longitudinal Section at Gage
X 250 Oxalic Acid, Electro

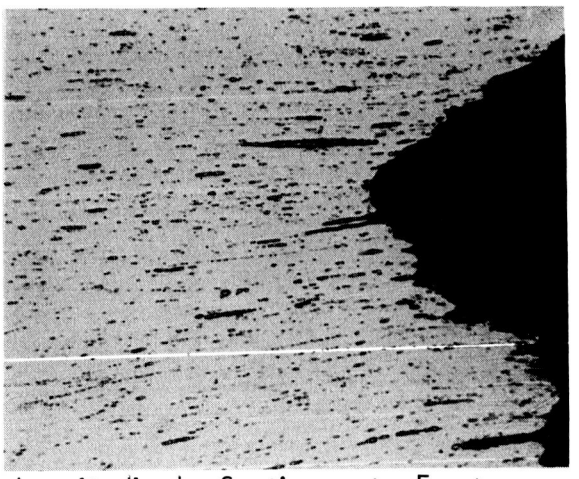

Longitudinal Section at Fracture
X 250 Oxalic Acid, Electro

FIGURE C 24 a PHOTOMICROGRAPHS OF
304 STAINLESS STEEL, ANNEALED

FAILED TENSILE SPECIMEN
30°R, UNIRRADIATED TEST

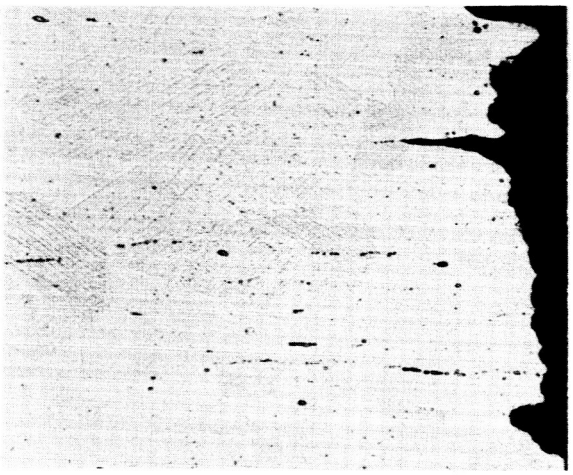

Longitudinal Section at Fracture
X 250 Oxalic Acid, Electro

FAILED TENSILE SPECIMEN
30°R, 1×10^{17} nvt TEST

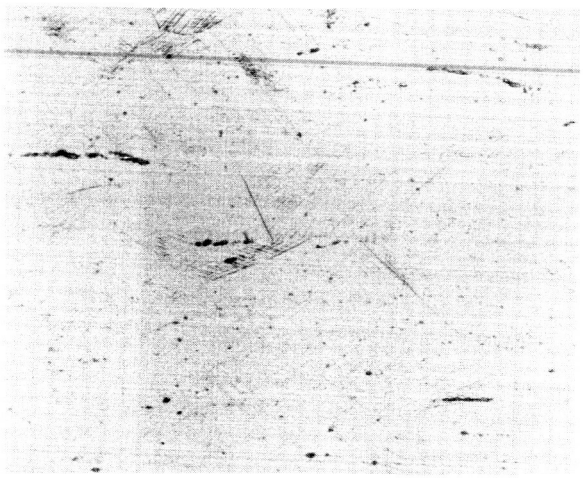

Longitudinal Section at Gage Mark
X 250 Oxalic Acid, Electro

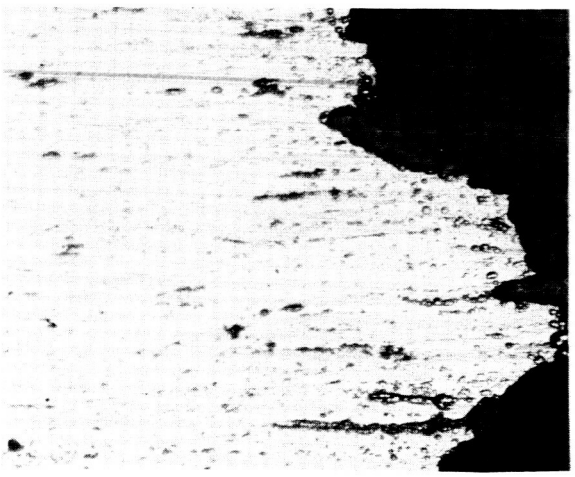

Longitudinal Section at Fracture
X 250 Oxalic Acid, Electro

FIGURE C 24 b PHOTOMICROGRAPHS OF
304 STAINLESS STEEL, ANNEALED

MATERIAL PEDIGREE SAMPLES

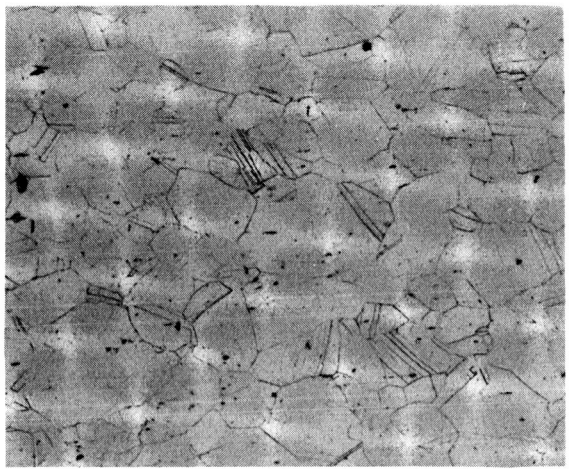

As Received - Longitudinal Section
X 100 Oxalic Acid Electrolytic

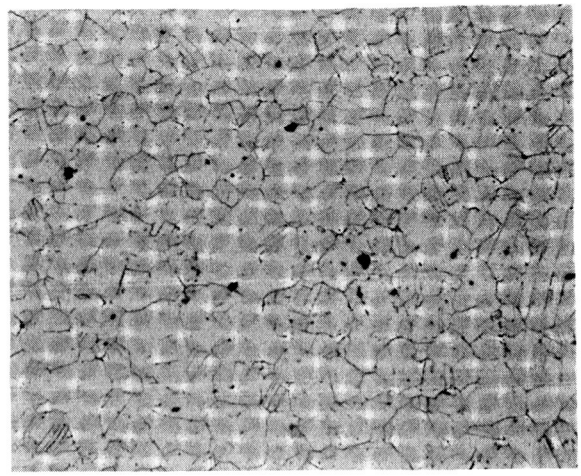

As Received - Transverse Section
X 100 Oxalic Acid Electrolytic

FAILED TENSILE SPECIMENS
ROOM TEMPERATURE TEST

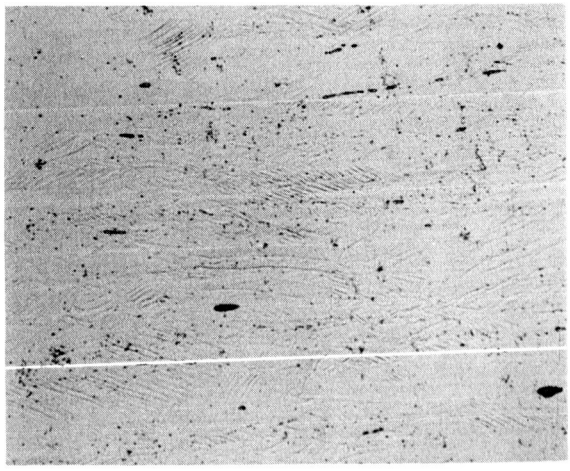

Longitudinal Section at Gage
X 250 Oxalic Acid Electrolytic

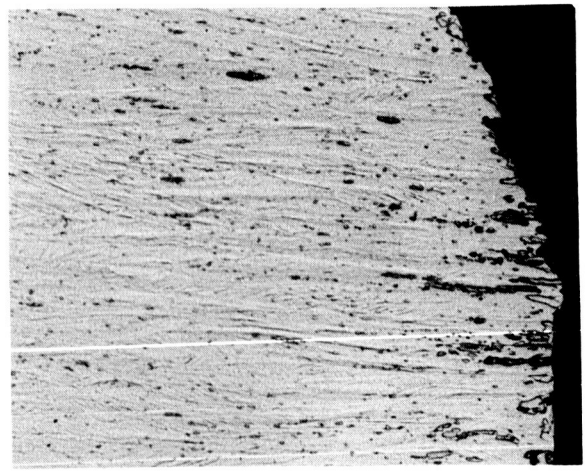

Longitudinal Section at Fracture
X 250 Oxalic Acid Electrolytic

FIGURE C 25 a PHOTOMICROGRAPHS OF
310 STAINLESS STEEL, ANNEALED

FAILED TENSILE SPECIMEN
30°R, UNIRRADIATED TEST

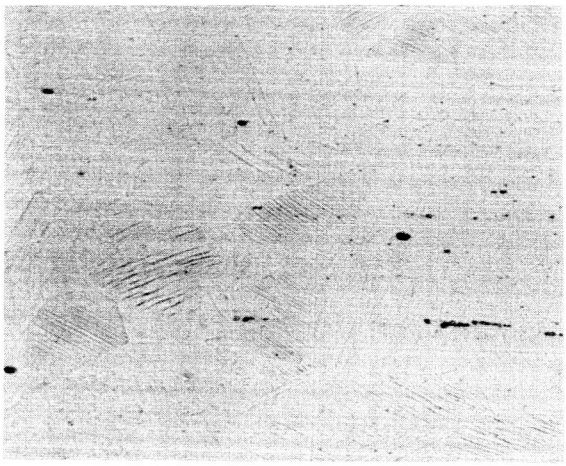

Longitudinal Section at Gage Mark
X 250 Oxalic Acid Electrolytic

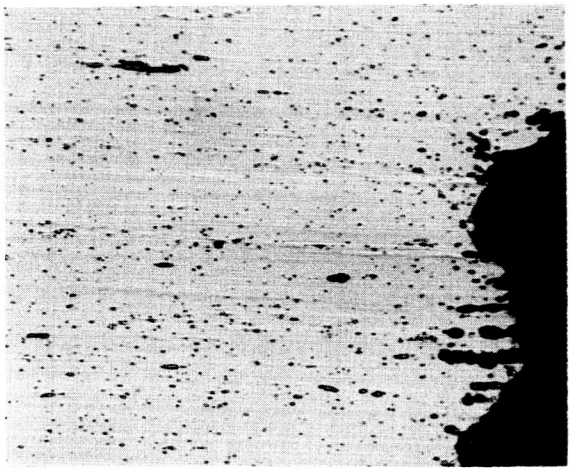

Longitudinal Section at Fracture
X 250 Oxalic Acid Electrolytic

FAILED TENSILE SPECIMEN
30°R, 1×10^{17} nvt TEST

Longitudinal Section at Fracture
X 250 Oxalic Acid Electrolytic

FIGURE C 25 b PHOTOMICROGRAPHS OF
310 STAINLESS STEEL, ANNEALED

MATERIAL PEDIGREE SAMPLES

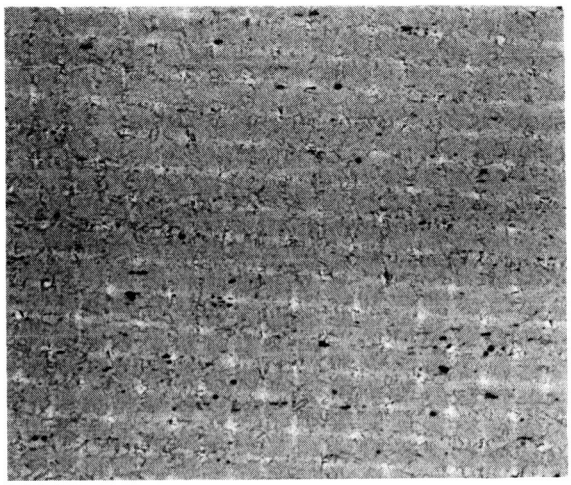

As Received - Longitudinal Section
X 100 $(NH_4)_2 S_2 O_8$, Electro

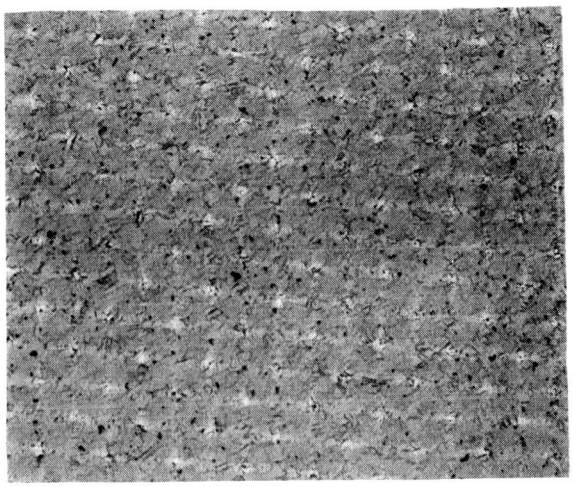

As Received - Transverse Section
X 100 $(NH_4)_2 S_2 O_8$, Electro

FAILED TENSILE SPECIMENS
ROOM TEMPERATURE TEST

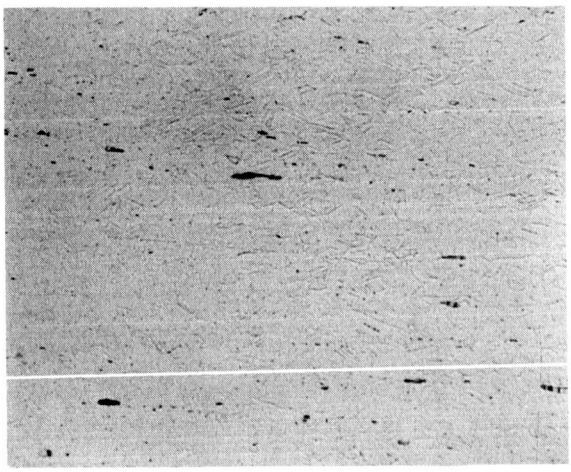

Longitudinal Section at Gage
X 250 $(NH_4)_2 S_2 O_8$, Electro

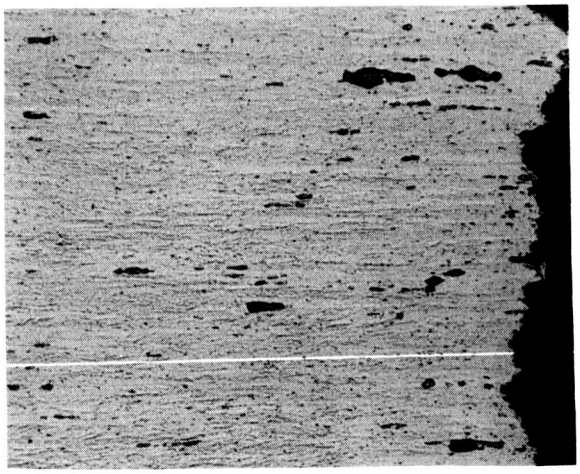

Longitudinal Section at Fracture
X 250 $(NH_4)_2 S_2 O_8$, Electro

FIGURE C 26 a PHOTOMICROGRAPHS OF
347 STAINLESS STEEL (ANNEALED)

FAILED TENSILE SPECIMEN
30°R, UNIRRADIATED TEST

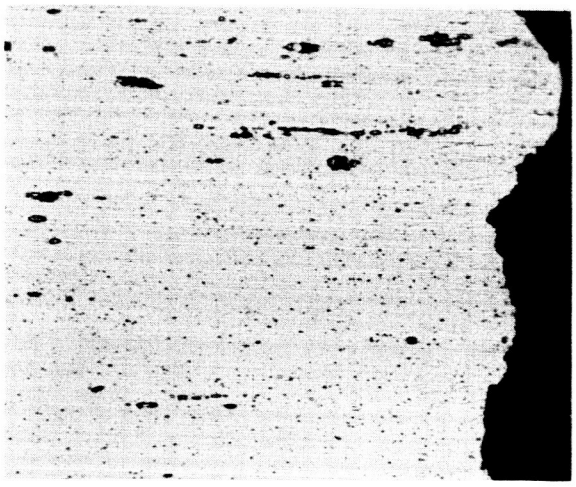

Longitudinal Section at Fracture
X 250 $(NH_4)_2 S_2 O_8$, Electro

FAILED TENSILE SPECIMEN
30°R, 1×10^{17} nvt TEST

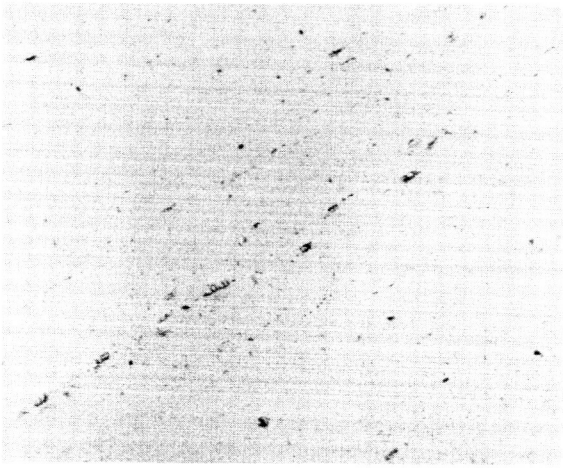

Longitudinal Section at Gage Mark
X 250 $(NH_4)_2 S_2 O_8$, Electro

Longitudinal Section at Fracture
X 250 $(NH_4)_2 S_2 O_8$, Electro

FIGURE C 26 b PHOTOMICROGRAPHS OF
347 STAINLESS STEEL (ANNEALED)

MATERIAL PEDIGREE SAMPLES

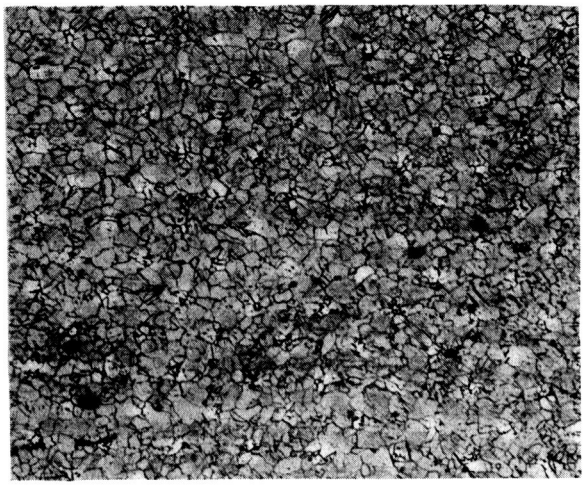

As Received - Longitudinal Section
X 100 Mixed Acid Etch

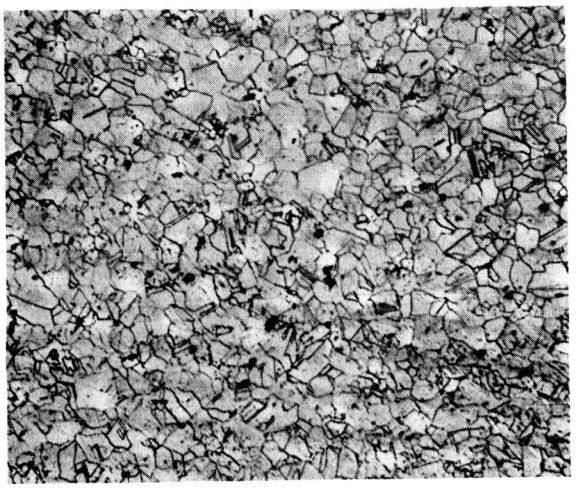

As Received - Transverse Section
X 100 Mixed Acid Etch

FAILED TENSILE SPECIMENS
ROOM TEMPERATURE TEST

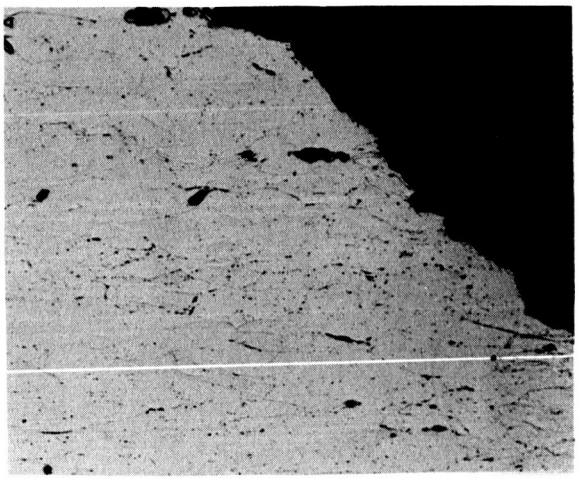

Longitudinal Section at Fracture
X 250 Mixed Acid Etch

FIGURE C 27 a PHOTOMICROGRAPHS OF
A 286 STAINLESS STEEL (AMS-5735)

FAILED TENSILE SPECIMEN
30°R, UNIRRADIATED TEST

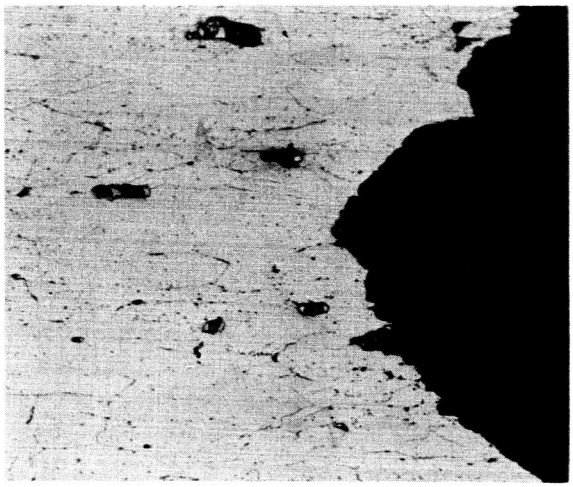

Longitudinal Section at Fracture
X 250 Mixed Acid Etch

FAILED TENSILE SPECIMEN
30°R, 1×10^{17} nvt TEST

Longitudinal Section at Fracture
X 250 Mixed Acid Etch

FIGURE C 27 b PHOTOMICROGRAPHS OF
A 286 STAINLESS STEEL (AMS-5735)

MATERIAL PEDIGREE SAMPLES

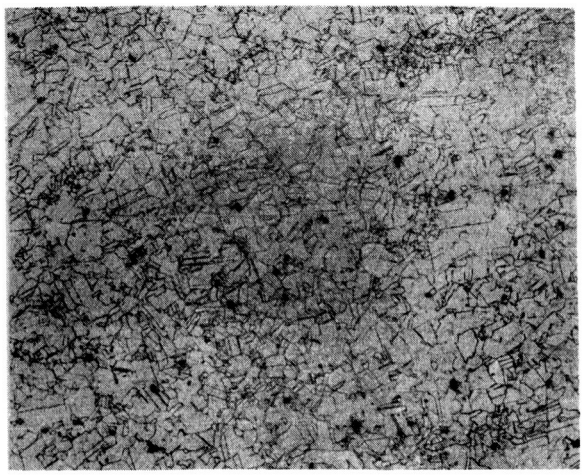

As Received - Longitudinal Section
X 100 Mixed Acid Etch

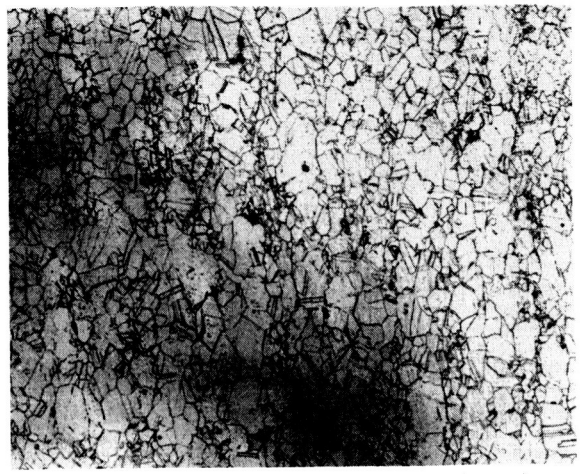

As Received - Transverse Section
X 100 Mixed Acid Etch

FAILED TENSILE SPECIMENS
ROOM TEMPERATURE TEST

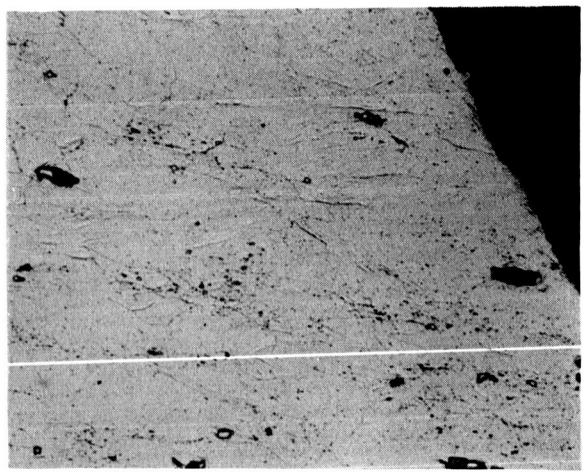

Longitudinal Section at Fracture
X 250 Mixed Acid Etch

FIGURE C 28 a PHOTOMICROGRAPHS OF
A 286 STAINLESS STEEL (AMS-5737)

FAILED TENSILE SPECIMEN
30°R, UNIRRADIATED TEST

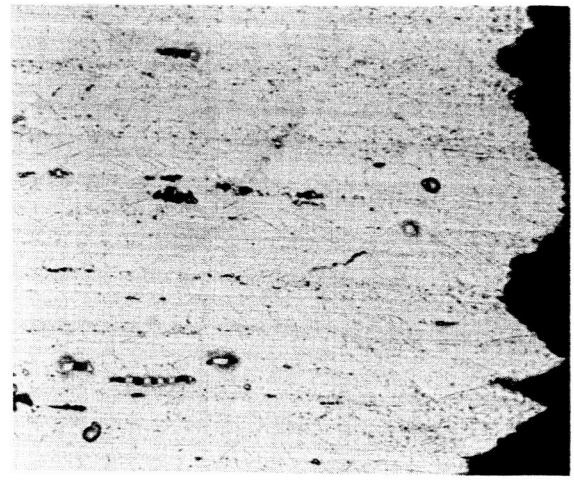

Longitudinal Section at Fracture
X 250 Mixed Acid Etch

FAILED TENSILE SPECIMEN
30°R, 1×10^{17} nvt TEST

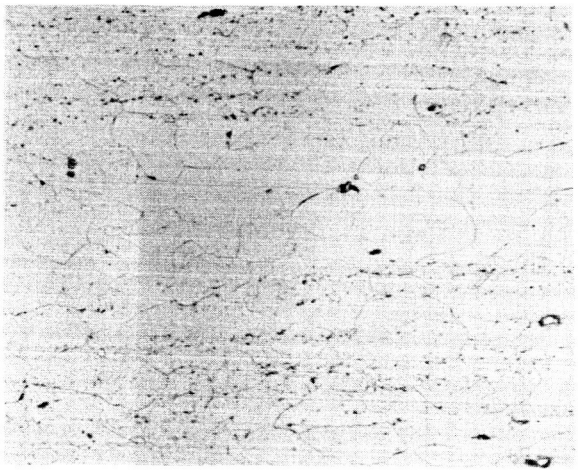

Longitudinal Section at Gage Mark
X 250 Mixed Acid Etch

Longitudinal Section at Fracture
X 250 Mixed Acid Etch

FIGURE C 28 b PHOTOMICROGRAPHS OF
A 286 STAINLESS STEEL (AMS-5737)

MATERIAL PEDIGREE SAMPLES

As Received
X 100

Longitudinal Section
5% Picral

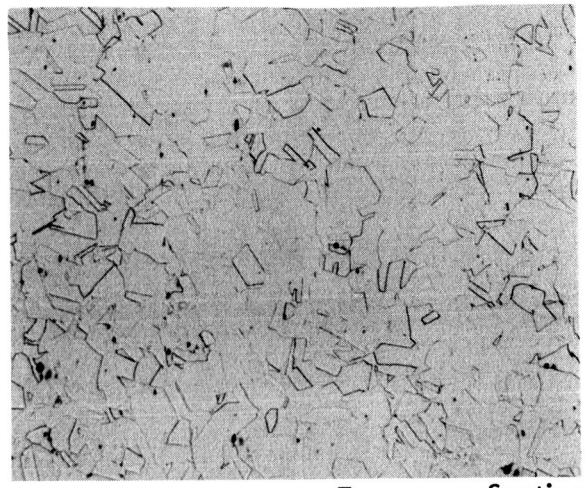

As Received
X 100

Transverse Section
5% Picral

FAILED TENSILE SPECIMENS
ROOM TEMPERATURE TEST

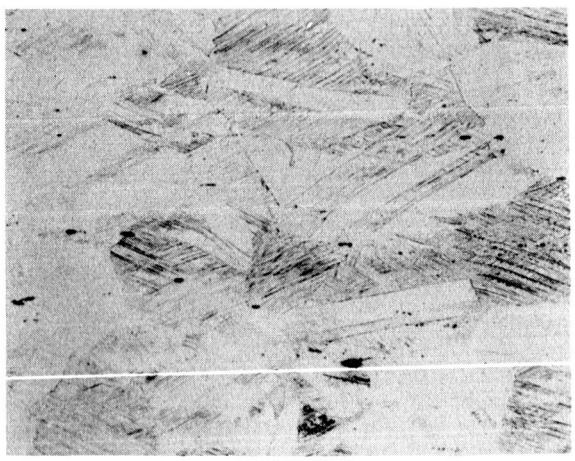

Longitudinal Section at Gage
X 250 Alternate Acid and Base
in Alcohol

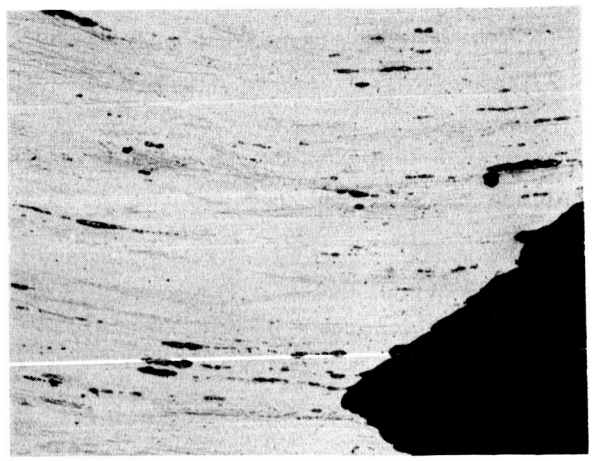

Longitudinal Section at Fracture
X 250 Alternate Acid and Base
in Alcohol

FIGURE C 29 a PHOTOMICROGRAPHS OF T 450
AUSTENITIC MANGANESE STEEL
(ANNEALED)

FAILED TENSILE SPECIMEN
30°R, UNIRRADIATED TEST

Longitudinal Section at Gage Mark
X 250 Alternate Acid and Base in Alcohol

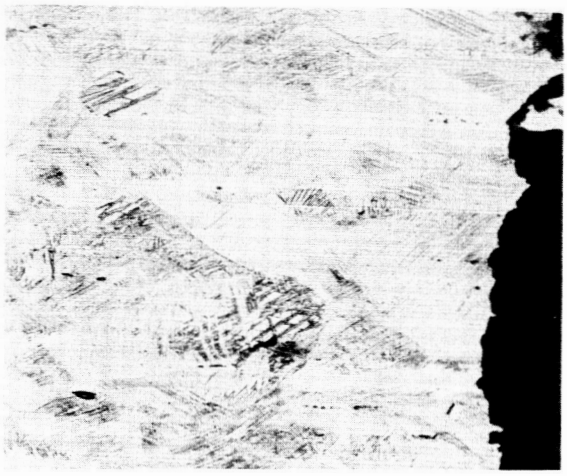

Longitudinal Section at Fracture
X 250 Alternate Acid and Base in Alcohol

FAILED TENSILE SPECIMEN
30°R, 1×10^{17} nvt TEST

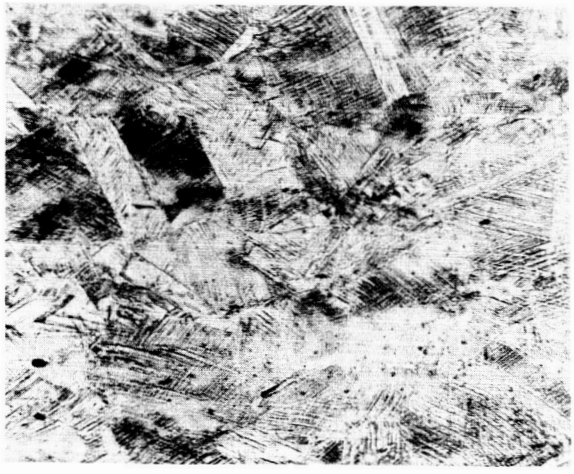

Longitudinal Section at Gage Mark
X 250 Alternate Acid and Base in Alcohol

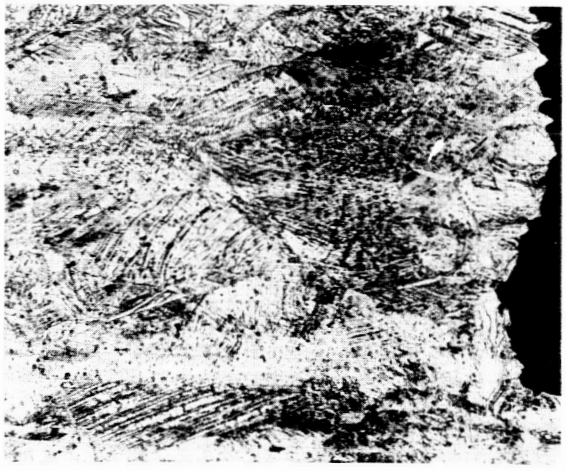

Longitudinal Section at Fracture
X 250 Alternate Acid and Base in Alcohol

FIGURE C 29 b PHOTOMICROGRAPHS OF T 450 AUSTENITIC MANGANESE STEEL (ANNEALED)

MATERIAL PEDIGREE SAMPLES

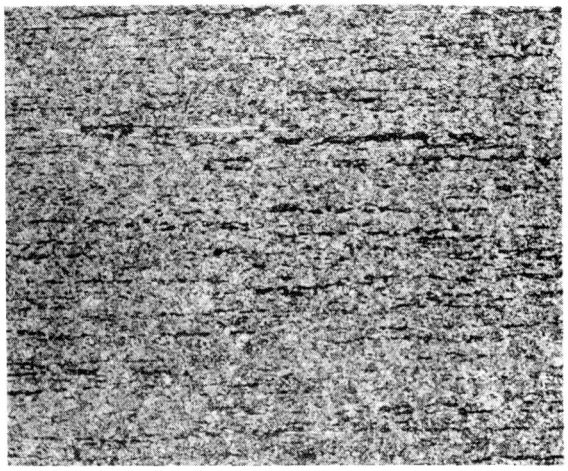

As Received - Longitudinal Section
X 100 Oxalic Acid, Electro

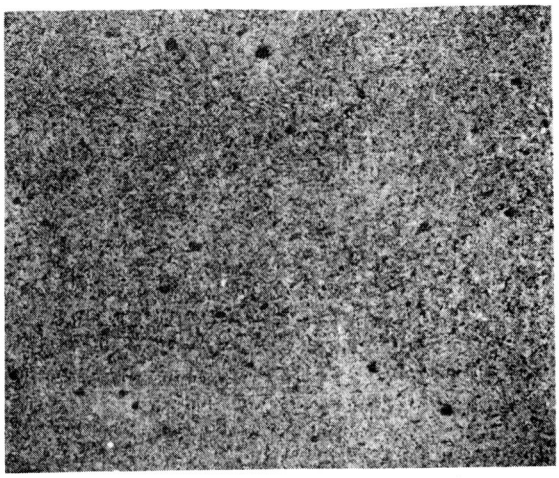

As Received - Transverse Section
X 100 Oxalic Acid, Electro

FAILED TENSILE SPECIMENS
ROOM TEMPERATURE TEST

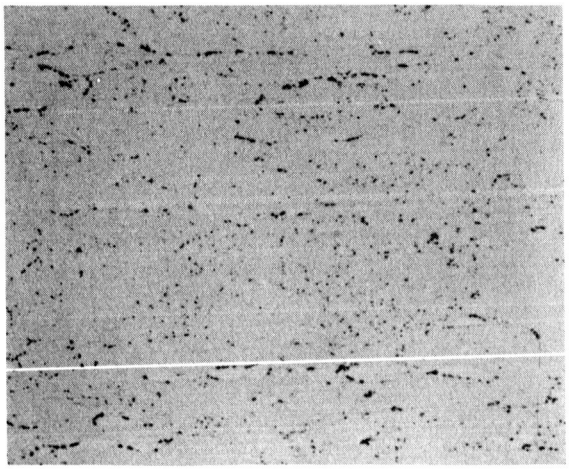

Longitudinal Section at Gage
X 250 Oxalic Acid, Electro

Longitudinal Section at Fracture
X 250 Oxalic Acid, Electro

FIGURE C 30 a PHOTOMICROGRAPHS OF AM 350 STAINLESS STEEL (SCT)

FAILED TENSILE SPECIMEN
30°R, UNIRRADIATED TEST

Longitudinal Section at Fracture
X 250 Oxalic Acid, Electro

FAILED TENSILE SPECIMEN
30°R, 1×10^{17} nvt TEST

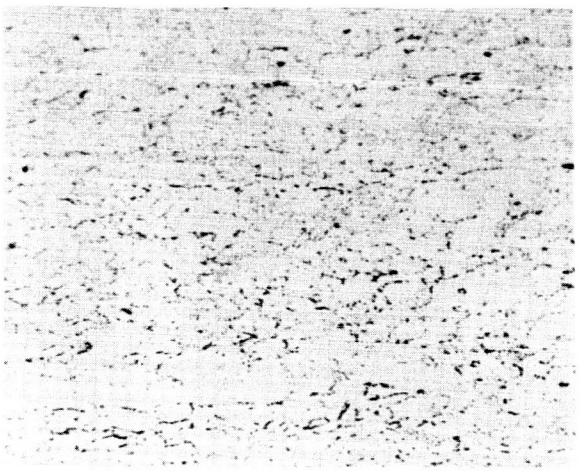

Longitudinal Section at Gage Mark
X 250 Oxalic Acid, Electro

Longitudinal Section at Fracture
X 250 Oxalic Acid, Electro

FIGURE C 30 b PHOTOMICROGRAPHS OF AM 350 STAINLESS STEEL (SCT)

MATERIAL PEDIGREE SAMPLES

FAILED TENSILE SPECIMENS
ROOM TEMPERATURE TEST

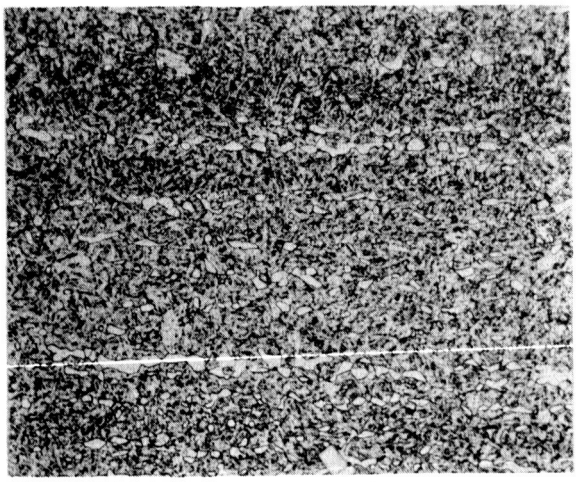

Longitudinal Section at Gage
X 250 HNO_3 - Acetic - Oxalic-Electro

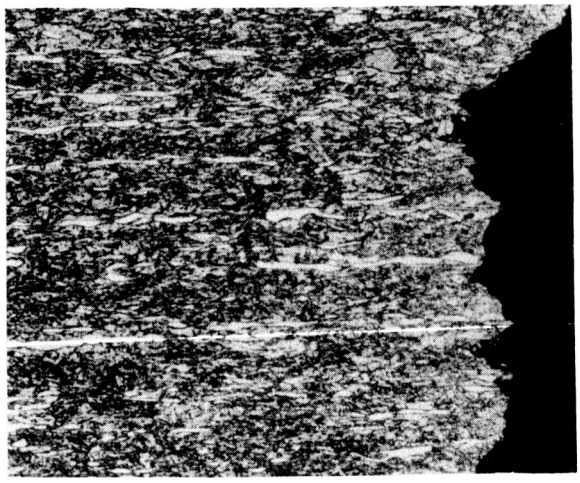

Longitudinal Section at Fracture
X 250 HNO_3- Acetic - Oxalic- Electro

FIGURE C 31 a PHOTOMICROGRAPHS OF
17-7 PH STAINLESS STEEL (RH-950)

FAILED TENSILE SPECIMEN
30°R, UNIRRADIATED TEST

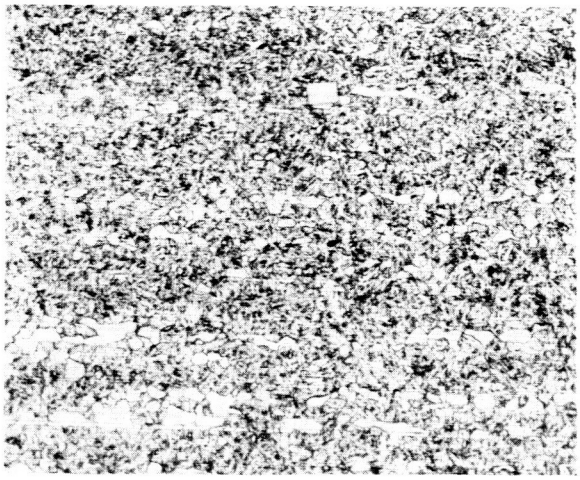

Longitudinal Section at Gage Mark
X 250 HNO_3 - Acetic - Oxalic-Electro

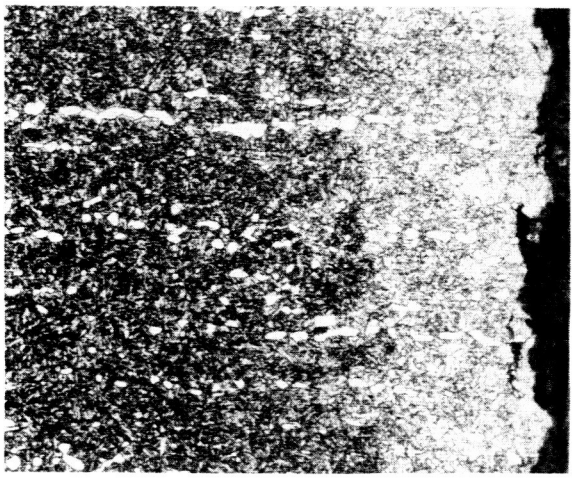

Longitudinal Section at Fracture
X 250 HNO_3 - Acetic - Oxalic - Electro

FAILED TENSILE SPECIMEN
30°R, 1×10^{17} nvt TEST

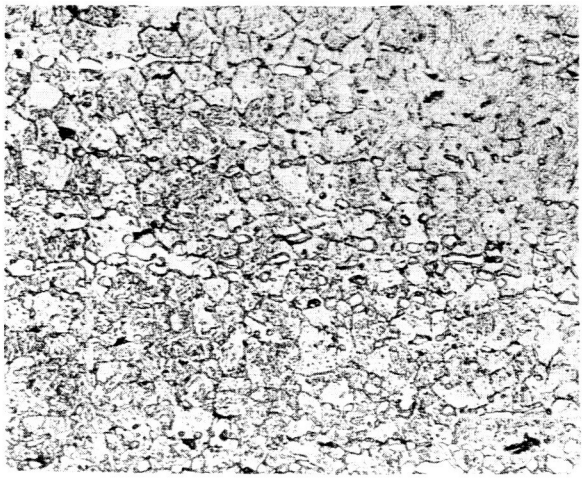

Longitudinal Section at Gage Mark
X 250 HNO_3 - Acetic-Oxalic-Electro

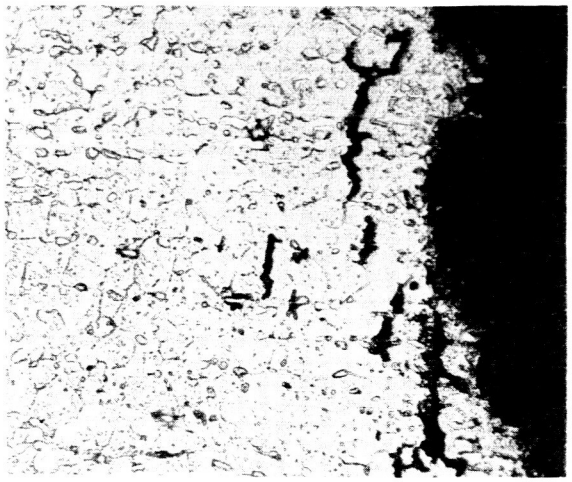

Longitudinal Section at Fracture
X 250 HNO_3-Acetic - Oxalic - Electro

FIGURE C 31 b PHOTOMICROGRAPHS OF
17-7 PH STAINLESS STEEL (RH-950)

MATERIAL PEDIGREE SAMPLES

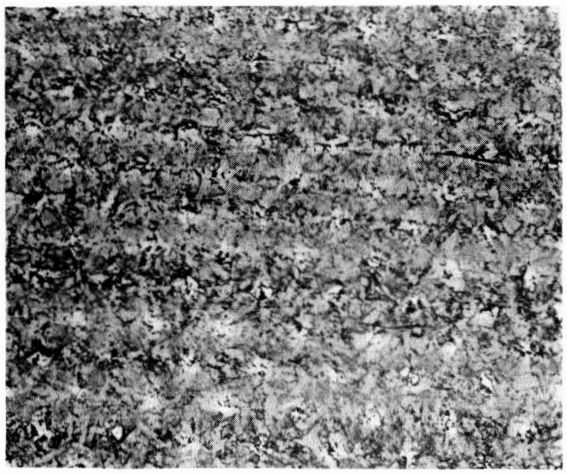

As Received - Longitudinal Section
X 200 Nital

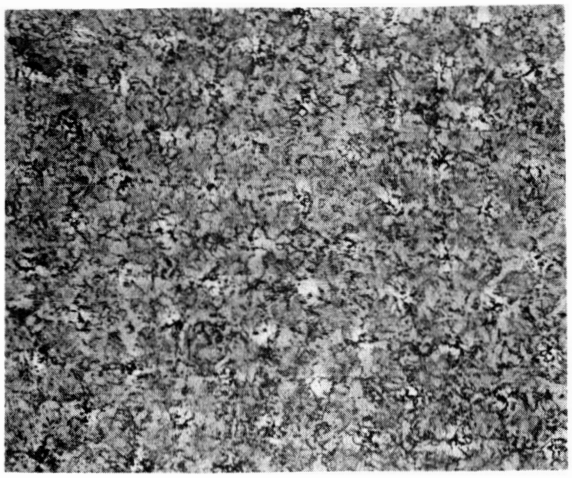

As Received - Transverse Section
X 200 Nital

FAILED TENSILE SPECIMENS
ROOM TEMPERATURE TEST

Longitudinal Section at Gage
X 250 Nital

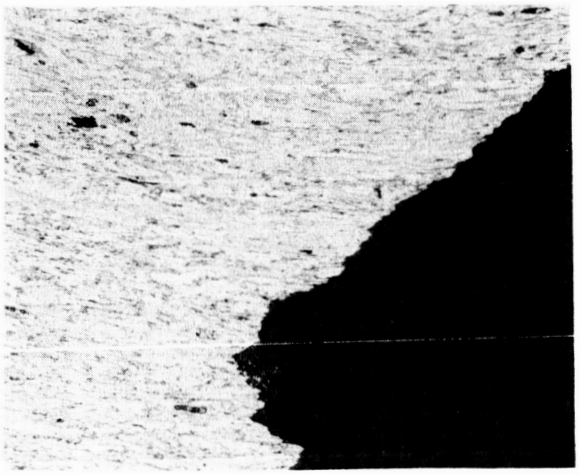

Longitudinal Section at Fracture
X 250 Nital

FIGURE C 32 a PHOTOMICROGRAPHS OF ASTM A 353 STEEL (NORMALIZED)

FAILED TENSILE SPECIMEN
30°R, UNIRRADIATED TEST

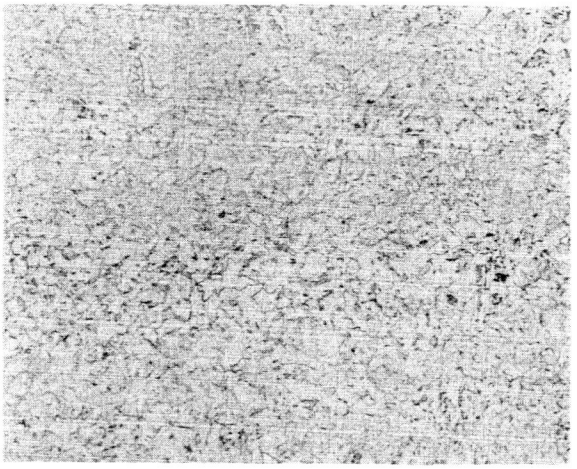

Longitudinal Section at Gage Mark
X 250 Nital

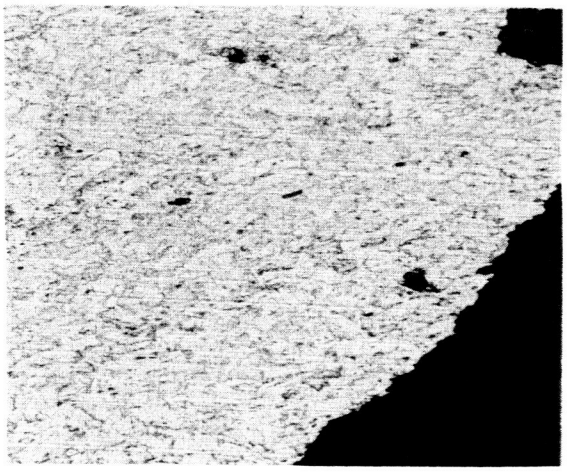

Longitudinal Section at Fracture
X 250 Nital

FAILED TENSILE SPECIMEN
30°R, 1×10^{17} nvt TEST

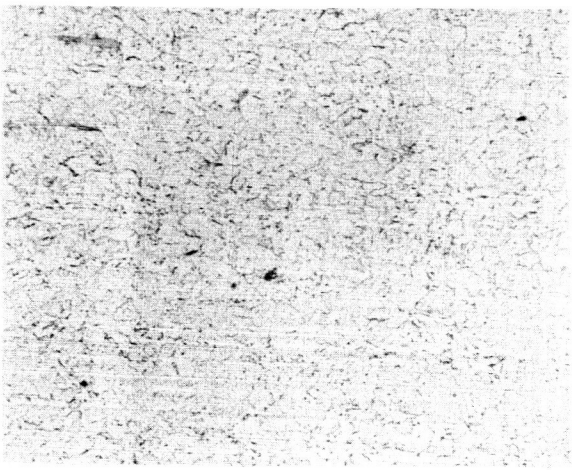

Longitudinal Section at Gage Mark
X 250 Nital

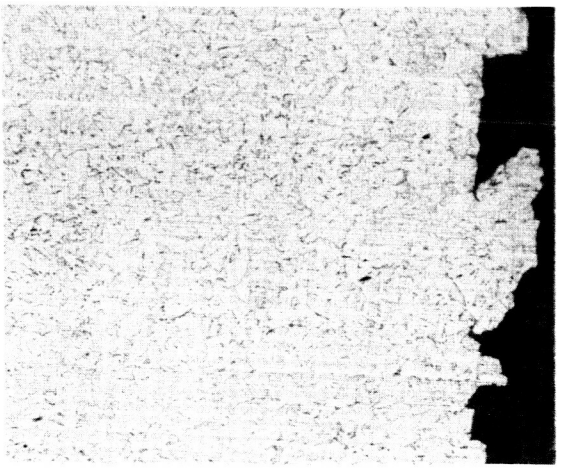

Longitudinal Section at Fracture
X 250 Nital

FIGURE C 32 b PHOTOMICROGRAPHS OF ASTM A 353 STEEL (NORMALIZED)

MATERIAL PEDIGREE SAMPLES

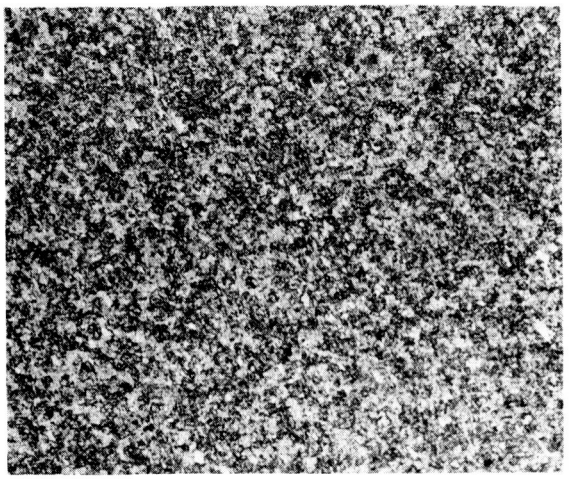

As Received - Mill Anneal
X 100 HCl and Picric in Alcohol

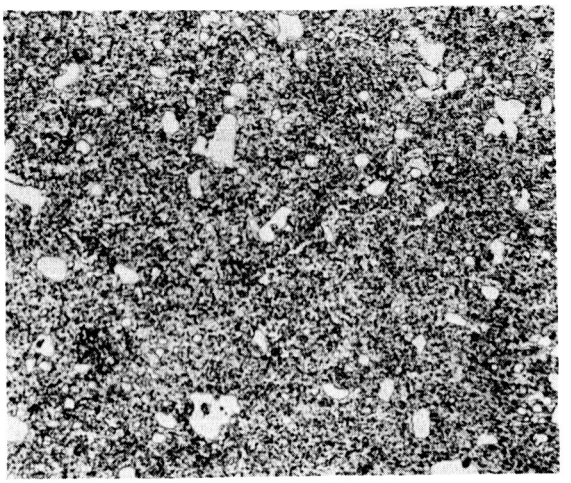

Quenched and Drawn to Rc 60
X 500 Vielella's Etch

FAILED TENSILE SPECIMENS
ROOM TEMPERATURE TEST

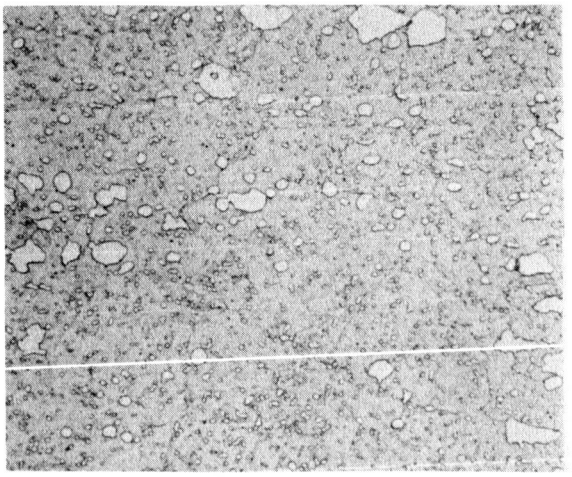

Longitudinal Section at Gage
X 250 HCl and Picric in Alcohol

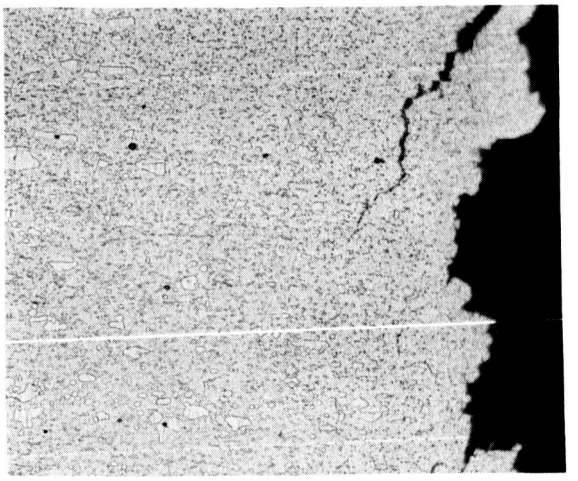

Longitudinal Section at Fracture
X 250 HCl and Picric in Alcohol

FIGURE C 33 a PHOTOMICROGRAPHS OF 440C STAINLESS STEEL (QUENCHED AND DRAWN)

FAILED TENSILE SPECIMEN
30°R, UNIRRADIATED TEST

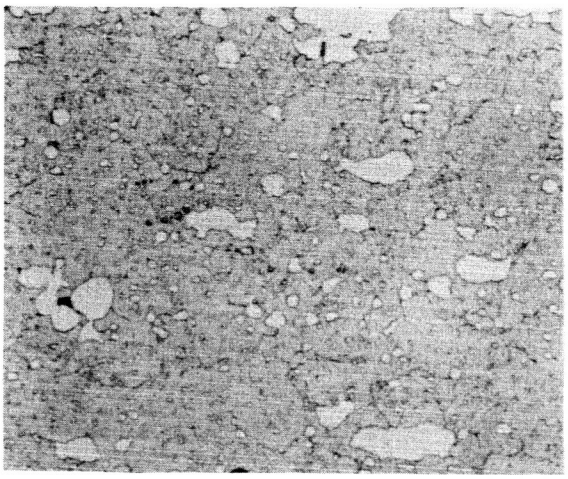

Longitudinal Section at Gage Mark
X 750 HCL and Picric in Alcohol

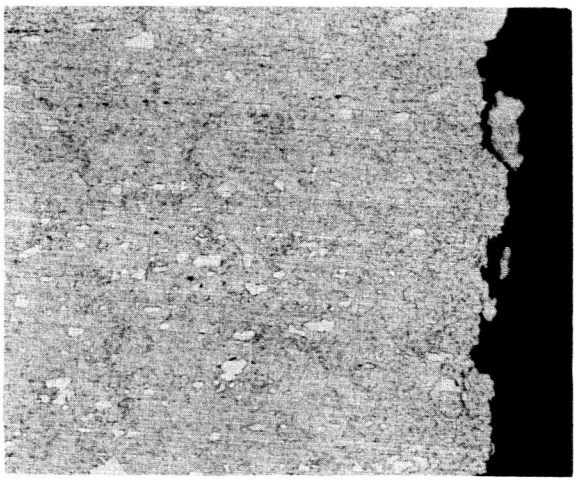

Longitudinal Section at Fracture
X 250 HCl and Picric in Alcohol

FAILED TENSILE SPECIMEN
30°R, 1×10^{17} nvt TEST

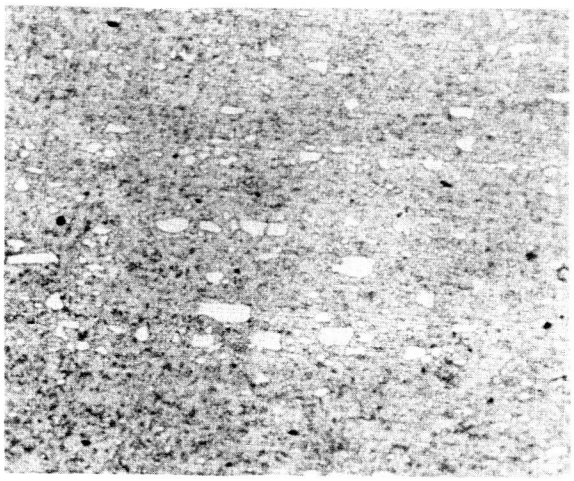

Longitudinal Section at Gage Mark
X 250 HCl and Picric in Alcohol

Longitudinal Section at Fracture
X 250 HCl and Picric in Alcohol

FIGURE C 33 b PHOTOMICROGRAPHS OF 440C STAINLESS STEEL (QUENCHED AND DRAWN)

APPENDIX D

Stress-Strain Diagrams

Typical stress-strain curves for each class of materials tested are shown in this appendix. The curves are presented as families; diagrams for each test condition of a material are superimposed on a common pair of coordinates to facilitate direct comparison. As explained in Section 3.2.2 of this report, actual strain measurements are possible for only some 2% total strain. Therefore, these plots are constructed curves based on stress measurements against time and elongation measurements from each specimen, not direct plots of dynamometer-extensometer signals.

Curves typical of Aluminum alloys 2014, 5086 and 7079 are presented as representative of the shape of the stress-strain functions for the copper bearing, the magnesium bearing and the zinc bearing aluminum alloys respectively. A family of curves for Aluminum 1099 is also shown to illustrate the significant change in shape of these plots at the three environmental conditions in this particular material indicative of the mechanisms discussed in Section 4.2.1.

Of the Titanium alloys, Titanium, 5% Al-2.5% Sn was selected as showing a characteristic shape for stress-strain curves. Curves from Titanium 55A are also shown since this relatively pure metal has a plastic behaviour significantly differing from the alloyed titaniums tested.

Curves of Inconel X were selected as typical of the aged nickel alloys, Inconel, Cold Drawn, as representative of the non-aged materials.

Curves of the Austenitic Steels were not included due to the experimental uncertainty of the exact location of major stress flucuation discussed in Section 6.4.1.

Type 17-7 PH Stainless Steel is typical of the non-austenitic steels showing brittle cryogenic behaviour. Stress-strain curves for Type AM-350 steel are presented to show the unusual cryogenic behaviour of this material; the stress drops significantly during the initial plastic deformation, as described in Section 6.4.2.1, and gradually recovers during increased straining so that the fracture load is approximately the same as the yield load.

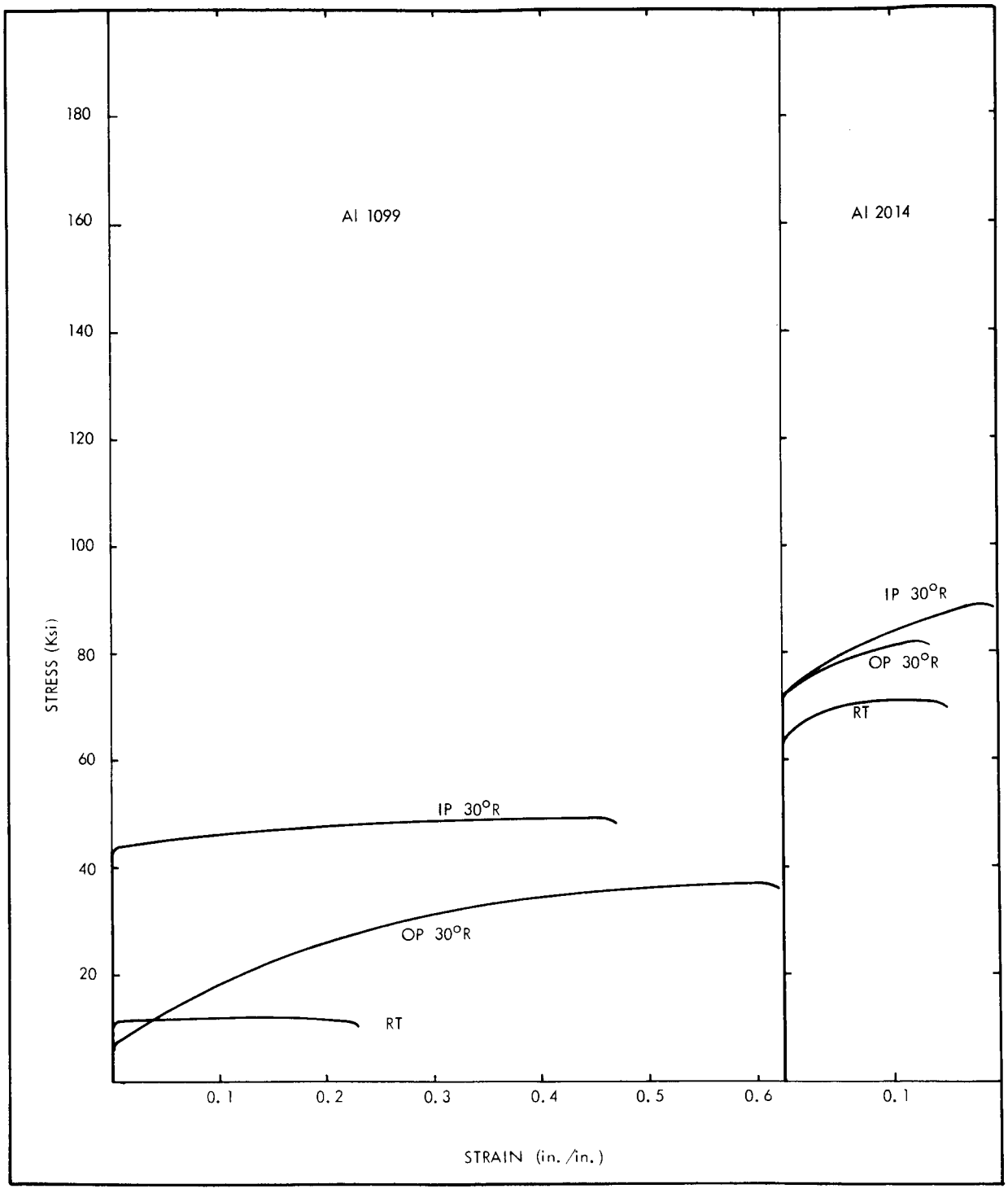

FIGURE D 1 TYPICAL STRESS-STRAIN CURVES FOR ALUMINUM 1099 AND ALUMINUM 2014

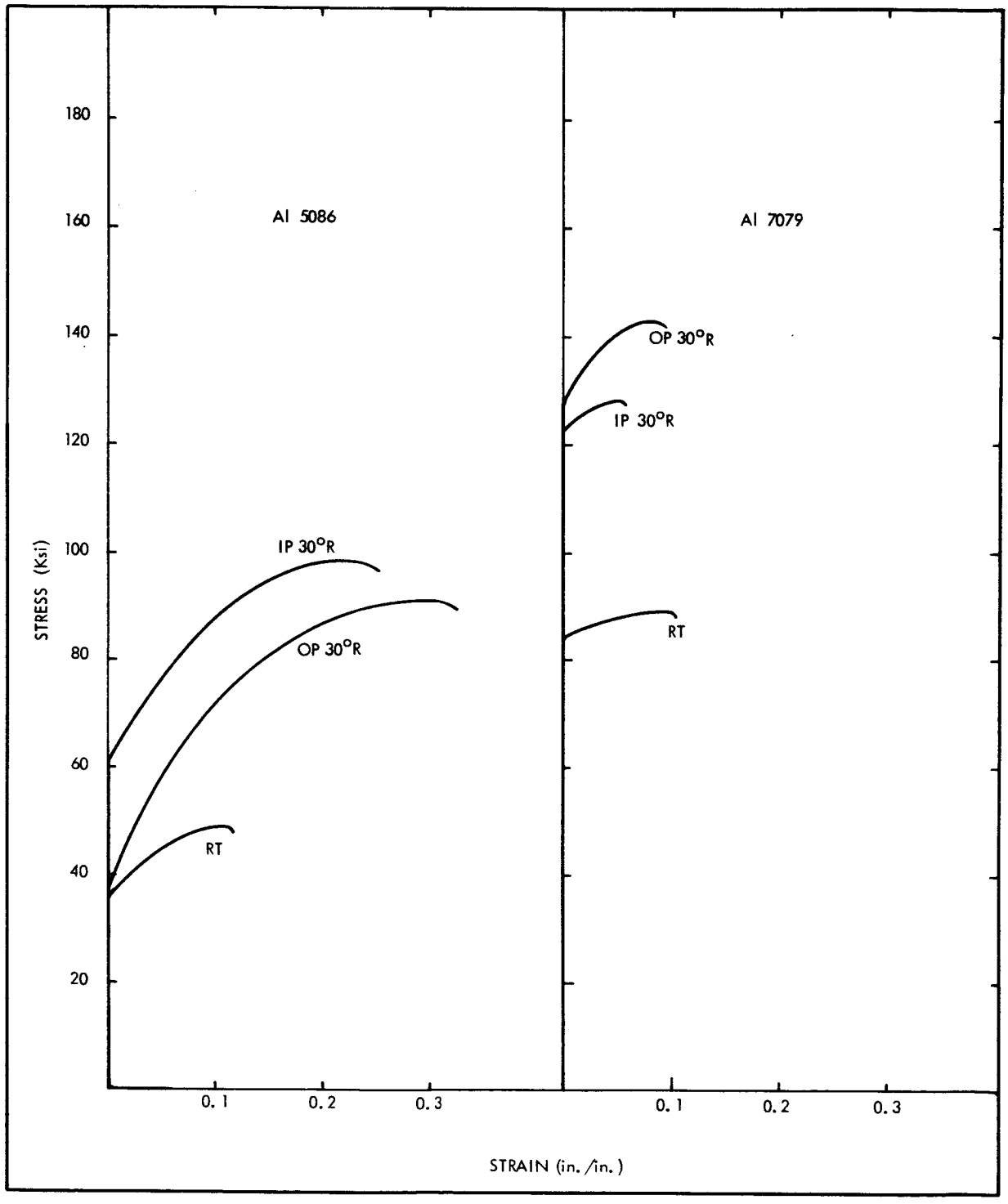

FIGURE D 2 TYPICAL STRESS-STRAIN CURVES FOR ALUMINUM 5086 AND ALUMINUM 7079

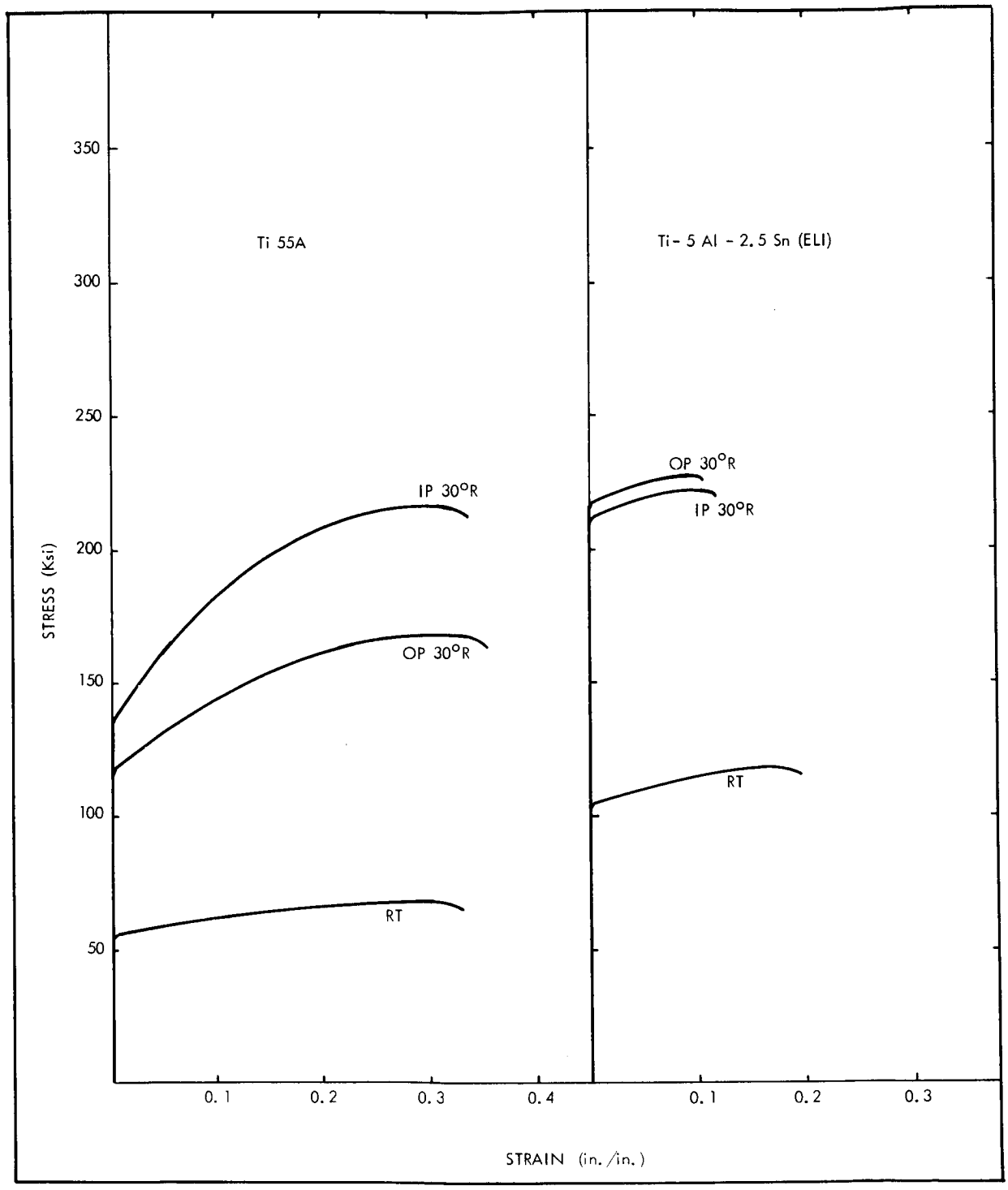

FIGURE D 3 TYPICAL STRESS-STRAIN CURVES FOR TITANIUM 55A AND TITANIUM-5Al-2.5 Sn (ELI)

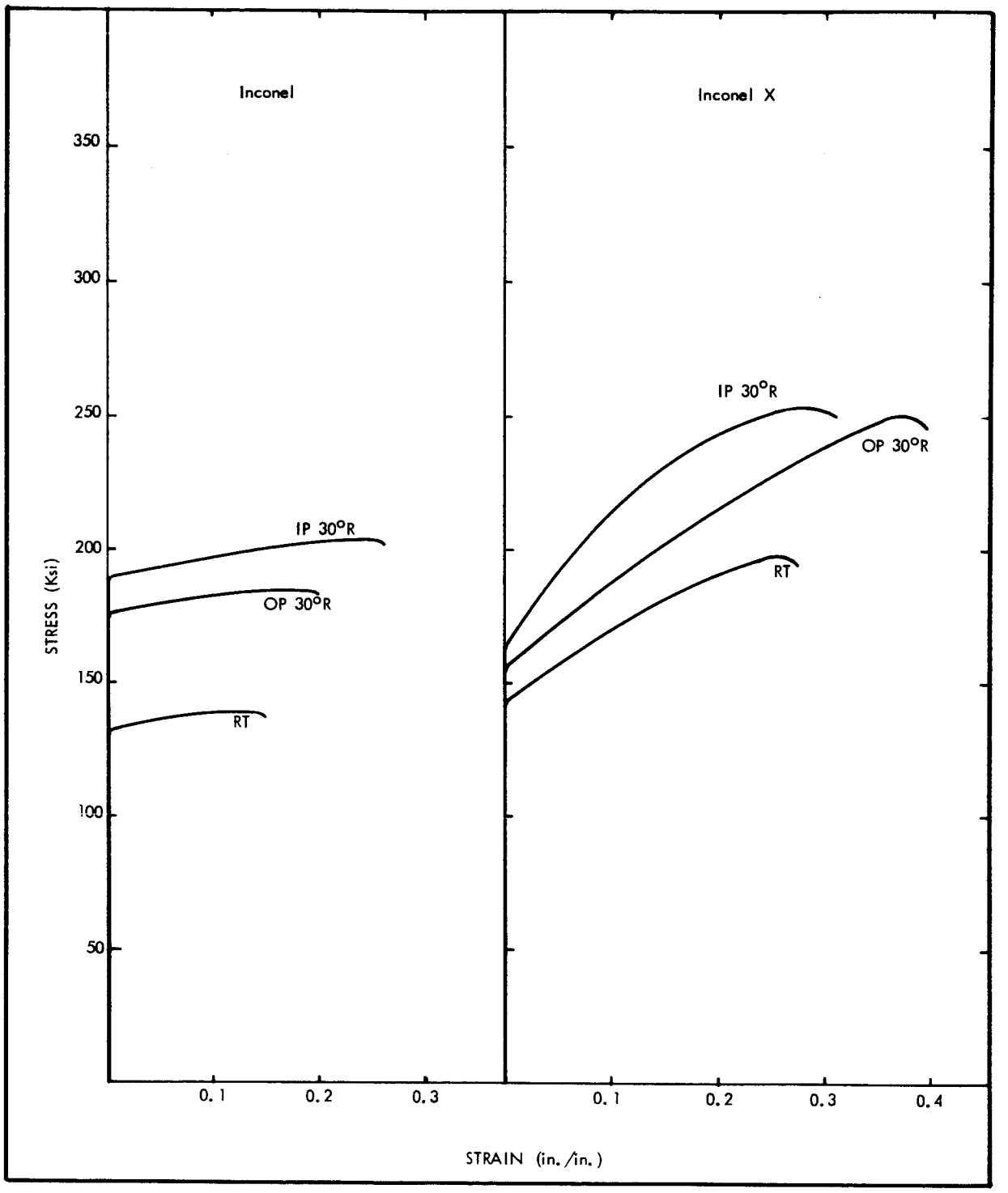

FIGURE D 4 TYPICAL STRESS-STRAIN CURVES FOR INCONEL AND INCONEL X

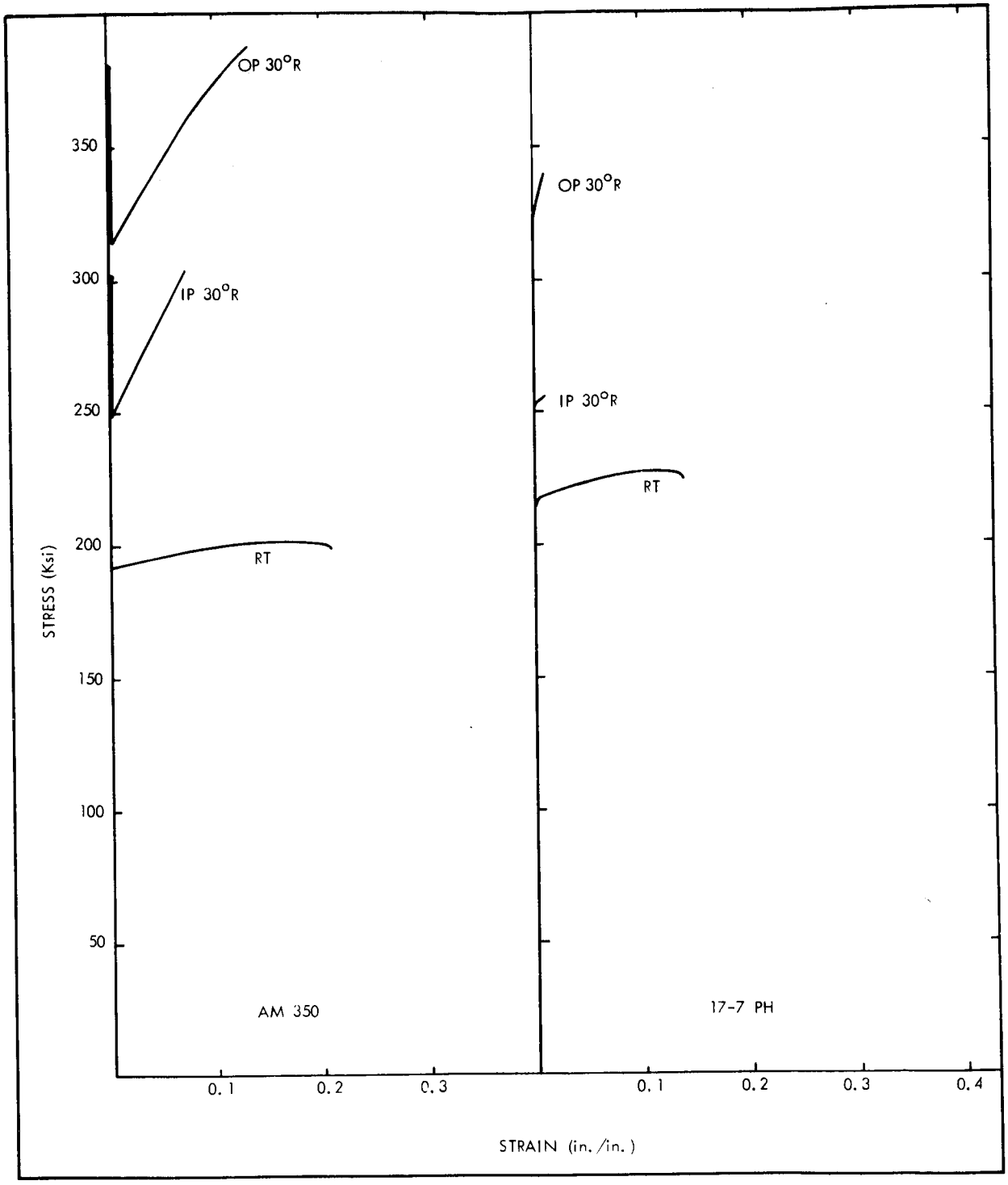

FIGURE D 5 TYPICAL STRESS-STRAIN CURVES FOR AM 350 AND 17-7 PH STAINLESS STEELS

APPENDIX E

DISTRIBUTION

NASA-Lewis Research Center (3)
21000 Brookpark Road
Cleveland, Ohio 44135
Attention: Charles L. Younger (NSD)

NASA-Lewis Research Center (1)
21000 Brookpark Road
Cleveland, Ohio 44135
Attention: T.J. Flanagan (P&SD)

NASA-Lewis Research Center (1)
21000 Brookpark Road
Cleveland, Ohio 44135
Attention: Norman T. Musial

NASA-Scientific & Technical
Information Facility (6)
Box 5700
Bethesda, Maryland 20014
Attention: NASA Representative
(CRT)

NASA-Lewis Research Center (2)
21000 Brookpark Road
Cleveland, Ohio 44135
Attention: Library

NASA-Lewis Research Center (1)
21000 Brookpark Road
Cleveland, Ohio 44135
Attention: Report Control Office

U.S. Atomic Energy Commission (3)
Technical Reports Library
Washington, D.C.

U. S. Atomic Energy Commission (1)
Division of Technical Information
Extension
P.O. Box 62
Oak Ridge, Tennessee 37831

National Aeronautics & Space
Administration (1)
Washington, D.C. 20546
Attention: George C. Deutsch
(Code RRM)

National Aeronautics & Space
Administration (1)
Washington, D.C. 20546
Attention: David Novik, Chief
(Code RNV)

AEC-NASA Space Nuclear Propulsion
Office (2)
U.S. Atomic Energy Commission
Washington, D.C. 20545
Attention: F.C. Schwenk

AEC-NASA Space Nuclear Propulsion
Office (1)
U.S. Atomic Energy Commission
Washington, D.C. 20545
Attention: J.E. Morrissey

National Aeronautics & Space
Administration (1)
Space Nuclear Propulsion Office-
Cleveland
Lewis Research Center
21000 Brookpark Road
Cleveland, Ohio 44135
Attention: L.C. Corrington

NASA-Lewis Research Center (3)
21000 Brookpark Road
Cleveland, Ohio 44135
Attention: M.H. Krasner

NASA-Lewis Research Center (1)
21000 Brookpark Road
Cleveland, Ohio 44135
Attention: H.J. Heppler, Jr.

NASA-Lewis Research Center (2)
21000 Brookpark Road
Cleveland, Ohio 44135
Attention: Dr. John C. Liwosz

NASA-Plum Brook Station (3)
Sandusky, Ohio 44870
Attention: Donald B. Crandall

NASA-Lewis Research Center (1)
21000 Brookpark Road
Cleveland, Ohio 44135
Attention: Office of Reliability &
Quality Assurance

NASA-Ames Research Center (1)
Moffett Field, California 94035
Attention: Library

NASA-Flight Research Center (1)
P.O. Box 273
Edwards, California 93523
Attention: Library

NASA-Goddard Space Flight Center (1)
Greenbelt, Maryland 20771
Attention: Library

Jet Propulsion Laboratory (1)
4800 Oak Grove Drive
Pasadena, California 91103
Attention: Library

NASA-Langley Research Center (1)
Langley Station
Hampton, Virginia 23365
Attention: Library

NASA-Manned Spacecraft Center (1)
Houston, Texas 77001
Attention: Library

NASA-Western Operations (1)
150 Pico Boulevard
Santa Monica, California 90406
Attention: Library

NASA-Marshall Space Flight Center (1)
Huntsville, Alabama 35812
Attention: Library

NASA-Marshall Space Flight Center (1)
Huntsville, Alabama 35812
Attention: W.Y. Jordan, P&VE-FN

NASA-Marshall Space Flight Center (1)
Huntsville, Alabama 35812
Attention: Dr. W.R. Lucas,
M-P & VE-M

NASA-Marshall Space Flight Center (1)
Huntsville, Alabama 35812
Attention: R.D. Shelton, M-RP-N

Aerojet-General Corporation (1)
P.O. Box 1947
Sacramento, California
Attention: W.A. Greenhow, Manager
Radiation Effects Program
Department 7431

Aerojet-General Corporation (2)
P.O. Box 1947
Sacramento, California
Attention: C.K. Soppet, Manager
Nuclear Operations

Aerojet-General Corporation (3)
P.O. Box 296
Azusa, California
Attention: C.N. Trent, Associate Director
NERVA Operations

Aerojet-General Corporation (1)
P.O. Box 1947
Sacramento, California
Attention: Dr. W. Weleff

Aerojet-General Nucleonics (1)
A Division of Aerojet-General
Corporation
P.O. Box 77
San Ramon, California 94583
Attention: G.A. Linenberger,
General Manager

Aluminum Company of America (1)
P.O. Box 1012
New Kensington, Pennsylvania
Attention: Edwin H. Spuhler

Argonne National Laboratories (1)
P.O. Box 299
Lemont, Illinois
Attention: T.H. Blewitt

Argonne National Laboratory (1)
Library Services Dept. 203-CE 125
9700 South Cass Avenue
Argonne, Illinois 60440
Attention: Report Section

Arthur D. Little Company, Inc. (1)
Acorn Park
Cambridge, Massachusetts
Attention: Charles A. Schulte

Atomics International (4)
P.O. Box 309
Canoga Park, California
Attention: F. E. Farhat, Librarian

Battelle Memorial Institute (1)
Northwest Laboratories
326 Building, 300 Area
Richland, Washington 99352
Attention: Dr. T. T. Claudson

Battelle Memorial Institute (1)
505 King Avenue
Columbus, Ohio 43201
Attention: D. J. Hammon, Radiation
Effects Information Center

Battelle Memorial Institute (1)
505 King Avenue
Columbus, Ohio 43201
Attention: Roger J. Runck

Battelle-Northwest (1)
P.O. Box 999
Richland, Washington
Attention: Spencer H. Bush

Beech Aircraft Corporation (1)
P.O. Box 631
Boulder, Colorado 80301
Attention: Technical Library

The Bendix Corporation (1)
Research Laboratory Division
Southfield, Michigan
Attention: Frank W. Poblenz,
Library Services

The Boeing Company (1)
Aerospace Group
P.O. Box 3707
Seattle, Washington 98124
Attention: Ruth E. Peerenboom,
Processes Supervisor

Brookhaven National Laboratory (1)
Upton Long Island, New York 11973
Attention: D. H. Gurinsky

Brookhaven National Laboratory (1)
Upton Long Island, New York 11973
Attention: Paul W. Levy, Department of Physics

Bureau of Naval Weapons (1)
Washington, D.C.
Attention: J.H. Terry, Captain, RRNU

California Institute of Technology (1)
1201 East California Street
Pasadena, California 91109
Attention: General Library

Carbone Company (1)
Toonton, New Jersey
Attention: E.P. Eaton

Carpenter Steel Company (1)
P.O. Box 662
Reading, Pennsylvania
Attention: Neil J. Culp

Department of the Army (1)
United States Army Munitions Command
Frankford Arsenal
Philadelphia, Pennsylvania
Attention: Librarian

Douglas Aircraft Company, Inc. (2)
Missile & Space Systems Division
3000 Ocean Park Blvd.
Santa Monica, California 90406
Attention: A2-260 Library

General Dynamics/Convair (1)
P.O. Box 1128
San Diego, California 92112
Attention: A. Hurlich, Manager
Materials & Processes Section,
Mail Zone 572-00

General Dynamics/Fort Worth (1)
P.O. Box 748
Fort Worth, Texas 76101
Attention: Mr. Bob Vollmer,
Administrative Assistant,
President's Office

General Electric Company (1)
Nuclear Materials & Propulsion Operation
P.O. Box 132
Cincinnati, Ohio 45215
Attention: J.W. Stephenson

Hughes Aircraft Company (1)
Nucleonics Division
Fullerton, California
Attention: Dr. A.M. Liebschutz

IIT Research Institute (1)
10 W. 35th Street
Chicago 16, Illinois
Attention: D.J. McPherson,
Vice President

International Nickel Company, Inc. (1)
Huntington Alloy Products Division
Huntington, West Virginia
Attention: E.B. Fernsler

Kaman Aircraft Corporation (1)
Kaman Nuclear Division
Colorado Springs, Colorado
Attention: Mary G. Brown, Librarian

Lockheed-California Company (1)
Burbank, California 91503
Attention: Dr. Lewis Larmore,
Chief Scientist

Lockheed-California Company (2)
Burbank, California 91503
Attention: Central Library, Bldg. 63
Scientific & Technical Information Center

Lockheed-California Company (1)
Burbank, California 91503
Attention: H.B. Wiley,
Engineering Research

Lockheed-Georgia Company (1)
Nuclear Laboratories
P.O. Box 128
Dawsonville, Georgia
Attention: Dr. M.M. Miller, Manager
Nuclear Aerospace Division

Lockheed-Georgia Company (15)
P.O. Box 2155
Sandusky, Ohio 44870
Attention: C. A. Schwanbeck

Lockheed-Georgia Company (1)
Nuclear Laboratories
P.O. Box 128
Dawsonville, Georgia
Attention: Information Center

Lockheed Missiles & Space Company (1)
3251 Hanover Street
Palo Alto, California
Attention: John C. McDonald,
Materials Research Staff

Lockheed Missiles & Space Company (2)
3251 Hanover Street
Palo Alto, California
Attention: Sci-Tech Information Center

Lockheed Missiles & Space Company (1)
3251 Hanover Street
Palo Alto, California
Attention: M.A. Steinberg, 52-30, 201

Lockheed Missiles & Space Company (1)
Sunnyvale, California
Attention: H.F. Plank, Nuclear Space
Programs

Los Alamos Scientific Laboratory (1)
P.O. Box 1663
Los Alamos, New Mexico 87544
Attention: Glen A. Graves

Los Alamos Scientific Laboratory (3)
P.O. Box 1663
Los Alamos, New Mexico 87544
Attention: Report Library

The Martin Company (1)
P.O. Box 179
Denver, Colorado 80201
Attention: F. R. Schwartzberg, G0534

Mechanical Properties Data Center (1)
Suttons Bay, Michigan 49682
Attention: Matthew J. Kanold,
Administrative Assistant

National Bureau of Standards (1)
Boulder, Colorado 80302
Attention: Cryogenic Data Center

National Bureau of Standards (1)
Cryogenic Engineering Laboratory
Boulder, Colorado 80302
Attention: R.P. Reed

North American Aviation (1)
Rocketdyne Division
6633 Canoga Avenue
Canoga Park, California
Attention: Technical Information Center

Northrop Corporation (1)
Norair Division
3901 W. Broadway
Hawthorne, California
Attention: Technical Information 3343-32

Oak Ridge National Laboratory (1)
Oak Ridge, Tennessee 37831
Attention: D.S. Billington

Ohio State University Libraries (1)
Serial Division
1858 Neil Avenue
Columbus, Ohio 43210

Pennsylvania State University (1)
105 Hammond Building
University Park, Pennsylvania 16802
Attention: Mr. Joseph Marin, Engineering Mechanics Department

Picatinny Arsenal (1)
Technical Information Section, SMUPA-VA6
Dover, New Jersey 07801
Attention: Commanding Officer

Purdue University (1)
Lafayette, Indiana
Attention: Librarian

Pure Carbon Company (1)
Wellsville Street
Saint Marys, Pennsylvania
Attention: Robert Paxon

Reynolds Metals Company (1)
6601 West Broad Street
Richmond, Virginia
Attention: L. E. Householder

Rice University (1)
P.O. Box 1892
Houston, Texas 77001
Attention: The Fondren Library

Rocketdyne (1)
A Division of North American Aviation, Inc.
6633 Canoga Avenue
Canoga Park, California
Attention: Mr. G. A. Fairboirn, D/596-174Z-2

Sandia Corporation (1)
P.O. Box 5800
Sandia Base
Albuquerque, New Mexico 87115
Attention: Technical Library

Southeastern Research Institute (1)
Birmingham, Alabama
Attention: J.R. Kattus

Special Metals, Inc. (1)
New Hartford, New York
Attention: Robert Neilsen

Titanium Metals Corporation of America (1)
233 Broadway
New York, New York
Attention: E.F. Erbin, Staff

TRW Systems (1)
Technical Information Center
One Space Park
Redondo Beach, California 90278

U.S. Air Force (1)
Air Force Weapons Laboratory
Kirtland AFB, New Mexico 87117
Attention: Technical Library (WLIL)

U.S. Air Force (1)
AF Materials Laboratory, Research & Technology Division, AFSC
Wright-Patterson AFB, Ohio 45433
Attention: Harold M. Hormann

U. S. Air Force (1)
Foreign Technology Division, TDEPR
Wright-Patterson AFB, Ohio 45433
Attention: Lt. Schauffle

U. S. Air Force (1)
AFML (MAAM) (1A)
Wright-Patterson AFB, Ohio 45433

U.S. Army Materials Research Agency (1)
Watertown Arsenal
Watertown, Massachusetts
Attention: T.S. DeSisto

U.S. Naval Research Laboratory (1)
Washington, D.C. 20390
Attention: Dr. Albert V.H. Masket, Mechanics Division, Code 6204

U. S. Naval Research Laboratory (1)
Washington, D.C. 20390
Attention: L.E. Steele, Head, Reactor Materials Branch, Metallurgy Division

United States Steel Corporation (1)
Monroeville, Pennsylvania
Attention: Waldo Rall

University of California (1)
Lawrence Radiation Laboratory
Berkeley, California
Attention: Technical Information Division

University of California (1)
Lawrence Radiation Laboratory
P.O. Box 808
Livermore, California
Attention: Technical Information Division

University of California (1)
Los Alamos Scientific Laboratory
P.O. Box 1663
Los Alamos, New Mexico 87544
Attention: W.L. Kirk

University of California (1)
405 Hilgard Avenue
Los Angeles, California 90024
Attention: Engineering & Mathematical Sciences Library

University of California (1)
University Research Library
Los Angeles, California 90024
Attention: Serials Department

University of Chicago (1)
5640 Ellis
Chicago, Illinois 60637
Attention: Institute of Metals Library

University of Colorado (1)
Engineering Research Center
Boulder, Colorado
Attention: K.D. Timmerhaus, Associate Dean of Engineering

University of Georgia Libraries (2)
Athens, Georgia 30601
Attention: Acquisitions Division

University of Michigan (1)
Ann Arbor, Michigan 48104
Attention: Robert G. Carter, University Library

Westinghouse Electric Corporation (1)
Astronuclear Laboratory
P.O. Box 10864
Pittsburgh, Pennsylvania 15235
Attention: Dr. D.E. Thomas, Manager Materials Department

Westinghouse Electric Corporation (1)
Metallurgical Division
Pittsburgh, Pennsylvania 15235
Attention: E.T. Wessel, Research & Development Center

A B S T R A C T

24695

The tensile properties for 33 polycrystalline structural materials including aluminum, titanium, nickel and iron alloys were obtained at -256.5°C (30°R) after irradiation exposure at this temperature to 10^{17} nvt ($E > 0.5$ Mev), at -256.5°C without previous irradiation, and at approximately 27°C (540°R) without previous irradiation. The data were evaluated statistically to permit identification of cryogenic effects and nuclear-cryogenic effects. A number of conclusions were drawn regarding suitability of certain of the materials for use in nuclear-cryogenic applications and regarding the need for further investigation.